

Tailoring electrospun nanofibers and electrosprayed nanoparticles to enhance cellular uptake of low bioavailability drugs

This thesis is submitted in partial fulfilment for the degree of Doctor of
Philosophy

Erum Noreen

June 2020

School of Human Sciences

London Metropolitan University

Acknowledgements

Most of all, I would like to express my deepest gratitude to my project supervisors, Dr Kenneth White (Professor in Molecular Bioscience), Dr Nick Chatterton, Dr Samir Nuseibeh and Dr Gemma Shearman, who had led me into this exciting multidisciplinary research arena of Biomedicine and given me great support and continual patience during my years of academic pursuit in the LMU, London. My deepest gratitude is also extended to Dr Gareth Williams for his constant encouragement and help in this PhD study.

This project could not complete without having help from the friends and colleagues around me. I would like to thank all the members in the Lab, the staff from LMU, especially lab technicians for providing the assistance in different ways. I am thankful to John Morgan, for his kind advices and patience.

Finally, I would like to thank my family for their constant support during the past tough years of doctoral study. Thanks Mom and Dad for your encouragement in this tough period. Completion of My degree was not possible without help of my brothers (Mazher and Dr Ather) and sisters (Dr Huma and Dr Anjum).

Dedication

To my mother, Parveen Akhter and Father Muhammad Hussain, who have taught me to work hard, be giving and never lose hope.

Abstract

This thesis describes colon targeted, fast dissolving delivery systems prepared through electrospraying and electrospinning. An overview of relevant literature on electrospraying and electrospinning is given at the start. Biodegradable polymer polyvinylpyrrolidone (PVP), and polycaprolactone (PCL) were used in the projects to produce nanomaterials using simple and straight forward techniques of electrospinning and electrospraying.

In the first project, preparation, and characterization of PCL and PVP nanoparticles, using coaxial electrospraying was carried out. Electrospayed nanocomposite coaxial nanoparticles with polyvinylpyrrolidone 10000 (PVP10) in the shell and polycaprolactone (PCL) 14000 in the core, were fabricated. Spherical, fiber-free particles were obtained with 5% solutions of polyvinylpyrrolidone. Confirmation of the presence of polycaprolactone inside the polyvinylpyrrolidone particles remained a challenge. Due to time constraints further work on this aspect of the project was abandoned, but a useful outcome was that low molecular weight PVP (av. mw10 kDa) could be used to prepare particles less than 100 nm.

For the second project, hemin was selected for preparation of formulations for treatment of anaemia, as current treatments have side effects like gastric irritation and low bioavailability. Electrospun nanofibers and electrospayed nanoparticles were tailored to enhance cellular uptake of low bioavailability drugs (hemin). DMF and MeOH was used to make hemin soluble. PVP-360 and eudragit L 100 were initially selected to make hemin formulations by electrospinning. A variety of electrospinning conditions were attempted and optimal conditions for producing high quality fibers were found to be 0.5 mL/hr, 14 cm (distance) and 12.22 kV (voltage) for PVP/1% (w/w) hemin fibers. Preliminary dissolution tests showed that PVP/ hemin fibres completely dissolved in PBS within 10 minutes. Whereas eudragit/hemin fibres took 2 to 3 days to dissolve. PVP-360 made hemin dissolve successfully in PBS, so further development was focused on developing PVP formulations.

DLS (Dynamic light scattering) gave two or three sizes of populations in biological media. The proportion of aggregates increased as the concentration of hemin increased which might be due to hydrogen bond between PVP and hemin.

Uptake from the nanoparticles obtained from hemin formulations was assessed in HepG2, THP-1 and Caco-2 cells. Fibers were generally well tolerated by HepG2 cells except when treated with fibers with 5% (w/w) hemin where there was loss of 76.7% of cells. According to the ferrozine iron assay there was a 22% increase in iron in cells treated with fibers with 1% (w/w) hemin preparation compared with 119% increase in iron in cells treated with 5% fibers, with respect to control. In THP-1 cells the viability after treatment with PVP hemin fibres decreased as the proportion of hemin in the fiber increased. An average viability of 70% was found in cells treated with 5% hemin preparation. The viability data showed that PVP fibers with hemin are not strongly toxic to THP-1 cells and are better tolerated in THP-1 in comparison to HepG2 cells and Caco-2 cells. There is a trend of increased iron uptake in THP-1 cells as the hemin content of fibers increased. The iron content of cells treated with 5% hemin fibers was found to be 100 times higher than control cells. There is significant increase in iron from 2 and 5 % hemin preparation in Caco-2 cells.

Electrospraying and electrospinning were successfully used for the production of nanomaterials. Nanoparticles less than 100 nm were successfully produced from PVP 10 kDa, which has not been reported before. Cellular uptake of iron from PVP-hemin formulations was demonstrated and is attributed to previously unobserved spontaneous formation of nanoparticles after dissolution of fibers.

Table of contents

Contents	Page number
Acknowledgments	2
Abstract	4
Table of contents	6
List of appendices	12
List of tables	13
List of figures	15
List of abbreviations	26
Chapter 1 – Introduction	28
1.1 Nanoscience, nanotechnology and its applications	28
1.2 Nanoparticles and diffusion through lipid bilayer	29
1.3 Nanomaterials as drug delivery system (DDS)	30
1.4 Electrohydrodynamics	31
1.4.1 Electrospinning	33
1.4.1.1 Coaxial Electrospinning	35
1.4.2 Electrospraying	36
1.4.2.1 Coaxial Electrospraying	36
1.4.3 Factors affecting electrohydrodynamic process	37
1.4.3.1 Solution properties	37

1.4.3.2 Processing parameters	38
1.4.3.3 Ambient parameters	40
1.5 Biodegradable polymers	40
1.5.1 Polyvinylpyrrolidone (PVP)	41
1.6 Formulation of drugs	42
Chapter 2: Preparation and characterization of nanoparticles for delivery of 5-flurouracil	44
2.1 Introduction	44
2.2 Methods and materials	45
2.2.1 Materials	45
2.2.2 General instruments	45
2.2.2.1 Infrared spectroscopy (IR)	46
2.2.2.2 Scanning electron microscopy (SEM)	46
2.2.2.3 Microscopy	46
2.2.2.4 NMR	46
2.2.2.5 Dynamic light scattering	46
2.2.3 Preparation of solutions	47
2.2.3.1 Polymer solutions	47
2.2.3.2 Sodium dodecyl sulphate (SDS) solution	47
2.2.4 Electro spraying	47
2.2.4.1 Single fluid electro spraying	47
2.2.4.2 Coaxial electro spraying	48
2.2.5 Method adopts for separation of PCL particles	49

2.2.5.1 Method 1	49
2.2.5.2 Method 2	49
2.3 Result and discussion	50
2.3.1 Electro spraying of polymer on foil	50
2.3.1.1 Characterization	67
2.3.1.1.1 Infrared (IR) Spectroscopy	67
2.3.1.1.2 Nuclear magnetic resonance (NMR)	69
2.3.2 Electro spraying of polymer in to distilled water	71
2.4 Conclusion	73
Chapter 3 – Preparation and characterization of novel formulation of hemin for better management of anaemia	75
3.1 Introduction	75
3.1.1 Iron and its availability in diet	75
3.1.2 Mechanisms of iron absorption	76
3.1.3 Regulation of iron absorption	76
3.1.4 Transportation and distribution of iron in the body	77
3.1.5 Deficiency of iron and its impact on human health	77
3.1.6 Prevention of iron deficiency: Food fortification & its limitations	78
3.1.7 Parenteral iron supplements	78
3.1.8 Oral iron supplements	79
3.1.9 Developments in iron supplements	80
3.1.10 Potential of heme and hemin as an iron supplement	81
3.1.11 Development of new hemin supplement	82
3.2 Aims and objectives	83

3.3 Materials and methods	84
3.3.1 Materials	84
3.3.2 Methods	84
3.3.2.1 Preparation electrospinning/electrospraying solution	84
3.3.2.2 Single fluid electrospinning/electrospraying	85
3.3.2.3 Dissolution studies	85
3.3.2.4 Characterization techniques of nanomaterial	86
3.3.2.4.1 Infrared spectroscopy (IR)	86
3.3.2.4.2 Ultraviolet-visible spectroscopy	86
3.3.2.4.3 X-ray diffraction	87
3.3.2.4.4 Energy disperse x-ray spectroscopy (EDX/EDS)	87
3.3.2.4.5 Scanning electron microscopy (SEM)	87
3.3.2.4.6 Microscopy	87
3.3.2.4.7 Dynamic light scattering	87
3.3.2.4.8 Differential Scanning Calorimetry (DSC)	89
3.3.2.4.9 Measurement of iron content in fibers (Ferrozine Assay)	89
3.4 Results and discussion	90
3.4.1 Development of Hemin-Polymer formulation	90
3.4.2 Absorption spectroscopy	107
3.4.3 Dissolution studies	112
3.4.4 Infrared spectroscopy	114
3.4.5 X-ray diffraction	116
3.4.6 Energy disperse x-ray spectroscopy (EDX)	117
3.4.7 Dynamic light scattering (DLS)	121

3.4.8 Differential Scanning Calorimetry (DSC)	125
3.4.9 Measurement of iron content in fibers	127
3.5 Discussion	129
Chapter 4 – Uptake of hemin-PVP nanoparticles by cultured cells – An in Vitro study	137
4.1 Introduction	137
4.2 Materials and methods	138
4.2.1 Materials	138
4.2.2 Methods	138
4.2.2.1 Preparation of hemin solutions for treatment of cells	138
4.2.2.2 Cell culture	139
4.2.2.3 Light microscopy	140
4.2.2.4 Cell viability assay	140
4.2.2.5 Perls staining of ferric iron	140
4.2.2.6 Ferrozine assay of cellular iron uptake ...	141
4.2.2.7 Bradford protein assay	143
4.3 Results	144
4.3.1 Uptake of Iron from PVP-Hemin Fibers by HepG2 Cells	144
4.3.2 Uptake of Iron from PVP-Hemin Fibers by THP-1 cells	148
4.3.3 Uptake of Iron from PVP-Hemin Fibers by Caco-2 cells	155
4.4 Discussion	159
Chapter 5 Future work	165
5.1 Potential for nanotechnology as drug delivery for cancer treatment	165

5.1.1 Burden of cancer	165
5.1.2 5-Fluorouracil: An example of chemotherapeutic drug	165
5.1.3 Formulation of 5 FU-PCL Nanoparticles for drug delivery	166
5.1.4 Potential for a formulation of 5FU-PVP Nanoparticles	167
5.2 PVP-Hemin formulation: Improvement in Hemin Formulation	167
5.2.1 PVP-Hemin Formulation: Scope for further work	168
References	169

List of Appendices

Appendix A	203
Appendix B	204
Appendix C	207
Appendix D.....	210
Appendix E.....	212
Appendix F	214
Appendix G.....	216

List of Tables

Table 2.1. Processing parameters used for CP _{V2M} of 5 % (w/v) solution in ethanol.....	56
Table 2.2. Processing parameters used for CP _{V2L} of 3% (w/v) solution in ethanol.....	58
Table 2.3. Processing parameters used for CP _{V2L} of 4% (w/v) solution in ethanol.....	59
Table 2.4. Processing parameters used for CP _{V2L} of 5% (w/v) solution in ethanol.....	61
Table 2.5. Processing parameters used for CP _{V2L} of 6% (w/v) solution in ethanol.....	62
Table 2.6. Size distribution of 100 particles from samples of CP _{V2L} . The data was obtained from Image J and processed through Graph Pad Prism.....	64
Table 2.7. The table shows the absorption band of representative functional groups in PCL and PVP.....	68
Table 3.1. Electrospinning conditions of PVP-360 with or without hemin with three different solvents. The voltages of the samples were adjusted until the needle stopped dripping. The images of fibres from these conditions are shown in figure 3.6.....	92
Table 3.2. Electrospinning conditions of PVP-Hemin 1% and Eudragit-Hemin 0.5% at different flow rates. The voltages of the samples were adjusted until the needle stopped dripping.....	94
Table 3.3. Electrospinning conditions of PVP 360 with different % hemin.....	99

Table 3.4. Electrospaying conditions for PVP 10 alone and with 1% hemin.....	101
Table 3.5. Electrospaying conditions of PVP 40 alone and with 1% Hemin.....	103
Table 3.6. Experimental conditions of electrospinning/electrospaying different percentages of PVP40 solution in methanol.....	106
Table 3.7. Molar extinction coefficient of hemin obtained in PVP-hemin complex in PBS, Ph 2 and SIF solution.....	111
Table 3.8. Diameter of fibers of PVP360 and Eudragit with and without hemin.....	132
Table 4.1. Preparation of standard concentrations of ferrous iron for the ferrozine assay.....	142
Table 4.2. Preparation of standard solutions for the Bradford protein assay.....	143
Table 4.3. Mean±SD of diameter 100 THP1 cells, measure with image J. Control (cell without treatment), FAC (positive control), PVP-fibers, P-H_0.5, P-H_1.0 and P-H_5.0 treated cells.....	152

List of Figures

Figure:1.1 A plot of average hydrophobicity verses relative membrane permeability of different nanoparticles (Pogodin., 2012).....	30
Figure 1.2. Single fluid electrohydrodynamic apparatus for electrospinning or electrospaying. Single fluid means only one type of solution is used for fibers or particle production. If particles are produced, the process is electrospaying and if fibers are produced the process is called electrospinning.....	31
Figure 1.3. An image of the ideal form of the cone-jet formed during the electrohydrodynamic experiment (Enayati et al., 2010). The arrow in figure pointing to cone formed during the process of electrospinning/ electrospaying and the dotted line means the starting of cone emerged from needle.....	32
Figure 1.4. Typical SEM of PVP 360 fibers.....	34
Figure 1.5. Co-axial particle or fiber production, using coaxial electrospaying or electrospinning. In this method two syringe pump and co-axial needle is used. The core and sheath solutions are different from each other.....	35
Figure 1.6. PVP 10 (10 kDa) Nanoparticles.....	36
Figure 1.7. Typical picture of beaded fibers of PVP 40 (40 kDa). SEM of 25% solution, image obtained of sample.....	39
Figure 1.8. Parameters that affect the diameter of nanomaterials. Diagram created from Chakraborty <i>et al.</i> , 2009.....	40
Figure 1.9. Structure of Polyvinylpyrrolidone.....	41
Figure 2.1. The chemical structure of the repeat unit in PCL.....	45
Figure 2.2. A photograph of the coaxial spinneret used in this study.....	48
Figure 2.3. Schematic representation of electrospaying into distilled water containing SDS.....	49

Figure 2.4. SEM of particles obtained from A) 4% (w/v) sample SP _{CH} (with a 1 mL/hr flow rate, 10.49 kV voltage 16 cm distance from tip to collector), B) 3% (w/v) sample SP _{CH} (with a 1 mL/hr flow rate, 10.49 kV voltage and 20 cm distance from tip to collector), C) 0.5% (w/v) sample SP _{CH} (with a 1 mL/hr flow rate, 17.63 kV voltage and 18 cm distance from tip to collector).....	50
Figure 2.5. SEM micrograph obtained for sample SP _{CH} 3 mentioned in table B1 in the appendix.....	51
Figure 2.6. Co-axial particle with PCL in core and PVP in shell.....	52
Figure 2.7. SEM micrograph obtained for sample CP _{VCH} 1 mentioned in table C1 in the appendix.....	52
Figure 2.8. SEM of sample from table C1 in appendix C with 5 %(w/v) PVP in ethanol in the shell A) CP _{VCH} 3 with 0.5% (w/v) PCL in 1,2- dichloroethane in the core, B) CP _{VCH} 2 with 2 % (w/v) PCL in 1,2- dichloroethane in the core.....	53
Figure 2.9. SEM of sample CP _{V2H} 5% solution was used in the shell with flow rate of 1.5 ml/hr and 3% solution was used for the core of flow rate of 0.25 ml/hr; at a 15 kV voltage and 10 cm tip to collector distance.....	53
Figure 2.10. SEM of sample CP _{V2M} 1 from table 2.1.....	56
Figure 2.11. SEM of sample CP _{V2L} 8 in table 2.3.....	56
Figure 2.12. (a1) SEM of particles (b1) frequency distribution graph of particles obtained for sample CP _{V2L} 11 from table 2.3. (a2) SEM and (b2) frequency distribution graph (but with a different scale from b1) of a dense area of same sample, showing that the average particle diameter is essentially independent on the particle density of the sample.....	62
Fig 2.13. (a) SEM and (b) frequency distribution graph of sample CP _{VCL} obtained from 4% PVP 10 in shell (with flow rate of 0.25 ml/hr) and 4% PCL 10-14 in core (with a flow rate of 1.0 ml/hr) with 10 cm tip to collector distance and voltage of 20 kV.....	65
Figure 2.14. SEM of sample CP _{VCL} , obtained from 4% PVP 10 and 4% PCL 10-14 with 10 cm tip to collector distance and flow rate of 0.25 mL/hr for core and 1mL/hr for	

shell and voltage of 20 kV. The sample was dissolved in distilled water and centrifuged the pellet was dispersed in (a1) distilled water and (b1) NaOH. The same sample of particles were directly treated with NaOH on foil (a1) 0.5 M and (b1) 2.5 M.....	66
Figure 2.15. SEM of sample CP _{VCL} , obtained from 4% PVP 10 with flow rate of 1.5ml/hr and 10% PCL 10-14 core with flow rate of 0.75 ml/hr at 18 kV voltage and 10 cm tip to collector distance.....	67
Figure 2.16. Comparison of IR of CP _{VCL} (sample in figure 2.16), PVP 10 and PCL 10-14.....	68
Fig 2.17. Comparison of IR of CP _{VCL} (sample in figure 2.19), PVP 10 and PCL 10-14.....	69
Figure 2.18. ¹ H NMR of PCL, PVP and sample CP _{VCL} (PVP/PCL coaxial particles with low flow rate that is 0.25 ml/hr of PCL) run in CDCl ₃ for sample in figure 2.16 (SEM).....	70
Figure 2.19. ¹ H NMR of PCL, PVP and sample CP _{VCL} (SEM in figure 2.19, the PCL was used in the sample at a high concentration (10%) and high flow rate, 0.75 ml/hr, 4% PVP was used with flow rate of 1.5 ml /hr).....	71
Figure 2.20. DLS graph of sample CP _{VCH} . 10% PVP (in core 0.5 ml/hr and in shell with 1.5ml/hr flow rate) at 20 kV voltage with 6.5 cm tip to surface of SDS solution.....	72
Figure 2.21. DLS graph of sample CP _{VCH} . 4% PCL (in core with 0.5ml/hr flow rate) and 5% PVP (in shell with 1.5ml/hr flow rate) at 20 kV voltage with 6.5 cm tip to surface of SDS solution.....	73
Figure 3.1. Pathways of iron absorption by the duodenum. A) heme and non-heme iron from dietary sources is taken up enterocytes brush border. Non-heme iron is reduced to Fe ²⁺ by the ferric reductase. Some of the non-heme iron transported in the form of Fe ³⁺ via the integrin-mobilferrin pathway (IMP).] B) Heme iron is transported via receptor mediated membrane endocytosis (HCP1), which is then oxygenated to Fe ²⁺ by the heme oxygenase. Fe ²⁺ is transported by the DMPT1 to the cytoplasm. FE ³⁺ is transported by IPM complex, which is reduced to Fe ⁺²	76

Figure 3.2. Cycle of iron utilisation & distribution in human body	77
Figure 3.3. Structure of a) heme, b) hemin.....	82
Figure 3.4. Solubility of Hemin in different solvents. Hemin was completely soluble in THF, DMAc and MeOH at the concentrations indicated, and partially soluble in EtOH. Hemin was not soluble in CHCl ₃ and formed a layer at the top of the solvent.....	91
Figure 3.5. Light microscopy of electrospun fibers. a) Fibers from an 18.2% solution of Eudragit L100 in DMAc and MeOH (1:5) and b) a 10% solution of PVP-360 in MeOH. The electrospinning conditions for these samples are given in Table 3.2. 0.5 ml/hr flow rate was used for both samples.....	93
Figure 3.6. Effect of solvent on the quality of PVP-360 fibers produced alone and with 1% hemin by electrospinning. The Electrospinning conditions for these samples are given in table 3.1. Solvents used in a1 and a2 (DMAc), b1 and b2 (EtOH) and c1 and c2 (MeOH).....	93
Figure 3.7. Effect of flowrate [layer 1(0.75mL/hr), 2(1 mL/hr) and 3(1.5mL/hr)] on quality of PVP-360 1% Hemin fibers. Panels: A) Light microscope images (100 x) B) SEM (mag 10k x) and C) histogram showing frequency distribution of fiber diameters from 25 fibers (as total number of fibers in each SEM are less) in each SEM image.....	95
Figure 3.8. Analysis of Eudragit-L100 alone. Panels: A) Light microscope image (mag 400 x) B) SEM (mag 10k x) and C) histogram of fiber diameter frequency distribution from 25 fibers in SEM image (25 fibers were selected as total number of fibers in SEM are less).....	96
Figure 3.9. Effect of flowrate [layer 1(0.5 mL/hr), 2(0.75mL/hr), 3(1 mL/hr) and 4(1.5mL/hr)] on quality of Eudragit-L100 0.5% Hemin fibers. Panels: A) Light microscope image (mag 100 x) B) SEM (mag 10k x) and C) histogram of fiber diameter frequency distribution from 25 fibers (as the total number of fibers in SEM are less) in each SEM image, at different flow rates. The diameter of fibers is increased with increasing flow rate except the sample collected at 0.75 mL/hr flow rate.....	97

Figure 3.10. Analysis of PVP-360 fibers with a range of hemin [layer 1 (0%), 2(0.25%), 3(0.5%), 4(1%) and 5(5%) content. Panels: A) image from light microscopy, B) SEM, C) histogram of frequency distribution from 50 fibers diameter in each SEM image, except for 0.25% hemin containing PVP fibers i.e. for 25 fibers (because the total number of fibers in SEM are less). The diameters are much smaller compared with PVP with 1% hemin. The electrospinning conditions of the samples are given in table 3.4.....100

Figure 3.11. Analysis of PVP-10 particles alone (layer 1) and with 1% hemin (layer 2). Panels: A) SEM (PVP-10 alone, mag 25k x, PVP-10 1%H mag 50k x), B) light microscope image (mag 100 x), C) histogram of frequency distribution from 100 particles diameter in each SEM image. The electrospaying conditions are given in table 3.4.....102

Figure 3.12. Analysis of PVP-40 (layer 1) and PVP-40/ 1% hemin (layer 2) particles. Panels: A) SEM (PVP40 alone, PVP-40 1%H), mag 25k x, B) SEM (PVP-10 alone, PVP-10 1%H), mag 10k x), C) histogram of frequency distribution from 100 particles diameter in each SEM image. The electrospaying conditions are given in table 3.5.....103

Figure 3.13. 15 % PVP-40 Nanoparticle SEM.....104

Figure 3.14. Material produced after Electrospaying/ Electrospinning of 25% PVP-40. Light microscope image at 400 x. The image is enlarged to confirm the presence of fibres. The picture shows the microscope slide part on right side and coverslip with material on left side to avoid misinterpretation due to dust on the slide and lens.....104

Figure 3.15. 40% PVP-40 Fibres. Light microscope image at 400 x. The electrospinning conditions of the sample are given in table 3.6.....105

Figure 3.16. Electrospinning of different %ages of PVP-40. SEM of fibers obtained from A) 25 (mag 10k x), B) 40 (mag 10k x) and C) 55% (mag 2k x) PVP-40. The electrospinning conditions of the samples are given in table 3.6. The scale in A,B and C panel are 2,2 and10 μ M respectively.....105

Figure 3.17. Absorption spectra of three different forms of PVP. A, B and C each image includes only PVP fiber or particles, physical mixture, hemin in PVP solution, hemin alone, and PVP-H samples. The abbreviations use for each set is given in

table 3.8. A) PVP-360 B) PVP-40 C) PVP-10 with 1% hemin and D) PVP 360 with different percentages of hemin.....	107
Figure 3.18. UV-visible spectra of A) PVPH100 (F-HCL) in HCl and PBS (F-PBS) or B) hemin in MeOH or DMSO.....	109
Figure 3.19 Absorption spectrum of PVP-360 with different percentages of hemin in PBS (phosphate buffer saline) layer 1, pH 2 (layer 2) and SIF (layer 3) of unspun and spun samples.	110
Figure 3.20. The relationship between concentration of hemin (0-5%) and absorbance obtained from UV-spectrum at λ_{max} in PBS layer 1, pH 2 (layer 2) and SIF (layer 3) in both without spun and spun samples.....	111
Figure 3.21. Dissolution of PH-1.0-F (A) and hemin alone (B) in PBS. Hemin alone in PBS shows undissolved hemin floating at the top.....	112
Figure 3.22. Dissolution of hemin formulations in PBS. Data are % release measured after spun at 400 nm in samples taken at indicated times. A) Set of PVP-360 formulations, B) set of PVP-40 formulations, C) set of PVP-10 formulations, D) comparison of hemin dissolved after 30 min from PVP-360 fibers with different % hemin. Data are the mean \pm SD of three independent assays carried out for all four sets.....	114
Figure 3.23. IR spectra of a PVP-360 set with 1% hemin. Comparison of IR spectra of 5 samples, PH-1.0-F, PVP-F, PH-1.0-M, PVP (polymer powder) and H (hemin)..	115
Figure 3.24. IR spectra of PVP 360 fibers containing 0.1-5% hemin.....	115
Figure 3.25. IR spectra of a PVP-10 set with 1% hemin. Comparison of IR spectra of 5 samples, PH-1.0-P, PVP-P, PH-1.0-M, PVP (polymer powder) and H (hemin)....	116
Figure 3.26. IR spectra of a PVP-40 set with 1% hemin. Comparison of IR spectra of 5 samples, PH-1.0P, PVP-P, PH-1.0-M, PVP (polymer powder) and H (hemin).....	116
Figure 3.27. X-ray Diffraction of PVP-360 powder and PVP-360 hemin fibers.....	117

Figure 3.28. Energy Dispersive spectroscopy analysis of PVP-360 fibers alone. This showed the presence of C, O, and Cu in the sample. The electrospinning condition of this sample are given in table 3.2.....	118
Figure 3.29. Energy Dispersive spectroscopy analysis of PVP-360-1%H fibers. This showed the presence of C, N, O, Cu, Fe and Cl in sample. The electrospinning conditions of this sample are given in table 3.2.....	118
Figure 3.30. Energy Dispersive spectroscopy analysis of PVP-360-5%H fibers. This showed the presence of C, O, Cu, Fe and Cl in sample. The electrospinning conditions of this sample are given in table 3.3.....	119
Figure 3.31. Energy Dispersive spectroscopy analysis of PVP-10 particles alone. This showed the presence of Al, Fe and Si in sample. The electrospinning condition of this sample are given in table 3.4.....	120
Figure 3.32. Energy Dispersive spectroscopy analysis of PVP-10-1%H particles. This showed the presence of Al, O, Fe and Si in sample. The electrospinning condition of this sample are given in table 3.4.....	120
Figure 3.33. Measurement of particles size of PVP-360 fibers containing 0-1% hemin using DLS in (a) water and (b) PBS.....	122
Figure 3.34. Three triple exponential fit for PVP 360 fibers in water at 25 °C (SSR= 0.010)	123
Figure 3.35. The triple exponential fit for PVP 360 containing 1% hemin fibers in water at 25 °C (SSR= 0.010).....	123
Figure 3.36 (a) Relative intensities of the two different populations with respect to the percentage of hemin in each sample, For all three graphs, the solution is represented by triangles for water and circles for PBS. In figures (b) and (c), additionally, the filled markers represent the fast relaxation times (i.e. small particles) and the unfilled markers represent the slow relaxation times (i.e. PVP aggregates)	125

Figure 3.37. DSC analysis of a PVP360 set of hemin formulations. P360 (polymer powder), H (hemin powder), PH-1.0-M (physical mixture of PVP360 and hemin), P360-F (PVP360 fibers) and PH-1.0-F (PVP360 and hemin fibers)	126
Figure 3.38. Iron content of dissolved PVP-hemin fibers in PBS as determined by a colourimetric assay.....	127
Figure 3.39. Image of solution of PVP-hemin fiber (0-5%) in SIF. It showed sedimentation of microparticulate.....	128
Figure 3.40. Iron content of dissolved PVP-hemin fibers in SIF as determined by a colourimetric assay. FAS was used to prepare standards.....	128
Figure 3.41. Iron content of dissolved PVP-hemin fibers in pH 2 solution determined by a colourimetric assay. FAS was used to prepare standards.....	129
Figure 3.42. The effect of flow rate of 10% PVP-360 / 1% hemin solution on diameter of fibers produced through electrospinning. The data is presented as mean (nm) + SD of diameters of 25 fibers, obtained from SEM and measured using Image J.....	130
Figure 3.43. The effect of flow rate of 18.2% Eudragit / 0.5% hemin solution on diameter of fibers produced through electrospinning. The data is represented as mean (nm)+SD of diameters of 25 fibers, obtained from SEM and measured using Image J.....	131
Figure 3.44 The dissolution process of PVP/hemin fibers in aqueous medium. Firstly, the fibers swell in aqueous medium, A) hemin molecule on surface of fibers joined and made macromolecules, PVP molecule intertwined with it. Hemin molecule imbedded in fibers were convert in to two size PVP/hemin particles B) nanoparticles 10-100 nm C) nanoparticles 100-1000 nm.....	136
Figure 4.1. Standard curve for the ferrozine assay. The data are means \pm SD of triplicate measurements.....	142

Figure 4.2. Standard curve for determination of concentration of protein in lysed cells. The data are means \pm SD of triplicates. Some of the error bars are hidden due to symbols.....144

Figure 4.3. Light microscope images of HepG2 cells; (a) control, no treatment, then treatment with (b) 100 μ M FAC, (c) PVP-360 only, PVP fibers containing hemin to give (d) 10 μ M, (e) 25 μ M, (f) 50 μ M, (g) 75 μ M, (h) 100 μ M, and (i) 500 μ M concentration of hemin. Cells were treated for 48 hr in serumfree medium and then viewed live. Healthy cells are elongated and flat; stressed cells appear rounded and either bright or granular and dark, which is the predominant appearance in panel (i).....145

Figure 4.4. Toxicity of PVP-hemin preparations to HepG 2 cells. Data are the mean+SD from three sets of data and are normalised to control, untreated cells. Treatments are 100 μ M FAC [FAC], PVP only fibers [PVP Only], PVP-hemin fibers producing: 10 μ M hemin [PVP-H_0.1], 25 μ M hemin [PVP-H_0.25], 50 μ M hemin [PVP-H_0.5], 100 μ M hemin [PVP-H_1.0] and 500 μ M hemin [PVP-H_5.0]. One-way Anova comparison of means indicated a significant difference between the control and cells treated with PVP-H_0.5 [**, $p < 0.01$] and PVP-H_5.0 [*** $p < 0.0001$].....146

Figure 4.5. Iron uptake by HepG2 cells. Data are the mean+SD from four sets of data. Treatments are 100 μ M FAC [FAC], PVP only fibers [PVP Only], PVP-hemin fibers producing: 10 μ M hemin [PVP-H_0.1], 50 μ M hemin [PVP-H_0.5], 100 μ M hemin [PVP-H_1.0] and 500 μ M hemin [PVP-H_5.0]. One-way Anova comparison of means indicated a significant difference between the control and cells treated with PVP-H_5.0 [** $p < 0.01$].....147

Figure 4.6. Preparations of PVP or PVP-hemin fibers in DMEM. There are four preparations: PVP-360 only, P-H_0.5, P-H_1.0 and P-H_5.0 in DMEM to make 0, 50 μ M, 100 μ M and 500 μ M of hemin solution. According to the solutions in figure 4.6 the colour of solution darkens as the percentage of hemin increases.....149

Figure 4.7. Treatment of THP-1 cells with PVP fibers only and PVP fibers containing (0.5, 1.0 and 5.0%) hemin. C is control without any treatment (1 ml of plain DMEM only), FAC contains 100 μ M of ferric ammonium citrate.....150

Figure 4.8. Light microscope images of THP-1 cells and frequency distribution graphs of cell diameter. (a1,2) Control cells without any treatment, (b1,2) cells treated with 100µM FAC, (c1,2) cells treated with PVP fibers.....151

Figure 4.9. Light microscope images of THP-1 cells and frequency distribution graphs of cell diameter. (a1,2) Cells treated with P-H_0.5 fibers, (b1,2) cells treated with P-H_1.0 fibers, (c1,2) cells treated with P-H_5.0 fibers.....152

Figure 4.10. Toxicity of hemin preparations to THP-1 cells. Data are mean+SD from four sets of cells. X-axis labels indicate untreated cells (Control), cells treated with 50µM FAC (FAC) as a positive control, cells treated with dissolved PVP fibers at 0.326% (w/v) (PVP only), cells treated with PVP-hemin fibers to give 25 µM (P-H_0.5), 50µM (P-H_1.0) and 250µM (P-H_5.0) hemin. One-way Anova comparison of means indicated a significant difference between the control/ FAC/ PVP only and cells treated with P-H_5.0 [* , p < 0.01].....153

Figure 4.11. Iron uptake by THP-1 cells. Data are mean+SD from five sets of cells. X-axis labels indicate untreated cells (Control), cells treated with 50µM FAC (FAC) as a positive control, cells treated with dissolved PVP fibers at 0.326% (w/v) (PVP only), cells treated with PVP-hemin fibers to give 25 µM (PH_0.5), 50µM (P-H_1.0) and 250µM (P-H_5.0) hemin. One-way Anova comparison of means indicated a significant difference between the control/ PVP only and cells treated with P-H_5.0 fibers [**, p < 0.005] and there is significant difference between cell treated with P-H_0.5 and P-H_5.0 [* , p < 0.05].....154

Figure 4.12. Light microscope images of Caco-2 cells; (a) control, no treatment, then treatment with (b) 100 µM FAC, (c) PVP-360 only, PVP fibers containing hemin to give (d) 100 µM, (e) 200 µM, (f) 500 µM concentration of hemin. The scale bar is 200 µM. Cells were treated for 48 hr in full medium and then viewed live. Healthy cells are elongated and flat; stressed cells appear rounded and either bright or granular and dark, which is the predominant appearance in panel (f).....155

Figure 4.13. Toxicity of PVP-hemin preparations to Caco-2 cells assessed by MTT assay. Data are the mean+SD from three sets of data and are normalised to control, untreated cells. Treatments are 100 µM FAC [FAC], PVP only fibers [PVP Only], PVP-hemin fibers producing: 100 µM hemin [PVP-H_1.0], 200 µM hemin [PVP-H_2.0]

and 500 μM hemin [PVP-H_5.0]. One-way Anova comparison of means indicated a significant difference between cells treated with PVP-H_5.0 [$** p < 0.05$] and control, FAC, PVP only, PVP-H_1.0 and PVP-H_2.0.....156

Figure 4.14. Iron uptake by Caco-2 cells. Data are the mean+SD from three sets of data. Treatments are 100 μM FAC [FAC], PVP only fibers [PVP Only], PVP-hemin fibers producing: 100 μM hemin [PVPH_1.0], 200 μM hemin [PVP-H_2.0] and 500 μM hemin [PVP-H_5.0]. One-way Anova comparison of means indicated a significant difference between the control and cells treated with PVP-H_5.0 [$* p < 0.05$].....157

Figure 4.15. Toxicity of PVP-hemin preparations (spun) to Caco-2 cells assessed by MTT assay. Data are the mean from one set of data and are normalised to control, untreated cells. Treatments are 100 μM FAC [FAC], PVP only fibers [PVP Only], PVP-hemin fibers producing: 100 μM hemin [PVP-H_1.0], 200 μM hemin [PVP-H_2.0] and 500 μM hemin [PVP-H_5.0].....158

Figure 4.16. Iron (spun) uptake by Caco-2 cells. Data are the mean from one set of data. Treatments are 100 μM FAC [FAC], PVP only fibers [PVP Only], PVP-hemin fibers producing: 100 μM hemin [PVPH_1.0], 200 μM hemin [PVP-H_2.0] and 500 μM hemin [PVP-H_5.0].....159

Figure 4.17. Uptake of NPs in intestinal lumen by paracellular transport (50-200 nm), transcellular transport (< 50 nm) and the M cells (200-5 μm). The uptake with specific route depends on particle size.....161

Figure 4.18. Schematic diagram of pathway of PVP/hemin fibers containing gastro-resistant capsule in body. Endocytosis is considered as entrance route of entrance of PVP/hemin NP in intestinal cells, as it has resemblance with heme. Heme enter in enterocytes by endocytosis.....164

Figure 5.1. Structure of 5-FU.....166

List of abbreviations
(arranged in an order as appeared in text)

SP _{CH}	PCL alone single fluid high molecular weight.
SP _C	PCL alone single fluid
CP _{Vc}	Combination coaxial PVP shell and PCL as core
CP _{VCL}	combination of coaxial PVP shell and PCL as core both of low molecular weight(L)
CP _{VCH}	combination of coaxial PVP shell and PCL as core both of high molecular weight(H)
CP _{V2}	PVP in both core and shell
CP _{V2H}	PVP high molecular weight both core and shell
CP _{V2M}	PVP in both shell and core with Medium molecular weight
CP _{V2L}	PVP with low molecular weight in both core and shell
PCL 45	PCL with molecular weight 45,000 g/mol (H)
PCL 10-14	PCL with molecular weight 10-14000 g/mol (L)
PVP 360	PVP with molecular 360,000 g/mol (H)
PVP 45	PVP with molecular weight 45,000 g/mol (M)
PVP 10	PVP with molecular weight 10,000 g/mol (L)
H	Hemin
PVP-360-F	PVP 360 fibers
PH-1.0-M	PVP-hemin (1%) physical mixture in PBS
H-P-PBS	Hemin in PVP solution in PBS
P40-P	PVP 40 particles
P10-P	PVP 10 particles

PVPH10	PVP-360 and 0.1% hemin fibers
PVPH25	PVP-360 and 0.25% hemin fibers
PVPH50	PVP-360 and 0.5% hemin fibers
PVPH75	PVP-360 and 0.75% hemin fibers
PVPH100 / PH-1.0-F/PH-1.0-P	PVP-360 and 1% hemin fibers/Particles
PVPH500	PVP-360 and 5% hemin fibers
F-HCl	PVP-360 and 1% hemin fibers in HCl
F-PBS	PVP-360 and 1% hemin fibers in DMSO
H-DMSO	Hemin in DMSO
H-MeOH	Hemin in MeOH
PVP	PVP polymer powder
PH-1.0-M	PVP-hemin physical mixture
PVP-F	PVP fibers or particles
PH-0.1-F	PVP hemin (0.1%) fibers
PH-0.25-F	PVP hemin (0.25%) fibers
PH-0.5-F	PVP hemin (0.5%) fibers
PH-0.75-F	PVP hemin (0.75%) fibers
PH-1.0-F	PVP hemin (1%) fibers or particles
PH-5.0-F	PVP hemin (5%) fibers

Chapter1

1.1 Nanoscience, Nanotechnology, and its applications

Nanoscience is an exciting diverse area of science that deals with the study of materials at atomic, molecular, macromolecular scale. Nanotechnology is the application of methodologies to the design, synthesis and characterisation of structures at the nanoscale i.e. size 1-100 nanometers. Nanotechnology is becoming increasingly pertinent as we are discovering that the physical properties and biological functions of many materials changes at sizes between a few nanometers to 100 nanometers (Whatmore, 2006).

Nanotechnology has been implemented across a wide range of fields. Nanomedicine is the implementation of nanotechnology in diagnosis, treatment and prevention of disease, improvement of human health and improving health outcomes (Ganipineni *et al.*, 2018). Nanodiagnostics deals with the use of nanodevices in making the diagnosis of health-related conditions. The technology has been playing a pivotal role in regenerative medicine by improving cell therapy and tissue engineering. There is another important area of medicine which is being revolutionized by nanotechnology and that is drug delivery systems (Patil *et al.*, 2008).

Many drugs have limitations in medical use due to poor bioavailability, inability to pass through the cell barrier, and lack of selectivity. However, the small size of nanomaterials can allow them to cross natural barriers in the human body hence they can play an important role in drug delivery (Reinholz *et al.*, 2018). Nanotechnology has been used extensively to formulate biocompatible nanomaterials which can play a role as carrier molecules (Xi *et al.*, 2012). Nanomaterials have revealed great potential as carriers for drugs, due to the small size, greater reactive area, and ability to diffuse through the cell barriers (Wilczewska, 2012).

Nanoparticles can penetrate and accumulate in the target tissue, which not only improves the bioavailability, but also helps to reduce unwanted side effects (Chauhan *et al.*, 2014), as less amount of drug is needed for the same action. Drug delivery systems based on nanoparticles can control the drug release and can give a sustained drug level and prolonged action. This can also reduce the risk of an acute surge in drug levels and potential side effects associated with it. Therefore,

the role of nanoparticles in the field of drug delivery needs to be explored (Shi *et al.*, 2010).

The focus of this research work is to produce polymeric nanomaterials for drug delivery. For example, Panyam (2004) reported a greater anti-proliferative activity of dexamethasone where biodegradable nanoparticles, made up of polylactic/glycolic acid (PLGA) and polylactic acid (PLA), were used for the cytoplasmic delivery of the drug. Research has also shown that nanomaterials could be used for targeted delivery of drugs in specific cells/tissues (Owais *et al.*, 1995). This is achieved due the small size of nanomaterial which allow penetrance to most tissues. Nanomaterials can also be tailored to respond to stimuli such as changing pH, temperature, light etc (Owais *et al.*, 1995).

There are some concerns associated with the use of nanoparticles as well. De Jong and Borm, 2008, have reviewed previous work looking into the possibility of side effects associated with nanoparticles. Although nanoparticles of gold/silica were considered to have toxicity, with modifications such as reducing the dose of stabilizer in the case of gold, or using amino-hexyl-aminopropyltrimethoxysilane as a surface modification in case of silica nanoparticles, significantly reduces the toxicity. However, not much evidence is available on the toxicity profile of organic nanoparticles. There is need of more research to establish the safety of nanoparticles in drug delivery systems and various other usages.

1.2 Nanoparticles and diffusion through lipid bilayer

Nature has designed phospholipid bilayers in order to protect cells from the external environment. The overall structure of the cell membrane (studded with proteins and possessing a hydrophobic core), is selectively permeable, and can act as a strong barrier for e.g. some proteins and drugs. Nanomaterials need to overcome this barrier to enter the cell (Pogodin and Baulin, 2010). Passive diffusion through the lipid bilayer generally occurs with small particles (less than 100 nm in diameter); however, high molecular weight species, including those larger than 100 nm in diameter, face difficulty in passive translocation. Instead, their transport through the membrane is generally considered to be mediated via pores, membrane fission and budding, surface aggregation, inclusion in the membrane or lipid membrane permeation (Pogodin *et al.*, 2012).

Pogodin (2011), modelled nanotubes of various diameters, translocated them through the lipid bilayer vertically, and calculated the energetic cost of their perpendicular translocation. Baulin drew the conclusion that simple translocation was unlikely to occur for single-walled carbon nanotubes (SWNTs), and the likely mechanism was an energy-dependent translocation such as endocytosis. However, insertion of short amino-functionalized SWNTs into the phospholipid bilayer was found to occur by passive diffusion (Kraszewski *et al.* 2012).

Simulations by Pogodin (2012) showed that the relative membrane permeability of a nanoparticle increases with the increase in the average hydrophobicity (number of homogenous particles). This is shown in figure 1.1, where number of nanoparticles represent hydrophobicity (36 = blue, 72 = green, 144 = black, 288 = red).

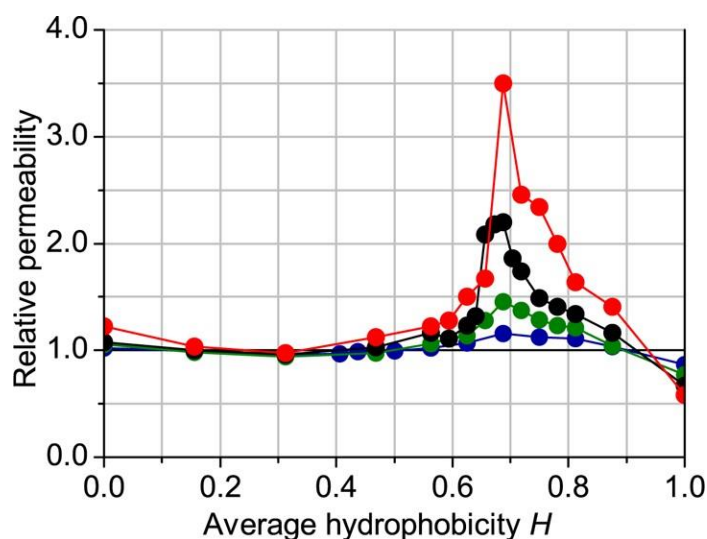


Figure:1.1 A plot of average hydrophobicity versus relative membrane permeability of different nanoparticles (Pogodin., 2012).

As stated previously, inspiration for this project came from extending this carbon nanotube work onto other nano-objects whose physical and chemical properties can be tailored more easily, namely electrospun or electrosprayed nanomaterials. Both processes (electrospinning and electrospraying) are explained in detail later in this chapter, as these are used in the production of nanomaterials made in this research work.

1.3 Nanomaterials as drug delivery system (DDS)

Nanomaterials with optimized physicochemical and biological properties are taken up by cells more easily, and they can be used as drug delivery systems of bioactive

compounds (Agrahari *et al.*, 2017; Wilczewska *et al.*, 2012). Liposomes, which are spherical vesicles composed of phospholipids and steroids, have been used to improve the therapeutic index of chemotherapeutic agents (Wilczewska, 2012).

Similarly, polymeric nanomaterials have been used as drug delivery systems. Sodium alginate has been used as a nano-carrier for carboplatin (an example of an anti-tumor drug), gelatin as a nano-carrier for rifampicin and PEGylated poly (lactic-co-glycolic acid) (PEGylated PLGA) as a carrier for doxorubicin (Wilczewska., 2012).

Polymers chosen are often biodegradable, such that polymer nanoparticles can undergo hydrolysis in the body and produce harmless metabolites. For example, Kumari *et al.* (2009) studied PLGA metabolism and reported minimal systemic toxicity.

1.4 Electrohydrodynamics

Electrospinning and electro spraying are sister technologies (Kostakova 2012; Zong 2017), combinedly described as electrohydrodynamics (Rodríguez-Tobías *et al.*, 2016). Electrohydrodynamics refers to the dynamics of electrically charged fluids (Chakraborty *et al.*, 2009). Electrospinning and electro spraying apparatus are similar and simple, consisting of a high voltage supply, syringe pump, collector, and syringe. If particles are produced, the process is called electro spraying and, if fibers are produced the process is called electro spinning. A schematic diagram of the apparatus used for electro spinning and electro spraying is shown in Figure 1.2.

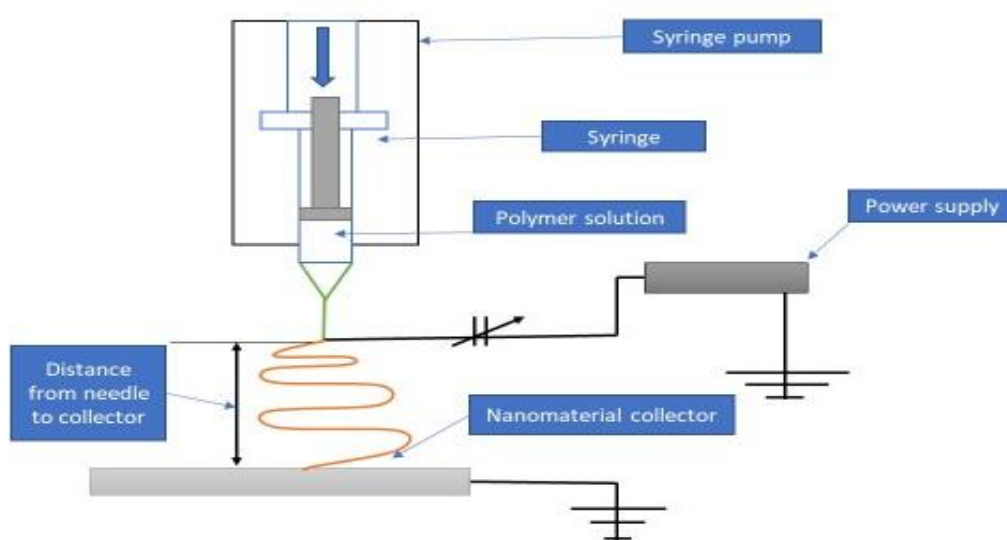


Figure 1.2. Single fluid electrohydrodynamic apparatus for electrospinning or electro spraying. Single fluid means only one type of solution is used for production of nanoparticles/nanofibers.

In electrohydrodynamics, there are numerous geometrical features and various types of cone-jet observable at the nozzle of the needle (or tip of the spinneret). The most stable and used mode is the cone-jet (Figure 1.3), as it produces almost uniform size particles and fibers (Enayati *et al.*, 2010).



Figure 1.3. Image of an ideal cone-jet from electrohydrodynamic process (Enayati *et al.*, 2010). The arrow pointing to cone formed during the process of electrospinning/electrospraying and the dotted line is the emerging point of the cone from the needle.

During the process of electrospinning and electrospinning, polymer chain entanglement occurs, which is responsible for the final morphology of the particles and fibers. The fewer the entanglements are, the smaller the diameter of particles and fibers would be. The number of entanglements can be calculated by equation 1.1 (Bock *et al.*, 2012).

$$(\eta_e)_{sol} = \varphi \frac{M_w}{M_e}$$

Equation 1.1 (Bock *et al.*, 2012).

Equation 1.1. (Bock *et al.*, 2012). Where $(\eta_e)_{sol}$ = entanglements per chain in solution, φ = polymer volume fraction, M_w = the average molecular weight (g/mol), M_e = the average entanglement molecular weight (g/mol).

Research has shown that the process of electrospinning occurs with one entanglement per chain ($(\eta_e)_{sol} = 2$). However, with 2.5 entanglements per polymer chain ($(\eta_e)_{sol} = 3.5$) electrospinning occurs, leading to the fibre formation. The entanglement constraint model can be used to estimate the M_e , if it is not known (Bock *et al.*, 2012).

Polymer concentration also dictates the outcome i.e. whether particle or fibre formation would occur. This introduces the concept of C_{ov} , which represents the critical chain overlap concentration, which is the point when the concentration of solution is equal to the concentration inside the radius of gyration of every single macromolecular chain and is inversely proportional to the intrinsic viscosity as shown in equation 1.2 (Bock *et al.*, 2012).

$$C_{ov} \propto 1/\eta$$

Equation 1.2 (Bock *et al.*, 2012).

Based on polymer concentration, regimes could be described as,

1. Dilute regime: when the concentration (C) is below C_{ov} resulting in no chain entanglements.
2. Semi-dilute unentangled regime: when the concentration, C , is above C_{ov} , and the concentration is large enough for chains to overlap but not enough to generate a significant degree of entanglement. Such a regime can be used to produce electrospayed films.

It is found that a semi-dilute moderately entangled regime is ideal for electrospaying of particles.

However, for $C/C_{ov} > 3$, molecular cohesion is generally too high for electrospaying and beaded fibers or fibers are electrospun, corresponding to the semi-dilute highly entangled regime. For optimal particle electrospaying, it is thus essential to work above C_{ent} (critical entanglement concentration) but not beyond $C/C_{ov} > 3$ (Bock *et al.*, 2012).

1.4.1 Electrospinning

Electrospinning is a versatile fibre forming process generally used to make macroporous scaffolds, which consist of randomly aligned nanofibers (Chew *et al.*, 2006). Formhal was the first to document production of nanoscale nanofibers in 1934, using viscoelastic solutions, by the method of electrospinning (Zhu *et al.*, 2017). The name electrospinning is derived from "electrostatic spinning", a term used in 1994. We find evidence of electrospinning in history since the end of the 19th to 20th century (Thakur, 2014). However only limited production and applications remained until 1990, when it was discovered that electrospinning can be carried out with organic polymers (Zhu *et al.*, 2017). In recent years with an

increase in the popularity of nanotechnology, electrospinning is becoming an area of increased interest.

Using this method, nanometer range fibers can be produced. A polymer solution or melt is passed through a narrow needle or nozzle which works as an electrode at the same time (figure 1.2). During this process, the utilized current varies from tens of nanoampere to several microampere (Zheng *et al.*, 2019). The setup of the electrospinning apparatus could be vertical or horizontal. With the application of high voltage, an electric field is produced between the electrode and a collector. Once electrostatic forces overcome the surface tension, polymer solution is ejected from the nozzle/needle tip in the form of a very thin and long jet. Fibers are collected on the surface of the collector (Kiyak and Cakmak, 2014).

Various types of collectors are available for electrospinning and electrospinning, and a metallic plate collector was used in this research work (Ulubayram *et al.*, 2015).

Electrospinning is a cost effective, simple, and versatile technique for the production of polymer fibers. These fibers have high surface area to volume ratios, making them suitable for scaffolds for tissue engineering, wound healing devices, semiconductors, cosmetics, textiles, filtration and drug-delivery systems (Mouthuy *et al.*, 2015). To augment functionality, researchers are increasingly attracted to integrate drugs into fibres (Chakraborty *et al.*, 2009). A typical SEM image of PVP 360 (polyvinylpyrrolidone 360 kDa) fibers is shown in figure 1.4.

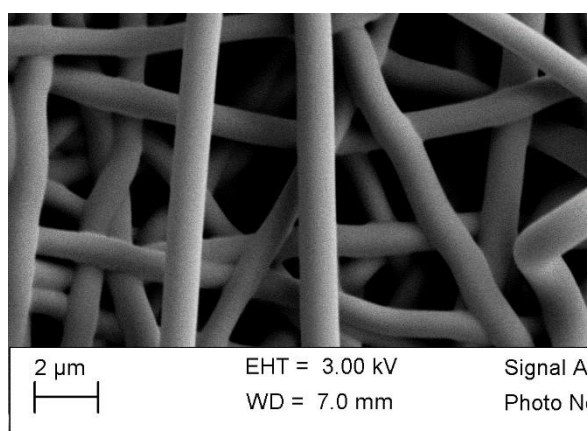


Figure 1.4. Typical SEM of PVP 360 fibers.

Various modifications of electrospinning techniques have been used in recent years, and one such variation is co-axial electrospinning.

1.4.1.1 Co-axial Electrospinning

In this method, two different polymer solutions (or possibly melts) are used. These polymer solutions from two different syringes are diverted towards the coaxial needle, resulting in formation of the Taylor cone. Evaporation of solvent happens during spinning and results in the solidification of a compound jet. Production of core shell nanofibers happens because of solidification. With this method, core shell nanofibers can be produced for the polymers which cannot be electrospun by the monoaxial electrospinning method. These fibers have multiple applications such as in microelectronics (Kiyak and Cakmak, 2014). This technique was used in this research project as well. The arrangement of apparatus is shown in figure 1.5.

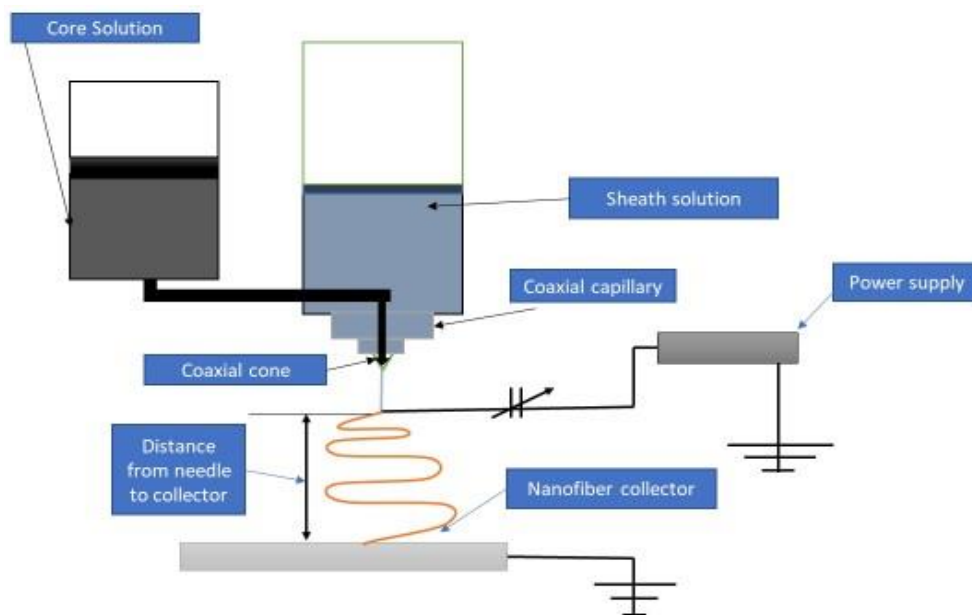


Figure 1.5. Production of co-axial particles or fibers using coaxial electrospinning or electrospinning. In this method two syringe pumps and a co-axial needle are used. The core and sheath solutions are different from each other.

Novel functionalities and properties of two different nanomaterials could be combined using co-axial electrospinning/electrospinning. Using this technique, fibers with multichannel, hollow, thin-wall and porous structures with tuneable inner structure, and large surface area have been produced. The polymeric nanofiber shell can be used as a diffusion barrier for delivery of drugs, facilitating the burst release of APIs (active pharmaceutical ingredients) (Zong *et al.*, 2017).

One of the limitations of the electrospinning is the requirement to ultrasonicate the fibers to control their length (Sawawi, 2013). An approach that may circumvent this is the use of electro spraying that generates particles rather than fibers.

1.4.2 Electro spraying

Poor solubility of numerous pharmaceutical ingredients results in their poor bioavailability. To overcome this issue, numerous methods have been implemented, one of which is electro spraying. Currently the process of electro spraying is implemented in various industries such as ceramics, food industry, paints etc. Drug delivery is another emerging field for the implementation of the electro spraying process (Smeets, 2017).

In electro spraying, solutions are sprayed in an electrostatic field, resulting in production of submicron polymer particles with distinctive functional nanostructures (Zhang *et al.*, 2009). A polymeric solution is pumped from a syringe at a constant rate through a needle attached to an electric field. When the polymer solution comes out from the needle, it forms a cone (Taylor cone). The jet of charged particles elongates and detaches from the cone. The solvent evaporates after the detachment of the droplets from the Taylor cone, nano-objects are generated and collected on the collecting plate (Cavalli *et al.*, 2011). A typical SEM image of PVP 10 particles produced by electro spraying is shown in figure 1.6.

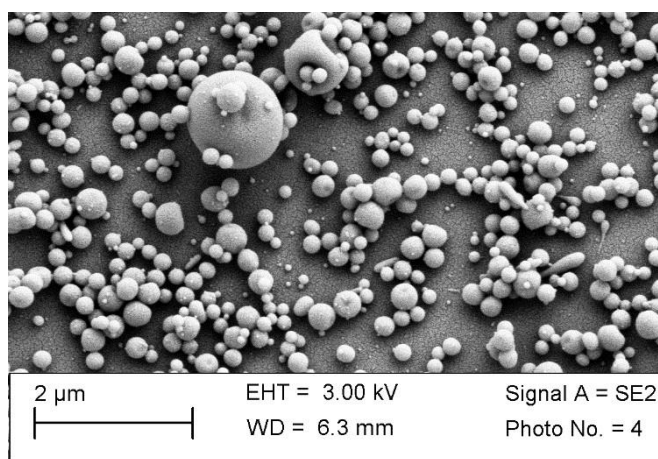


Figure 1.6. PVP 10 (10 kDa) Nanoparticles produced by electro spraying.

1.4.2.1 Co-axial electro spraying

Co-axial electro spraying is a nano-encapsulation process based on a single jet electro spraying. It has been developed to engineer multifunctional nanoparticles

with improved qualities and efficiency. In co-axial electrospinning, a co-axial nozzle is used which contains an inner and an outer needle. Two different liquids from co-axial needles are ejected using syringe pumps. An electrode is placed under the nozzle and an electric field is generated, which results in the formation of Taylor cone at the nozzle. The jet flow containing sheath and core fluids is eventually broken down into nanoparticles, which are collected on the collector (see figure 1.5).

There are minor variations to the coaxial electrospinning apparatus such as size of the needles, and the distance between the nozzle and ground electrode could vary. Also, aluminium foil could be used which serves as both collector and the ground electrode. Several parameters such as voltage, flow rate, solution properties etc could affect the outcome (Zhang *et al.*, 2012).

1.4.3 Factors affecting the electrohydrodynamic process

Various factors can affect the nanofiber formation during the electrospinning procedure. Indeed, the qualities of nanofibers produced can be tuned by the choice of the polymer, viscosity, flow rate and voltage applied to the polymer solution (Ramakrishna *et al.*, 2005). These factors can be divided into solution properties and processing parameters.

1.4.3.1 Solution properties

Several characteristics of the polymer solution can influence the outcome of electrospinning. The surface tension of the solution has an important impact on the process of electrospinning. Solutions with higher surface tension require a higher applied voltage for nanofiber production (Gazquez *et al.*, 2017).

The other significant characteristics are the molecular weight and viscosity of the solution. Increased molecular weight increases chain entanglement of the solution leading to greater viscosity (Li and Wang, 2013).

The viscosity of the polymer solution creates a profound effect on the morphology of fibers. High viscosity of polymer solution results in formation of smooth fibers whereas, low viscosity favours formation of beaded fibers. The viscosity of a solution is related to the chain entanglement between polymer chains. The extent of chain entanglement tells whether fibres or particles would be formed during electrospinning (Ramakrishna *et al.*, 2005).

Another important character to consider is the conductivity. In each electric field, conductivity of the solution determines the voltage needed to be applied. The conductivity can be increased by adding salts (as salt increases the ionic concentration of the solution) which improves fiber formation (Gazquez *et al.*, 2017).

The choice of solvent is also crucial. Solvents with larger dielectric constant and higher conductivity contain higher charge density in the polymer solution. In this case, the jet will carry more charge density and more elongated forces will be executed on the jet. Self-repulsion and excess of charge under electric field will produce straighten and small diameter fibers and particles (Xu *et al.*, 2017).

1.4.3.2 Processing parameters

Processing parameters such as voltage and flow rate have an effect on the diameter of the nanomaterials formed (Dhanalakshmi *et al.*, 2015). Some of the relevant parameters are discussed below.

The diameter of nanofibers and particles decrease with an increase in the voltage, as it provides surface charge to the jet causing greater electro repulsive forces. However, very high voltages facilitate the flow of polymer thus increasing the diameter. In addition to this, beaded fibers are obtained at high voltage (Okutan *et al.*, 2014). The SEM of PVP 40 (Polyvinylpyrrolidone MW 40,000 g/mol) with beaded fibers is given in figure 1.7. The concentration of solution was 25% (w/v), flow rate was 0.5 mL/hr, the distance from the needle tip to the collector was 14 cm and, the voltage was 16.25 kV.

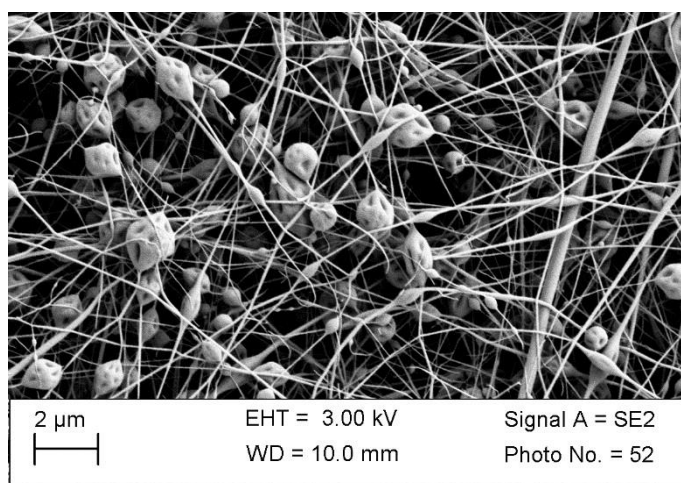


Figure 1.7. Typical picture of beaded fibers of PVP 40 (40 kDa). SEM image of fibers produced from a 25% (w/v) solution.

The next parameter to consider is the flow rate. Low flow rate will result in inhibition of the electrospinning process, whereas high flow rate can result in the formation of beaded fibers. This happens due to the reduced time available for solvent evaporation (Okutan *et al.*, 2014). The rate of the feeding affects the solution transfer and jet velocity. A lower flow rate of solution is required to obtain solid material with complete evaporation of solvent (Bhardwaj and Kundu, 2010).

The collector plate is another important parameter. The architectural deposition of particles or fibers and the electrical field are strongly influenced by the collector's characteristics (Alfaro De Prá *et al.*, 2017). The collector is normally used as a conductive surface. Aluminium foil is mostly used as a collector but transferring the fibers or particles from the foil could be challenging. Different types of collectors such as liquid bath, wire mesh, parallel or gridded bar rotating wheel or rod, grids or pins can be used to solve the problem (Li and Wang, 2013).

The diameter of the spinneret tip does not affect the fiber's diameter, but it affects the flow rate of polymer solution. It also affects the size and shape of the solution-air interface. Various types of spinneret designs are found in the literature. The simplest one is the hypodermic needle with blunted flat tip, which has been used extensively in this project. Additionally, a co-axial spinneret has been used in this project, which consists of two concentric needles which can be used for the formation of core-shell or hollow fibers (Robb and Lennox, 2011).

Tip to collector distance affects the diameter and morphology of the particles/fibers. An important aspect in electrospaying and electrospinning is the evaporation of the solvent during the journey of polymer solution from tip to collector. Optimum distance is required for successful production of particles/fibers. If the distance is short, complete solvent evaporation will not be possible, but too long a distance will result in beaded fibers (Li and Wang, 2013).

The dimensions of the nanomaterial can have an impact, for example, on penetration in the cell. Therefore, it is particularly important to control this factor (Garmarudi *et al.*, 2010). Parameters which influence the diameter of nanofibers and nanoparticles are summarized in figure 1.8.

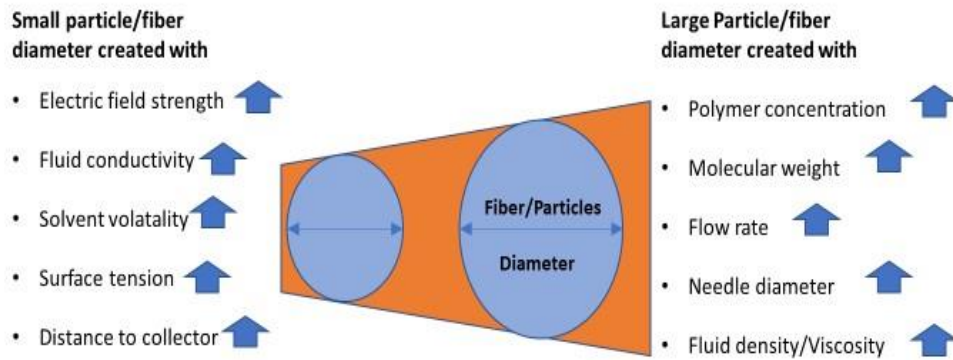


Figure 1.8. Parameters that affect the diameter of nanomaterials. Diagram created from Chakraborty *et al.*, 2009.

1.4.3.3 Ambient parameters

Temperature and relative humidity can affect the diameter of particles or fibers. The diameter of the particles or fibers decreases with an increase in the relative humidity or temperature (İçoğlu and Oğulata, 2017). Higher temperatures produce smaller diameter fibers due to more rapid evaporation of the solvent. Low humidity facilitates the flow of solution and thus increases fiber diameter.

1.5 Biodegradable polymers

Biodegradable polymers can easily be degraded through the action of enzymes and/or chemical deterioration associated with living organisms (Vroman and Tighzert, 2009).

Polymers could be broadly classified as synthetic and natural biodegradable polymers. Some examples of naturally existing biodegradable polymers include polysaccharides (starch, cellulose, hyaluronic acid etc.) and proteins (collagen, albumin etc.). Examples of synthetic biodegradable polymers are polyesters (such as polylactones, polycarbonates), polyanhydrides, polyurethane etc. Natural biodegradable polymers have good biocompatibility, but due to undesirable properties such as antigenicity have not been widely investigated. Synthetic biodegradable polymers are more versatile and have a wide range of applications (Doppaladupi *et al.*, 2014).

The biodegradable nature of polymers makes them very desirable for use in drug delivery, tissue engineering, gene therapy, temporary coating on devices etc. The choice of polymer depends on the mechanical needs for the application. For example, in a drug delivery application, the choice of biodegradable polymer will be governed by the time taken to release the drug. When used as suture material, the rate of degradation should be long enough to allow sufficient strength until the healing of the tissue is achieved (Doppaladupi *et al*, 2014).

For this research project, we have used PVP (polyvinylpyrrolidone) and PCL (polycaprolactone) as the biodegradable polymers.

1.5.1 Polyvinylpyrrolidone (PVP)

PVP was used as the carrier in both projects undertaken in this thesis, therefore it is discussed in the first chapter of the report (the other polymers used will be briefly discussed in relevant chapters). PVP has a well-defined structure: it contains N-vinylpyrrolidone monomers and synthesized by polymerization in isopropanol or water (Aria *et al.*, 2016; Kadajji and Betageri, 2011). The structure of PVP is shown in figure 1.9. PVP is available in various molecular weights; three different molecular weights PVP (10,000, 40,000 and 360,000 Da) were used in this research work.

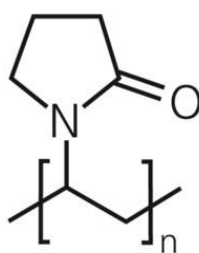


Figure 1.9. Structure of polyvinylpyrrolidone

PVP or povidone has been widely used in many applications in pharmaceutical technology, medicine, and cosmetic science. This is owing to its chemical and physical properties such as being colourless, physiologically compatible, chemically inert, pH-stable, temperature-resistant, and non-ionic (Rasekh *et al.*, 2014). PVP has a high glass transition thus increases the temperature of the amorphous drug which enhances the conversion to more stable crystalline form (Lopez *et al.*, 2014). It has good film making characteristics, adhesive properties, and high complexing

quality. The film forming property of PVP was used in the initial project described in chapter 2 to improve the quality of PCL nanoparticles. PVP exhibits special properties such as high solubility in organic solvents or water. Consequently, PVP is broadly used to improve the solubility of poorly water-soluble drugs in simple pharmaceutical formulations (Kadajji and Betageri, 2011).

Many active ingredients are poorly soluble which limits their bioavailability. Solubilizing agents like PVP can be used to solve this problem by forming soluble complexes with active ingredients hence enhancing dissolution or solubility of the active ingredients. The solubilizing quality of PVP was used in the second project of this thesis (hemin formulation), in which PVP solubilized the hydrophobic compound hemin (discussed in chapters 3 and 4).

1.6 Formulation of drugs

Nanomaterials have gained attention in recent years due to their physicochemical properties. Nanomaterials made of biodegradable biopolymers, synthetic polymers, metal oxides and metals are a significant innovation for targeted drug delivery (Banerjee *et al.*, 2017). The projects discussed in this thesis are based on the production of polymeric nanomaterials which will be used as carriers of the active pharmacological ingredients (APIs): 5-fluorouracil (5-FU) and hemin. Both of these drugs are currently administered intravenously (Regazzoni *et al.*, 1996) (Schiller *et al.*, 2004). The aim of this project is to develop an orally administered targeted delivery system for these active ingredients.

There are various routes of drug administration such as oral, nasal, inhalation, intramuscular, intravenous, subcutaneous, transdermal, transmucosal, rectal and topical (Mignani *et al.*, 2013). The enteral route has distinctive high patient acceptability, as well as high convenience. Through the enteral route medicines are swallowed or absorbed sublingually. However, there are limitations to the oral route, including intake of the drug with food and/or with other medication, and the drug's metabolism in the gastrointestinal tract and liver can have significant impact on its absorption and bioavailability (Finkel (PharmD.) *et al.*, 2009). This project focusses on the design of formulations for oral administration.

Enteric coated tablets are designed to prevent dissolution and release of drug in gastric acid, and the rate of the drug release is predominantly determined by the drug delivery system used. This allows controlled release of the drug. The

formulation of gastro-resistant and controlled released medicine has many benefits (Lozoya-Agullo *et al.*, 2018; Zema *et al.*, 2013). The purpose of controlled release medicine is to lower toxicity, have a better therapeutic efficacy, to reduce fluctuation in plasma levels and to reduce number of doses needed per day, which would improve patient compliance (Prajapati *et al.*, 2011). The aim of the second project was to create a formulation of gastro-resistant capsules for the release of hemin in the intestine.

In recent years, the focus on prolonged release medicines, which release their contents in the intestine, has increased (Macchi *et al.*, 2015; Modi *et al.*, 2012). Both local and systemic delivery of drug is possible in the colon. In certain colonic diseases targeted delivery is beneficial, for example for colon cancer, colitis, local infection, and Crohn's disease. Targeted delivery to the colon has benefits as lower dose of the drug would be required hence fewer systemic side effects (Lozoya-Agullo *et al.*, 2018). In the first project we targeted the colon for delivery of 5-FU (an anticancer drug) and in the second project intestine was targeted for the uptake of hemin (for treatment of anaemia). The aim was to reduce the side effects and improve the bioavailability of these APIs. 5-FU metabolizes in the intestine by uracil reductase or dihydropyrimidine dehydrogenase (Wilson *et al.*, 2012), due to which it has short half-life. This problem was planned to be addressed by targeted delivery of 5-FU to the colon in colorectal cancer. Oral iron supplements cause gastric irritation and only a small quantity (1-2 mg) of iron is absorbed from the intestine in a day (Coad and Pedley, 2014). Therefore, a gastro resistant formulation was planned to improve the bioavailability of hemin and reduce the gastric side effects.

Chapter 2

Preparation and characterization of Polycaprolactone and Polyvinylpyrrolidone nanoparticles

2.1 Introduction

Synthesis of polycaprolactone (PCL) nanoparticles is an appealing approach, as PCL based therapeutic delivery devices have many advantages. These include high permeability for small drug molecules, and during degradation, failure to generate an acidic environment (as is the case with polylactides and glycolides) which can be useful for the sustained release delivery of proteins or peptides. Additionally, PCL has slow degradation speeds (more than one year) as compared to poly lactic-co-glycolic acid (PLGA) and, this quality makes PCL a more suitable choice for long term delivery systems (Enayati *et al.*, 2010). This chapter describes attempts to formulate and characterise NPs of this type. Background theory and an outline of the practical details of the electrospinning and electrospaying processes were provided in Chapter 1.

During this phase of the project, NP electrospaying was carried out on two different substrates: foil and distilled water.

Firstly, electrospaying was carried out in the conventional way, collecting the particles on aluminium foil, which was wrapped on a metal collector (discussed in section 2.3.1).

The second approach involved liquid–liquid electro-dispersion, or dispersion of a liquid in a bath of another liquid (Barrero *et al.*, 2004), (discussed in section 2.3.2).

The main advantage of this approach was that PCL particles were automatically collected in the liquid phase, making it more convenient. PCL was initially selected as a polymer to produce nanoparticles. The structure of PCL is shown in figure 2.1. PCL is biodegradable and has less immunogenicity and toxicity than many other polymer systems (Celan *et al.*, 2013). It is used in drug delivery, tissue engineering and additive manufacturing (Kotula *et al.*, 2017).

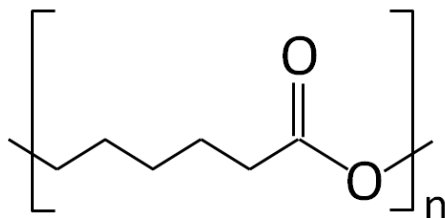


Figure 2.1. The chemical structure of the repeat unit in PCL

The degradation of PCL is reproducible and predictable, and this quality is used in bone and tissue engineering (Bose *et al.*, 2018). It has been combined with PEG to form a copolymer for production of nanoparticles by precipitation (Danafer, 2016).

Attempts to modify the surface characteristics of the NPs were also undertaken. This involved using co-axial electrospraying (discussed in chapter 1), generating NPs which had PCL in the core and PVP in the shell.

Once the various forms of PCL/PVP containing NPs were generated, they were characterised by using scanning electron microscopy (SEM), infrared spectroscopy (IR), and nuclear magnetic resonance spectroscopy (NMR). The next steps involved attempting to form NPs loaded with the model drug and assessing bioavailability of these NPs as potential DDS (drug delivery system).

2.2 Method and materials

2.2.1 Materials

The polymers polycaprolactone (PCL), (M.W 10,000-14,000 & 45,000) and polyvinylpyrrolidone (PVP) (M.W 10,000, 40,000 & 360,000) were purchased from Sigma Aldrich. 1,2-dichloroethane was purchased from Fisher Scientific. Distilled water and absolute ethanol were of analytical grade. Sodium dodecyl sulphate (SDS) (FW 288.38 Da) GC grade was purchased from Sigma Aldrich.

2.2.2 General instruments

Precise characterization of nanomaterials produced by electrospraying or electrospinning is crucial to associate nanomaterial physicochemical properties with cellular response. It is also essential for meaningful, accurate and reproducible results (Shang *et al.*, 2014). In this part of the thesis, different techniques used for characterization of nanomaterial are discussed.

2.2.2.1 Infrared spectroscopy (IR)

FTIR spectra of samples were obtained using an Agilent Cary 630 FTIR spectrometer with diamond ATR attachment and Microlab PC software. A small quantity of sample was placed on the platform with the help of spatula. The knob was rotated till the screw touched the sample. The IR spectra of samples were collected against background. The range of wavelength used was 4000-400 cm^{-1} , with resolution of 4.

2.2.2.2 Scanning electron microscopy (SEM)

The instrument used for SEM was a Zeiss Supra 55VP FEGSEM. The imaging conditions were 3kV accelerating voltage, a small (20 micron) aperture for good depth of focus, and high current mode for good resolution. Samples were mounted on 12 mm diameter aluminium SEM stubs using carbon sticky tabs. Gold sputter-coating was achieved using a Polaron SC7640 sputter coater, with a coating time of 40-60 seconds to give 5-10 nanometres thickness coating.

2.2.2.3 Microscopy

An Olympus X81 light microscope was used to take the images of fibers and particles at magnifications of 100x and 400x.

2.2.2.4 NMR

A Bruker Avance 500 MHz spectrometer was used for ^1H NMR. CDCl_3 was used as the solvent for all samples.

2.2.2.5 Dynamic light scattering

A Brookhaven Nanobrook Omni particle size analyser was used to measure the particle size distribution in solution, with supporting BIC Particle Solutions (version 2.6) software. Measurements were performed at 22°C at an angle of 90°. The EPSRC Equipment Loan Pool is gratefully acknowledged for the loan and use of the Brookhaven Nanobrook Omni particle size analyser.

2.2.3 Preparation of solutions

2.2.3.1 Polymer solutions

0.25 - 10% (w/v) PCL solutions were made by adding PCL (M.W 10000-14,000 & 45,000) into 1,2-dichloroethane at room temperature. The solution was continuously stirred until the required amount of PCL was dissolved in 1,2-dichloroethane. 1-10% (w/v) PVP-360 solutions were made by dissolving an appropriate amount in distilled water or absolute ethanol.

When electrospaying directly into water, 0.25-5% (w/v) PCL solutions were made by adding appropriate amounts of PCL (M.W 45,000) to acetic acid at room temperature. The solution was continuously stirred until the required amount was dissolved in acetic acid and 5% and 10% (w/v) PVP solutions were made by dissolving appropriate amounts in distilled water.

2.2.3.2 Sodium dodecyl sulphate (SDS) solution

5% (w/v) solution of SDS (sodium dodecyl sulphate) was made by stirring an accurate amount in distilled water at room temperature (22°C) until SDS had completely dissolved.

2.2.4 Electrospaying

2.2.4.1 Single fluid electrospaying

Electrospaying was performed at $22^{\circ}\text{C} \pm 3^{\circ}\text{C}$. The spinneret was attached to the syringe (5 mL), which was filled with the polymer solution. The syringe was attached to the syringe pump (ColeParmer pump (78-9100C)). A power supply (FuG Elektronik HCP 35 – 65000, supplied by Omiran Ltd, UK) with voltages ranging from 10 - 20 kV and 16-20 cm tip to collector distance was used. The needle was attached to the positive electrode and the collector to the grounded electrode. Aluminium foil was wrapped on the metal collector. The solution was ejected from the needle at a controlled rate between 0.25 mL/hr and 1.5 mL/hr.

2.2.4.2 Co-axial electrospaying

The setup of coaxial electrospaying is same as the single fluid set up, but two syringe pumps and the coaxial spinneret were used. A photograph of the co-axial spinneret is given in figure 2.2. In the case of collection on foil, 5% PVP (flow rate 1.5 mL/hr) was used as the 'shell' fluid and 4% PCL (flow rate of 0.25-0.5 mL/hr) was used for the 'core'. The voltage used ranged from 15-20 kV and the tip to collector distance was between 10-20 cm.



Figure 2.2. A photograph of the co-axial spinneret used in this project. It shows the structure of the concentric nozzle.

Co-axial electrospaying was also used for electrospaying in distilled water (80 ml), in which 10 % PVP 360 in distilled water was used in the shell and 0.5-5% PCL 45 in acetic acid was used for the core of the co-axial spinneret. The collector distance ranged from 5-10 cm and the voltage used was between 15-20 kV. 5% SDS was used for collection of nanomaterial, which was stirred continuously to prevent agglomeration of PCL particles. The apparatus of co-axial electrospaying in liquid is shown in figure 2.3.

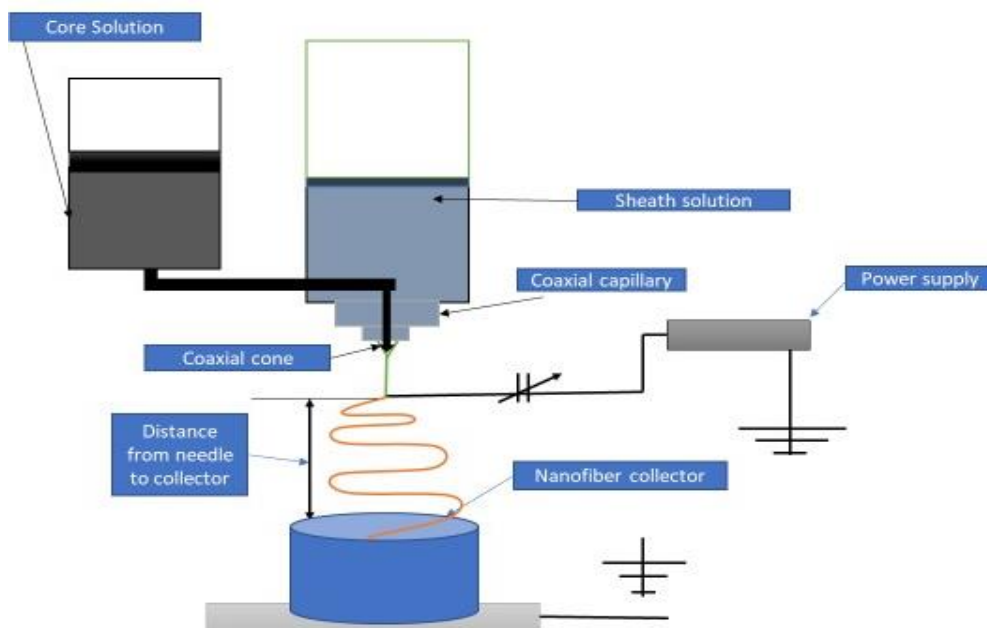


Figure 2.3. Schematic representation of electrospaying into distilled water containing SDS.

2.2.5 Methods attempted for separation of core PCL particles

2.2.5.1 Method 1

PVP is a water-soluble polymer (Oliveira *et al.*, 2011) and to confirm the presence of PCL in coaxial particles, the mat was dissolved in distilled water. The solution was centrifuged twice for 10 minutes at 25000 g (at highest speed available on centrifuge). The supernatant was removed, in this way the PVP was removed from the PCL particles. The pellet was dispersed in the distilled water and NaOH solution (1.25 M), the solution was then dried on two different SEM stubs. NaOH was used to prevent aggregation of the PCL particles. The SEM images of the dried distilled water and NaOH treated pellet are shown in figure 2.14a1 and 2.14b1, respectively.

2.2.5.2 Method 2

0.026% and 0.05% (w/v) of brilliant green dye was incorporated in the 4% PCL solution to enhance visibility of the core. The electrospaying was carried out with same conditions as mentioned in figure 2.13. The samples were collected on foil and both samples were dissolved in few mL of distilled water. Samples were transferred in eppendorf tubes and centrifuged at 25000 g at 22 °C for 10 minutes. Dark black pellets appeared at the bottom of the Eppendorf tubes. Pellets were spread on a carbon tab for SEM.

2.3 Results and discussion

2.3.1 Electro spraying of polymer on foil

Previous work by Zhou and co-workers (2016) used electro spraying with a range of PCL solutions to produce microspheres of controlled size and shape. They found that PCL solution concentration and molecular weight have a clear effect on morphology and the formation of the particles. The aim of this work differs significantly from Zhou's, in that this project aimed to produce PCL nanoparticles instead of microspheres as they should have enhanced cellular uptake and be more effective as DDS.

Firstly, the results obtained from single fluid electro spraying of PCL 45 (molecular weight of 45,000 g/mol) on foil is discussed. Initially 5-10% (w/v) solutions of PCL 45 in 1,2-dichloroethane were used for electro spraying, but SEM micrographs indicated that the particles produced were larger than expected (i.e. 3-10 μM). Further experiments were then performed using PCL at lower concentration 0.25 - 5% (w/v), as lower concentrations are known to reduce particle diameters (Jagtap *et al.*, 2012). Some representative SEM micrographs of those samples are shown in figures 2.4 (the rest of the SEMs are given in appendix A).

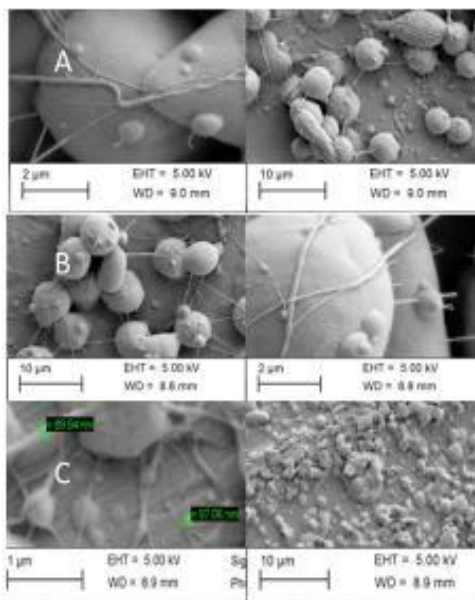


Figure 2.4. SEM of particles obtained from A) 4% (w/v) sample SPCH (with a 1 mL/hr flow rate, 10.49 kV voltage 16 cm distance from tip to collector), B) 3% (w/v) sample SPCH (with a 1 mL/hr flow rate, 10.49 kV voltage and 20 cm distance from tip to collector), C) 0.5% (w/v) sample SPCH (with a 1 mL/hr flow rate, 17.63 kV voltage and 18 cm distance from tip to collector).

According to these results, the particles made from 3% and 4% (w/v) solutions appear to be more circular when compared with the particles made from the lower concentration PCL solutions. The samples obtained from 3% and 4% (w/v) solutions have particle sizes with diameters around 4 – 5 μm . Conversely, particles made from 0.5 % (w/v) PCL are of various sizes, with some particles smaller than 100 nm and these have been highlighted in figure 2.4C. The prevalence of these smaller particles or nanoparticles observed at 0.5% PCL led to further investigation of the electrospaying parameters for this solution. The experimental conditions for this investigation are summarized in table B1 of appendix B.

As per table B1 in appendix, thirteen different processing parameters ($\text{SP}_{\text{CH}} 1$ - $\text{SP}_{\text{CH}} 13$) were tested for electrospaying, out of which seven sets of conditions (with voltage from 15-20 kV, 18-20 cm tip to collector distance and flow rate 1-1.5 mL/hr) resulted in continuous electrospaying of material. The rest of the conditions resulted in spitting along with intermittent electrospaying.

There are many similarities observed in the SEM micrographs described in table B1. Figure 2.5 shows an indicative micrograph with the remainder given in appendix B.

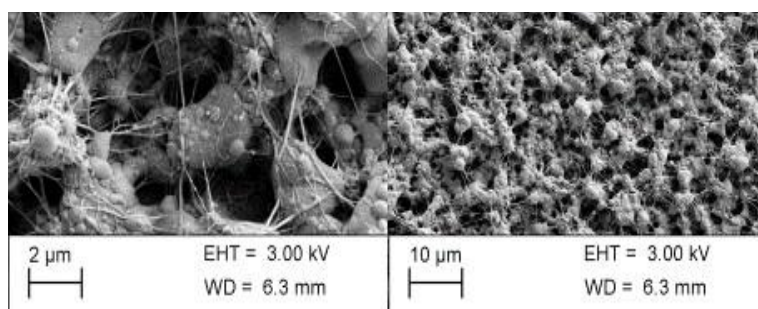


Figure 2.5. SEM micrograph obtained for sample $\text{SP}_{\text{CH}} 3$ mentioned in table B1 in the appendix B.

The SEM images of particles produced from 0.5% (w/v) PCL solution showed production of fibres along with non-spherical particles (see, for example figure 2.5). To overcome the problem of particle nonuniformity, PVP was used since it is widely reported in the literature to improve the morphology of the particles (Jaberolansar *et al.*, 2016; Seo *et al.*, 2018). The aim of this work was to coat the PCL particles with PVP by using co-axial electrospaying. This was carried out to produce spherical fibre free PCL particles. The diagram of a co-axial particle is shown in figure 2.6.

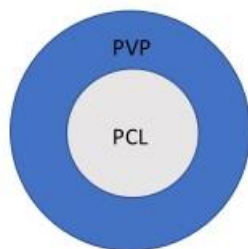


Figure 2.6. Co-axial particle with PCL in core and PVP in shell.

Further experiments were performed on PCL 45 and PVP 360 (360,000 Da) using the method of coaxial electrospinning (CP_{VCH}). Initially, 5% (w/v) PVP 360 was dissolved in water as the shell and 4% (w/v) PCL 45 was dissolved in 1,2-dichloroethane as the core. A range of samples were collected under various electrospinning parameters, as shown in Table C1 of appendix C.

A representative SEM micrograph from the experiments summarised in table C1 is shown in figure 2.7 and the rest are given in appendix C.

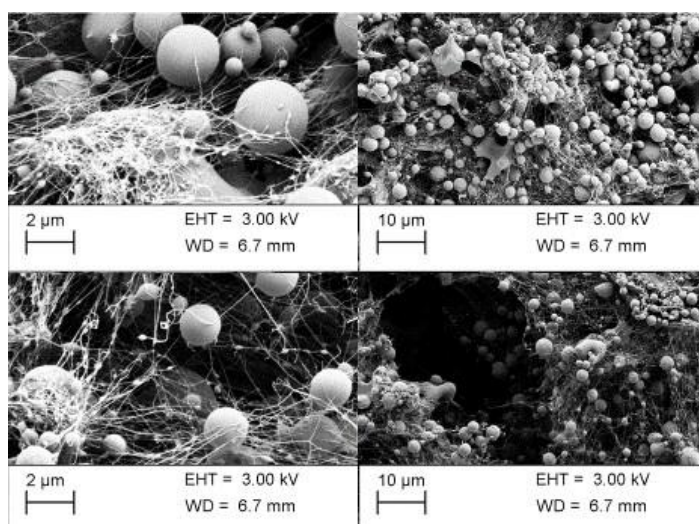


Figure 2.7. SEM micrograph obtained for sample CP_{VCH} 1 mentioned in table C1 in the appendix.

The SEM micrographs resulting from the experiments detailed in Table C1, indicated that the PVP coated PCL particles seemed to be more spherical than particles obtained using PCL alone. However, it was also clear that fibres were still present (see figure 2.7). It was suggested that an alternative solvent for PVP might influence the morphology observed in the nanomaterials. PVP is freely soluble in ethanol as well as water so coaxial-electrospinning was carried out by keeping PVP in ethanol in the shell and PCL in 1, 2-dichloroethane in the core.

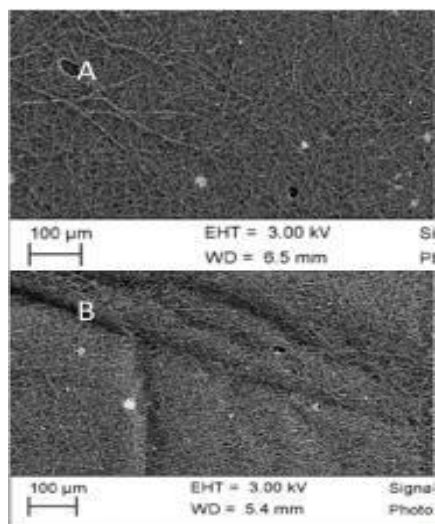


Figure 2.8. SEM of sample from table C1 in appendix C with 5 % (w/v) PVP in ethanol in the shell A) CP_{VCH} 3 with 0.5% (w/v) PCL in 1,2- dichloroethane in the core, B) CP_{VCH} 2 with 2 % (w/v) PCL in 1,2- dichloroethane in the core.

The SEM images of these samples showed that using ethanol as the solvent for PVP (M.W 360,000 Da) resulted in a whole mesh of fibres. Distilled water seemed to be a more suitable solvent for obtaining particles. The PVP solution in ethanol resulted in fibre formation as ethanol is more volatile and evaporated more readily and hence left the solution more viscous (noticed by observation) (Pillay *et al.*, 2013). In addition to the solvent, the molecular weight of polymer also affects the fibre or particle production.

To investigate whether the fibres observed in figure 2.7 were due to the PVP or PCL in the samples, a co-axial electrospaying experiment was carried out by keeping PVP (in water) in both the core and shell. A representative SEM micrograph from those samples is shown in Figure 2.9.

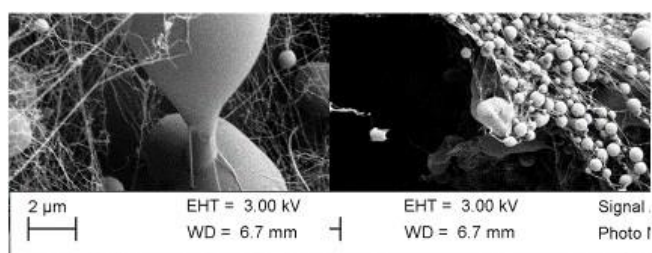


Figure 2.9. SEM of sample CP_{V2H} 5% solution was used in the shell with flow rate of 1.5 mL/hr and 3% solution was used for the core with flow rate of 0.25 mL/hr: at a 15 kV voltage and 10 cm tip to collector distance.

The SEM image shown in figure 2.9 indicated that PVP is most likely responsible for the production of fibres, in addition to coating the PCL nanoparticles. However, this is not definitive.

These initial experiments demonstrated that fibre-free samples containing both PVP and PCL were challenging to make. Recent work indicated that lower concentrations and lower molecular weights were likely to favour (nano)particles over nanofibres (Gómez-Mascaraque *et al.*, 2016). Therefore, it was decided that the next stage of the project was to work on lower molecular weight PVP (40 and 10) and PCL (10-14).

In this section of the report, the work carried out on lower molecular weight of PVP 40 (MW 40,000), PVP 10 (MW 10,000) and PCL 10-14 (MW 10-14,000) is discussed.

The first lower molecular weight (MW) polymer investigated in this part of the study was the target shell polymer, PVP. The earlier studies described in the previous section had used PVP with a MW of 360,000. The PVP chosen for this part had a significantly lower MW of 40,000 (PVP 40). Our initial focus in this part of the project was to investigate whether we could generate fibre-free particles. For that aim, it was decided to keep the system as simple as possible, so co-axial electrospaying was attempted using both PVP (in distilled water) as the core and the shell fluids. A range of solutions with concentrations between 8-10% (w/v) of PVP 40 dissolved in distilled water were electrospayed. However, all these samples led to spitting and dripping rather than electrospaying. The solvent was then changed from distilled water to ethanol, in a similar manner to Kostakova (2012) who had successfully electrospayed PVP 40. A range of samples were collected under varying electrospaying conditions (table 2.1) where the observation 'spitting' refers to an unstable spray whereas 'dripping' is the formation of larger droplets. Electrospaying or spraying is therefore the target, which achieves a smooth spray producing nanoparticles.

Sample code	PVP flow rate (mL hr⁻¹)	PVP flow rate (mL hr⁻¹)	Distance (cm) from tip of needle to collector	Voltage (kV) of the apparatus	Observation
CPV _{2M} 1	0.25	1	10	19	Electrospaying (getting particles)

CP _{V2M} 2	0.25	1	20	10	Spitting (drops were collecting on foil)
CP _{V2M} 3	0.25	1	20	11	Spitting + spraying
CP _{V2M} 4	0.25	1	20	12	Spitting + spraying
CP _{V2M} 5	0.25	1	20	13	Spitting + spraying
CP _{V2M} 6	0.25	1	20	14	Spitting + spraying
CP _{V2M} 7	0.25	1	20	15	Mostly spraying then spitting
CP _{V2M} 8	0.25	1	20	16	Electrospraying
CP _{V2M} 9	0.25	1	20	17	Electrospraying
CP _{V2M} 10	0.25	1	20	18	Electrospraying
CP _{V2M} 11	0.25	1	20	19	Electrospraying & dripping (collecting drops fastly)
CP _{V2M} 12	0.25	1	20	20	Electrospraying + some dripping
CP _{V2M} 13	0.25	1	30	10	Dripping
CP _{V2M} 14	0.25	1	30	11	Fast spraying
CP _{V2M} 15	0.25	1	30	12	Fast spitting & Electrospaying
CP _{V2M} 16	0.25	1	30	13	Spitting & Electrospaying
CP _{V2M} 18	0.25	1	30	15	Spitting and Electrospaying
CP _{V2M} 19	0.25	1	30	16	Spraying and spitting

CP _{V2M} 20	0.25	1	30	17	Spraying and spitting
CP _{V2M} 21	0.25	1	10	20	Spraying and spitting
CP _{V2M} 22	0.25	1	30	19	Electrospraying
CP _{V2M} 23	0.25	1	30	20	Electrospraying

Table 2.1. Processing parameters used for CP_{V2M} of 5 % (w/v) solution in ethanol.

A representative SEM micrograph from table 2.1 is given in figure 2.10 and the rest are given in appendix E.

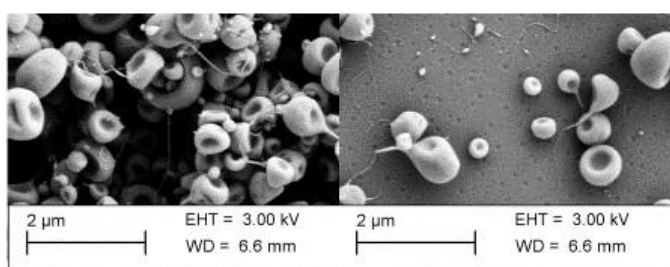


Figure 2.10. SEM of sample CP_{V2M} 1 from table 2.1.

It is clear from figure 2.10 that 40,000 M.W PVP gave fibre-free donut shape particles, which are rather similar in size (around 500 µm). Similar samples were made using PVP 10. Again, experiments initially focussed on electrospaying where both the core and shell fluids comprised of PVP 10 in ethanol. A representative SEM micrograph is shown in figure 2.11.

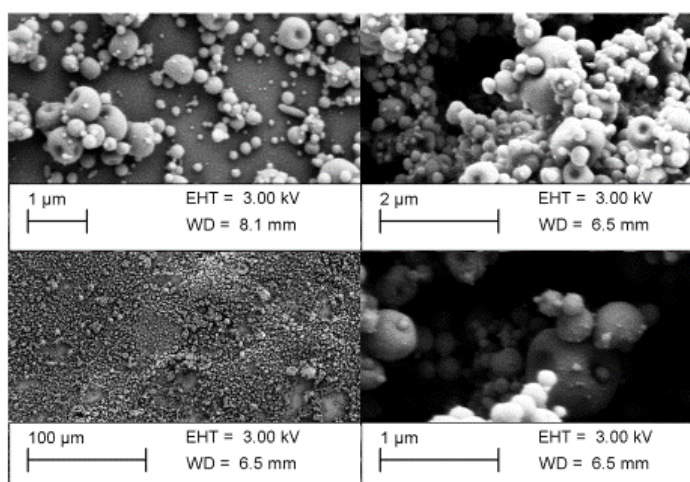


Figure 2.11. SEM of sample CP_{V2L} 8 in table 2.3.

It is apparent from figure 2.11 that the resulting NPs (from PVP 10) were more regular shaped and smaller (some are less than 100 nm) than those obtained with PVP 40. It was therefore decided to focus on PVP 10 in greater detail.

Co-axial electro spraying was carried out using 3-6% (w/v) solutions of PVP 10. A wide range of processing parameters was used for each concentration of polymer solution. The details of the processing parameters are given in tables (2.2-2.5). During these investigations, the effect of concentration on morphology and particle size was assessed.

Sample code	PVP flow rate (mL hr⁻¹)	PVP flow rate (mL hr⁻¹)	Distance (cm) from tip of needle to collector	Voltage (kV) of the apparatus	Observation
CP _{V2L} 1	0.25	1.00	10.00	10.00	Spitting
CP _{V2L} 2	0.25	1.00	10.00	15.00	Spitting +spraying
CP _{V2L} 3	0.25	1.00	10.00	20.00	Spitting +spraying collecting sample
CP _{V2L} 4	0.15	0.75	10.00	10.00	Spitting + spraying
CP _{V2L} 5	0.15	0.75	10.00	15.00	Spitting less +more spraying collecting sample
CP _{V2L} 6	0.15	0.75	10.00	20.00	Spraying (collecting sample)
CP _{V2L} 7	0.25	1.00	20.00	10.00	Spitting +spraying
CP _{V2L} 8	0.25	1.00	20.00	15.00	Spitting
CP _{V2L} 9	0.25	1.00	20.00	20.00	Electrospraying and spitting
CP _{V2L} 10	0.15	0.75	20.00	10.00	Dripping

CP _{V2L} 11	0.15	0.75	20.00	15.00	Spitting +spraying
CP _{V2L} 12	0.15	0.75	20.00	20.00	Spitting +spraying
CP _{V2L} 13	0.25	1.00	30.00	10.00	dripping
CP _{V2L} 14	0.25	1.00	30.00	15.00	spitting +spraying
CP _{V2L} 15	0.25	1.00	30.00	20.00	spitting +spraying
CP _{V2L} 16	0.15	0.75	30.00	10.00	dripping +spitting
CP _{V2L} 17	0.15	0.75	30.00	15.00	spitting +spraying
CP _{V2L} 18	0.15	0.75	30.00	20.00	spitting +spraying

Table 2.2. Processing parameters used for CP_{V2L} of 3% (w/v) solution in ethanol.

Sample code	PVP flow rate (mL hr⁻¹)	PVP flow rate (mL hr⁻¹)	Distance (cm) from tip of needle to collector	Voltage (kV) of the apparatus	Observation
CP _{V2L} 1	0.25	1.00	10.00	10.00	Spitting +spraying
CP _{V2L} 2	0.25	1.00	10.00	11.00	Spitting +spraying
CP _{V2L} 3	0.25	1.00	10.00	12.00	Spitting +spraying
CP _{V2L} 4	0.25	1.00	10.00	13.00	Sparking
CP _{V2L} 5	0.25	1.00	10.00	14.00	Spitting +spraying
CP _{V2L} 6	0.15	1.00	10.00	15.00	Spitting +spraying
CP _{V2L} 7	0.15	1.00	10.00	16.00	Spitting +spraying
CP _{V2L} 8	0.15	1.00	10.00	17.00	Spitting +spraying
CP _{V2L} 9	0.25	1.00	10.00	18.00	Spitting
CP _{V2L} 10	0.25	1.00	10.00	19.00	Dripping
CP _{V2L} 11	0.25	1.00	10.00	20.00	Spitting +spraying

CP _{V2L} 12	0.25	0.75	10.00	20.00	Mostly spraying
CP _{V2L} 13	0.25	0.75	10.00	15.00	Fast dripping
CP _{V2L} 14	0.25	0.75	10.00	10.00	Dripping
CP _{V2L} 15	0.25	1.00	20.00	10.00	Dripping
CP _{V2L} 16	0.25	1.00	20.00	15.00	Drpping &electrospraying
CP _{V2L} 17	0.25	1.00	20.00	20.00	Dripping & electrospraying collected sample
CP _{V2L} 18	0.25	0.75	30.00	15.00	Spitting & electrospraying
CP _{V2L} 19	0.25	0.75	30	17	Spitting &electrospraying
CP _{V2L} 20	0.25	0.75	30	18	Spitting + spraying
CP _{V2L} 21	0.25	0.75	30	20	Spitting and spraying
CP _{V2L} 22	0.25	0.75	30	21	Spitting and spraying
CP _{V2L} 23	0.25	0.75	30	22	Spitting & spraying & sparking
CP _{V2L} 24	0.25	1	30	10	Dripping
CP _{V2L} 25	0.25	1	30	15	Spitting and spraying
CP _{V2L} 26	0.25	1	30	20	Spitting and spraying
CP _{V2L} 27	0.25	1	30	22	Spitting and spraying
CP _{V2L} 28	0.25	1	30	23	Spitting and spraying & sparking

Table 2.3. Processing parameters used for CP_{V2L} of 4% (w/v) solution in ethanol.

Sample code	PVP flow rate (mL hr⁻¹)	PVP flow rate (mL hr⁻¹)	Distance (cm) from tip of needle to collector	Voltage (kV) of the apparatus	Observation
CP _{V2L} 1	0.25	1.00	30.00	21.00	Spitting + spraying
CP _{V2L} 2	0.25	1.00	30.00	22.00	Spitting + spraying
CP _{V2L} 3	0.25	1.00	30.00	23.00	Spitting + spraying
CP _{V2L} 4	0.25	1.00	30.00	24.00	Sparking
CP _{V2L} 5	0.25	0.75	30.00	20.00	Spitting + spraying
CP _{V2L} 6	0.15	0.75	30.00	20.00	Spitting + spraying
CP _{V2L} 7	0.15	0.75	30.00	22.00	Spitting + spraying
CP _{V2L} 8	0.15	0.75	20.00	15.00	Spitting + spraying
CP _{V2L} 9	0.25	1.00	20.00	15.00	Spitting + spraying
CP _{V2L} 10	0.25	1.00	20.00	16.00	Spitting
CP _{V2L} 11	0.25	1.00	20.00	17.00	Spitting + spraying
CP _{V2L} 12	0.25	1.00	20.00	18.00	Spitting + spraying
CP _{V2L} 13	0.25	1.00	20.00	19.00	Spitting + spraying
CP _{V2L} 14	0.25	1.00	20.00	20.00	Spitting + spraying
CP _{V2L} 15	0.25	1.00	20.00	21.00	Spitting + spraying
CP _{V2L} 16	0.25	1.00	20.00	22.00	Spitting + spraying
CP _{V2L} 17	0.25	1.00	10.00	10.00	Fast spitting (fast spraying)
CP _{V2L} 18	0.25	1.00	10.00	15.00	Spitting
CP _{V2L} 19	0.25	1.00	10.00	16.00	Spitting
CP _{V2L} 20	0.25	1.00	10.00	17.00	Spitting + spraying

CP _{V2L} 21	0.25	1.00	10.00	18.00	Spitting and spraying
CP _{V2L} 22	0.25	1.00	10.00	19.00	Spitting and spraying
CP _{V2L} 23	0.25	1.00	10.00	20.00	Spitting (very less) +electrospraying

Table 2.4. Processing parameters used for CP_{V2L} of 5% (w/v) solution in ethanol.

Sample code	PVP flow rate (mL hr ⁻¹)	PVP flow rate (mL hr ⁻¹)	Distance (cm) from tip of needle to collector	Voltage(kV) of the apparatus	Observation
CP _{V2L} 1	0.25	1.00	10.00	10.00	Spitting + spraying (got inside and outside circle because of dripping)
CP _{V2L} 2	0.25	1.00	10.00	15.00	Spitting + spraying
CP _{V2L} 3	0.25	1.00	10.00	16.00	Spitting + spraying
CP _{V2L} 4	0.25	1.00	10.00	17.00	Sparking
CP _{V2L} 5	0.25	1.00	10.00	18.00	Spitting + spraying
CP _{V2L} 6	0.25	1.00	10.00	19.00	Spitting + spraying
CP _{V2L} 7	0.25	1.00	10.00	20.00	Spitting + spraying collecting sample
CP _{V2L} 8	0.15	0.75	10.00	20.00	Spitting + spraying collected sample
CP _{V2L} 9	0.25	1.00	20.00	10.00	Dripping current zero

CP _{V2L} 10	0.25	1.00	20.00	15.00	Spitting + spraying
CP _{V2L} 11	0.25	1.00	20.00	20.00	Spitting + spraying
CP _{V2L} 12	0.25	1.00	30.00	10.00	Dripping no current
CP _{V2L} 13	0.25	1.00	30.00	15.00	Spitting + spraying
CP _{V2L} 14	0.25	1.00	30.00	20.00	Spitting + spraying

Table 2.5. Processing parameters used for CP_{V2L} of 6% (w/v) solution in ethanol.

The samples collected at a voltage of 20 kV with 10 cm distance were the only ones that were successfully electrospayed. A representative SEM and frequency distribution of particle size is shown

In figure 2.12a1. Figure 2.12a2 shows a SEM micrograph from the same sample as that shown in figure 2.12a1, but in a region that is more densely populated with particles. This picture showed the effect of it on particle size and other properties.

The rest of the images of these samples are given in appendix F.

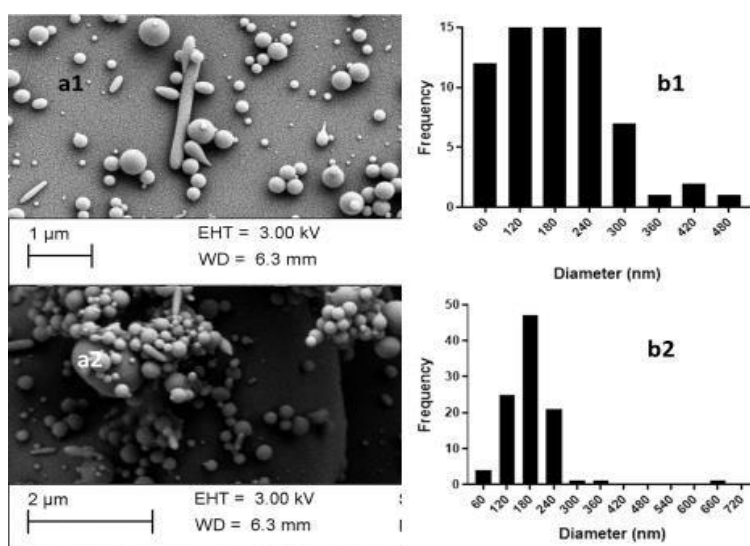


Figure 2.12. (a1) SEM of particles (b1) frequency distribution graph of particles obtained for sample CP_{V2L} 11 from table 2.3. (a2) SEM and (b2) frequency

distribution graph (but with a different scale from b1) of a dense area of same sample, showing that the average particle diameter is essentially independent on the particle density of the sample.

A comparison of figure 2.12b1 and figure 2.12b2 indicates that the diameter of particles in dense and sparse areas are similar but the ratio of numbers of particles that lie in the 0 – 200 nm or 200 - 400 nm ranges are different.

SEM micrographs of the 3-6% (w/v) solution of PVP 10 shows that the concentration of the polymer solution does not make a large difference to the particle size (the SEMs are given in appendix F).

The size distribution of particles containing minimum particle size diameter, maximum particle size diameter and mean \pm SD of all processed images obtained from CP_{V2L} are given in Table 2.6.

Sample code	Figure No	No of particles diameter measure	Minimum size particle diameter (nm)	Maximum size particle diameter (nm)	Mean \pm SD (nm)
CP _{V2L} 11	2.14 in table 2.3	100.00	50.82	460.19	178.6 \pm 80.8
CP _{V2L} 11	2.15 in table 2.3	100.00	65.93	684.50	185.25 \pm 72.5
CP _{V2L} 12	F1 in table 2.3	100.00	21.98	447.44	180.45 \pm 79.3
CP _{V2L} 23	F2 in table 2.4	100.00	45.44	352.72	177.17 \pm 74.04
CP _{V2L} 7	F3 in table 2.5	100.00	22.47	1033.00	186.45 \pm 156.09
CP _{V2L} 8	F4 in table 2.5	100.00	22.47	638.15	
CP _{V2L} 3	F5 in table 2.2	100.00	16.66	290.91	

Table 2.6. Size distribution of 100 particles from samples of CP_{V2L}. The data was obtained from Image J and processed through Graph Pad Prism.

The minimum particle size was found to be 16.66 nm as per data compiled from 7 samples in table 2.6. In this project, the aim was to produce particles less than 100 nm and, according to the data compiled in table 2.6, this aim has been achieved.

All the samples recorded in Table 2.6 have a minimum diameter less than 100 nm with the mean of all samples found to be less than 201 nm. The maximum particle size was found to be 1033.00 nm. The D'Agostino & Pearson normality test was carried out for all sample mentioned in table 2.6. The sample shown in figure 2.12 failed the normality test, presumably because of outlier large particles.

After successful production of PVP 10 nanoparticles, PCL 10-14 was incorporated in PVP 10 nanoparticles. As the aim of this research project was the production of PCL nanoparticles, PCL 10-14 was used in the core and PVP 10 was selected for the

formation of the shell of the particles. An SEM image of the sample CP_{VCL} is given in figure 2.13.

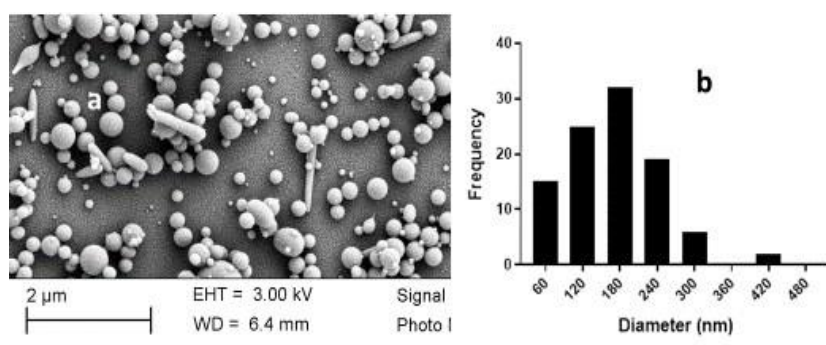


Fig 2.13. (a) SEM and (b) frequency distribution graph of sample CP_{VCL} obtained from 4% PVP 10 in shell (with flow rate of 0.25 mL/hr) and 4% PCL 10-14 in core (with a flow rate of 1.0 mL/hr) with 10 cm tip to collector distance and voltage of 20 kV.

The diameter for 100 particles of sample CP_{VCL} was determined using Image J. The minimum particle diameter was found to be 29.85 nm; the maximum particle diameter was 422.41 nm and mean of the sample was ~180 nm. PVP/PCL particles in figure 2.13 passed all the normality tests, which means the frequency distribution graph is bell shaped and the data is normally distributed.

The results of this research work confirmed that we produced nanoparticles much smaller than reported before. Liposomal nanoparticles have been used as a drug delivery system. According to Wilczewska and coworkers (2012), most of liposomal particles range from 80 – 300 nm. Park *et al.* (2009) used PEGylated PLGA nanoparticles for the improved delivery of doxorubicin, where the average diameter of particles was 130 nm. Bilensoy *et al.* (2009) studied various nanoparticles for the delivery of mitomycin C for bladder tumours. The average size of chitosan particles was 291 nm, and PCL nanoparticles used had an average size of 179 nm, Poly-L-lysine-PCL nanoparticles diameter was 190 nm, and Chitosan-PCL nanoparticle size was 336 nm. Particles produced in this project are smaller than the work published by Wilczewska in 2012.

A range of tests were carried out to confirm the presence of PCL inside PVP particles. These are summarised below.

The SEMs of the dried distilled water and NaOH treated pellet are given in figures 2.14a1 and 2.14b1, respectively. The procedure of collection of this sample is given in section 2.3.5.1. The SEM of the material did not confirm the presence of PCL

nanoparticles. One of the reasons could be that NaOH hydrolysed the PCL polymer backbone (McInnes *et al.*, 2018). The effect of 0.5 M and 2.5 M NaOH was directly observed on PVP/PCL particles, by applying 100 μ L of NaOH solution and observing the changes by SEM. SEM images of the samples are given in figures 2.14a2 and 2.14b2, indicating loss of all particulate material, and hence treatment with NaOH was not found useful for the separation of PCL particles.

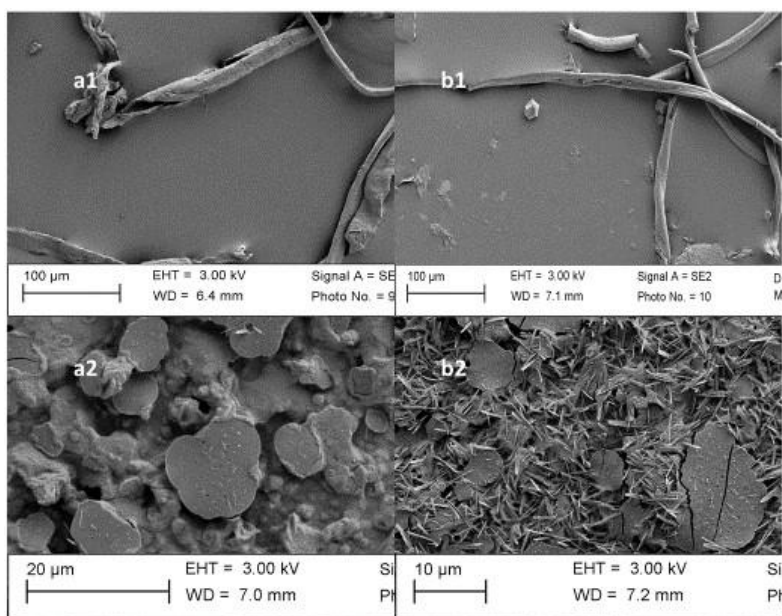


Figure 2.14. SEM of sample CP_{VCL} , obtained from 4% PVP 10 and 4% PCL 10-14 with 10 cm tip to collector distance and flow rate of 0.25 mL/hr for core and 1mL/hr for shell and voltage of 20 kV. The sample was dissolved in distilled water and centrifuged the pellet was dispersed in (a1) distilled water and (b1) NaOH. The same sample of particles were directly treated with NaOH on foil (a1) 0.5 M and (b1) 2.5 M.

Brilliant green dye was incorporated in PCL solutions to aid identification of PCL nanoparticles, as NaOH treatment failed to separate PCL particles from the preparations. The dissolution of different dyes was tested in PCL solutions. Brilliant blue was found to be insoluble in 1,2-dichloroethane, the solvent used to make the PCL solution. Brilliant green dye was used by Loon and Barefoot (2003) at 0.05% (w/v), which was found to be soluble in PCL solution. 0.026% and 0.05% (w/v) of brilliant green were used in this experiment. The dye was incorporated in 4% PCL solutions, the electro spraying was carried out with same conditions as mentioned in figure 2.13. Samples were collected on foil and both samples were dissolved in few mL of distilled water. Samples were transferred in eppendorf tubes and centrifuged at 25000 g at 22 $^{\circ}$ C for 10 minutes. The SEM of the pellet did not

confirm the presence of PCL particles. The result obtained from treatment of CP_{VCL} nanoparticles remained inconclusive.

Further experiments were carried out to confirm the presence PCL in the core of particles. Rhodamine b, which is a fluorescent dye (Yilmaz and Soylak, 2018) was selected, as this dye gives a neon yellow light when exposed to ultraviolet light. Firstly 0.05% (w/v) of dye was incorporated into a preparation of CP_{VCL}. The flow rate of PCL was kept the same (0.25 mL/hr) as mentioned in the figure 2.13. The pink colour dye confirmed that the flow of PCL is not continuous, and IR and NMR did not confirm PCL presence in the sample, due to which the flow rate of PCL was increased to 0.5, 0.75 and 1 mL/hr.

The SEM of the samples run at flow rate of 0.75 mL/hr with 10% PCL is given in figure 2.15. The SEM showed that electrospinning did not produce particles at the higher flow rate.

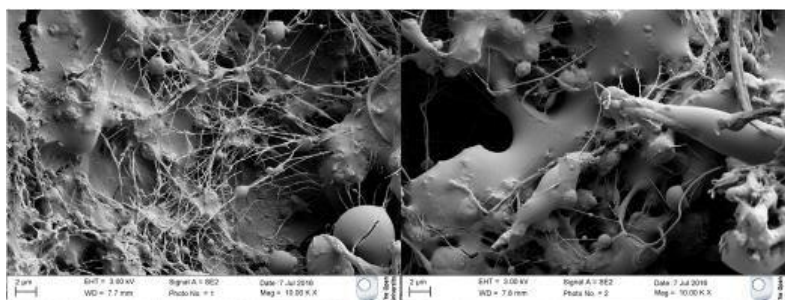


Figure 2.15. SEM of sample CP_{VCL}, obtained from 4% PVP 10 with flow rate of 1.5 mL/hr and 10% PCL 10-14 core with flow rate of 0.75 mL/hr at 18 kV voltage and 10 cm tip to collector distance.

2.3.1.1 Characterization

2.3.1.1.1 Infrared (IR) Spectroscopy

IR spectroscopy is a classical tool used for the determination of the structure of molecules. The chemical composition and architecture of molecules is sensitive to IR light (Barth, 2007). IR spectroscopy results from the vibration of atoms and bonds in a molecule, in which the fraction of incident radiation is absorbed at a specific energy. During this work, it was primarily used to elucidate the presence or absence of a polymer. To this aim, the IR of a pure sample of PCL and PVP and CP_{VCL} sample (with low flow rate 0.25 mL/hr of PCL in core) nanoparticles was obtained to confirm the presence of both in that same sample (figure 2.13). Table 2.7 shows the absorption band of representative functional groups in PCL and PVP.

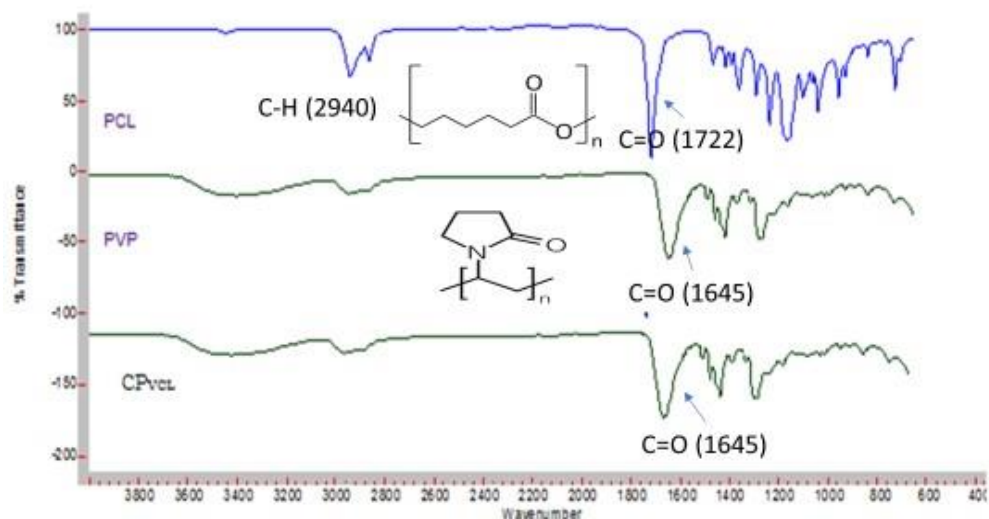


Figure 2.16. Comparison of IR of CP_{VCL} (sample in figure 2.13), PVP 10 and PCL 10-14.

Absorption band (cm ⁻¹)	Functional group	Reference
PCL		
2940-2860	C-H	(Abderrahim et al., 2016)
1722	C=O	
1238	C-O-C (asymmetric)	
1160	C-O-C (Symmetric)	
PVP		
1645	C=O	(Gutul et al., 2014).
1287.6, 1437.8, 1422.4	C-N, attachment of CH ₂ in pyrrole ring	

Table 2.7. The table shows the absorption bands of representative functional groups in PCL and PVP.

The peak at 1645 cm⁻¹ for CP_{VCL} in figure 2.16 resembles the C=O peak of PVP in the same figure. The other absorption bands at 1280 cm⁻¹, 1422 cm⁻¹ and 1437cm⁻¹ for CP_{VCL} resemble the peaks in the PVP spectrum around the same wavenumber for the C-N stretch. The distinctive peaks of PCL spectrum were not found in the CP_{VCL}

spectrum. Due to this, NMR was carried out to further investigate the presence (or absence) of PCL in this sample.

The FTIR spectrum of sample CP_{VCL} prepared with a high flow of PCL (0.75 mL/hr) in the core, compared with PCL 10-14 and PVP 10 IR is given in figure 2.17.

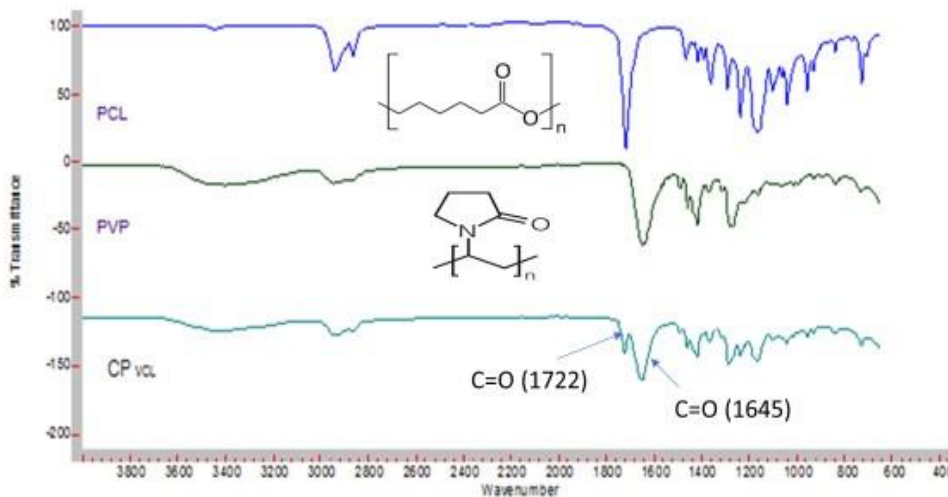


Fig 2.17. Comparison of IR of CP_{VCL} (sample in figure 2.15), PVP 10 and PCL 10-14, indicating the presence of PCL in the CP_{VCL} preparation.

The comparison of IR of PCL 10-14, and PVP 10 with CP_{VCL} at a high flow rate of PCL (0.75 mL/hr) confirmed that the absorption bands at 2940 cm⁻¹ and 2860 cm⁻¹ are due to the C-H groups and at 1722 cm⁻¹ is due to a stretching vibration of the ester carbonyl (C=O) in CP_{VCL}. These match with peaks in the IR spectra of PCL, suggesting that PCL is present in the sample. The absorption band at 1645 cm⁻¹ in CP_{VCL} was assigned to C=O group which resembles the peak in the PVP spectrum. This shows that both PCL and PVP are present in the sample CP_{VCL} (in figure 2.13), which clarifies that an increased flow rate affected the sample composition and enhanced incorporation of PCL in the particles.

2.3.1.1.2 Nuclear Magnetic Resonance (NMR)

This technique is widely used for the analysis and identification of the organic compounds. ¹H NMR was carried out in this section, which determines the chemical environment of protons in a compound (Balci, 2005).

NMR spectra of pure samples of PCL and PVP, and of CP_{VCL} nanoparticles prepared at low flow rate 0.25 mL/hr of PCL, were obtained to confirm the presence of both PCL and PVP in CP_{VCL} (figure 2.13). The NMR spectrum showed four peaks in the

case of PCL, as shown in figure 2.18, but the peak at 4.06 ppm (e), which represents the two methylene protons adjacent to the carboxylic acid group, is distinctive. The other peaks for PCL are further upfield, and less significant for comparative purposes as these are more likely to overlap with the peaks from PVP.

The comparison of ^1H NMR spectra of PCL, PVP and CP_{VCL} particles in figure 2.18 clearly showed that the CP_{VCL} sample contains PVP, but it did not confirm the presence of PCL, because the distinctive peak of PCL at 4.06 ppm is not seen in the CP_{VCL} sample. The pattern of peaks found in the CP_{VCL} spectrum resembles the pattern of PVP NMR peaks in figure 2.18. Both IR and NMR analysis indicate that particles prepared at a low flow rate (0.25 mL/hr) of PCL in the core did not contain detectable amounts of PCL.

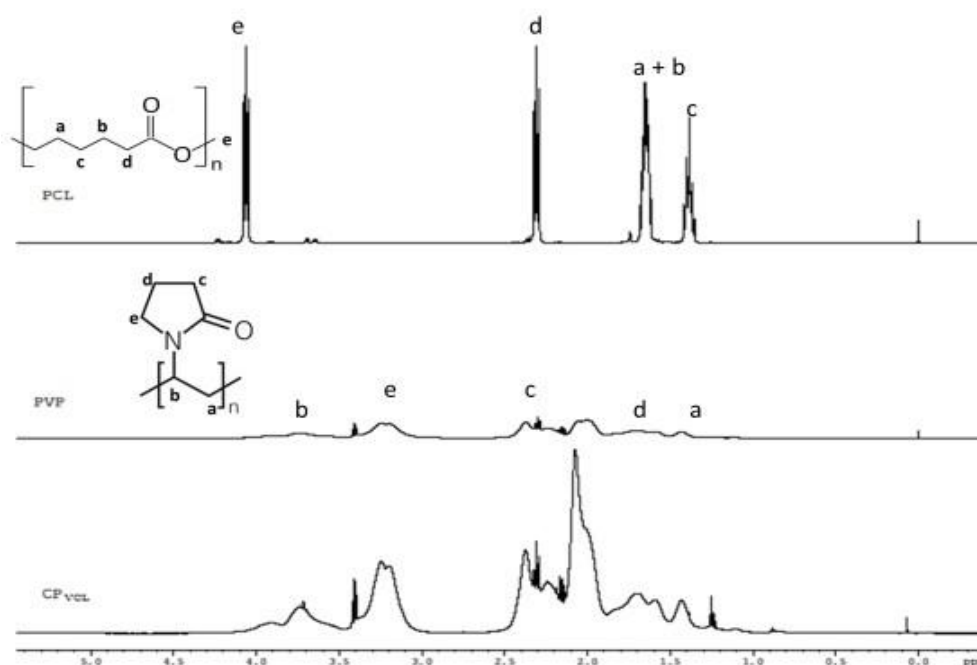


Figure 2.18 ^1H NMR of PCL, PVP and sample CP_{VCL} (PVP/PCL coaxial particles with low flow rate that is 0.25 mL/hr of PCL) run in CDCl_3 for sample in figure 2.13 (SEM).

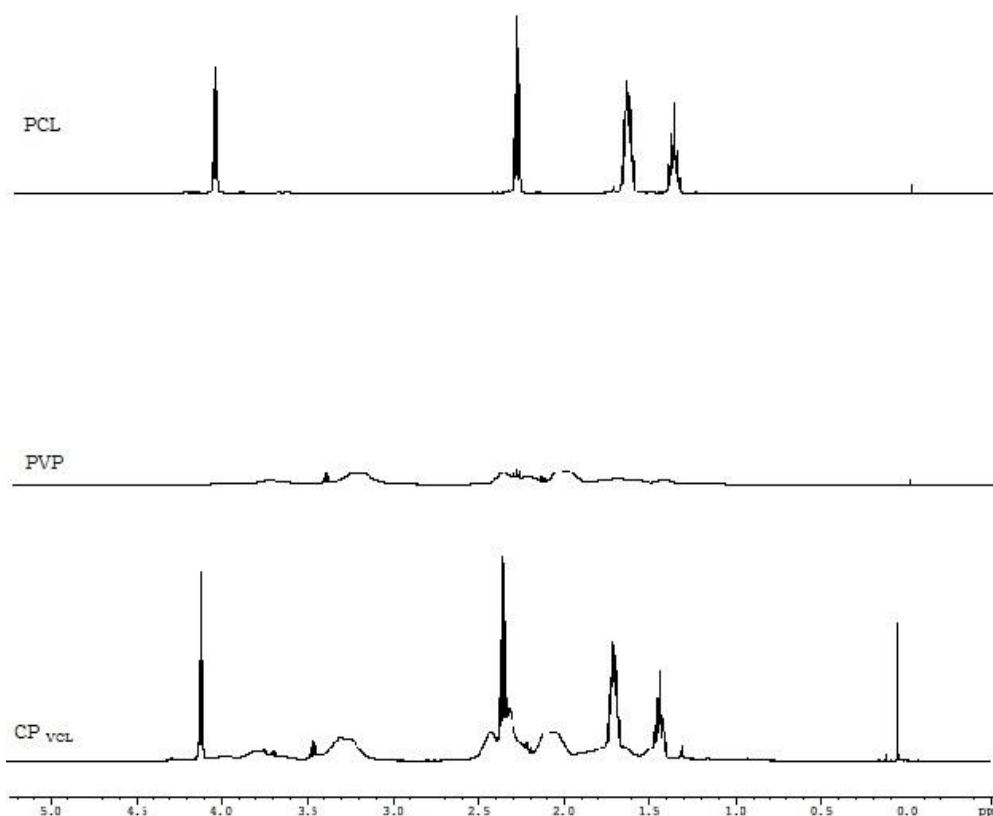


Figure 2.19. ^1H NMR of PCL, PVP and sample CP_{vcl} (SEM in figure 2.15, the PCL was used in the sample at a high concentration (10%) and high flow rate, 0.75 mL/hr, 4% PVP was used with flow rate of 1.5 mL/hr).

When the flow rate and concentration of PCL is increased in the coaxial electrospaying experiment both the ^1H NMR and IR (Figure 2.19 and 2.17) obtained from those samples confirms the presence of PCL but the SEM (figure 2.15) confirmed that the sample consists of lumps rather than nanoparticles.

2.3.2 Electrospaying of polymer in to distilled water

The plan of this work was to obtain PCL particles of smaller size, using a coaxial electrospaying strategy with water-soluble PVP as the shell polymer. Given the difficulties, described above, of generating core-shell nanoparticles that retain PCL, it was decided to attempt collection of particles into water directly, following a technique described by Luo *et al.* (2015). The particles would be generated with the higher flow rate of PCL, which allows the PCL and PVP components to remain together. As the shell polymer PVP is water soluble, the hope was that the PVP from

CP_{VCH} particles would dissolve in water, leaving free PCL particles that could be collected directly.

The presence of particles collected after electro spraying into water was determined using dynamic light scattering (DLS). In these experiments coaxial electro sprayed material was collected in an aqueous solution of 5% (w/v) SDS, in which the SDS acts as an excipient. Samples (CP_{VCH}) with concentrations of 0.25% - 5% (PCL) and 5 % or 10% (PVP) were used for particle size measurement. A representative graph is given in figure 2.20.

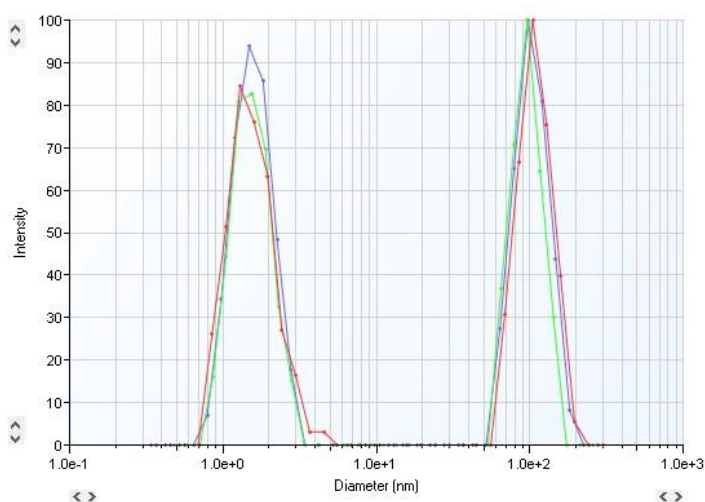


Figure 2.20. DLS graph of sample CP_{VCH}. 10% PVP (in core 0.5 mL/hr and in shell with 1.5 mL/hr flow rate) at 20 kV voltage with 6.5 cm tip to surface of SDS solution.

Figure 2.20 shows two main particle size distributions, one at around 1.5 nm and the other at approximately 100 nm. The first peak is representative of SDS for which the hydrodynamic radius of micelles in solution (in the absence of added salt) is known to be around 1.95 nm (Missel *et al.*, 1980). The second peak is possibly due to PVP-SDS aggregates. This has previously been observed by Prasad *et al.* (2006) for PVP40 and SDS where the hydrodynamic radius was found to increase with an increasing SDS concentration (specifically, from 108 nm at 4.15 mM, i.e. half the CMC (critical micelle concentration), to 158 nm at 24.9 mM) (Prasad *et al.*, 2006). The DLS graph of a further sample is given in figure 2.21, where three particle size distributions are seen. This is typical of the DLS graphs obtained for this set of samples.

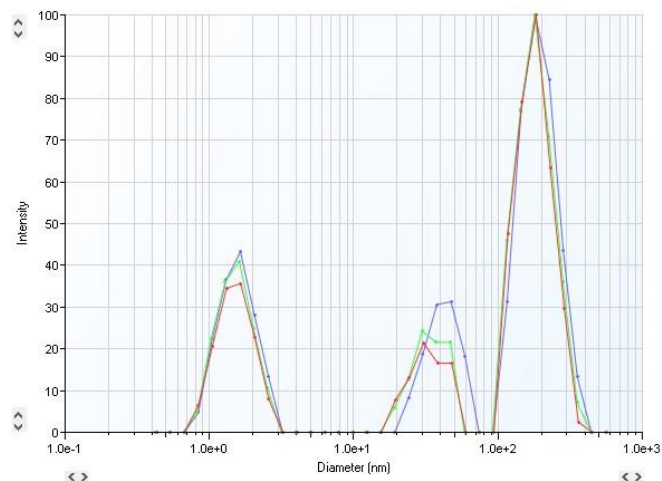


Figure 2.21. DLS graph of sample CP_{VCH}. 4% PCL (in core with 0.5 mL/hr flow rate) and 5% PVP (in shell with 1.5 mL/hr flow rate) at 20 kV voltage with 6.5 cm from the tip to the surface of the SDS solution.

As with figure 2.20, the two extreme particle size distributions (~1.5 nm and 200 nm) are still seen; however, a third peak denoting another particle size can also be seen at ~ 50 nm, for which we postulate that it could potentially be due to suspended PCL nanoparticles. The comparison of the result of electro spraying into liquid with already published work, shows that Luo *et al.* (2015) used static solvent displacement to collect near-monodisperse polymeric particles with diameters between 100 nm and 10 μ m. Pinto Reis *et al.* (2006) achieved a 50–300 nm size range of monodisperse polymeric NPs by solvent displacement.

After the collection of PCL particles in the liquid, the separation of these particles from water remained a significant challenge.

2.4 Conclusion

Electrospraying parameters play an important role in the production of nanomaterial but the molecular weight of polymer and the nature of the solvent both have a significant effect on production of particles as well. PVP 360 and PCL 45 both produce fibres, however low molecular weight PVP (10 & 40) had fewer entanglements and hence it can produce fibre free particles. Low molecular weight PVP therefore successfully gave nanoparticles with less than 100 nm diameter, but the formulation of PCL (10-14) nanoparticles remained a challenge and there were problems in identifying the presence of PCL in the particles produced.

The electro spray precipitation technique, which involves electro spraying directly into aqueous media, described by Luo *et al.* (2015), gave smaller nanoparticles in

comparison to either electrospray or agitated solvent displacement alone. This technique enabled us to get particles less than 100 nm, compared with the more standard electrospray technique producing particles of around 4-5 μm . The same molecular weight of both polymers was used in electrospray precipitation and these experiments gave particles less than 100 nm. This suggests that electrospray precipitation can give smaller particles than electrospraying on foil. The particle size can be further decreased by the adding surfactant and reducing the concentration of polymer solution further. However, the collection of nanoparticles from the solvent (distilled water) remained a challenge, even when the solvent was centrifuged at high RCF (relative centrifugal force).

Due to time constraints further work on this aspect of the project was abandoned as production of PCL nanoparticles was unsuccessful.

Chapter 3

Preparation and characterization of novel formulation of hemin for better management of anaemia

3.1 Introduction

Iron is the most abundant element on planet Earth. According to estimates, the core of the Earth is predominantly composed of iron and nickel, and the 6% of Earth's mantle is also compos

ed of iron. Similarly, iron is abundant in the human physiological system and it is an essential element required (Himmelfarb, 2007).

In 1932, it was established that iron is required for the synthesis of hemoglobin, which is a carrier of oxygen in humans (McDowell, 2017). It has been recognized that iron is required for numerous physiological processes, such as transport of oxygen, synthesis of deoxyribonucleic acid (DNA) and transport of electrons in the production of ATP (Abbaspour *et al.*, 2014).

The importance of iron for human life is further established by the health conditions which can result from its imbalance in the human body. Both its deficiency as well as its excess in the human body can lead to pathologies. Low iron can result in iron deficiency anaemia. Similarly, excess iron could lead to a condition known as haemochromatosis, in which the excess free iron can lead to the formation of free radicals which can cause tissue damage (Abbaspour *et al.*, 2014).

In the first part of the chapter, the absorption and utilisation of iron in the human body will be discussed briefly.

3.1.1 Iron and its availability in diet

Iron is vital for the synthesis of haemoglobin and myoglobin, flavin-containing iron enzymes, cytochromes, catalase, some hormones, and neurotransmitters (Abbaspour *et al.*, 2014). The daily adult iron requirement is 8 - 18 mg, but only 1-2 mg iron is absorbed, through the proximal intestine (duodenum) (Johnson-Wimbley and Graham, 2011). The remaining iron required for normal body maintenance is recycled from the breakdown of senescent RBCs (Coad and Pedley, 2014). In the diet, iron is present as heme (in the form of haemoglobin and

myoglobin, mainly from red meat), and non-heme forms from white meat, vegetables and cereals (Conrad and Umbreit, 2002). Components in the diet such as phytates and tannins can reduce, whereas ascorbic acid can increase, iron absorption (Fuqua *et al.*, 2012; Lynch and Cook, 1980).

3.1.2 Mechanisms of iron absorption

Figure 3.1 describes the three molecular pathways for the intestinal iron absorption, involving the heme transporter HCP1, the transporter of divalent metals DMT1 and the integrin-mobilferrin pathway. Once the heme is internalised, heme-oxygenase degrades the heme and releases the iron (West and Oates, 2008). Hemin formulations used in this work will therefore be able to release the iron from the hemin inside the duodenal cells, which is described later in chapter 4.

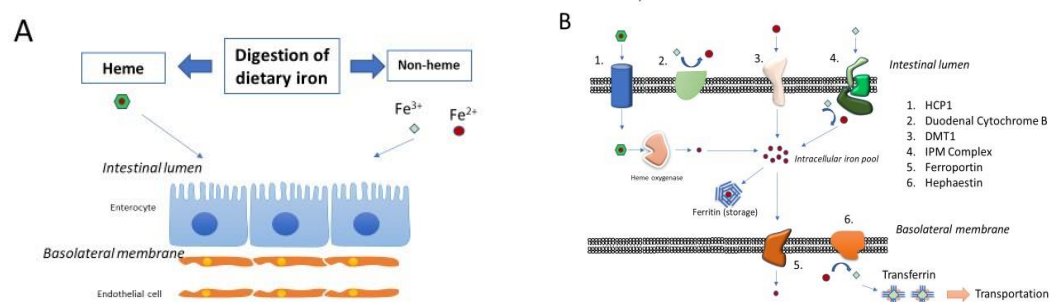


Figure 3.1. Intestinal pathways of iron absorption A) heme and non-heme iron is taken up enterocytes brush border. Non-heme iron is reduced to Fe^{2+} by the ferric reductase. Some of the non-heme iron transported in the form of Fe^{3+} via the integrin-mobilferrin pathway (IMP).] B) Heme is transported via receptor mediated membrane endocytosis of HCP1, and heme Fe^{2+} is released by the heme oxygenase. Fe^{2+} is transported by the ferroportin to the cytoplasm. Fe^{3+} can be imported by the integrin-mobilferrin (IMP) complex, and then reduced to Fe^{2+} .

3.1.3 Regulation of iron absorption

Iron is regulated closely in the human body, as both deficiency and excess, can be harmful (Kew, 2014). Hepcidin, a peptide produced by liver, exerts a negative control on the absorption of dietary iron by reducing the expression of DMT-1 receptors in the duodenum (Bergamaschi *et al.*, 2017). Another hormone, erythroferrone (ERFE) acts directly on the liver to decrease the hepcidin production

resulting in an increase in iron absorption (Hanudel *et al.*, 2018), in response to an increased demand for red blood cell synthesis.

3.1.4 Transport and distribution of iron in the body

Fe²⁺ is exported into the circulation through ferroportin. Hephaestin, a membrane-bound ferroxidase converts Fe²⁺ to Fe³⁺. Fe³⁺ binds to the plasma protein transferrin for transportation to the cells (Fuqua *et al.*, 2012). See Figure 3.2.

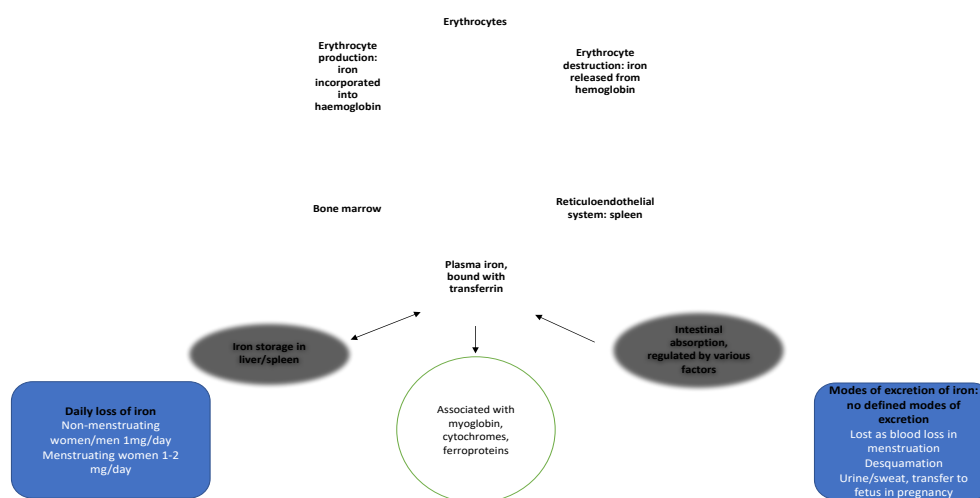


Figure 3.2. Cycle of iron utilisation & distribution in human body diagram modified from “Distribution of Body Iron – All About Blood,” n.d.

3.1.5 Iron deficiency anaemia and its impact on human health

Anaemia is defined as a low oxygen-carrying capacity of RBCs, or low hemoglobin concentration <13 g/dL in an adult male or <12 g/dL in an adult female (“Anaemia - iron deficiency - NICE CKS,” n.d. & (“WHO | Anaemia,” n.d.).

The causes of iron deficiency anaemia (IDA) include poor diet, gastrointestinal bleeding, menstrual losses, malabsorption syndromes, or pregnancy (“Anaemia - iron deficiency - NICE CKS,” n.d.). Worldwide, IDA is one of the most significant nutritional problems (Yang *et al.*, 2016). Anaemia could increase maternal mortality and morbidity, premature births and low birth weight, developmental delays (WHO, 2017). IDA is common in both underdeveloped and developed countries (Ezzati *et al.*, 2002).

3.1.6 Prevention of iron deficiency: Food fortification and its limitations

Universal iron fortification of cereals has been attempted. However, there are concerns for example it will not be suitable for people with haemochromatosis, and bioavailability is limited (Waldvogel-Abramowski *et al.*, 2014). A double-blind randomised control trial published by Zimmerman. *et al.* in 2010 showed that children who received iron fortified biscuits had higher levels of faecal calprotectin, increased enterobacteria and fewer microfloras (lactobacilli and bifidobacteria), but no improvement in anaemia/iron status.

3.1.7 Parenteral iron supplements

Intravenous (IV) preparations of iron are effective treatments for anemia, but are only administered at in-patients clinics where facilities are available. Whilst generally successful, IV administration can sometimes have side effects such as anaphylaxis (Silverstein and Rodgers., 2004). Some of the common formulations used are iron dextran, iron sucrose, ferric carboxymaltose, and iron isomaltoside (Araya and Zaritsky, 2017).

However, as there is evidence of significant side effects from IV iron transfusion, the Medicine and Healthcare Products Regulatory Agency (MHRA) published guidelines on its safety and use. The evidence suggests that intravenous iron does not result in a faster increase in haemoglobin production when compared to oral iron supplements, provided oral iron supplements are taken as advised and intestinal absorption is not affected ("British National Formulary (BNF) 70," n.d.). Also, intravenous iron administration is associated with significant risk of serious hypersensitivity reactions. The hypersensitivity reactions are not only limited to first administration, in fact this could happen at any subsequent administration. Hence, every time, a person is having an intravenous iron administration, trained staff and resuscitation facilities should be available ("Intravenous iron and serious hypersensitivity reactions," n.d.; Litton *et al.*, 2013).

Based on the above, in 2013 the MHRA published a document which suggested that intravenous iron should only be reserved for treatment when oral iron supplements are ineffective.

3.1.8 Oral iron supplements

Oral iron supplements are widely used for the prevention and treatment of iron deficiency. There are various iron formulations available in the form of ferrous salts such as ferrous sulphate, ferrous fumarate, and ferrous gluconate (BNF, 2015). According to the BNF (2015), there is no significant difference between the various ferrous formulations in terms of absorption of iron.

Ferrous sulphate is available as 200 mg tablets. Each 200 mg tablet of ferrous sulphate is equivalent to 65 mg of ferrous iron. The daily recommended dose for treatment for an adult is 130-195 mg ferrous iron (2-3 tablets) in divided doses, whereas the prophylactic dose is 65 mg ferrous iron (1 tablet) daily. Ferrous fumarate is available in tablet form, usually 210 mg. Each 210 mg tablet is approximating to 65-70 mg of elemental iron. The recommended dose of ferrous fumarate for iron deficiency anaemia is one tablet two to three times a day, whereas prophylactic dose is one tablet once or twice a day ("About the eMC - electronic Medicines Compendium (eMC)," n.d.).

Fei (2015) looked at the intestinal absorption of the orally administered ferrous salts, and evidence suggests that only 10-15 % is actually absorbed (Fie, 2015). In iron deficiency anaemia, there are low levels of stored iron in the body, so that higher daily doses are needed. According to the BNF (2015), the total dose of elemental iron needed to be given for IDA is 100 – 200 mg daily. Hence, this results in 2-3 daily doses of oral iron and it can cause GI (gastrointestinal) side effects such as heartburn, epigastric discomfort, nausea, constipation, diarrhoea, and constipation/faecal impaction. Thus, higher doses are associated with issues such as intolerance of oral formulations and reduced cost-effectiveness (Johnson-Wimbley and Graham, 2011; Sazawal *et al.*, 2006)

According to Fei (2015), these side effects result in poor compliance with the treatment, which could be as low as 40-60%. The ferrous salts are best absorbed on an empty stomach but to reduce the side effects some patients take it with food; however, this may cause further deterioration in iron absorption (Abbaspour *et al.*, 2014).

Animal trials have shown an increase in systemic infections, alteration of gut bacteria and changes in the pro-inflammatory signalling from gut epithelium following treatment with iron supplements (Carrier *et al.*, 2002). Kortman *et al.* (2012) evaluated the impact of iron supplements on the gut bacterial flora. The importance of gut flora (the microbiome) is well established and is known to affect

the immune system and provide protection against pathogenic microbes. An *in vitro* experiment was designed by Kortman *et al.* (2012) using the differentiated monolayers of intestinal epithelial cell lines. Characteristics such as bacterial attachment, infiltration and translocation were studied using a panel of enteric pathogens. The panel was exposed to iron rich conditions. The results of the experiment suggested oral iron supplements can increase growth and virulence of enteric pathogens.

Supplements with the ferric form of iron are better tolerated but have poor absorption (Seril *et al.*, 2002). As we have seen in previous sections that the ferrous form of iron is more soluble than the ferric form (“Iron Deficiency Anemia,” n.d.). Chelation has been considered to improve the bioavailability of ferric iron; however, it has shown increased risk of colon cancer in rodents (Seril *et al.*, 2002). The WHO recommend the use of ferrous over ferric salts due to better bioavailability, in which 10 – 15 % of iron is absorbed. The ferric form has poor solubility in an alkaline environment and needs to be converted to the ferrous form before being absorbed, and the bioavailability is 3 – 4 times less than ferrous salts (Santiago, 2012).

Therefore, tailoring the iron in a nano formulation could help to overcome above mentioned issues. This research describes efforts to develop a novel oral iron preparation which could be better tolerated with improved bioavailability compared with formulations currently available.

3.1.9 Developments in iron supplements

Due to the disadvantages and side effects of available iron supplements, researchers are constantly working to develop formulations which are safer and have improved bioavailability.

Pereira *et al.* (2014), developed organic acid-modified Fe(III) oxo-hydroxide nanomaterials. The preparation of iron hydroxide adipate tartrate (IHAT) showed ~80% relative bioavailability when compared to Fe(II) sulfate in humans. IHAT did not accumulate in the intestinal mucosa and promoted a beneficial microbiota. Also, the research showed that IHAT is less toxic than Fe(II) sulfate/ascorbate.

Latunde-Dada *et al.* (2014), assessed the efficacy of IHAT on iron-deficient and iron-sufficient Swiss mice. The mice were given ferrous sulphate or nano Fe(III) [acidic concentrated solution of Fe(III) was added to adipic and tartaric acid solutions]. The

research showed that absorption of nano Fe(III) was significantly increased in iron-deficient mice compared to iron-sufficient mice.

Powell *et al.* (2014) studied 2-5 nm Fe(III) oxo-hydroxide, which is less ordered and more readily bioavailable compared to its pure synthetic analogue ferrihydrite. They co-precipitated, the ferrihydrite with tartrate inclusion, which resulted in stabilization of the cross links. The murine models showed that gastrointestinal uptake was independent of luminal Fe(III) reduction to Fe(II) and absorption was equivalent to that of ferrous sulphate. The side effect of ferrous sulphate was not found in Powell's formulation. However, the bioavailability is not significantly better than the ferrous sulphate and crucially these are unstable in acidic environment, which poses a barrier for oral administration.

Shafie *et al.* (2016) demonstrated that a single dose of nanoparticles containing iron showed more bioavailability compared to a single dose of ferrous sulfate, in rats in which iron deficiency anemia was induced. This was measured by levels of haemoglobin in control and experimental groups using the formulation from Powell's group (Pereira *et al.* 2014).

3.1.10 Potential of heme and hemin as an iron supplement

Heme could be an alternative to inorganic iron supplements. It has a different absorption pathway by duodenal cells. The transporter for heme is not well characterized (Conrad and Umbreit, 2002; Gaitán *et al.*, 2012). HCP 1 is primarily a folate transporter, but it has low affinity for heme transport as well (Le Blanc *et al.*, 2012).

Heme is a prosthetic group, and it is present in cellular hemoproteins which execute diverse biological functions, such as: oxygen transport, oxygen sensing, cell respiration and metabolism, cell growth, cell self-renewal, and differentiation, all needed for survival and function of organisms (Tsiftoglou *et al.*, 2006).

Heme and hemin structures are given in figure 3.3 a and b respectively. Heme is a metallo-compound, comprising of an iron atom bound to a tetrapyrrole ring system known as protoporphyrin, through its four nitrogen atoms. Iron in hemoglobin is in the ferrous (Fe^{2+}) form, which allows reversible binding with molecular oxygen (Berg *et al.*, 2002).

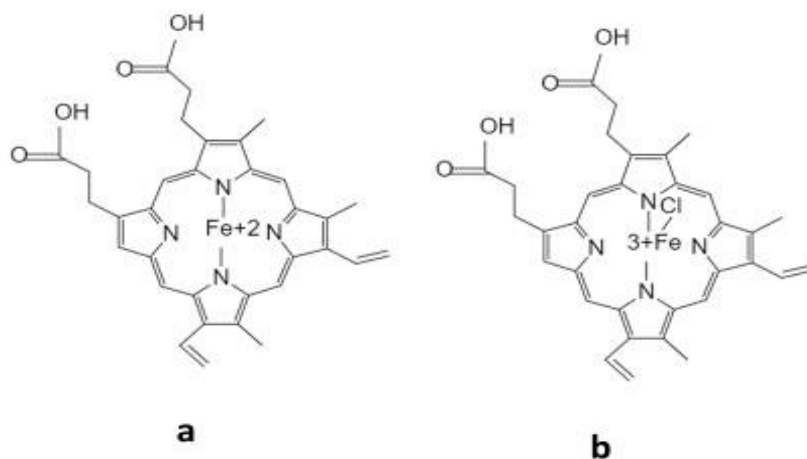


Figure 3.3. Structure of a) heme, b) hemin.

Heme iron polypeptide (HIP) has been developed as a heme formulation derived from bovine haemoglobin and is highly soluble (Naraju *et al.*, 2013). It was seen earlier that there is a separate pathway for absorption of heme. Heme absorption is generally not affected by food; hence it can be taken on empty stomach or with food. The Canadian Agency for Drugs and Technologies published a review paper in 2007 comparing the efficacy of HIP, oral ferrous salts and IV iron. The paper concluded that the available evidence for HIP evaluation is limited and more research is needed to determine its efficacy. In a randomised control trial, patients with chronic kidney disease were given HIP or IV iron. The results showed that HIP had similar efficacy to IV iron in maintaining haemoglobin levels.

However, patients who received IV Iron had higher levels of ferritin, the significance of which is unclear. Both HIP and IV iron had similar profiles of side effects (Nagaraju *et al.*, 2013).

Hemin is the oxidized form of iron protoporphyrin IX, which is an essential growth promoter (Tsiftoglou *et al.*, 2006). Structurally hemin contains a chloro ligand, which is not present in heme. Hemin is insoluble at neutral pH but is soluble in sodium hydroxide. In sodium hydroxide, the chloro ligand is substituted by a hydroxyl group, which results in the formation of hematin (Egan *et al.*, 1999a).

3.1.11 Development of new hemin supplement

This research is aimed at developing an oral iron supplement with improved stability and bioavailability. Therefore, if hemin is used for oral iron supplements, it should be soluble in physiological media and able to resist the harsh environment

of the GI tract (Span et al., 2016a). The Lipinski rule of 5 determines whether a drug is orally active or not. According to the Lipinski rule of 5, it is not easy to make hemin soluble because its molecular weight and log P values are out of the range. As hemin is the poorly soluble drug, it needs to be delivered efficiently, which can be achieved with nano formulations.

To achieve these objectives, Eudragit L 100 and PVP-360 were used in the initial experiments. PVP is very well tolerated, amphipathic, cost-effective, available in various sizes, has been used in health products for many years, and hence more data is available.

PVP forms molecular adducts with substances, which can help solubilization or precipitation of some substances. This property of PVP was shown to enhance hemin solubility in physiological medium (Melent'eva et al., 1980).

The use of electrospraying and electrospinning to create micro/nano particles and micro/nanofibers of the PVP and hemin to enhance its uptake, was investigated.

3.2 Aim and objectives

The aim of the research project was to gain insight into the characteristics that affect the uptake of nanofibres and their associated cargo (such as a drug with low bioavailability, hemin) by cells.

To address the aim, the following objectives were attempted

1. Development of ultra-fine nanofibres (diameters less than 100 nm) by electrospinning.
2. Production of nanofibres and nanoparticles containing hemin.
3. Measurement of hemin release from nanoformulaions.
4. The treatment of cells with nanofibers/nanoparticles containing hemin, and to monitor hemin uptake by ferrozine assay of iron and Perls staining of iron in cells.

3.3 Material and methods

3.3.1 Materials

Hemin (molecular weight= 651.9 Da) was purchased from Calbiochem. Polyvinylpyrrolidone (PVP) (average MW 360,000, 40,000 and 10,000 Da) was purchased from Sigma Aldrich. Poly(ethylene oxide) (PEO) (average MW 100,000 Da) was purchased from Acros Organics. Poly(vinyl alcohol) (PVA) (average MW 89,000-98,000 Da) analytical grade was obtained from Sigma Aldrich. MeOH (methanol), EtOH (ethanol), CHCl₃ (chloroform), THF (tetrahydrofuran), DMAc (dimethylacetamide), DMF (dimethylformamide) were manufactured by Fisher, and were of analytical grade and Eudragit L 100 was bought from Fluka. All other materials were used of analytical grade and used as provided.

3.3.2 Methods

3.3.2.1 Preparation of electrospinning/ electro spraying solutions

All solutions were % (w/v) unless otherwise stated. 10 % solutions of PVP were made in MeOH as it gave nice smooth fibers. However, this solution caused clogging on the electrospinning needle, presumably because MeOH is a low boiling solvent (64.7 °C) (Bertini *et al.*, 1979). Subsequently DMF, which is a high boiling solvent, 153 °C, (Admin, 2010) was used with MeOH in the ratio of MeOH:DMF 7:3 to avoid this problem. Hemin solutions were made in DMF at 16.66 mg/mL. 15% PVP solutions were prepared in MeOH. Hemin in DMF, was added to the 15% PVP solution to achieve a final concentration of 10 % PVP with final ratio of MeOH and DMF 7:3. Hemin was added to the PVP solution to make a range of percentages from 0.1-5%. All solutions were stirred until completely dissolved. Solutions for electrospinning with Eudragit L 100 were made to 18.2% (w/v) in MeOH: DMAc (4:1) as this solvent combination gave smooth, particle-free fibers according to SEM and light microscopy. Hemin formulations with Eudragit L 100 were made with 26% Eudragit L 100 in MeOH: DMAc (4:1). Hemin was separately dissolved in DMAc (3.33mg/ml) and added to the 26% Eudragit L 100 solution to obtain 0.5 % hemin in 18.2 % of Eudragit L 100. The final ratio of MeOH to DMAc was 5:1. The use of other polymers is described in the results section 3.3.1.

PVA nanofibers were successfully made by Nigadiman (2015), using deionized water as solvent. In this study PVA was mixed in deionized water to make 10% PVA

solution, then heated at 100°C for two hours while mixing with a spatula, resulting in a thick paste.

3.3.2.2 Single fluid electrospinning/electrospraying

The electrospinning solution was loaded into a 5 mL syringe, avoiding the formation of air bubbles.

The spinneret was attached directly to the syringe. Flow from the syringe was controlled by a ColeParmer pump (78-9100C). The negative, ground electrode of a high voltage DC supply (FuG Elektronik HCP 35 – 65000, supplied by Omiran Ltd, UK) was connected to the collector (dimension 20 X 20 cm) and the positive electrode to the spinneret. The collector was wrapped with aluminum foil. Polymer solution was ejected from the spinneret and voltage applied to the spinneret. The experiment was performed under ambient conditions at room temperature. An illustration of the electrospinning/electrospraying apparatus is given in chapter one, figure 1.2. The voltage range was 10-20 kV and the distance from tip to collector was kept between 12-15 cm.

3.3.2.3 Dissolution studies

In vitro dissolution tests were carried out for sets of PVP-360 fibers containing hemin in 10 mL or 100 mL of dissolution buffer. A standard dissolution apparatus was not used because it was not possible to prepare the large amounts of formulation, 6.52 g for 1 dm³, needed for each sample. Instead 65.2 mg of hemin PVP-360-1% fibers were added to 10 mL of isotonic phosphate-buffered saline (PBS), which when fully dissolved would create a 100 µM preparation of hemin. To measure the amount of dissolved fibers, duplicate 200 µL aliquots were collected up to 50 hrs as shown in the dissolution graphs in results and discussion section. The volume of the solution was maintained by addition of 400 µL of PBS. The aliquots were centrifuged at 14000 rpm to remove undissolved material then 180 µL of supernatant was transferred to a 96 well plate. Hemin dissolution was assessed by absorbance at 400 nm in an Omega FLUOStar plate reader (BMG LabTech, Aylesbury, UK), based on peak absorption of the visible spectrum (Figure 3.17). This experiment was repeated 3 times.

Dissolution of fibers was compared with controls of i) a physical mixture of PVP-360 and hemin powders added to the dissolution medium, ii) dissolution of hemin in a solution of PVP-360 in PBS and iii) dissolution of hemin powder alone.

Dissolution studies were done in the same pattern for preparations made with PVP-40 and PVP-10 except particles were dissolved *in situ* on the collection foil rather than in a glass bottle, due to the low yields and stickiness of the material. The foil was folded from the side and the PBS was poured on to the sample. The solution was transferred to a centrifuge tube by pipette. The dissolution experiment was only done once for PVP-40 and PVP-10 as it was difficult to produce enough quantities of the material for analysis. To make the data reliable the experiment needs to be repeated at least twice.

3.3.2.4 Characterization techniques of nanomaterial

Precise characterization of nanomaterials made from electrospaying or electrospinning is crucial to associate nanomaterial physicochemical properties with cellular response. It is also essential for meaningful, accurate and reproducible results (Shang *et al.*, 2014). In this part of the thesis different techniques used for characterization of hemin containing nanomaterials are discussed.

3.3.2.4.1 Infrared spectroscopy (IR)

FTIR instrument and method for obtaining IR spectrum is given in section 2.2.2.1.

3.3.2.4.2 Ultraviolet-visible spectroscopy

The UV-visible spectra of hemin preparations in PBS were obtained using a Shimadzu UV-1800 ultraviolet spectrophotometer over a wavelength range of 200-600 nm. The spectra were used for measuring λ_{max} for a range of concentrations of hemin, 10, 25, 50, 75, 100 and 500 μM , obtained by dissolution of PVP-hemin fibers with hemin content 0.1-5%. UV-visible spectra were also measured for preparations of PVP-40 and PVP-10 particles alone and with hemin. Spectra were also measured for the controls including fibers of PVP only, a physical mixture of PVP and hemin, hemin dissolved in a PVP solution and hemin alone in PBS. These

solutions were kept on a stirrer for five days before reading. Spectra were also taken of solutions of hemin in selected solvents.

3.3.2.4.3 X-ray diffraction

The X-ray diffraction data was collected using a Philips PW1830 powder diffractometer operating at 40 kV and 25 mA, with Cu K α radiation ($\lambda=1.5418$ Å).

3.3.2.4.4 Energy dispersive X-ray spectroscopy (EDX/EDS)

The instrument used for EDX was an Oxford Instruments Aztec Energy EDS control / acquisition software, with Oxford Instruments Xmax50 (50 mm²) detector. EDX analysis was carried out at the Open University by Gordon Imalach.

3.3.2.4.5 Scanning electron microscopy (SEM)

The instrument used for SEM was a Zeiss Supra 55VP FEGSEM. The imaging conditions were 3kV accelerating voltage, 20 micron aperture for good depth of focus, and high current mode for good resolution. Samples were mounted on 12 mm diameter aluminium SEM stubs using carbon sticky tabs. Gold sputter-coating was achieved using a Polaron SC7640 sputter coater, with a coating time of 4060 seconds to give 5-10 nanometres thickness coating. SEMs of all samples were carried out.

3.3.2.4.6 Microscopy

An Olympus X81 light microscope used to take the images of fibers and particles at magnifications of 100x and 400x.

3.3.2.4.7 Dynamic light scattering

A Malvern Zetasizer Nano-ZS system was used to measure the particle size of dissolved PVP preparations. 65.2 mg of PVP fibers only or PVP with hemin in different proportions, were dissolved in 10 mL of PBS or water. Each solution was

stirred gently until the fibers were completely dissolved and 2 mL of solution was then transferred to a plastic cuvette. Three different data fitting algorithms were considered when fitting the normalized field autocorrelation functions obtained for each solution:

- (a) the general purpose (GP) NNLS (non-negative least squares) algorithm developed by Malvern as part of their proprietary software,
- (b) the CONTIN function, a well-known NNLS algorithm often used for DLS analysis, and
- (c) a triple exponential function.

The triple exponential mentioned above is given by:

$$g^{(1)}(\tau) = A_1 \exp\left(-\frac{\tau}{\tau_1}\right) + A_2 \exp\left(-\frac{\tau}{\tau_2}\right) + A_3 \exp\left(-\frac{\tau}{\tau_3}\right)$$

Where the sum of the first two relative amplitudes A_1 and A_2 equals 1. The solutions were unable to be filtered and hence it is assumed that the third decay mode is likely to be due to dust and will not be considered further during the analysis.

From application of the Stokes-Einstein equation for the diffusion coefficient (D_0):

$$D_0 = k_B T / 6\pi\eta_0 R_H$$

where k_B is the Boltzmann constant ($1.381 \times 10^{-23} \text{ J K}^{-1}$), T is the temperature (here 25 °C i.e. 298.15 K) and μ is the dynamic viscosity of the solvent (i.e. $8.90 \times 10^{-4} \text{ Pa}\cdot\text{s}$ for water at 25 °C), and knowing the values of the decay times (τ) where:

$$\tau = \frac{1}{D_0 q^2}$$

for which q^2 reflects the distance the particle travels and can be calculated as:

$$q = \frac{4\pi n}{\lambda} \sin\left(\frac{\theta}{2}\right)$$

where $\lambda = 633 \times 10^{-9} \text{ m}$ and $\theta = 173^\circ$, the hydrodynamic radii (R_H) can be obtained.

The triple exponential was found to fit well to the data here and therefore was used for detailed data analysis, although the Malvern GP NNLS algorithm is also used in this chapter for comparison purposes only.

3.3.2.4.8 Differential Scanning Calorimetry (DSC)

A Mettler Toledo DSC822 Differential Scanning Calorimeter (maximum 700 °C), with Mettler 'Star' software V.9 for control/acquisition/analysis, and Labplant RP100 Intracooler for sub-ambient cooling to -60 °C was used in this research work. Maximum cell temperature is rated to 700 °C but maximum operating temperature was limited by the sample pan material. Aluminium pans were used, limiting a safe maximum temperature to about 600 °C. Heating rates were made variable up to 50 °C/min, though 10 °C/min is a more common rate.

3.3.2.4.9 Measurement of iron content in fibers (Ferrozine Assay)

This technique was adapted from a method used to measure total cellular iron by a colourimetric method using ferrozine (Fish, 1988) for cultured cells (Riemer *et al.* 2004). It was used here to measure total hemin available in PBS, SIF (simulated intestinal fluid) and pH 2 solution after dissolving PVP-hemin nanofibers. 6.52 mg/mL of fibers of PVP only or PVP with hemin in different proportions were dissolved in PBS and SIF. Each solution was stirred gently until the fibers were completely dissolved. Portions of the samples were spun at 12,000 rpm for 5 min, to remove small amounts of brown precipitate. The hemin was measured in both spun and unspun solutions and compared with standard FAS (ferrous ammonium sulphate) solution. 100 µL aliquots of each solution were treated with 100 µL of iron releasing solution made up of 4.5% (w/v) KMnO₄ and 1.4 M HCl freshly mixed in a 1:1 ratio. The iron releasing solution digests proteins and heme to which iron is bound and releases the iron. Here this treatment was used to release iron from hemin wrapped in PVP. The samples were incubated at 60 °C for 2 hours in a heating cabinet. The samples were cooled to room temperature, and the volume of each sample was made up to 1.0 mL accurately with deionized water. 100 µL of iron detection solution (2.5 M ammonium acetate, 1 M ascorbic acid, 6.5 mM ferrozine) was added to each sample. The iron detection solution was made by adding 9.7 g ammonium acetate and 8.8 g ascorbic acid to about 10 mL of water, so that the volume was less than 25 mL. The mixture was heated for complete dissolution, 80 mg of ferrozine were dissolved, and the volume was adjusted to 25

mL (Riemer *et al.*, 2004). The ascorbic acid in the iron detection solution reduces Fe^{3+} to Fe^{2+} . It is the ferrous form of iron which binds to ferrozine and gives a purple colour (Jeitner, 2014; Riemer *et al.*, 2004; Yamamoto *et al.*, 2010). The samples were centrifuged at 12,000 rpm for 5 mins. 200 μL centrifuged samples were taken for measurement of absorbance at 592 nm, with correction for light scattering at 750 nm in a FluoStar Omega plate reader (BMG LabTech, Aylesbury, UK), in a 96-well plate.

Standards were prepared from a fresh solution of ferrous ammonium sulfate (FAS), made by dissolving 0.392 g of FAS in 10 mL of water to make a 0.1 M solution. Stock solutions of 1 mM and 100 μM were prepared by serial dilution in which 1 mL of each concentration was diluted 10 times by addition of 9 ml water. Standards were prepared and 100 μL of each standard was used for a standard curve.

3.4 Results

The aim of the work described in this report was to develop a formulation using the technique of electrospinning or electrospraying to create nano- / micro- sized formulations to improve the bioavailability of hemin, as a novel DDS (drug delivery system).

3.4.1 Development of a Hemin-Polymer formulation

Hemin is poorly soluble in water and therefore a suitable organic solvent for electrospinning is needed.

Also, in the initial phase of the work, a variety of polymers compatible with drug formulation were assessed, with the aim of identifying polymer and hemin mixes that could be prepared in compatible solvents.

The solubility of hemin was checked in different solvents. Methanol, DMAc, DMF and THF were found to be good solvents for hemin. Hemin is partially soluble in EtOH as well. Solutions of hemin in THF, DMAc, MeOH, EtOH and CHCl_3 are shown in figure 3.4.

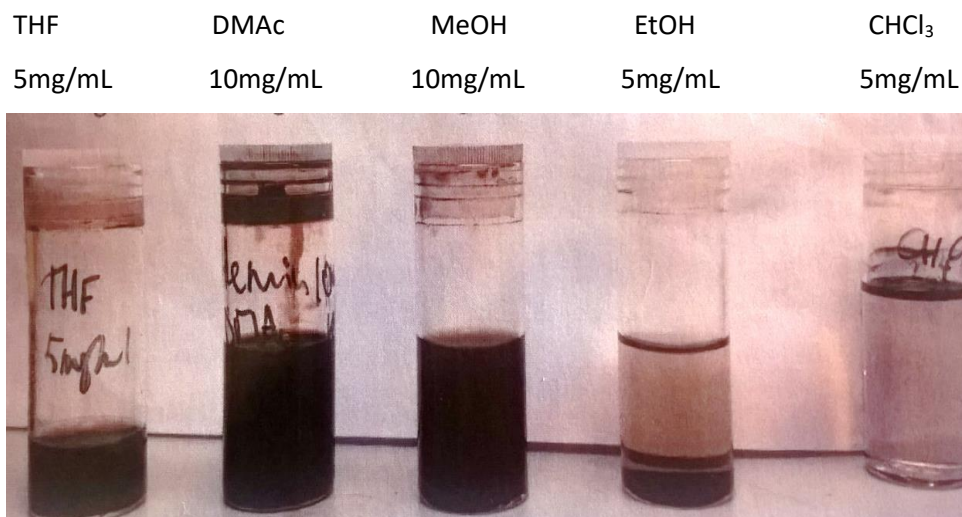


Figure 3.4. Solubility of Hemin in different solvents. Hemin was completely soluble in THF, DMAc and MeOH at the concentrations indicated, and partially soluble in EtOH. Hemin was not soluble in CHCl₃ and formed a layer at the top of the solvent.

A selection of biocompatible polymers was assessed for suitability for the formulation. PVA (polyvinyl alcohol), PEO (polyethylene oxide), Eudragit L 100 and PVP-360 were investigated as materials for production of nanofibers by electrospinning.

Attempts were made to prepare a solution of PVA in water (Nigadiman 2015) but the result was a paste of PVA contained bubbles which disappeared after a week. The paste did not remain stable for long as microbial growth was observed after 10 days. The PVA paste was not suitable for electrospinning and behaved like an anti-thixotropic material (behaves like a solid when force is applied). PVA was found to be insoluble in THF and DMF. For these reasons PVA was not investigated as a carrier for the hemin further. It is mentioned by Nigadiman (2015) as well that additional force was needed to extrude the solution from the syringe, due to the high viscosity.

PEO did not dissolve in cool or hot water, but 20% PEO made a creamy solution when heated at 70 °C for 50 minutes in ethanol. The solution produced crystals after removing from heat within 10 minutes, and hence was impossible to use for electrospinning.

Eudragit L 100 was selected because it is designed to limit release of API at pH 2 but would allow a sustained release at pH 6 (Cetin *et al.*, 2010). This is the requirement for the hemin formulation, as it is required to be released in the intestine to avoid

gastric irritation and to promote duodenal uptake (Illangakoon *et al.*, 2014).

Eudragit L 100 was soluble in a combination of DMAc and methanol (1:5).

PVP-360 was found to be soluble in EtOH, MeOH, DMAc and deionized water. 10% PVP 360 has been used to make fast dissolving fibers carrying either caffeine or paracetamol (Illangakoon *et al.*, 2014).

After comparing results from the above experiments, Eudragit L 100 and PVP 360 were selected as being suitable candidates for electrospinning with hemin.

The conditions for electrospinning in the first set of fibers prepared from PVP are given in table 3.1. 10% PVP-360 was prepared in MeOH and electrospun initially. Later in the project, DMF (30%) was mixed with MeOH as solvent to avoid clogging of the needle during electrospinning.

Sample	Solvent	% PVP (w/v)	% Hemin (w/v)	Flow rate (mL.hr ⁻¹)	Distance (cm) from tip to collector	Voltage (kV)	Observation
a1	DMAc	10	0	0.5	14	11.67	Electrospraying
a2	DMAc	10	0.1	0.5	14	11.67	Electrospraying
b1	EtOH	10	0	0.75	12	13.28	Electrospinning
b2	EtOH	10	0.1	0.75	14	13.55	Electrospinning
c1	MeOH	10	0	1	14	8.18	Electrospinning
c2	MeOH	10	0.1	1	14	11.32	Electrospinning

Table 3.1. Electrospinning conditions of PVP-360 with or without hemin with three different solvents. The voltages of the samples were adjusted until the needle stopped dripping. The images of fibres from these conditions are shown in figure 3.6.

18.2% Eudragit L 100 was made in MeOH and DMAc, the solution was electrospun according to conditions mentioned in table 3.2. As shown in the image from light microscopy (figure 3.5), 18.2% of Eudragit L 100 and 10% of PVP 360 gave particle-free fibers (figure 3.5). Both polymers gave a thick, consistent mat of fibers which was easy to produce and peel from the collector.

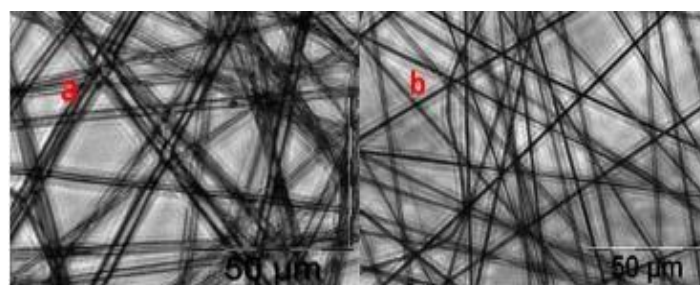


Figure 3.5. Light microscopy of electrospun fibers. a) Fibers from an 18.2% solution of Eudragit L 100 in DMAc and MeOH (1:5) and b) a 10% solution of PVP-360 in MeOH. The electrospinning conditions for these samples are given in table 3.2. The flow rate used for both samples was 0.5 mL/hr.

Following these preliminary preparations, solutions of PVP 360 in DMAc, EtOH and MeOH were electrospun to select the best solvent for production of fibers. Images from light microscopy of electrospun preparations of PVP alone and with 1% hemin in these solvents are shown in figure 3.6.

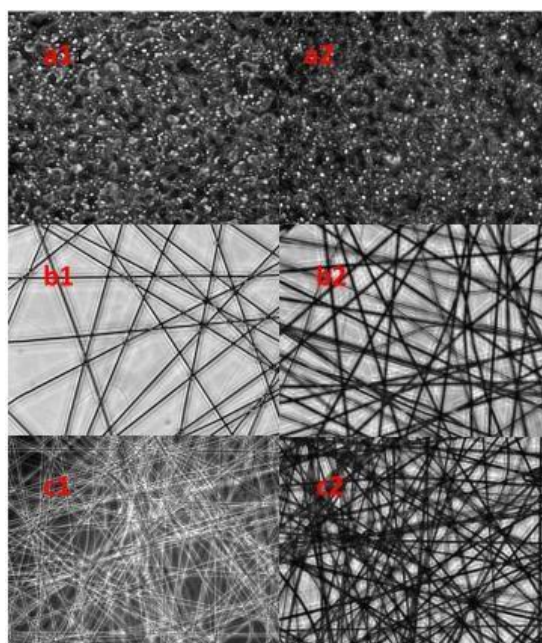


Figure 3.6. Effect of solvent on the quality of PVP-360 fibers produced alone and with 1% hemin by electrospinning. The electrospinning conditions for these samples are given in table 3.1. Solvents used were: a1 and a2 (DMAc), b1 and b2 (EtOH) and c1 and c2 (MeOH).

As seen in the light microscopy images, PVP could successfully be electrospun into fibers from solutions prepared in MeOH and EtOH but not DMAc. Because hemin

was found to be more soluble in MeOH compared to EtOH, MeOH was chosen as a solvent for PVP. The electrospinning conditions for the samples shown in figure 3.6 are given in table 3.1.

Electrospinning was carried out at four different flow rates (0.5, 0.75, 1.0 and 1.5 mL/hr) for both Eudragit L100 / hemin solutions and PVP / hemin solutions. The details of all experimental conditions are given in table 3.2.

10% PVP 1% Hemin in methanol				
S.no	Flow rate (mLhr⁻¹)	Distance (cm)	Voltage (kV)	Observation
1	0.5	14	12.22	Electrospinnig
2	0.75	14	14.12	Electrospinnig
3	1.0	14	14.12	Electrospinnig
4	1.5	14	14.12	Electrospinnig
5 PVP ALONE	1.0	14	8.18	Electrospinnig
18.2% Eudragit 0.5% Hemin prepared in a mixture of methanol and DMAc (5:1)				
1	0.5	14	14.29	Electrospinnig
2	0.75	14	13.99	Electrospinnig
3	1.0	14	16.01	Electrospinnig
4	1.5	14	16.01	Electrospinnig
5 Eudragit 18.2% alone	0.5	14	14.29	Electrospinnig

Table 3.2. Electrospinning conditions of PVP-Hemin 1% and Eudragit-Hemin 0.5% at different flow rates. The voltages of the samples were adjusted until the needle stopped dripping.

Scanning electron microscopy (SEM) was used to assess fiber or particle quality, including the degree of uniform and homogeneous fiber/particle appearance, and fiber/particle diameter (Alyami *et al.*, 2017; Oréfice *et al.*, 2001; “Imaging fibers

with a SEM," n.d.). The diameter of particles or fibers was measured from the SEM images using image J (Hotaling *et al.*, 2015).

SEM and light microscope pictures of PVP-360 1% hemin fibers obtained under different flow rates (except 0.5 mL/hr in table 3.2), and the frequency distribution graphs of fiber diameter, are shown in figure 3.7.

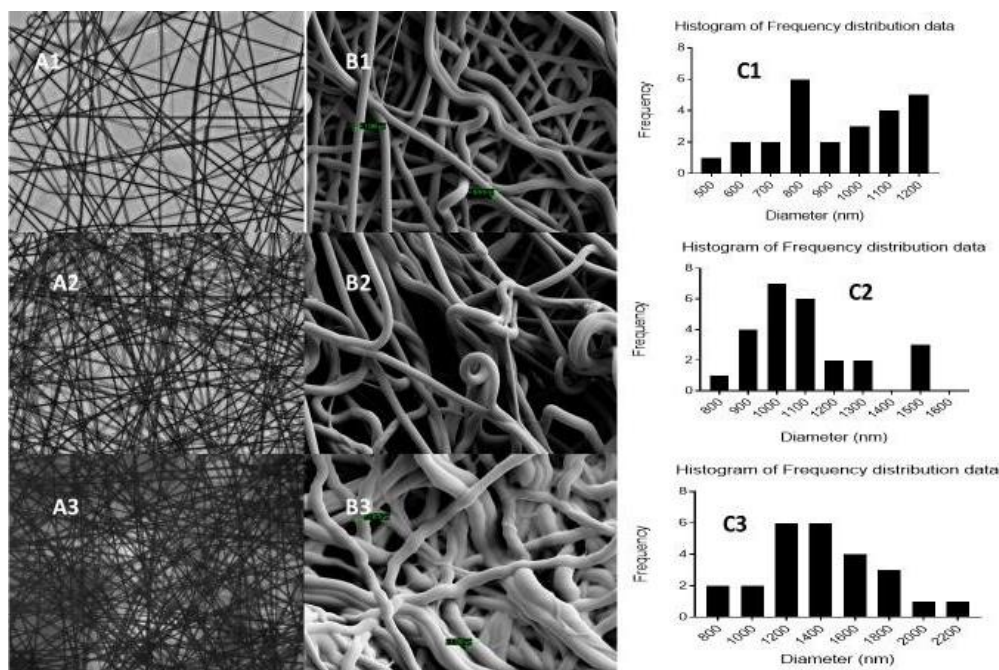


Figure 3.7. Effect of flowrate [layer 1(0.75mL/hr), 2(1 mL/hr) and 3(1.5mL/hr)] on quality of PVP-360 1% Hemin fibers. Panels: A) Light microscope images (100 x) B) SEM (mag 10k x) and C) histogram showing frequency distribution of fiber diameters from 25 fibers (as total number of fibers in each SEM are less) in each SEM image.

Electrospinning of 10 % PVP-360 / 1% hemin solutions in MeOH produced smooth, bead-free fibers at flow rates of 0.75, 1.0 and 1.5 mL/hr. According to the SEM images, the diameter of individual fibers varies with even one fiber at different points having different diameters, especially at the highest flow rate 1.5 mL/hr. The mean diameters (in nm) and standard deviation of fibers for all flow rates from lower to higher are 922.8 ± 203.4 , 1111 ± 187.0 and 1409 ± 326.9 . The means show that lower flow rates gave smaller diameters. The result showed that the standard deviation of diameter of 1.0 mL/hr flow rate fibers are varying least from the mean fiber diameter. It means that the fibers in 1.0 mL/hr sample is more homogenous than those produced at other flow rates. The D'Agostino & Pearson, normality tests were carried out with GraphPad prism for the frequency distributions shown in figure 3.7. All three samples passed the normality test. It means the mean, median

and mode of samples are almost the same, and the data is normally distributed, and samples are true representative of the whole population.

Figure 3.8 shows the light microscope image, SEM image, and frequency distribution graph of fibers produced from 18.2% Eudragit in MeOH:DMAc (5:1). Details of experimental conditions for these samples are given in table 3.2.

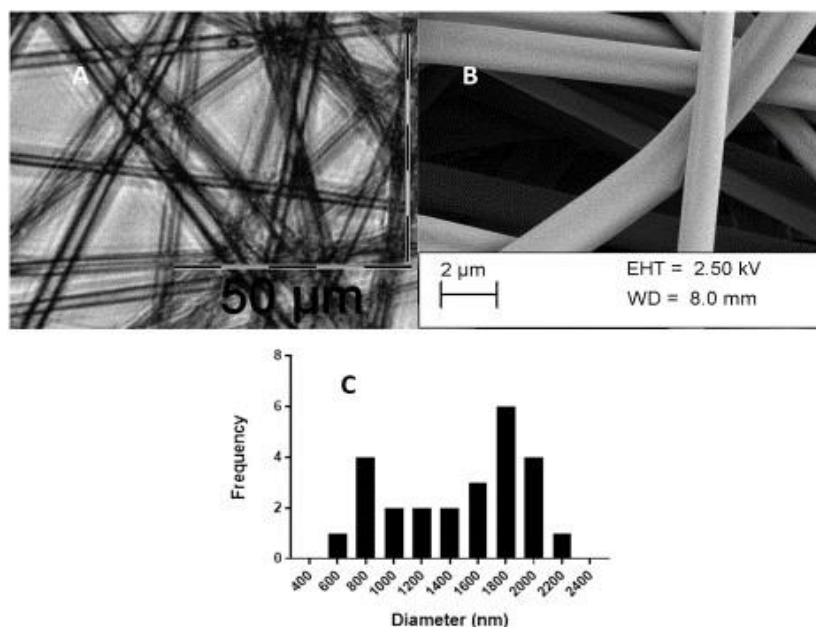


Figure 3.8. Analysis of Eudragit L 100 alone. Panels: A) Light microscope image (mag 400 x) B) SEM (mag 10k x) and C) histogram of fiber diameter frequency distribution from 25 fibers in SEM image (25 fibers were selected as total number of fibers in SEM are less).

The mean diameters (nm) and SD of Eudragit L 100 fibers shown in figure 3.8 is 1480.5 ± 477.5 nm. The sample passed the D'Agostino & Pearson normality tests, which means that the data has a normal distribution and the fibers are homogenous. The frequency distribution graph is not bell shaped, and this may be due to the smaller sample size used.

Figure 3.9 shows the light microscope image, SEM images, and frequency distribution graphs of fibers produced from 18.2% Eudragit / 0.5% hemin in MeOH:DMAc (5:1) at four different flow rates. Details of experimental conditions for these samples are given in table 3.2.

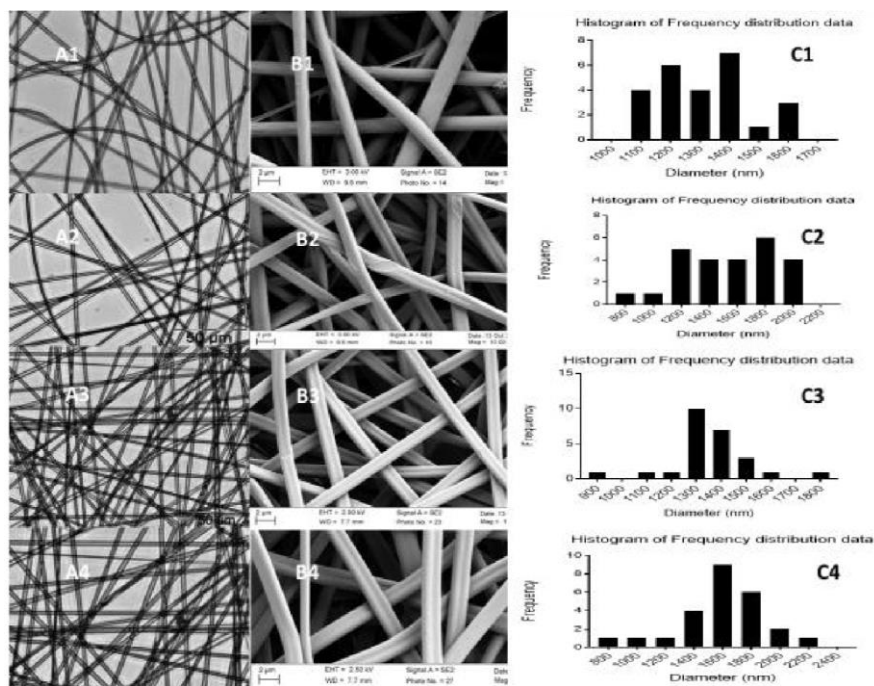


Figure 3.9. Effect of flowrate [layer 1(0.5 mL/hr), 2(0.75mL/hr), 3(1 mL/hr) and 4(1.5mL/hr)] on quality of Eudragit L 100 0.5% Hemin fibers. Panels: A) Light microscope image (mag 100 x) B) SEM (mag 10k x) and C) histogram of fiber diameter frequency distribution from 25 fibers (as the total number of fibers in SEM are less) in each SEM image, at different flow rates. The diameter of fibers increased with increasing flow rate except the sample collected at 0.75 mL/hr flow rate.

As shown in panels B of figure 3.9, fibers obtained from Eudragit L 100 and hemin are smooth, homogeneous, uniform and particle free for each flow rate. The SEM images reveal the fibers to be flat with a depression in the middle, as though two fibers are joined, especially at flow rates 0.75, 1.0 and 1.5 mL/hr. The mean diameters and SD of all flow rates (0.5, 0.75, 1 and 1.5 mL/hr) from lower to higher are 1320 ± 152 , 1561 ± 326.6 , 1348 ± 157.6 and 1608 ± 314.8 nm, respectively. According to the mean, the fibers with smallest diameter are produced at the lowest flow rate, 0.5 mL/hr. On the other hand, the mean diameter of 1 mL/hr flow rate fibers is lower than those produced at 0.75 mL/hr, confirmed by physical appearance of the fibers in the SEM images. The standard deviation is highest for 0.75 mL/hr flow rate, which means the diameter of fibers of 0.75 mL/hr flow rate vary more from mean than other flow rates. As with the PVP-360 Hemin samples the D'Agostino & Pearson normality test was carried out for the four Eudragit hemin samples as well. All four samples with four different flow rates passed the normality tests, which means that the data has a normal distribution and the fibers are homogenous. The diameter of Eudragit L 100 fibers are larger than Eudragit L

100 / 0.5% hemin fibers, except for 0.75 and 1.5 mL/hr flow rate samples, as shown in figure 3.9. This is a similar result to PVP fibers (figure 3.7) and PVP/hemin fibers (figure 3.10). It means hemin is affecting the diameter of polymer fiber. In comparison to PVP fibers, Eudragit L100 fibers are thicker, perhaps because of their dual nature.

The focus of this project was to create a formulation that can deliver iron safely in the small intestine. Central to this is a requirement that the formulation can dissolve rapidly in the conditions found in the small intestine, especially the pH, but with the normally insoluble hemin maintained in a soluble form. Accordingly, before proceeding further with the development of the fibers, preliminary dissolution tests were carried out on PVP / hemin and Eudragit /hemin fibers. If the fibers did not dissolve easily, or released free hemin after dissolution, then they would not be useful. The solubility of both types of fibers was checked in PBS (isotonic phosphate-buffered saline). PVP / hemin fibers dissolved readily within 10 minutes, but in contrast Eudragit / hemin fibers took 2-3 days to dissolve. These preliminary tests showed that PVP is a better choice for a hemin formulation because the digestion time of drugs in the gastrointestinal tract is 10 hours (Lee *et al.*, 2014) and if the formulation does not dissolve in that time it will be excreted without absorption. Accordingly, further development focused on PVP fibres.

To find out the extent to which hemin can be incorporated into PVP-360 fibers, the hemin was added to create a 50-fold range of percentages, 0.1, 0.25, 0.5, 0.75, 1, 5% (w/w) final concentration of hemin in the fibres, using 10% PVP-360 to prepare fibers. The experimental conditions for these samples are given in table 3.3.

10% PVP with different % Hemin				
S. no	% Hemin	Flowrate (mL hr⁻¹)	Distance (cm) tip to collector	Voltage (kV)
1	0.1	0.75, 0.5	14	12.81 14.96
2	0.25	0.5	14	14.26
3	0.5	0.5, 0.25	14	15.30 18.11
4	0.75	0.5	14	13.75
5	1.0	1.0	14	14.12
6	5.0	0.75, 0.5	14	11.20 18.38

Table 3.3. Electrospinning conditions of PVP 360 with different % hemin.

Fibers were successfully obtained at all concentrations and images from light microscopy and SEM, together with frequency distribution histograms, of PVP-360 fibers with 0, 0.25, 0.5, 1.0 and 5.0% hemin are shown in figure 3.10.

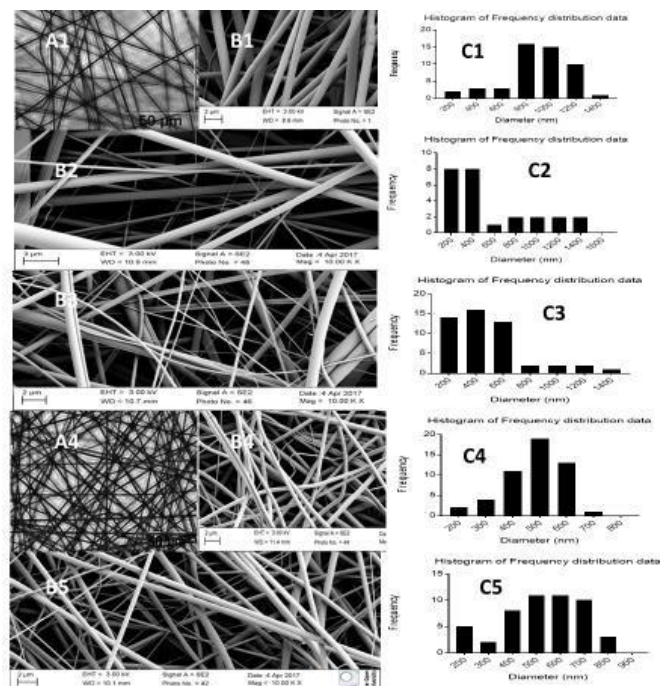


Figure 3.10. Analysis of PVP-360 fibers with a range of hemin [layer 1 (0%), 2(0.25%), 3(0.5%), 4(1%) and 5(5%) content. Panels: A) image from light microscopy, B) SEM, C) histogram of frequency distribution from 50 fibers diameter in each SEM image, except for 0.25% hemin containing PVP fibers i.e. for 25 fibers (because the total number of fibers in the SEM image are few). The diameters are much smaller in comparison with PVP with 1% hemin. The electrospinning conditions of the samples are given in table 3.3.

PVP fibers with 0.1 and 0.75 % are not presented in figure 3.10. As shown in figure 3.10, fibers of PVP360 / 0.25% hemin are mostly of diameter 200-400nm, these fibers have wide range of fiber diameter, some of them are thick but, for PVP-360 / 0.5% hemin are mostly from 200 to 600 nm. PVP-360 fibers are of larger diameter (881.9 ± 243 nm) than PVP-360 / hemin fibers. The mean diameter and SD of PVP-360 / hemin (0.25, 0.5, 1 and 5%) fibers are 579.1 ± 407.8 , 489.2 ± 267.7 , 479.1 ± 102.8 , 525.6 ± 160.3 nm, respectively. The diameter of PVP-360 / 1% hemin fibers have the least standard deviation, indicating a greater homogeneity than the other preparations. PVP-360 / 0.5% hemin failed the normality test mentioned earlier. PVP-360 only and with 0.25, 1 and 5% hemin passed the normality test. A normal distribution can be interpreted as an indicator of homogeneity, with a unimodal distribution. There is a possibility of a bi- or even tri modal distribution for the 0.25 and 0.5% fibers – this could be caused by fibers being dual or triple, visible through electron micrograph.

All the work described so far was carried out with PVP-360. To extend the work further it was decided to assess smaller forms of PVP, and work with PVP-40, average mw 40,000 Da, and PVP-10, average mw 10,000 Da. One of the reasons for working with all three forms of PVP is to compare their toxicity and uptake of the iron carried in hemin, in cultured cells, which will enable selection of a better carrier for hemin. Some work was already done on PVP-10 and PVP-40 in the initial stages of this project, so it was already known that these two-molecular weights can give fiber free particles, and so were included for comparison with PVP-fibers. 4% PVP-10 and 5% PVP-40 solutions were selected because previous work (in chapter 2 in section 2.3.1) had shown that they gave round fiber-free particles.

A 4% PVP-10 solution in methanol was selected for particle formation. The experimental conditions of electrospaying for PVP-10 alone and PVP-10 with 1% hemin are given in table 3.4.

4% PVP-10 in methanol					
S.no	% Hemin (w/v)	Flow rate (mLhr⁻¹)	Distance to collector (cm)	Voltage (kV)	Humidity (%)
1	0	0.5	14	17.16	24
2	1	0.5	14	17.16	23

Table 3.4. Electrospaying conditions for PVP 10 alone and with 1% hemin.

SEM and light microscope images of particles obtained under the conditions mentioned in table 3.4 are given in figure 3.11.

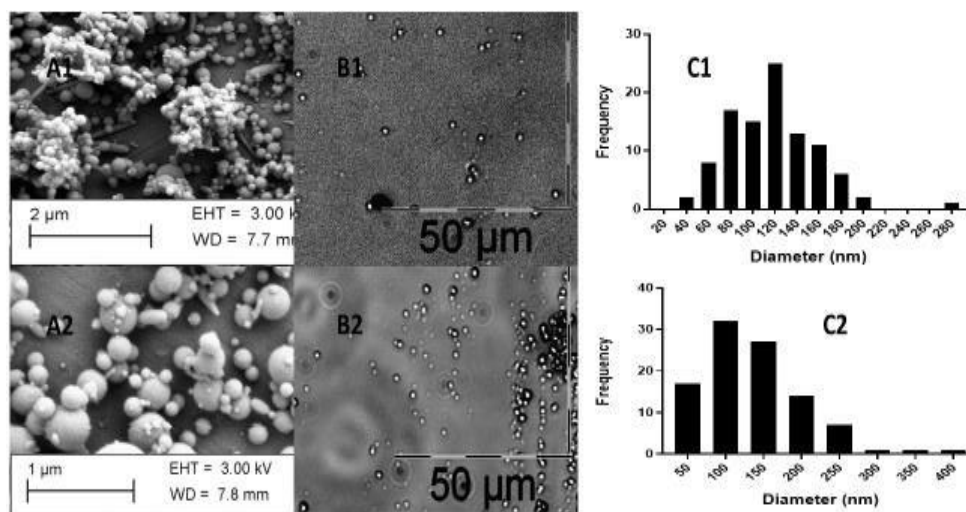


Figure 3.11. Analysis of PVP-10 particles alone (layer 1) and with 1% hemin (layer 2). Panels: A) SEM (PVP-10 alone, mag 25k x, PVP-10 1%H mag 50k x), B) light microscope image (mag 100 x), C) histogram of frequency distribution from 100 particles diameter in each SEM image. The electro spraying conditions are given in table 3.4.

The SEM images in figure 3.11 clearly showed the successful production of fiber-free particles under the conditions given in table 3.4. The light microscope pictures showed only a few particles in both samples, which means that the particles are too small to be visible under the resolution of a light microscope. The mean diameters (in nm) and standard deviation of PVP-10 and PVP-10/1% hemin nanoparticles were 118.2 ± 39.5 and 137.4 ± 67.0 . The D'Agostino & Pearson, normality test was carried out with GraphPad prism for the frequency distributions in figure 3.11. Both, PVP-10 nanoparticles, and PVP-10/1% hemin nanoparticles passed the normality test. In contrast to the outcome of hemin containing PVP-360 fibers (figure 3.7), the hemin containing PVP-10 nanoparticles mean diameter is larger than PVP-10 nanoparticles. As seen in the SEM images, PVP-10 nanoparticles have narrower range of size (40-280 nm) compared with PVP-10/1% hemin nanoparticles.

After working on PVP-10, it was found that the electro spraying was not productive (low yield) and it was difficult to remove particles from the foil. It was decided to make particles from PVP-40, which had been done previously successfully (chapter 2 in section number 2.3.1). So, 5% of PVP-40 was selected for particle production as it gave round, fiber-free particles. The electro spraying conditions for PVP-40 only and PVP-40 / 1% hemin are given in table 3.5 and examples of particles are shown in figure 3.12.

5% PVP 40 in methanol				
S.no	% Hemin (w/v)	Flowrate (mLhr ⁻¹)	Distance to collector (cm)	Voltage (kV)
1	0	0.5	14	12.25
2	1	0.5	14	14.20

Table 3.5. Electro spraying conditions of PVP 40 alone and with 1% Hemin.

The SEMs of the samples mentioned in table 3.5 are shown in figure 3.12.

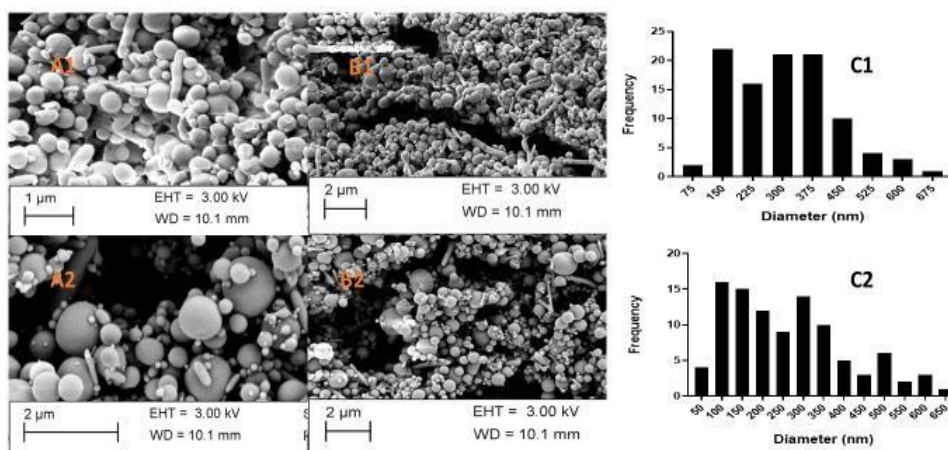


Figure 3.12. Analysis of PVP-40 (layer 1) and PVP-40/ 1% hemin (layer 2) particles. Panels: A) SEM (PVP40 alone, PVP-40 1%H), mag 25k x, B) SEM (PVP-10 alone, PVP-10 1%H), mag 10k x), C) histogram of frequency distribution from 100 particles diameter in each SEM image. The electro spraying conditions are given in table 3.5.

The images in figure 3.12, show that it is possible to prepare particles from PVP-40. After successful production of PVP-40 particles, PVP-40/hemin particles were made. Firstly, 1% hemin was added to a 5% solution of PVP-40 in MeOH. The proportion of PVP-40 to hemin was 50:1.

The mean diameters (in nm) and standard deviation of PVP-40 and PVP-40/1% hemin nanoparticles were 303.3 ± 125.0 and 264.3 ± 147.6 . The hemin containing PVP-40 nanoparticles' mean diameter is slightly smaller by about 10% than that of PVP-40 nanoparticles, but the standard deviation is larger. Some of the particles are elongated in shape for both PVP-40 and PVP-40/1% hemin particles (figure 3.12).

Dissolution tests for PVP-10 hemin and PVP-40 hemin were carried out and are discussed later (figure 3.22 B and C).

Different percentages of PVP-40 were tested to find out whether it was possible to produce fibers. 15 % PVP-40 also gave particles, as shown by SEM analysis in figure 3.13.

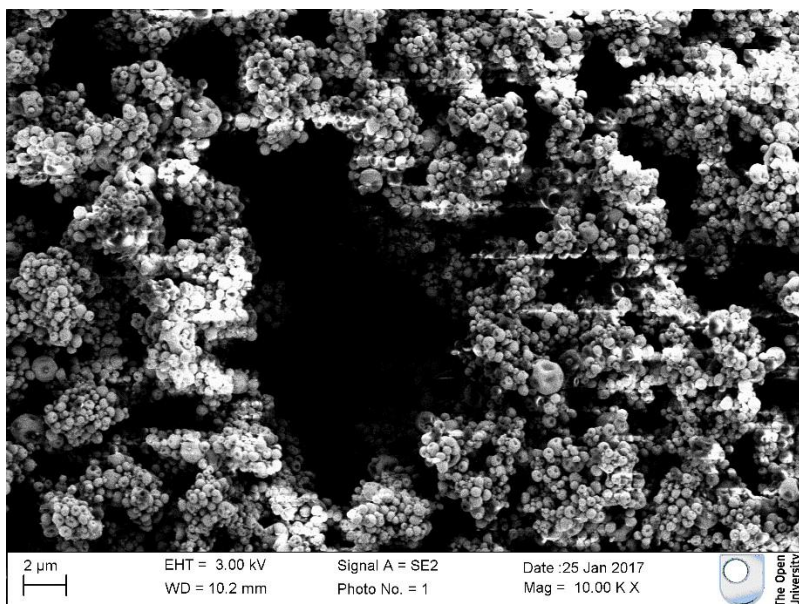


Figure 3.13. 15 % PVP-40 Nanoparticle SEM.

Most of the particles in figure 3.13 are donut shaped. In comparison to 15 % the 25 % PVP-40 solution gave mixture of particles and fibres. The light microscope picture of a sample is given in figure 3.14.

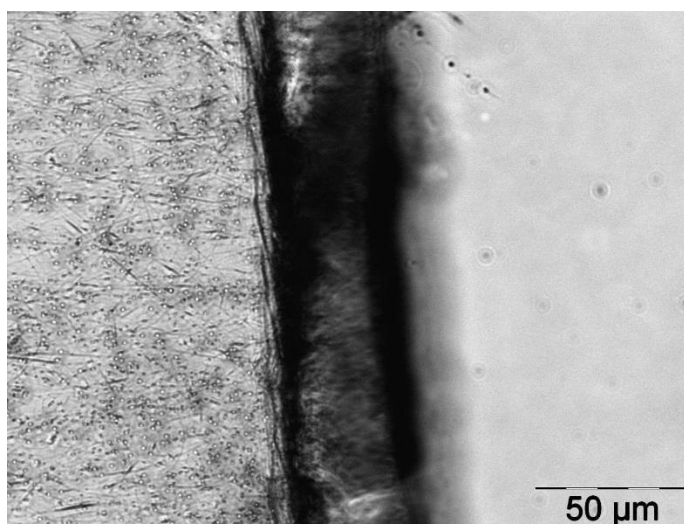


Figure 3.14. Material produced after Electrospaying/ Electrospinning of 25% PVP-40. Light microscope image at 400 x. The image is enlarged to confirm the presence of fibres. The picture shows the microscope slide part on right side and coverslip

with material on left side to avoid misinterpretation due to dust on the slide and lens.

After this 40% PVP-40 was electrospun, and this showed a significant presence of fibres. The light microscope picture of 40% of PVP-40 at 400 x is given in figure 3.15.

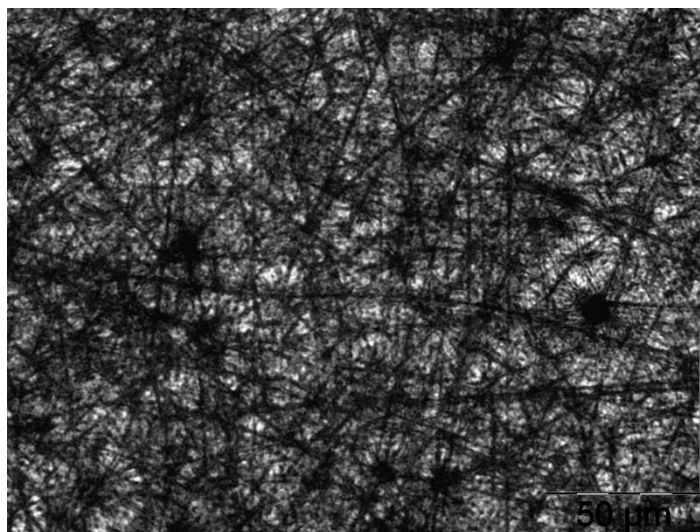


Figure 3.15. 40% PVP-40 Fibres. Light microscope image at 400 x. The electrospinning conditions of the sample are given in table 3.6.

Figure 3.15 clearly shows the presence of fibres, but to confirm whether this preparation still contained particles, SEM analysis was necessary. The SEM images of electrohydrodynamically-formulated material prepared from 25, 40 and 55% (w/v) solutions of PVP 40 are shown in figure 3.16.

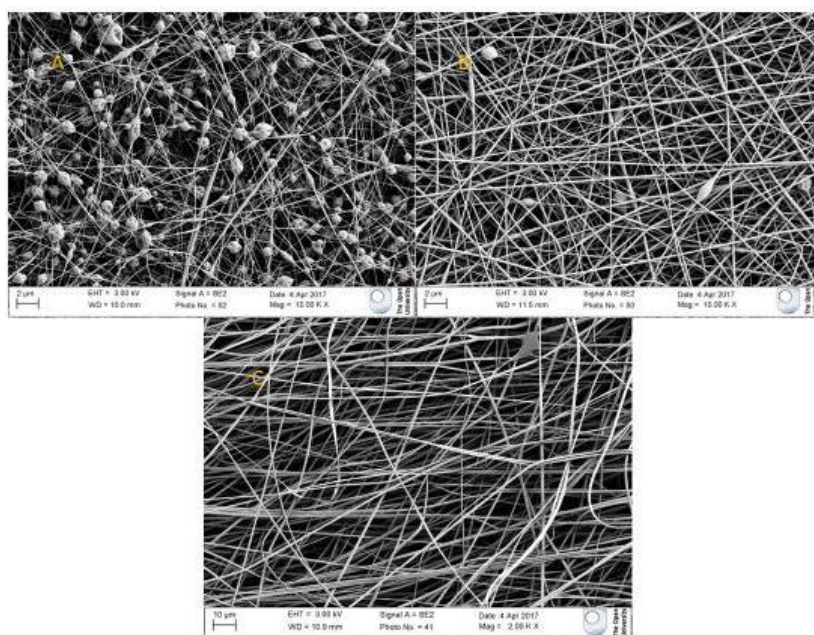


Figure 3.16. Electrospinning of different percentages of PVP-40. SEM of fibers obtained from A) 25 (mag 10k x), B) 40 (mag 10k x) and C) 55% (mag 2k x) PVP-40.

The electrospinning conditions of the samples are given in table 3.6. The scale in panels A, B and C are 2, 2 and 10 μM , respectively.

According to the SEM image in figure 3.16, the 25% (w/v) solution of PVP-40 produced particles containing fibers but the other two percentages produced fibers which were free from particles. The 40% solution produced fibers with three particles in the whole image (figure 3.16B), and no particles were observed in the fibers produced from the 55% solution (figure 13.6C). The diameter of fibers obtained from 25, 40 and 55% of PVP-40 were approximately 200, 300 and 3000 nm respectively, according to the scales shown on the SEM images. As the percentage of the polymer increased, the viscosity (seen by observation) of the spinning solution also rises ultimately resulting in thicker fibers. The conditions of electrospinning or electro spraying for PVP-40 for 15, 25, 40 and 55% solution in methanol are given in table 3.6.

PVP-40 in methanol					
S.no	% PVP-40 (w/v)	Flowrate (mL.hr⁻¹)	Distance to collector (cm)	Voltage (kV)	Humidity (%)
1	15	0.5	14	14.64	23
2	25	0.5	14	16.25	24
3	40	0.5	14	18.22	24
4	55	0.5	14	17.20	23

Table 3.6. Experimental conditions of electrospinning/electro spraying different percentages of PVP40 solution in methanol.

If 1% hemin is to be incorporated into the 55% (w/v) solution of PVP-40, this would require a 5.5% (w/v) solution of hemin in MeOH which could be diluted 10x with 60% (w/v) PVP-40 to produce an electrospinnable solution of 55% (w/v) PVP-40 hemin with 0.55% (w/v) hemin, with a ratio of PVP-40: hemin of 100:1 in the fibers. The solubility of hemin in methanol is about 10 mg/mL or 1% (w/v) and when a 5% hemin formulation was made with 10% PVP-360 methanol the hemin did not dissolve completely and settled in the bottom. This made it impossible to make a

formulation of PVP-40 fibers with 1% hemin. In future work it might be worth trying PVP-40 at 45% and 50% as well.

In the next section the absorption studies carried out on solutions of PVP-360, PVP-40 and PVP-10 containing hemin will be discussed in detail.

3.4.2 Absorption spectroscopy

Spectra of fiber of PVP/ hemin solutions were measured to see if the spectral properties of hemin were altered by PVP, to measure the extinction coefficient of hemin in PVP, and to assess the molecular form of hemin – monomer or dimer in the PVP complex. Hemin solubilizes in aqueous solution by complexing with PVP, and it is found as a monomer in a neutral solution of PVP-hemin complexes (Inamura *et al.*, 1989).

The absorption spectra obtained for hemin formulations with PVP-360, PVP-40 and PVP-10 are given in figure 3.17 A, B and C, respectively. In all cases a concentration of 100 μ M hemin was prepared for the three groups of formulations. For example, 65.2 mg of PVPH100 was dissolved in 10 mL of PBS, to achieve 100 μ M hemin, since hemin has a MW 652 Da.

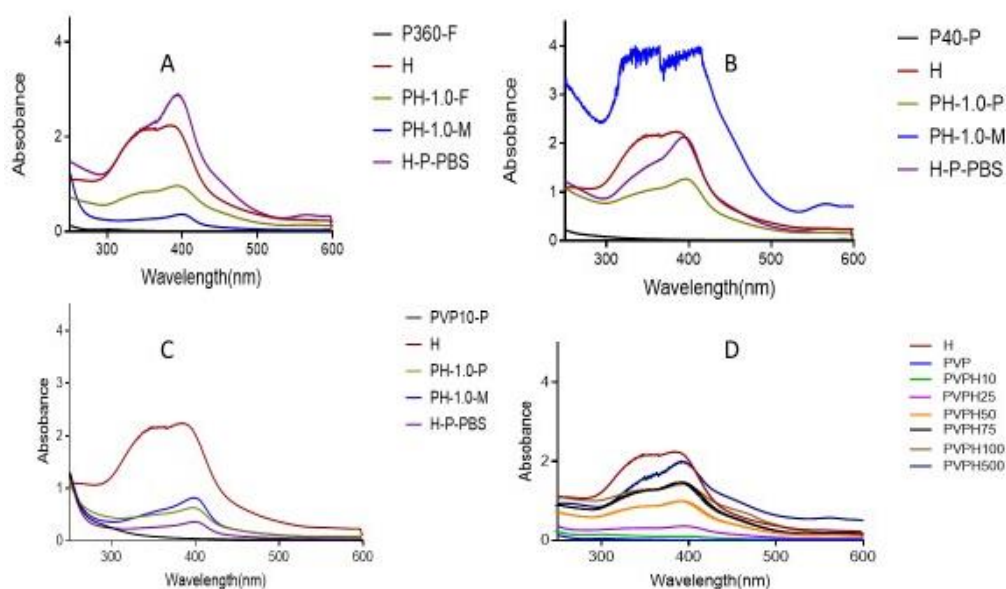


Figure 3.17. Absorption spectra of hemin formulations made with three different forms of PVP. A) PVP-360 B) PVP-40 C) PVP-10 all with 1% hemin and D) PVP 360 with different percentages of hemin. Each image A, B and C includes PVP-only fibers or particles,

a physical mixture of PVP and hemin, hemin dissolved in a PVP solution, hemin alone, and PVP-H samples.

The λ_{\max} for all formulations or mixtures containing hemin, and for hemin alone, was found to be 400 nm, which was also found by Han *et al.* (2013). This value of λ_{\max} was used in dissolution experiments to measure formation of soluble hemin-PVP complexes at different time intervals (section 3.4.3). All formulations or mixtures containing hemin and hemin alone showed a shoulder in the absorption spectrum with a peak around 360 nm. This is indicative of a state of dimerization, known to occur to hemin in aqueous media (Kremer, 1989; Golnak *et al.*, 2015). To confirm this interpretation, spectra of hemin were taken in solvents in which hemin is known to be monomeric, DMSO and MeOH (Figure 3.18B). Organic solutions of hemin have a sharp Soret band, indicating that the hemin is monomeric (Brown and Lantzke, 1969). In the same series of measurements spectra were also taken of PVP-360 hemin fibers dissolved in PBS (phosphate-buffered saline) and HCl (figure 3.18A).

As expected, a single sharp Soret band at 400nm was found with solutions of hemin in DMSO or MeOH (Figure 3.18B) whereas a broad Soret band, with peaks at 360 and 400nm were found for solutions of PVP-hemin fibers dissolved in PBS or 2M HCl (figure 3.18A).

The absorbance at λ_{\max} of PH-1.0-F is low as compared to hemin in pre-dissolved PVP and hemin in PBS, as shown in figure 3.17A. Hemin in PBS did not dissolve completely. Similarly, the physical mixture of PVP and hemin and hemin added to PVP solution in PBS did not dissolve completely, but more than hemin alone in PBS. Absorbances at around 400 nm in the case of hemin formulations of PVP-40 and PVP-10 are lower than of hemin in pre-dissolved PVP and hemin in PBS. So, it was important to compare physical mix, hemin in pre-dissolved PVP and hemin in PBS by using DLS, to find out if it is worth using controls as hemin formulation instead of making fibers or particles.

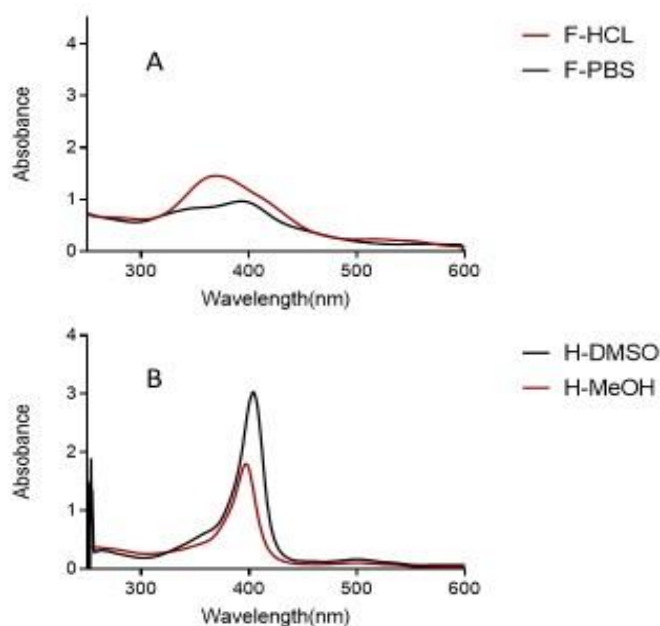


Figure 3.18. UV-visible spectra of A) PVPH100 (F-HCL) in HCl and PBS (F-PBS) or B) hemin in MeOH or DMSO. The concentration of hemin in all the solutions is 100 μM .

Three different solutions, pH 2, SIF and PBS, were made to study simulated release of hemin from PVP-hemin nanofibers in the stomach, intestine and blood respectively. The UV-visible spectra obtained from the three different solutions are given in figure 3.19. The absorbances were measured with and without centrifugation of each solution, to observe absorption differences due to formation of macroscopic complexes.

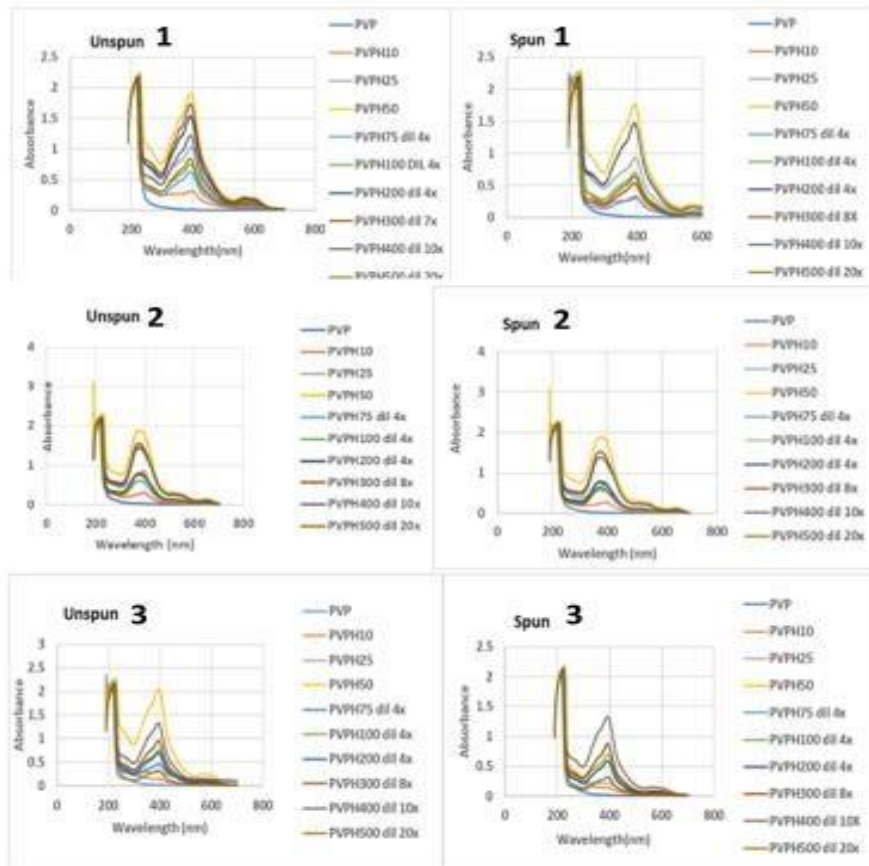


Figure 3.19 Absorption spectra of PVP-360 with different percentages of hemin in PBS (phosphate buffer saline) layer 1, pH 2 (layer 2) and SIF (layer 3) of unspun and spun samples.

The graphs (figure 3.20) were drawn between concentration of hemin and absorbance (at λ_{max}) to measure extinction coefficients for each solution. The wavelengths used were those of highest absorbance, 394.5, 376 and 394 nm for PBS, pH 2 and SIF solution, respectively. The calculation was carried out for both spun and unspun solutions.

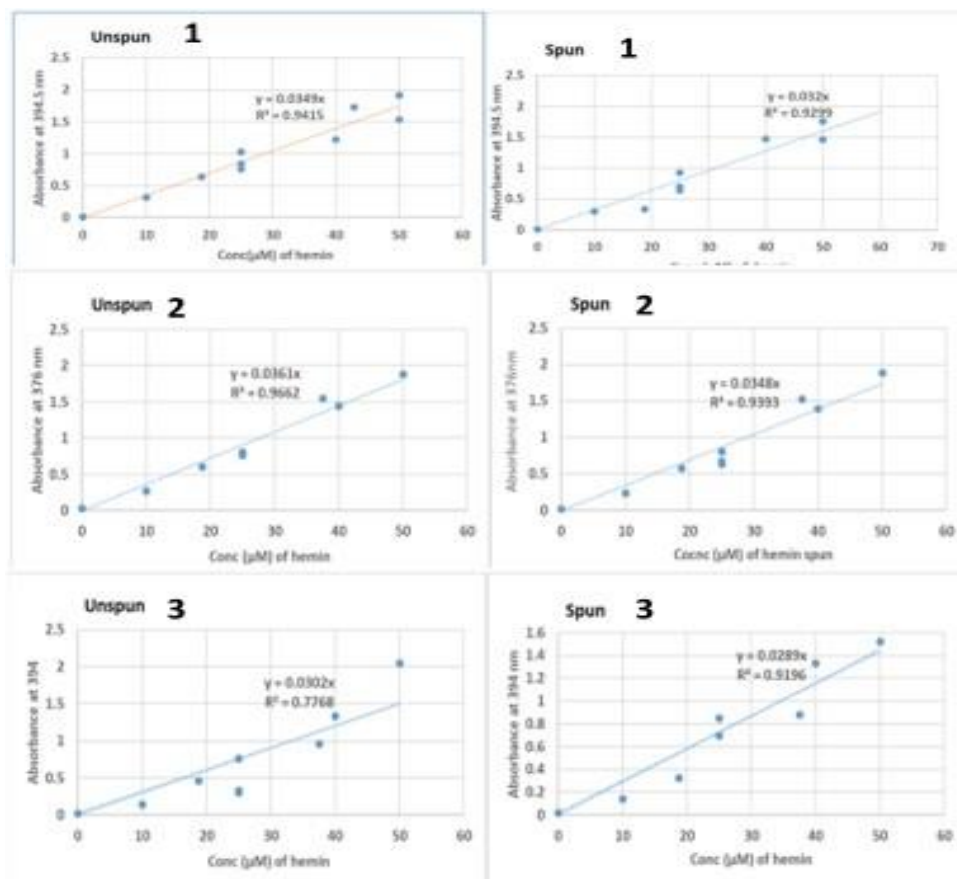


Figure 3.20. The relationship between concentration of hemin and absorbance obtained from UV-visible spectra at λ_{max} in PBS layer 1, pH 2 (layer 2) and SIF (layer 3) in both spun and unspun samples.

The molar extinction coefficient obtained from each solution (unspun and spun) is given in table 3.7.

Solution	Unspun ($M^{-1}cm^{-1}$)	Spun ($M^{-1}cm^{-1}$)
PBS at wavelength 394.5 nm	3.49×10^4	3.2×10^4
pH 2 at wavelength 376 nm	3.61×10^4	3.48×10^4
SIF at wavelength 394 nm	3.02×10^4	2.89×10^4

Table 3.7. Molar extinction coefficients obtained from hemin in PVP-hemin complexes in PBS, pH 2 and SIF solution. The extinction coefficient was found higher in pH 2 than other two solutions. The extinction coefficient of spun solution in each case is lower than normal solution.

According to data in table 3.7 the extinction coefficient of PVP-hemin complex is highest in pH 2 solution which represent the stomach in the human body. The

extinction coefficient of spun solutions is less than unspun solutions and can be attributed to formation of fine macroparticulate material. The precipitate is not immediately obvious and was first noticed when fresh solutions were left overnight. The differences in extinction coefficient could be explained by differences in solubility and or pH. Accurate measurement of the extinction coefficients will require independent measurement of iron concentrations in the solutions, instead of using estimates.

3.4.3 Dissolution studies

Dissolution tests are used to simulate the availability of the active substance (API) from a formulation and model the duration of time for complete release of the active substance from the dosage form into solution. In preliminary studies, the solubility of PVP-360-H fibers and hemin alone were compared in PBS. In the first trial a quick comparison was made between PVP-360 hemin fibers and hemin alone, dissolving in 10 mL PBS to produce a 100 μ M solution of hemin (figure 3.21). PVP-360 hemin fibers were found to dissolve rapidly and completely within 10 minutes in PBS at room temperature (figure 3.21 B), whereas hemin hardly dissolved (figure 3.21A).

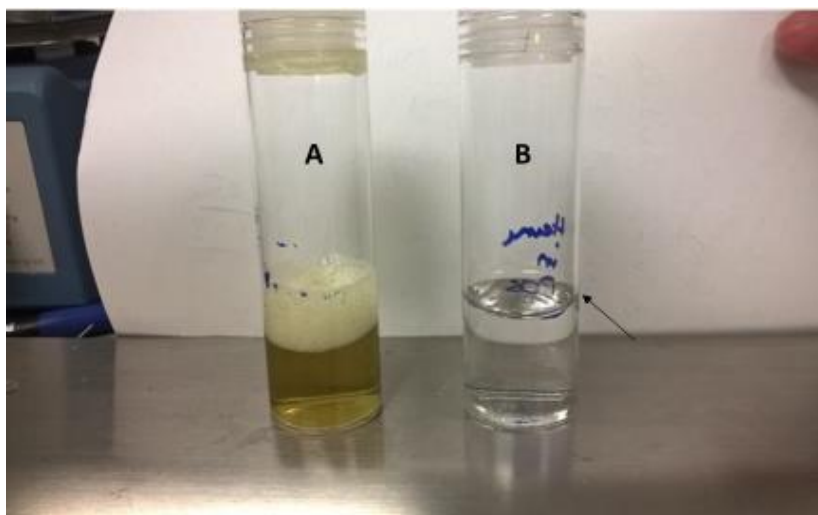


Figure 3.21. Dissolution of PH-1.0-F (A) and hemin alone (B) in PBS. The arrow indicates hemin alone in PBS is undissolved, floating at the top of the PBS.

In the next set of experiments, dissolution of PVP-360 fibers containing 1% hemin was compared with three controls: dissolution of i) a physical mix of PVP 360 and hemin powders with the same mass as the PVP and hemin components of the fibers, ii) hemin powder in PBS with PVP pre-dissolved, and iii) hemin powder alone. To make 100 μ M of hemin in 10 mL PBS, 65.2 mg PH-1.0-F was used. Control sets

were dissolved in 100 mL of PBS, whereas fibers were dissolved in 10 mL due to limited supplies as it takes a day to produce enough fibers for a single experiment in 100 mL PBS. Three sets of dissolution tests were carried out with separate preparations of fibers.

The dissolution graphs for this experiment are shown in part A of figure 3.22. The graphs confirm that hemin in fibers dissolved completely and rapidly within 10 minutes (PH-1.0-F in Figure 3.22A) whereas the physical mix (PH-1.0-M) and hemin added to pre-dissolved PVP (H-PVP 360-PBS) control formulations, took several days to completely dissolve. Hemin alone (H in Figure 3.22A) eventually dissolved to about 30 μM , over a period of six days.

The dissolution test was also carried out for a set of PVP-40 and PVP-10 formulations, with a similar outcome, that the electrospayed formulations containing hemin dissolved much more rapidly than the controls (Figure 3.22 B and C). The electrospayed formulations of PVP-40 and PVP-10 could not be weighed accurately, and PBS was added directly to material stuck on to the collecting foil, and the particles dissolved immediately. The final concentrations of hemin that were achieved were much lower than the target of 100 μM due to the inaccurate measurement of particle mass. The extinction coefficient of hemin in different forms of PVP was assumed to be the same or considered not to vary much. An attempt was made to measure iron content of dissolved hemin fiber preparations using MCP-AES, but the technique consistently produced under-estimates, and further work is needed establish conditions for accurate measurement.

It was of interest to find out the upper limit of hemin release when part of a composite in PVP-360 fibers. PVP-360 fibers were prepared with a range of hemin content 0.1, 0.25, 0.5, 0.75, 1 and 5% (w/w) and dissolved in PBS for 30 min. The data (Figure 3.22D) showed that there was limited enhancement of hemin release beyond a fiber content of 1%. This showed the saturation limit for hemin and suggests there may be no advantage in preparing fibers with more than 1% content of hemin. The relation between hemin release and percentage of hemin is not directly proportioned as shown in panel D of figure 3.22. This might be due to changes in the interaction between hemin and PVP at the higher concentrations of hemin, which lead to formation of greater proportions of macro-particulate material higher.

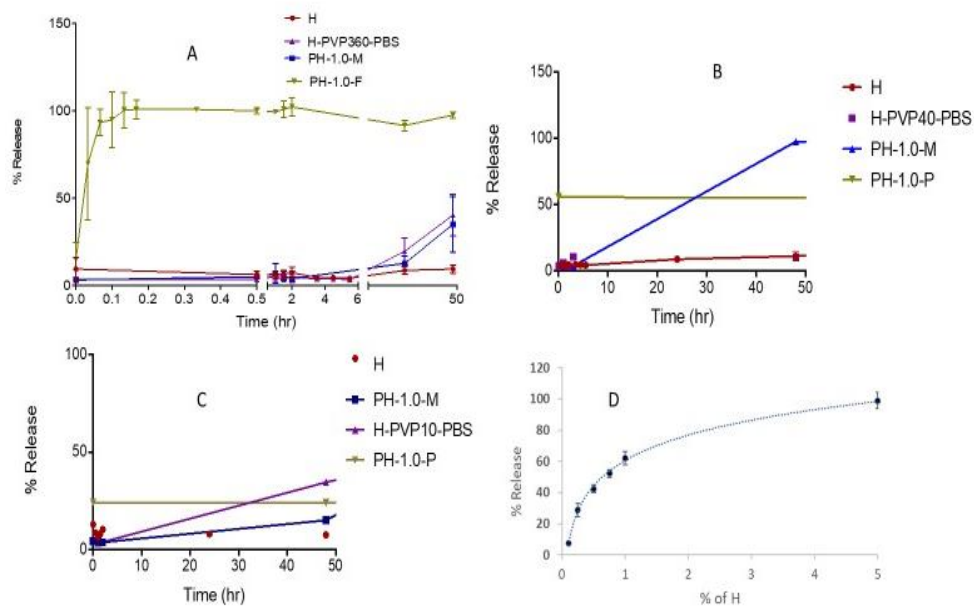


Figure 3.22. Dissolution of hemin formulations in PBS. Data are % release measured after spun at 400 nm in samples taken at indicated times. A) Set of PVP-360 formulations, B) set of PVP-40 formulations, C) set of PVP-10 formulations, D) comparison of hemin dissolved after 30 min from PVP-360 fibers with different % hemin. Data are the mean \pm SD of three independent assays carried out for all four sets.

3.4.4 Infrared (IR) spectroscopy

This technique was used to determine the potential interactions between functional groups in the sample.

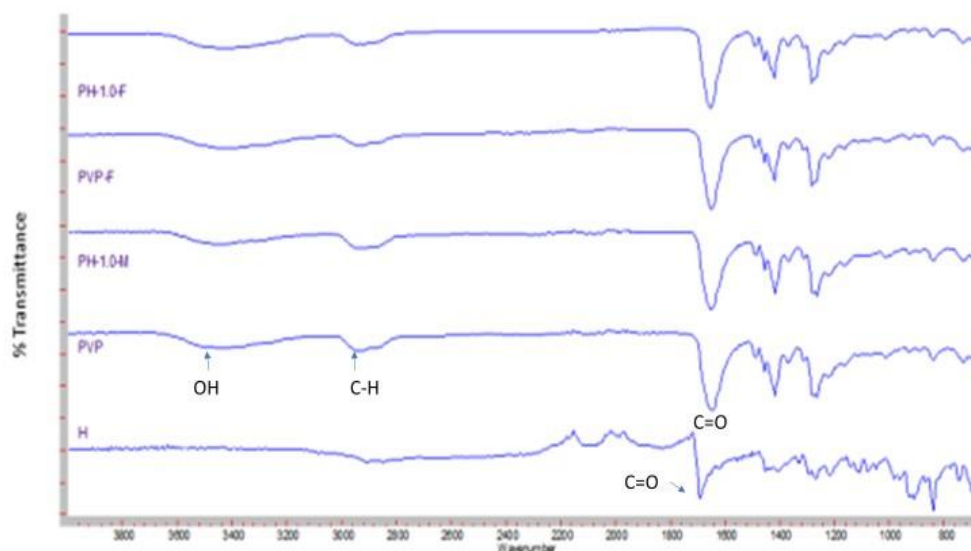


Figure 3.23. IR spectra of a PVP-360 set with 1% hemin. Comparison of IR spectra of 5 samples, PH-1.0-F, PVP-F, PH-1.0-M, PVP (polymer powder) and H (hemin).

The IR spectra of all samples containing PVP are similar. Hemin has a carbonyl peak was at 1700 cm^{-1} , and other peaks at 1272 due to C-N stretching, and 939 and 841 cm^{-1} indicating C-H bonding vibration (Zhang *et al.*, n.d.) The distinct IR spectrum of hemin is masked when mixed with PVP, due to the low content, 1%, of hemin in the formulations. The peaks present in the hemin at 3500 and 2919 cm^{-1} due to C-H and hydroxyl stretching are not found. It seemed that this technique is not useful to confirm the presence of hemin, or to study its bonding interaction with PVP.

The IR spectra of PVP fibers with 0.1-5% hemin, and spectra of PVP-40, PVP-10 particles with hemin are given in figures 3.24, 3.25 and 3.26, respectively. They all show a similar outcome, that any potential signals from hemin cannot be detected.

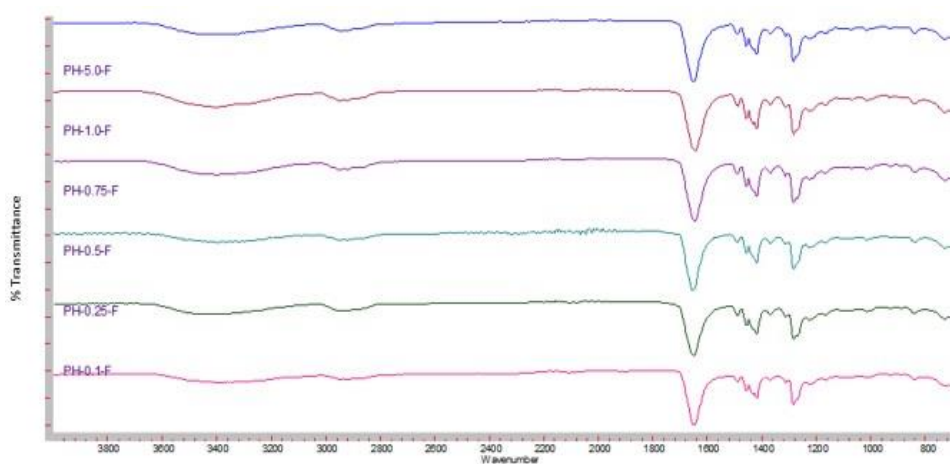


Figure 3.24. IR spectra of PVP 360 fibers containing 0.1-5% hemin.

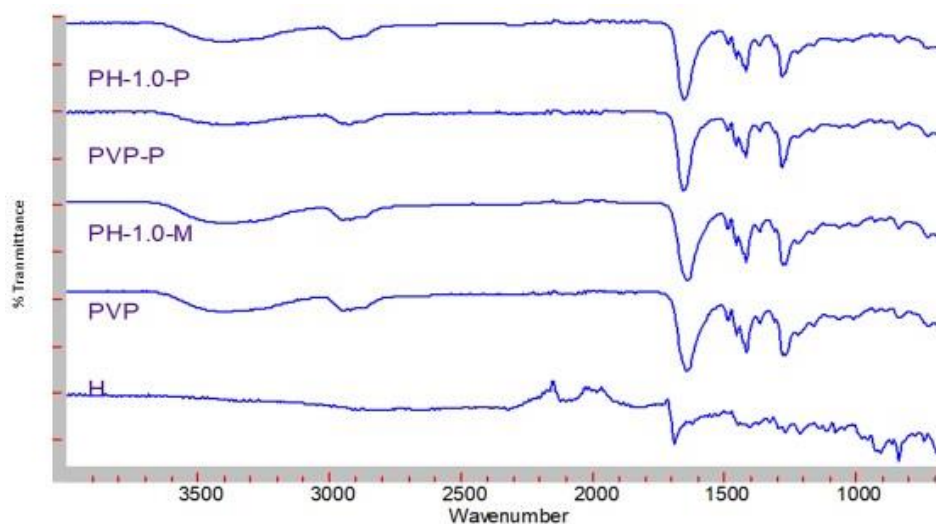


Figure 3.25. IR spectra of a PVP-10 set with 1% hemin. Comparison of IR spectra of 5 samples, PH-1.0P, PVP-P, PH-1.0-M, PVP (polymer powder) and H (hemin).

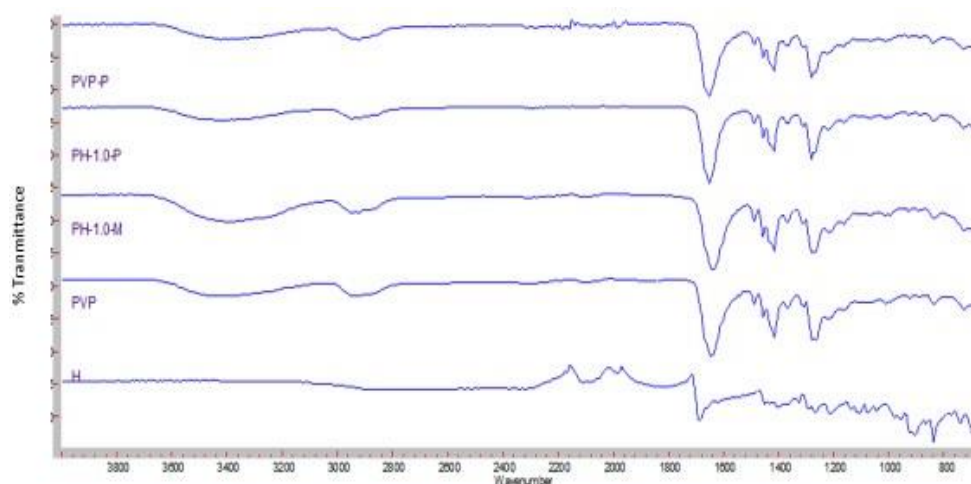


Figure 3.26. IR spectra of a PVP-40 set with 1% hemin. Comparison of IR spectra of 5 samples, PH-1.0P, PVP-P, PH-1.0-M, PVP (polymer powder) and H (hemin).

3.4.5 X-ray diffraction

X-ray diffraction was undertaken to find out the physical state of hemin embedded in PVP-360 nanofibers, whether it was distributed homogeneously or whether it was present in crystalline forms. The X ray diffraction spectrum of PVP powder and PVP-360 / hemin fiber are given in figure 3.27. In terms of the PVP, the two broad peaks at around 13° and 21° reflect the amorphous nature of PVP. The two sharp peaks seen in both XRD patterns are due to reflections from the aluminium

substrate (111) and (222) planes. Although there is a high signal to noise ratio in the PVP-hemin XRD pattern, the incorporation of hemin into PVP fibers does not show any significant sharp peaks other than those from the aluminium, suggesting that there are no crystalline regions i.e. the hemin is no longer crystalline so likely to be dispersed through the sample. However, the amorphous signals appear to have shifted slightly to lower 2θ . Unfortunately, because the machine needed maintenance only a single session of analysis was possible. Hemin alone and a physical mix of hemin and PVP powders need to be analysed and compared for completing this section. Samples need to be run for a longer time in order to reduce the signal to noise ratio.

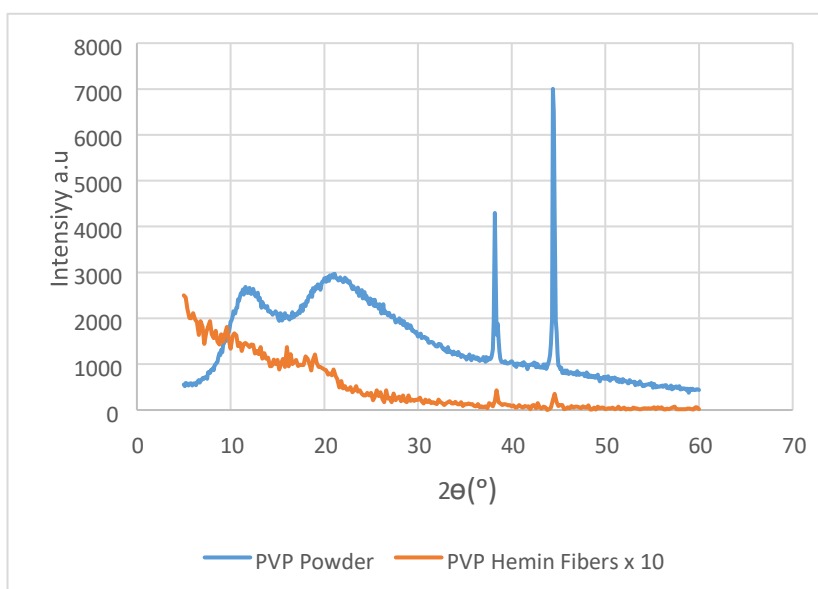


Figure 3.27. X-ray Diffraction of PVP-360 powder and PVP-360 hemin fibers

3.4.6 Energy dispersive X-ray spectroscopy (EDX)

EDX is known as energy dispersive X-ray spectroscopy, which is sometimes denoted by EDS as well, and is used for elemental analysis and distribution in a sample. It was carried out to confirm the presence of iron in samples. It was only carried out on a few samples because of equipment failure. The EDX of PVP-360 fibers alone and with 1 and 5% hemin are given in figures 3.28, 3.29 and 3.30, respectively.

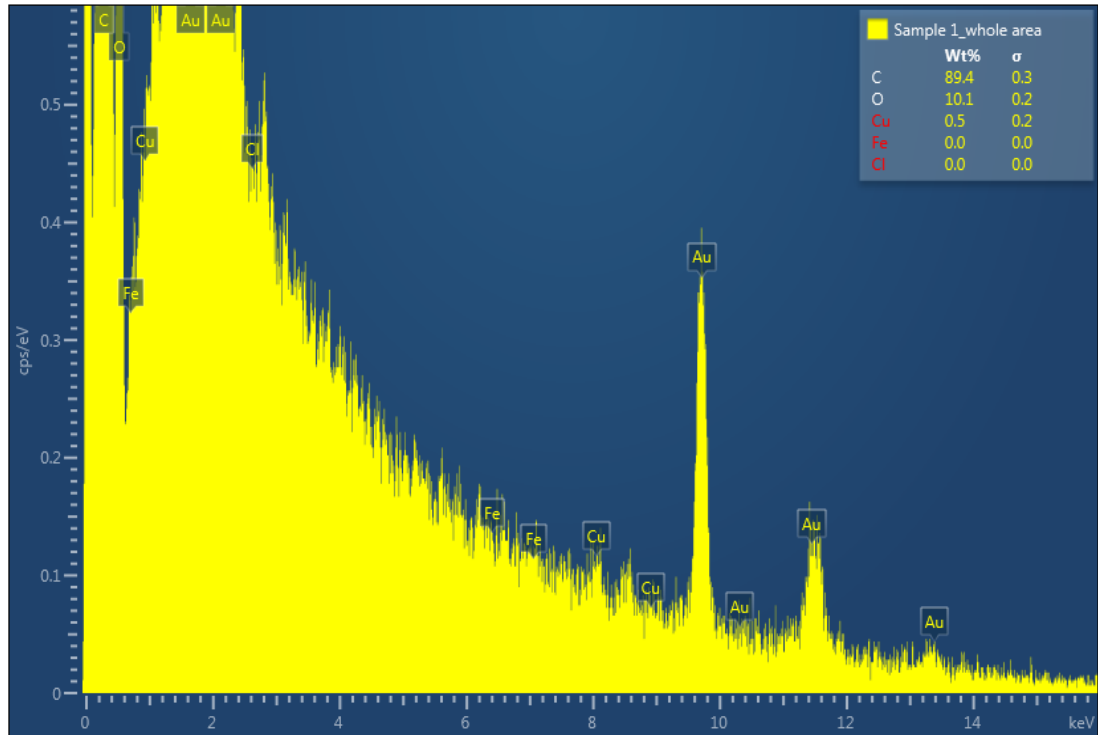


Figure 3.28. Energy Dispersive Spectroscopy analysis of PVP-360 fibers with no hemin.

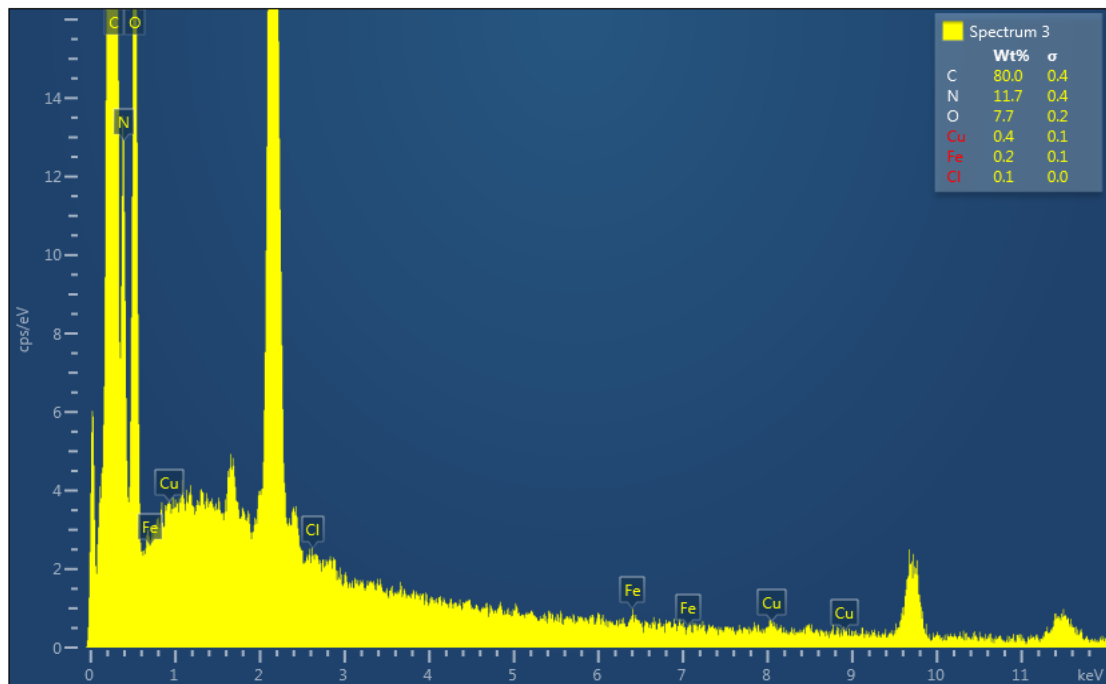


Figure 3.29. Energy Dispersive spectroscopy analysis of PVP-360-1%H fibers. This showed the presence of C, N, O, Cu, Fe and Cl in sample. The electrospinning conditions of this sample are given in table 3.2.

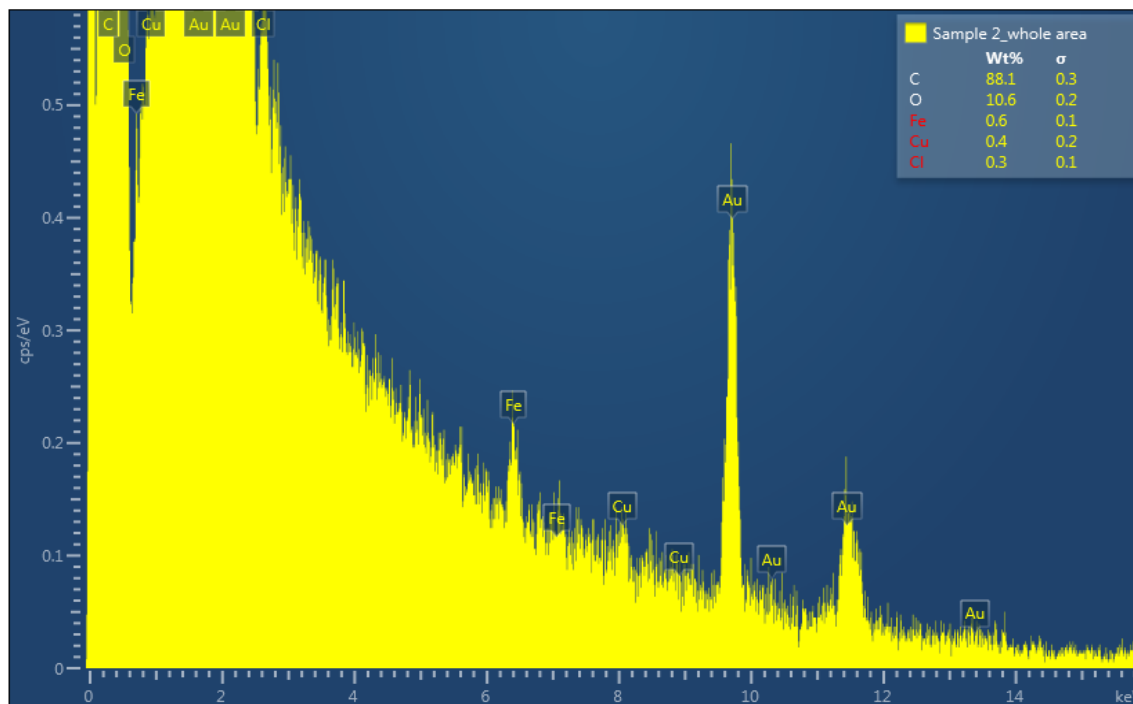


Figure 3.30. Energy Dispersive spectroscopy analysis of PVP-360-5%H fibers. This showed the presence of C, O, Cu, Fe and Cl in sample. The electrospinning conditions of this sample are given in table 3.3.

The EDX shown in figure 3.28 of PVP-360 fibers without hemin showed the presence of elements C, O and Cu, whereas EDX analysis of PVP-360 with 1% or 5% (w/w) hemin showed the additional presence of Fe and Cl which are part of hemin. We would not expect to see any Fe signal in the EDX spectrum shown in figure 3.28 as PVP itself does not contain any iron so this analysis confirmed the absence of hemin in the sample. The percentage of Fe detected by EDX is low; in the sample with 1% hemin it is 0.2% by weight and in the sample with 5% hemin it is 0.6%. 11.7 % N was found in the sample with 1% hemin which was found in both hemin and PVP structure as well. It's difficult to explain the low value of N – it should be present at about 13%, or more, in all samples, but it may be caused by a habitual EDX issue with low Z (atomic number) detection (“Using SEM/EDS for the Quantitative Analysis of Light Elements,” 2015). Gazulla in 2012, used a super ultra-thin window to get over this issue of nitrogen.

The EDX of PVP-10 particles only and with 1% hemin is given in figure 3.31 and 3.32, respectively.

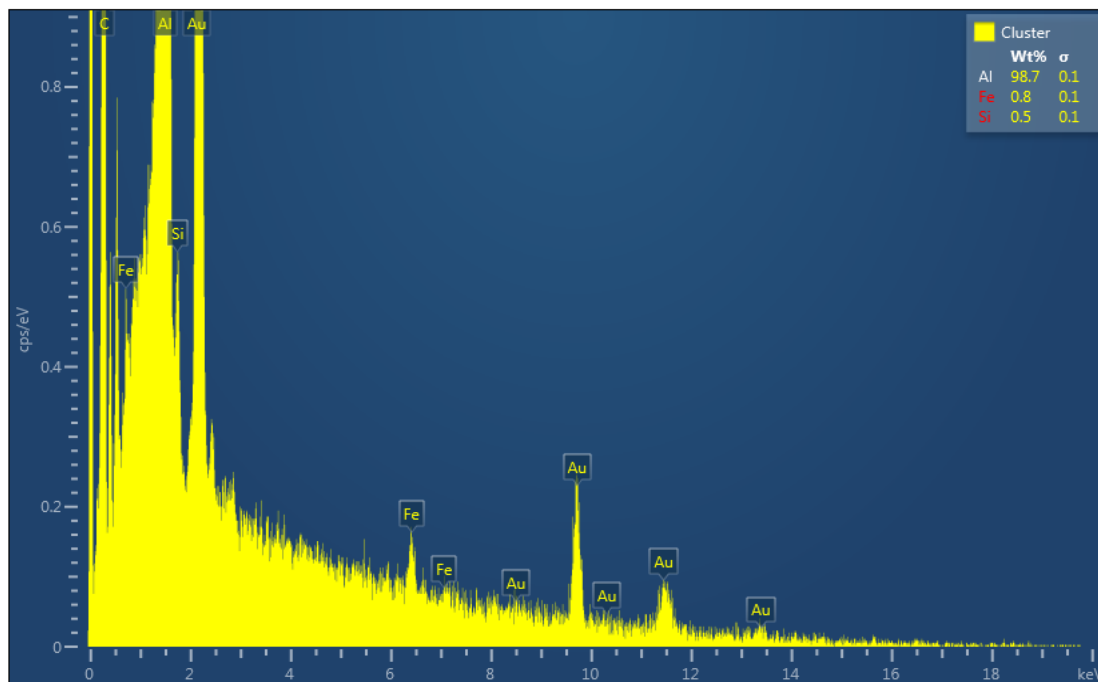


Figure 3.31. Energy Dispersive spectroscopy analysis of PVP-10 particles alone. This showed the presence of Al, Fe and Si in sample. The electrospinning condition of this sample are given in table 3.4.

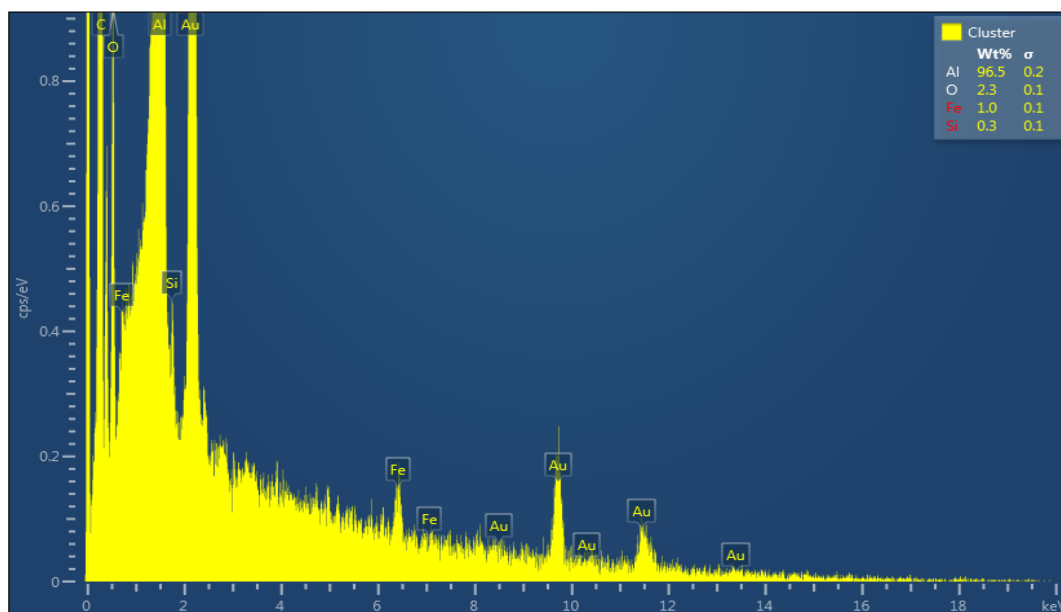


Figure 3.32. Energy Dispersive spectroscopy analysis of PVP-10-1%H particles. This showed the presence of Al, O, Fe and Si in sample. The electrospinning condition of this sample are given in table 3.4.

EDX of particles of PVP-10 alone (figure 3.31) showed the presence of Al, Fe and Si, with Fe at 0.8% (w/w) in this sample. The elements found in PVP-10 / 1% hemin particles (Figure 3.32) are Al, O, Fe and Si. Fe was measured at 1% (w/w) in the

sample. Fresh samples of PVP-10 alone and with 1% hemin are needed to repeat the EDX to confirm the presence of hemin in the sample. The very high percentage of aluminium, 96.5% suggests that there was no sample in this analysis. Carbon is expected as the major element.

Overall, the EDX analysis provided some confirmation that hemin was incorporated into fibers, but quantitation is not reliable.

3.4.7 Dynamic light scattering (DLS)

DLS is used to determine the size of particles simply and readily in a biological media. This technique has low sensitivity for small particles and interference could be possible for light sensitive objects (Cho *et al.*, 2013). There is another downside of using DLS which is mentioned by Mahl *et al.* (2011), that it can produce artefacts as large particles scatter light more strongly. This may produce false results if the sample is polydisperse. This technique was used here to determine the size of the particles obtained through the dissolution of PVP-360 fibres, and hemin containing PVP-360 fibres, in either HPLC-grade water or PBS. The size of particles determines how particles can be transported inside cells (Shang *et al.*, 2014), where smaller particles may possibly move through passive diffusion inside the cells without use of energy (Yang and Hinner, 2014). However, high molecular weight species, including those larger than 100 nm e.g. carbon nanotubes, face difficulty in such passive translocation. Instead, their transport through the membrane is generally considered to be via pores, membrane fission and budding, surface aggregation, inclusion in the membrane or lipid membrane permeation (Pogodin *et al.*, 2012).

Previous research has found that PVP, a water-soluble polymer, exists in the monomeric state (confirmed through estimation of the radius of gyration) when in the dilute regime. In the semi dilute regime, aggregates of approximately 2-3 times the size of the monomer also seen (Sun and King, 1996). For PVP360, the concentration, which denotes the start of the semi-dilute regime is approximately 10.5 mg/mL (Finch., 1984), although Sun and King (1996) reported aggregates for concentrations lower than this. This was evidenced by the presence of both fast and slow relaxation trends in the autocorrelation function, then fitted to a double exponential to estimate the sizes of the two populations. Sun and King (1996) also postulated that the aggregation was likely due to the hydrogen bonding network of water linking the molecules of PVP together through the carbonyl groups. This aggregation was significantly reduced when a denaturing agent (thiourea) was

added. This was believed to be due to the thiourea disrupting the non-covalent hydrogen-bonding network i.e. acting as a chaotropic agent.

The graphs shown in figures 3.33a and 3.33b are the outputs obtained after analysis of the autocorrelation functions by Malvern proprietary software of PVP360 and PVP360-hemin solutions in water and in PBS, respectively. For figure 3.33a, the graph showed that there were two size populations of particles in the dissolution medium for the PVP 360 in water alone, agreeing with Sun and King (1996), even though here the concentration of PVP 360 was lower than the predicted overlap concentration. As the percentage of hemin in the PVP fibres is increased, the relative proportion of aggregated particles as opposed to monomers also increased, as does the size of the aggregate implying that as the quantity of hemin is increasing, particles are aggregating more.

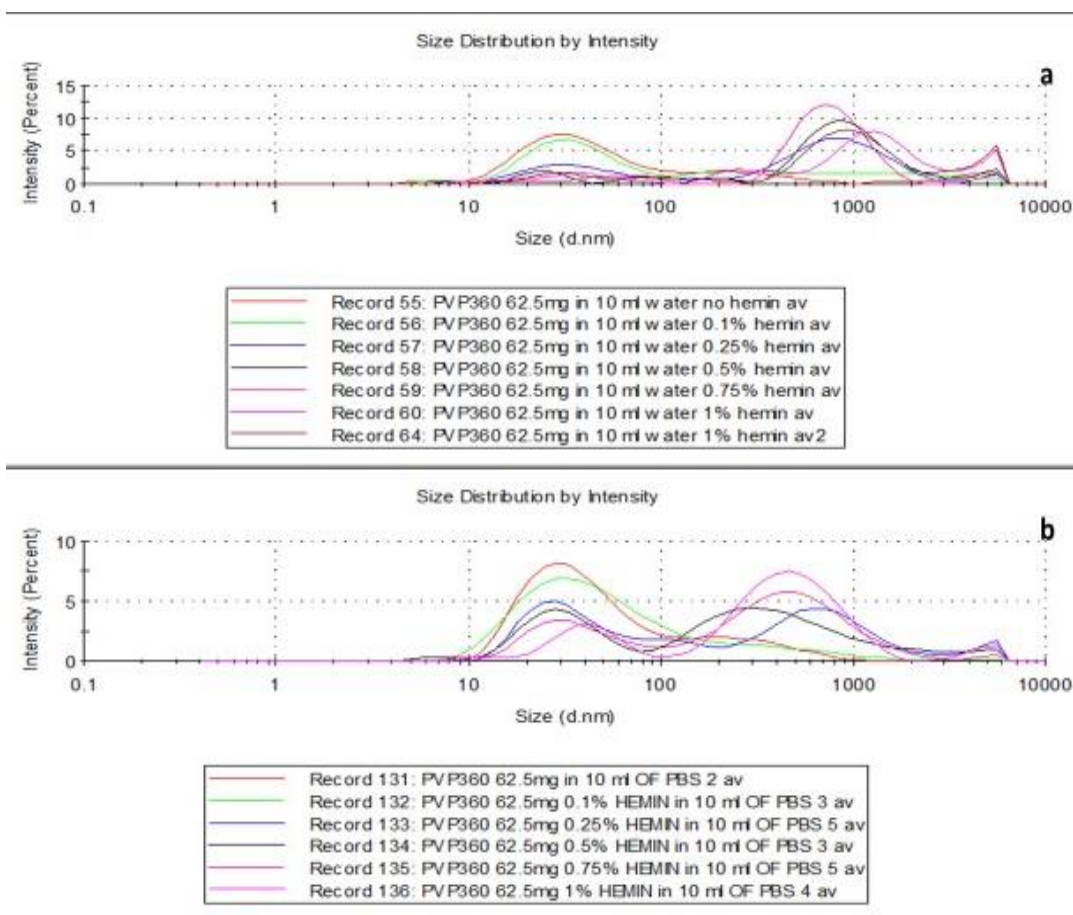


Figure 3.33. Measurement of particles size of PVP-360 fibers containing 0-1% hemin using DLS in (a) water and (b) PBS.

Triple exponential fits were carried out on the autocorrelation functions for the PVP 360-hemin solutions and found to closely fit the data. Exemplar fits are shown in figures 3.34 and 3.35, with further examples given in the appendix.

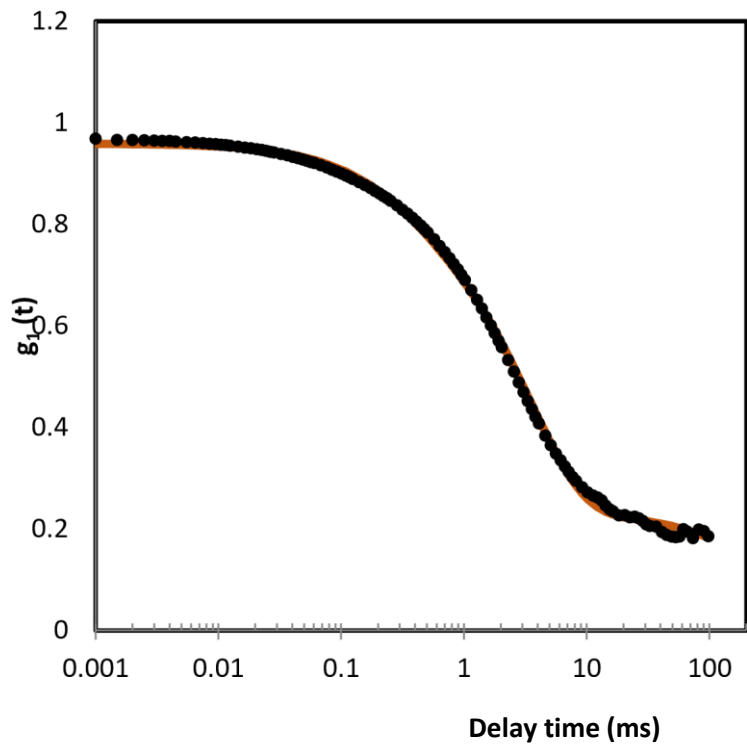


Figure 3.34. The triple exponential fit for PVP 360 fibers in water at 25 °C [SSR(sum of square of regression)= 0.010]

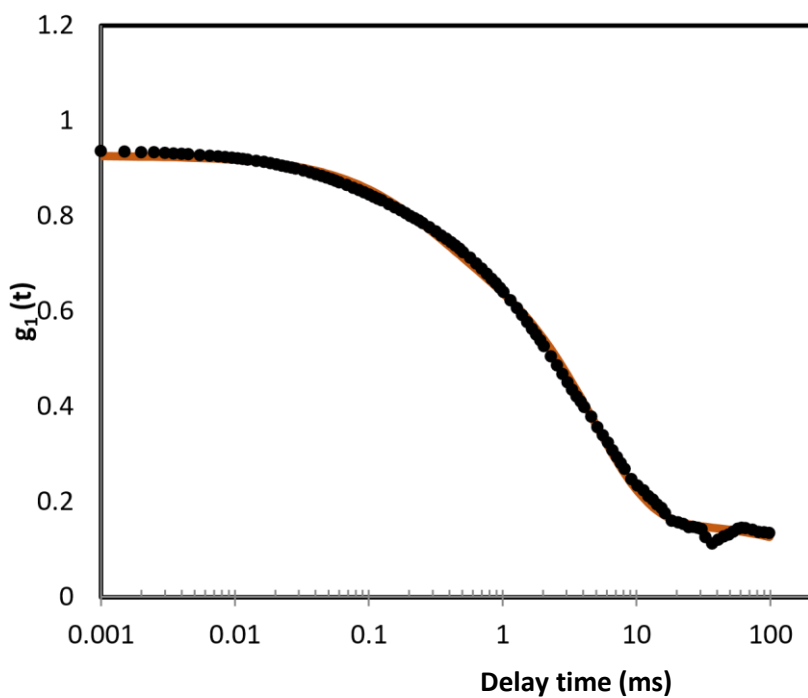


Figure 3.35. The triple exponential fit for PVP 360 containing 1% hemin fibers in water at 25 °C (SSR= 0.010)

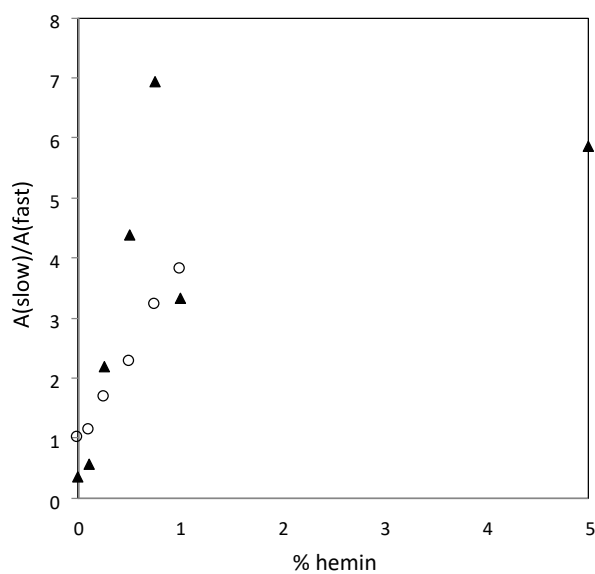
The ratio of the intensities of the two populations is plotted in figure 3.36 (a) in both water and PBS, showing an almost linear response for both until 1 % hemin,

which reflects the gradual shift away from the monomeric PVP form and towards aggregates. This is unexpected as the PVP concentration itself was not changed and suggests that hemin itself may create hydrogen bonds with PVP (C=O of PVP with H-O of hemin) thus forming aggregates, possibly in order to stabilize the monomeric form of hemin.

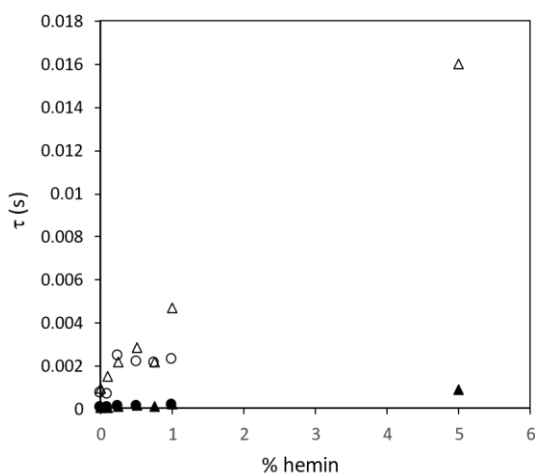
Figures 3.36 (b) and (c) show the relaxation rates and estimated sizes of the two PVP populations, both in water and in PBS. In water, with increasing hemin, the relaxation rates of both PVP populations increased, leading to increased aggregate sizes. However, in PBS, although the smaller population appears to follow a similar trend for increased hemin concentration, the aggregates appear to reach a finite relaxation rate and hence size estimated at around 400 nm.

A difference in behaviour of PVP-hemin when in PBS as opposed to water was also seen in the ratio of intensities of the two populations, where the population of the aggregates appears to increase more slowly when in PBS than in water. These two features are proposed to be due to the inherent chaotropic nature of PBS, which can disrupt hydrogen bonding networks.

(a)



(b)



(c)

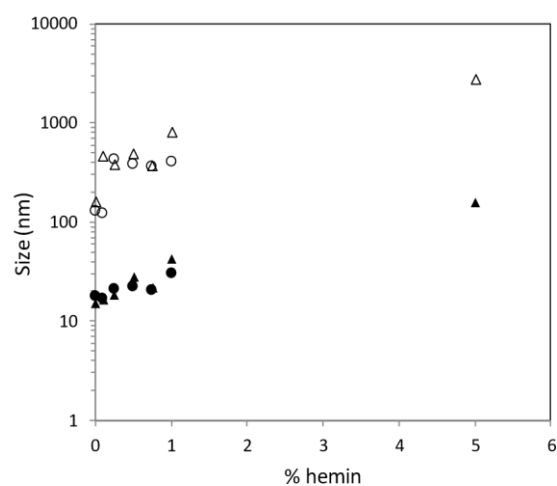


Figure 3.36 (a) Relative intensities of the two different populations with respect to the percentage of hemin in each sample. For all three graphs, the solution is represented by triangles for water and circles for PBS. In figures (b) and (c), additionally, the filled markers represent the fast relaxation times (i.e. small particles) and the unfilled markers represent the slow relaxation times (i.e. PVP aggregates).

3.4.8 Differential Scanning Calorimetry (DSC)

The differential scanning calorimetry (DSC) curves of pure PVP 360 and hemin confirmed that there was no melting peak in the case of hemin (as hemin is exothermic), whereas there is a clear endothermic peak for PVP. PVP 360 showed

a broad endothermic peak around 110 °C corresponding to dehydration (Baskakova *et al.*, 2016; Illangakoon *et al.*, 2014a). PVP is mostly an amorphous polymer that can undergo a transition phase when heated or cooled at a specific temperature, known as the glass transition temperature (T_g), where the polymer is in a partial rubbery and partial glassy phase. Similar to data from Illangakoon *et al.* (2014b), the transition temperature of PVP was 40-120 °C. This study has shown that hemin inclusions in polymers had no significant effects on DSC result of polymers and polymeric nanocomposites. However, no coherent conclusion has been drawn about the effect of hemin inclusions on the T_g . Strong interactions and possible covalent bonding between hemin and polymer matrix most likely result in an increase in the T_g . This study also showed that there was no significant effect on the T_g of PVP fibers with hemin incorporated at 1 wt% (figure 3.37). This may be attributed to the lack of strong non-covalent bonds between the hemin and the PVP or because hemin has no isotherm (Khan *et al.*, 2013). The endothermic peaks of P360, PH-1.0-M, PH-1.0-F are almost same (i.e. around 110 °C). This technique was not useful to confirm the presence of hemin in PH-1.0F fibers. The peak of P360-F was slightly different from P360, PH-1.0-F and PH-1.0-M. The endothermic peak for P360-F was around 150 °C, the reason for the change in the shape of this peak is not known.

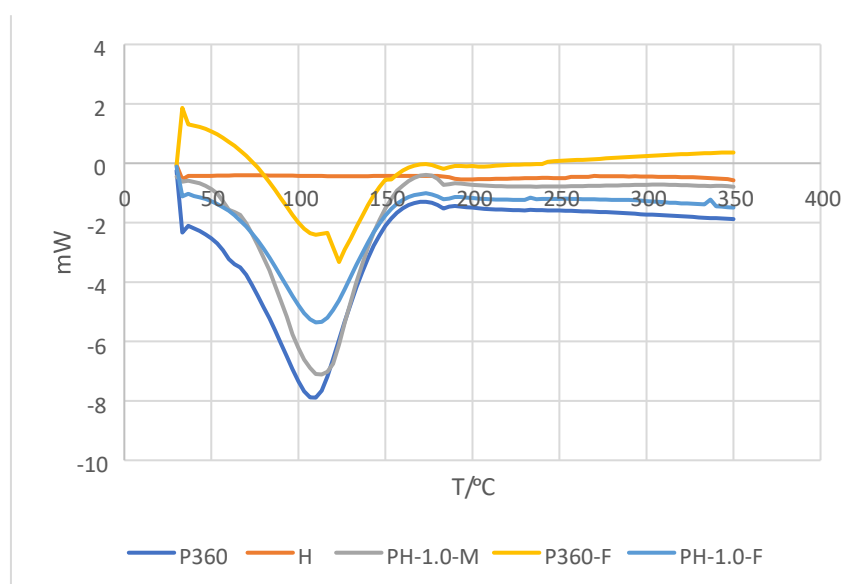


Figure 3.37. DSC analysis of a PVP 360 set of hemin formulations. P360 (polymer powder), H (hemin powder), PH-1.0-M (physical mixture of PVP 360 and hemin), P360-F (PVP360 fibers) and PH-1.0-F (PVP 360 and hemin fibers).

3.4.9 Measurement of iron content in fibers

In this section, the experiments were conducted to find out the available iron content in PVP/hemin fibers. The measurement was conducted on both unspun and spun solutions of PVP/hemin in different biological media, by using the ferrozine assay. This was carried out to find out the effect of formation of macroparticulates on the available content of iron.

The graphs obtained from the ferrozine assay of PVP-hemin fibers in PBS, SIF, and pH 2 solutions are shown in figures 3.38, 3.40 and 3.41, respectively. Standards were made using a soluble form (FAS) of iron and compared with iron bound in PVP fibers.

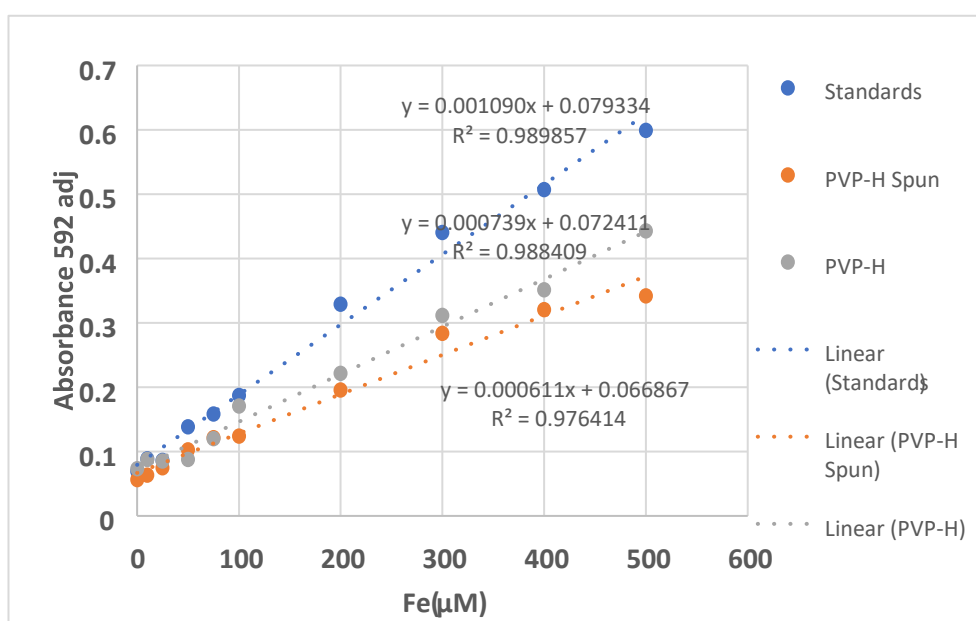


Figure 3.38. Iron content of dissolved PVP-hemin fibers in PBS determined by a colourimetric assay. FAS was used to prepare standards. Fibers were dissolved to prepare a solution containing 500 µM hemin and diluted accordingly. Aliquots of fiber solutions were spun at 12,000 g for 5 min prior to assay to provide pairs of unspun and spun solutions of fibers. The measured value of iron content in fibers was about 36.36% less than expected. 14.28% of iron content in dissolved fibers was lost by centrifugation, due to formation of insoluble brown macroparticulate material.

The results from the ferrozine assay shown in figure 3.38 indicate that PVP affected the assay. The quantity of iron differed by 36.36% in PBS and this needed to be confirmed by comparing three types of samples (standard, spun and unspun) using ICP-AES. The solution of dissolved fibers of PVP-hemin in SIF is shown in figure 3.39.



Figure 3.39. Image of solutions of PVP-hemin fibers (0-5%) in SIF after centrifugation. Sedimentation of macroparticulate material can be seen in the image, with increasing amounts as the percentage of hemin in the fibres increases.

The results obtained from ferrozine assay carried out on PVP-hemin fibers in SIF is shown in figure 3.40.

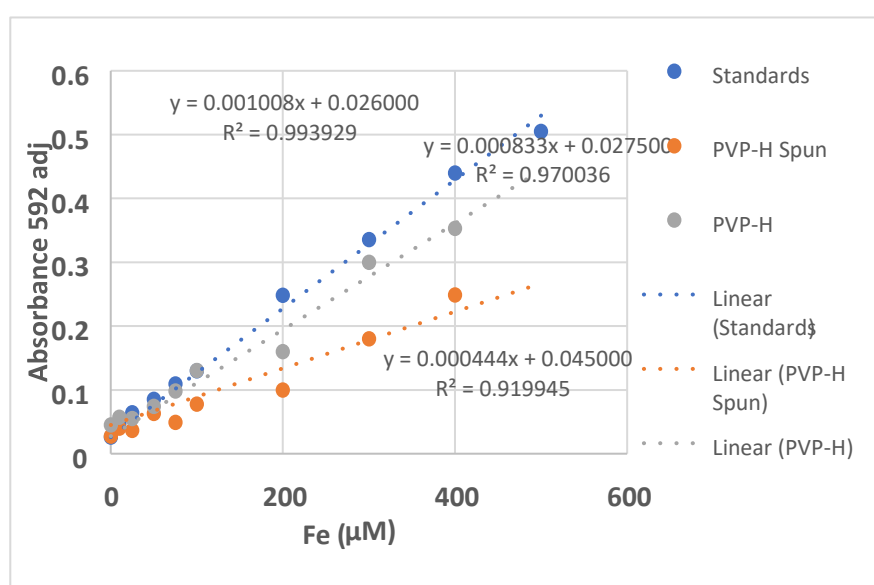


Figure 3.40. Iron content of dissolved PVP-hemin fibers in SIF as determined by a colourimetric assay. FAS was used to prepare standards. Fibers were dissolved to prepare a solution containing 500 µM hemin and diluted accordingly. Aliquots of fiber solutions were spun at 12,000 g for 5 min prior to assay to provide pairs of unspun and spun solutions of fibers. The measured value of iron content in fibers was about 20% less than expected. 50% of iron content in dissolved fibers was lost by centrifugation, due to formation of insoluble brown macroparticulate material.

The results obtained from ferrozine assay carried out on PVP-hemin fibers in pH 2 is given in figure 3.41.

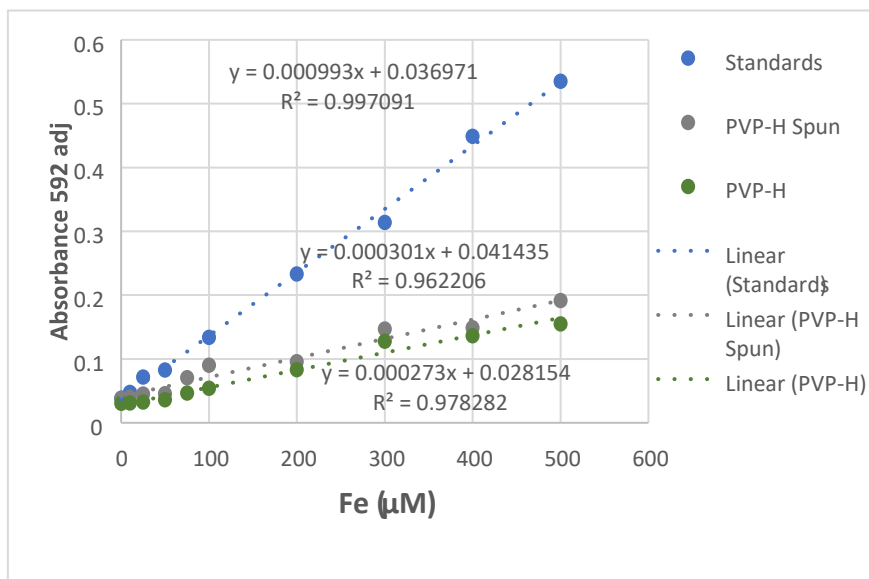


Figure 3.41 Iron content of PVP-hemin fibers dissolved in pH 2 solution determined by a colourimetric assay. FAS was used to prepare standards. Fibers were dissolved to prepare a solution containing 500 µM hemin and diluted accordingly. Aliquots of fiber solutions were spun at 12,000g for 5 min prior to assay to provide pairs of unspun and spun solutions of fibers. The measured value of iron content in fibers was about 69% less than expected. 9.3% of iron content in dissolved fibers was lost by centrifugation, due to formation of insoluble brown macroparticulate material.

The comparison of results from the ferrozine assay showed that iron content was less available in pH 2, only 31% compared with same concentration of standards.

The ferrozine assay consistently gave lower measurements of iron content across several independent sets of assays. The assay was designed to include strong denaturing chemical steps to liberate iron from heme embedded in heme-proteins (Riemer *et al.* 2014). When applied to solutions of PVP polymer fibers containing hemin the assay underestimated iron content by a significant margin, about 20, 40 and 70% in the three sets of data presented. This could indicate a very tight association between hemin and PVP, possibly dependent on pH and ionic environment. Further investigation needs to be carried out to determine the iron content in PVP/hemin formulations, using another technique such as ICP-AES (inductive coupled plasma atomic emission spectroscopy).

3.5 Discussion

The aim of the later part of the work described in this report was to develop a formulation using the technique of electrospinning or electrospraying to create

nano- / micro- sized formulations to improve the bioavailability of hemin, as a supplement to treat anaemia. Hemin is poorly soluble in water and has not been widely used as an iron supplement, and only used intravenously, and seemed a good candidate for exploiting electrohydrodynamic approaches to enhance solubility and availability.

In the early stages a suitable organic solvent for electrospinning was identified. Also, in the initial phase of the work, a variety of polymers compatible with drug formulation were assessed, with the aim of identifying polymer and hemin mixes that could be prepared in compatible solvents. Eudragit L100 (in DMAc and MeOH) and PVP 360 (in MeOH and DMF) were selected as being suitable candidates for electrospinning with hemin, as hemin is soluble in these solvents as well. Eudragit L 100/hemin and PVP 360/hemin gave thick consistent fibers. The effect of flow rate on Eudragit L 100/hemin and PVP 360/hemin was also studied. The correlation between diameter and flow rate of electrospinning of PVP 360/hemin and Eudragit L100/hemin fibers is shown in figures 3.42 and 3.43, respectively.

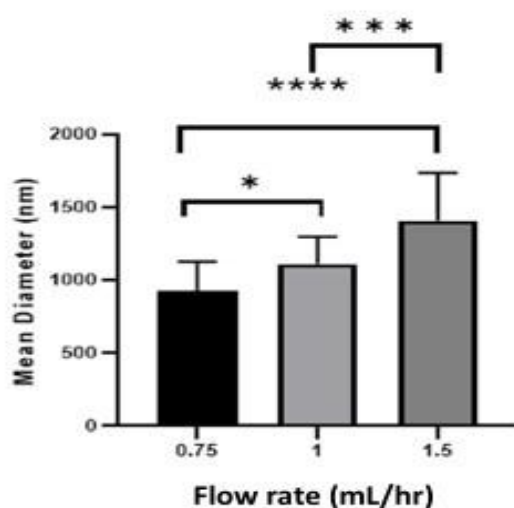


Figure 3.42. The effect of flow rate of 10% PVP-360 / 1% hemin solution on diameter of fibers produced through electrospinning. The data are presented as mean (nm) + SD of diameters of 25 fibers, obtained from SEM and measured using Image J. There is a direct relation between flow rate and diameter. One-way Anova comparison of means indicated a significant difference between the diameter of the fibers with flow rate 0.75 mL/hr and diameter of the fibers with flow rate 1.0 and 1.5 mL/hr [* , p <0.05]. The diameter of fibers prepared at 1 mL/hr flow rate were significantly different from diameters fibers prepared at 1.5 mL/hr flow rate [* , p < 0.05].

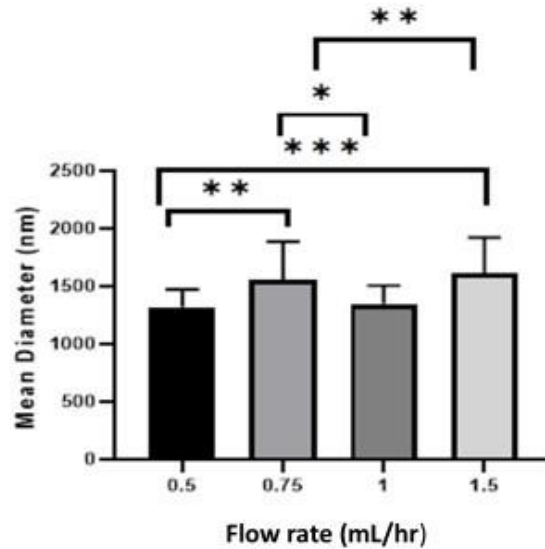


Figure 3.43. The effect of flow rate of 18.2% Eudragit / 0.5% hemin solution on diameter of fibers produced through electrospinning. The data are presented as mean (nm)+SD of diameters of 25 fibers, obtained from SEM and measured using Image J. There is no direct relation between flow rate and diameter of fiber. One-way Anova comparison of means indicated some significant differences between pairs of means as indicated by * $p < 0.05$, ** $p < 0.01$, *** $p < 0.005$.

A trend for increasing diameter with increasing flow rate has been observed for 8% PVA (0.5, 1, 1.2, 1.5, and 2 mL/hr), 25 % nylon (0.1, 0.5, 1, 1.5, and 2 mL/hr) and 4% PVP (0.5, 0.7, 1, 1.2, and 1.5 mL/hr) (Jabur *et al.*, 2018). Experiments carried out in this research for PVP produced a similar trend, except for Eudragit. As it is clear from the work carried out in chapter 3, that the mean diameter of Eudragit L 100 fibers (1480.5 nm) are larger than Eudragit / 0.5% hemin fibers (1320 nm), except for 0.75 and 1.5 mL/hr flow rate sample in figure 3.9. This is similar to the effect of hemin on PVP fibers, which can be seen from figure 3.7, PVP-fibers and PVP/hemin fibers (figure 3.10). The diameter of fibers of both polymers with and without hemin is given in table 3.8. Johnson mentioned the same behaviour i.e. the inclusion of drug reduces the fiber diameter due to a decrease in the fiber's alignment (Johnson *et al.*, 2016).

PH-1.0-F flow rate 1 mL.hr ⁻¹		Eudragit-hemin fibers flow rate 0.5 mL.hr ⁻¹
Diameter (Mean±SD nm)	479.1 ± 102.8	1348 ± 157.6
PVP fiber flow rate 1 mL.hr ⁻¹		Eudragit fiber flow rate 0.5 mL.hr ⁻¹

Diameter (Mean±SD nm)	881.9 ± 243	1480.5 ± 477.5
------------------------------	-------------	----------------

Table 3.8. Diameter of fibers of PVP360 and Eudragit with and without hemin

According to SEM, PVP 360/Eudragit and hemin fibers are smooth, homogeneous, uniform and particle free for each flow rate. In comparison to PVP fibers, Eudragit fibers are thicker, perhaps because of their dual nature, as if two fibers are joined together, indicated from SEMs of Eudragit fibers in section 3.8 and 3.9. Eudragit fibers are flat in appearance. The reason behind this is the traditional one-fluid electrospinning shares characteristics of both electro spraying and conventional solution dry spinning. During the process, methanol evaporated very quickly. This would make the electrospinning process very sensitive to small changes in the environment and thus result in nanofibers with a wide range of sizes and generate a solid “skin” on the surfaces of collected fibers with some solvent still trapped inside the fiber bodies. After spinning, the solvent contained in the fibers diffused out into the atmosphere, and the resulting barometric pressure distorted the cylindrical fibers to the flat morphology (Yu *et al.*, 2014). Yu produced Eudragit fibers of 1280 nm diameter compared with 1300-1500 nm from the research carried out in this project, which was quite similar.

The focus of this project was to create a formulation that can deliver iron safely in the small intestine. Central to this is the requirement that the formulation can dissolve rapidly in the conditions found in the small intestine, especially the pH, but with a normally insoluble hemin maintained in a soluble form. Before proceeding further with the development of the fibers, preliminary dissolution tests were carried out on PVP / hemin and Eudragit /hemin fibers. If the fibers did not dissolve easily or released free hemin after dissolution, this would limit their usefulness. The solubility of both types of fibers was assessed in PBS (isotonic phosphate-buffered saline). PVP / hemin fibers dissolved readily within 10 minutes, but in contrast Eudragit / hemin fibers took 2-3 days to dissolve. These preliminary tests showed that PVP is a better choice for a hemin formulation because the digestion time of drugs in the gastrointestinal tract is 10 hours (Lee *et al.*, 2014) and if the formulation does not dissolve in that time it will be excreted without absorption. Accordingly, further development focused on PVP fibres.

To find out the extent to which hemin can be incorporated into PVP-360 fibers, hemin was added to create a 50-fold range of percentages, 0.1, 0.25, 0.5, 0.75, 1, 5% (w/w), final concentration of hemin in the fibres, using 10% PVP-360 to prepare fibers. All the work described so far was carried out with PVP-360. To extend the work further it was decided to assess smaller forms of PVP, i.e. PVP-40, average mw 40,000 Da, and PVP-10, average mw 10,000 Da. One of the reasons for working with all three forms of PVP was to compare their toxicity and the bioavailability of the iron carried in hemin in cultured cells, which would enable selection of the best carrier for hemin. The SEM images of PVP-10 and PVP-40 clearly showed the successful production of fiber-free particles under the conditions given in table 3.6 and 3.7. Electrospaying with PVP-10 and PVP-40 was not productive due to low yields and it was difficult to remove material from the collecting foil. Consequently, the cell work with lower molecular weight PVP was not carried out. The λ_{\max} for PVP is around 225 nm and that of hemin was found to be 400 nm, known as the Soret band, which was also found by Han *et al.* (2013). The λ_{\max} of PVP-hemin formulations, 397 nm, was used in dissolution tests. Aqueous solutions of hemin have a broad Soret band, indicative of dimerization (Kremer, 1989) and this was found to be the case for hemin-PVP mixtures (figures. 3.17, 3.18A). Organic solutions of hemin have a sharp Soret band, indicating that the hemin is monomeric (Brown and Lantzke, 1969), and this was confirmed for solutions of hemin in DMSO and MeOH (figure. 3.18B). It appears therefore that hemin is electrospun as a monomer but assumes a dimeric configuration at some stage. Alternatively, and perhaps more likely, during dissolution in PBS or DMEM for cell culture, hemin changes into the dimeric form, as these are aqueous solutions with broad Soret absorption bands. Inamura *et al.* (1989), explained that doublet and broad soret bands represent dimerization of hemin in the PVP-hemin complexes. The comparison of this with the UV-visible spectrum of PVP-hemin complexes in PBS (figure 3.19 layer 1) and SIF (figure 3.19 layer3) confirmed that the complex is dimeric in these two solutions. The broad soret band of PVP-hemin complex in pH 2 also gave the indication of presence of dimeric form.

Dissolution tests were used to simulate the availability of the hemin from the formulation and to model the time duration for complete release of it from the dosage form into solution. In this research the release of free hemin was not observed, but instead, the PVP-hemin fibres dissolved quickly to form substantial amounts of insoluble material as well as a nanoparticulate form of hemin. PVP made hemin soluble in PBS. Hemin in fibers dissolved completely and rapidly within 10 minutes (PH-1.0-F in Figure 3.22A) whereas the physical mix of PVP and hemin

(PH-1.0-M) and hemin added to pre-dissolved PVP (H-PVP 360-PBS), took several days to completely dissolve. Hemin alone (H in Figure 3.22A) eventually dissolved in PBS to about 30 μM , over a period of six days. The dissolution test was also carried out for a set of PVP-40 and PVP-10 formulations, with a similar outcome, that the electrospayed formulations containing hemin dissolved much more rapidly than the controls. As mentioned earlier, due to low yield and difficulty in removing the formulation from the foil, the work on PVP-10 and PVP-40 was carried out at a preliminary level. PVP-360 fibers were prepared with a range of hemin content 0.1, 0.25, 0.5, 0.75, 1 and 5% (w/w) and dissolved in PBS for 30 min. The data (Figure 3.22D) showed that there was limited enhancement of hemin solubility beyond a fiber content of 1%. This showed the saturation limit for hemin and suggests that there may be no advantage in preparing fibers with more than 1% content of hemin. FTIR spectroscopy was used to determine the functional groups in the sample. The spectra of hemin alone and of hemin containing sample were measured to confirm the presence of hemin in the sample, and to assess molecular interactions. All four sets of IR spectra confirmed that this technique is not beneficial to assess the presence of hemin in PVP/hemin fibers or particles. The distinct IR spectrum of hemin was masked when mixed with PVP, due to the low content, 1% or 5%, of hemin in the formulations.

EDX was used for elemental analysis of the sample. It was carried out to confirm the presence of iron in samples. The percentage of Fe and N was found lower than the actual percentages in the formulation. This is likely to be caused by a habitual SEM issue with low sensitivity for atoms with low atomic number ("Using SEM/EDS for the Quantitative Analysis of Light Elements," 2015). Gazulla in 2012, used a super ultra-thin window to try to get over this issue for nitrogen.

DLS was used to determine the size of particles simply and readily in biological media. This technique was used here to determine the size of the particles obtained through the dissolution of PVP-360 fibres, and hemin containing PVP-360 fibres, in either HPLC-grade water or PBS. The size of particles determines how particles can move into the cells (Shang *et al.*, 2014), where smaller molecules may possibly move through passive diffusion inside the cells without use of energy (Yang and Hinner, 2014). However, high molecular weight species, including those larger than 100 nm e.g. carbon nanotubes, face difficulty in such passive translocation. Instead, their transport through the membrane is generally considered to be affected via pores, membrane fission and budding, surface aggregation, inclusion in the membrane or lipid membrane permeation (Pogodin *et al.*, 2012).

Previous research has found that PVP, a water-soluble polymer, exists in the monomeric state (confirmed through estimation of the radius of gyration) when in the dilute regime (lower than 10.5 mg/mL) but in the semi dilute regime, aggregates of approximately 2-3 times the size of the monomer are also seen (Sun and King, 1996). The overlap concentration, which denotes the start of the semidilute regime is approximately 10.5 mg/mL (Finch., 1984), although Sun and King (1996) reported aggregates for concentrations lower than this. This was evidenced by the presence of both fast and slow relaxation trends in the autocorrelation function, then fitted to a double exponential to estimate the sizes of the two populations. Triple exponential fits were carried out on the autocorrelation functions for the PVP 360-hemin solutions and found to closely fit the data. Sun and King (1996) also postulated that the aggregation was likely to be due to the hydrogen bonding network of water linking the molecules of PVP together through the carbonyl groups.

According to DLS there are two size populations of particles in the dissolution medium for the PVP 360 in water alone, agreeing with Sun and King (1996), even though here the concentration of PVP 360 was lower (6.52 mg/mL) than the predicted overlap concentration. As the percentage of hemin in the PVP fibres is increased, the relative proportion of aggregated particles, as opposed to monomers, also increases, as does the size of the aggregate.

A model was made to describe the behaviour of hemin/PVP fiber in biological media. It is based on the results obtained from dissolution experiments and DLS. PVP/hemin fibers in aqueous solution transfer in to two size populations (10-100 nm and 100-1000 nm) PVP/hemin particles (hemin wrapped with PVP). However, some of the hemin which was on the surface of the fibers intertwined with PVP aggregated and formed insoluble hemin-PVP complexes. The schematic diagram of this phenomenon is given in figure 3.44.

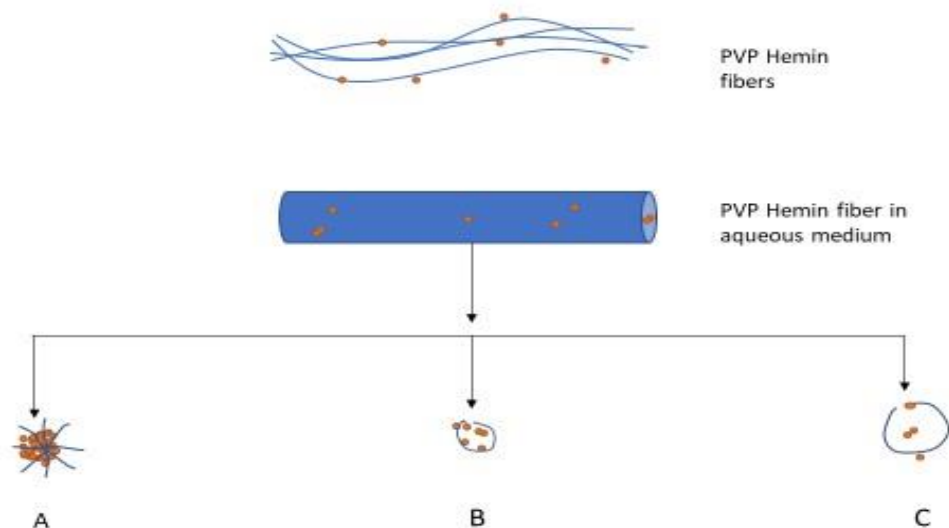


Figure 3.44. The dissolution process of PVP/hemin fibers in aqueous medium. Firstly, the fibers swell in aqueous medium, A) hemin molecule on surface of fibers joined and made macromolecules, PVP molecule intertwined with it. Hemin molecule imbedded in fibers were convert in to two size PVP/hemin particles B) nanoparticles 10-100 nm C) nanoparticles 100-1000 nm.

The described work in this chapter has revealed unusual behaviour of monolithic PVP-API composite nanofibers, in which the API interacts with polymer to form nanoparticles or insoluble aggregates, rather than dissociating as free API from the polymer. The molecular basis for this behaviour is not clear and requires further investigation. Future work in developing the potential of this system for delivery of hemin could include coaxial formulations with sheath polymers stable in gastric conditions, with a PVP core. Despite the formation of insoluble aggregates, the rapid solubility of PVP-hemin fibers to form stable soluble preparations of hemin suggested the possibility of cellular uptake, the focus of the next chapter.

Chapter 4

Uptake of hemin-PVP nanoparticles by cultured cells – an *in vitro* study

4.1 Introduction

In this project, hemin loaded PVP fibers were prepared for the first time, as a potential new formulation for treatment of anemia. The fibers have been found to dissolve rapidly in physiological buffers, creating solubilised hemin packed in PVP nanoparticles. To assess the bioavailability of the iron in the hemin nanoparticles some preliminary studies were carried out *in vitro*, to assess iron uptake from the NPs by a variety of cultured cell models. It was also important to assess any potential toxicity of the hemin fibers.

Three types of cells were used to assess cytotoxicity, uptake, and storage of iron. Firstly, HepG2 human hepatoma cells were selected as a model for liver cells (hepatocytes). Liver is the major organ of iron storage and helps to maintain the homeostasis of body iron levels. Liver can sense the level of iron in the body and respond by controlling uptake of iron from the diet, through the release of the regulatory hormone hepcidin (Anderson and Shah, 2013). HepG2 cells have been used to model iron homeostasis and regulation in the liver, latterly to investigate the molecular mechanisms by which production of hepcidin is regulated (Kulaksiz *et al.*, 2004).

The human monocyte cell line THP-1 was selected as a model for an important cell type that has a major role in systemic iron homeostasis, the monocyte-macrophage system (Andriopoulos and Pantopoulos, 2006; Ludwiczek, 2003). Macrophages capture and recycle senescent erythrocytes, extracting the iron from haemoglobin and exporting it for re-use (Silva and Faustino, 2015). Macrophages are present throughout the body and those associated with the liver and spleen, recycle old red blood cells. Liver macrophages are also called Kupffer cells and it is possible to co-culture THP1 and HepG2 cells to model the interactions between Kupffer cells and hepatocytes (Matak *et al.*, 2009). THP-1 monocytes can be easily differentiated into macrophages and can provide a convenient model for characterising uptake of hemin nanoparticles by endocytic and phagocytic pathways.

Caco-2 cells, a cell line derived from human colon cancer (Lea, 2015), was selected as a third cell line because it has been widely used as a model for absorption of dietary components, including different formulations of iron (Tako *et al.*, 2016). Caco-2 cells have been used in co-culture with HepG2 cells to model uptake and first-pass metabolism.

In this chapter experiments are described in which the safety of hemin-NPs is assessed through assay of toxicity to cultured cells (Molinari *et al.*, 2005). Iron uptake by cells was measured by a chemical assay based on chelation of Fe^{2+} by the chromophore ferrozine (Hirayama and Nagasawa, 2017). Had time permitted later work would have assessed the bioavailability of iron from hemin-NPs, by increase of iron stored in cells, measured by the levels of the intracellular iron storage protein ferritin (Knutson, 2017).

4.2 Materials and Methods

4.2.1 Materials

Hemin (relative molecular mass 651.9) was obtained from Calbiochem (Merck, UK). Polyvinylpyrrolidone (PVP) (average relative molecular mass 360,000), ferric ammonium citrate, ferrous ammonium sulphate, ferrozine, neocuproine, PSG (penicillin, streptomycin, glutamine), nonessential amino acids and FBS (fetal bovine serum) were all purchased from Sigma Aldrich. Methanol, ethanol, chloroform, dimethylformamide and trypsin were bought from Fisher. HepG2, THP-1 and Caco-2 cells were purchased from the European Collection of Cell Cultures (ECCAC, Salisbury, UK). Dulbecco's Modified Eagle Medium (DMEM), EMEM, RPMI-1640 were obtained from BioWest (VWR, UK). Ferrozine (3-(2-pyridyl)-5,6-bis(phenyl sulfonic acid)-1,2,4-triazine), and neocuproine (2,9dimethyl(1,10-phenanthroline)) were from Sigma Aldrich.

4.2.2 Methods

4.2.2.1 Preparation of hemin solutions for treatment of cells

Amounts of solid preparations of nanofibers were added to plain cell culture medium (DMEM) based on the mass of PVP-hemin fibers with 1% (w/w) content of hemin, needed to create a concentration of iron of 100 μM . For 10 mL of DMEM, 65.2 mg of PVP-hemin (1%) was added, containing 652 μg of hemin, or 1 μmole . Control treatments included DMEM containing 65.2 mg of PVP nanofibers or 65.2 mg of PVP powder. Fibers containing a range of hemin from 0.1 to 5% (w/w) were used, all

dissolved at 65.2 mg per 10 mL medium, giving a range of iron concentrations of 10 to 500 μ M.

Each preparation of fiber was placed in a sterile plastic petri dish in a microbiological safety cabinet with the air flow switched off to avoid loss of the very light fibers. The fibers were exposed to UV light for 30 minutes for sterilization, and then 10 mL of DMEM was added to each petri dish. At this point the air flow of the safety cabinet was turned on, to provide the normal environment for handling cell cultures in a sterile way. The fibers were dissolved completely by pipetting the mixtures. Fresh solutions were prepared immediately before each set of treatments.

4.2.2.2 Cell culture

HepG2 cells were cultured in DMEM medium, supplemented with 10% (v/v) FBS, 0.05% penicillin and 2% streptomycin. THP-1 cells were cultured in RPMI 1640 medium, supplemented with 10% (v/v) FBS, 0.05% penicillin and 2% streptomycin. Caco-2 cells were cultured in EMEM medium with non-essential amino acids, supplemented with 10% (v/v) FBS, 2 mM glutamine, 0.05% penicillin and 2% streptomycin. Cells were maintained at 37 °C in 5% (v/v) CO₂ and sub-cultured twice a week. HepG2 and Caco-2 cells were grown in 25 or 75 cm² flasks and detached by treatment with 0.02% (w/v) trypsin in PBS with 1 mM EDTA. THP-1 cells were centrifuged at 150 *g* and the medium replaced. Generally, cells were subcultured at a dilution of 1:3 to 1:5.

For treatments, cells were seeded at about 2×10^5 cells/mL in 6-, 24- or 96-well plates. HepG2 cells could grow to 80% confluency, usually in two days before the treatment. Growth medium was removed and replaced with plain medium containing a range of concentrations of hemin solutions (PVP-only, 0.1, 0.25, 0.5, 0.75, 1 and 5% hemin containing PVP solutions). Cells were treated with 100 μ M ferric ammonium citrate (FAC) as a positive control for iron uptake. Negative controls of cells without treatment and a blank well without cells were performed for each analysis. The cells were treated with the PVP-hemin solutions for 48 hours.

4.2.2.3 Light microscopy

An Olympus X81 inverted light microscope was used to take the images of cells at magnifications of 100x and 200x.

4.2.2.4 Cell viability assay

The MTT assay (Mosmann, 1983) was carried out to quantify metabolic activity in cells, representing total cell number, as a means of measuring the potential toxicity of the PVP nanofiber treatments. The assay is based on the reduction of the yellow tetrazolium salt MTT (3-(4,5-dimethylthiazol-2-yl)-2,5-diphenyltetrazoliumbromide) to a purple MTT-formazan crystal (Mossmann, 1983). Viable cells reduce MTT into formazan mainly by the action of succinate dehydrogenase enzymes in the mitochondria, dead cells lose this ability (Gomez Perez *et al.*, 2017). Hence, the percentage of viable cells relative to untreated controls was quantified by the MTT assay. 96-well tissue culture plates were seeded with the cells (5×10^4 cells/mL growth medium) and left overnight. Growth medium was replaced by plain medium containing nanofiber solutions comprised of iron over a range of 0 to 500 μ M, 100 μ M FAC and plain medium only as control. Treatments were performed in triplicate and incubated for another 24 h. The medium from each well was removed by aspiration at the end of the treatment and cells were washed with 200 μ L PBS per well. 50 μ L of 1.0 mg/mL MTT solution in plain DMEM was added to each well and the plate incubated for 4 h at 37 °C. The MTT solution was then removed and 50 μ L of DMSO was added to dissolve the MTT-formazan crystals, by orbital rotation for 15 min. The optical density was determined at 590 and 650 nm for each well using a FluoStar plate reader (BMG Labtech, Aylesbury, UK).

4.2.2.5 Perls staining of ferric iron

HepG2 cells were cultured on coverslips to about 80% confluency and treated with PVP-hemin nanofibers as described above. The cells were washed with PBS twice and then fixed by treating with 4% paraformaldehyde/ PBS for 30 minutes at room temperature. Cells were washed with PBS once, then treated with 70% EtOH for storage at -20 °C, or the staining procedure was continued at this stage. Cells were hydrated with distilled water for 5 min, before staining. The water was drained off and the cells treated with a freshly prepared 1:1 mixture of 2% (v/v) HCl and 2%

(w/v) potassium ferrocyanide (freshly prepared) solution for 15 minutes. The cells were washed with water five times, and then counterstained with 1% (w/v) aqueous neutral red for 30 min. After washing with water twice, cells were dehydrated rapidly with alcohol. Coverslips were mounted onto microscope slides with 50% (v/v) PBS in glycerol (Bancroft, 1982).

4.2.2.6 Ferrozine assay of cellular iron uptake

Total cellular iron was measured to assess iron uptake by a colourimetric method using ferrozine (Fish, 1988) adapted for cultured cells (Riemer *et al.* 2004). HepG2 cells were grown and treated with PVP-hemin nanofibers in 24-well plates. After treatment, medium was discarded, the cells were washed with PBS and then lysed by addition 250 μ L of 50 mM NaOH, followed by incubation with rotation at room temperature for 2 h. 100 μ L aliquots of cell lysate were treated with 100 μ L of iron releasing solution made up of 4.5% (w/v) KMnO_4 and 1.4 M HCl freshly mixed in a 1:1 ratio. The iron releasing solution digests proteins to which iron is bound and releases the iron. The samples were incubated at 60°C for 2 hours in a fume hood as chlorine gas is released during heating. The samples were cooled to room temperature, and the volume of each sample was made up to 500 μ L accurately with deionized water. 25 μ L of iron detection solution (2.5 M ammonium acetate, 1 M ascorbic acid, 6.5 mM neocuproine, 6.5 mM ferrozine) was added to each sample, mixed, incubated for 30 min. The iron detection solution was made by adding 9.7 g ammonium acetate and 8.8 g ascorbic acid to about 10 mL of water, so that the volume was less than 25 mL. The mixture was heated for complete dissolution, 43 mg of neocuproine and 80 mg of ferrozine were dissolved, and the volume was adjusted to 25 mL. Cu^{2+} is also present in cells and can bind ferrozine. To avoid interference from copper ions the selective copper chelator neocuproine was included in the solution (Riemer *et al.* 2004). The ascorbic acid in the iron detection solution reduces Fe^{+3} to Fe^{+2} . It is the ferrous form of iron which binds to ferrozine and gives a purple colour (Jeitner, 2014; Riemer *et al.*, 2004; Yamamoto *et al.*, 2010). After incubation the samples were centrifuged at 12,000 rpm for 5 min and 200 μ L taken for measurement of absorbance at 550 nm, with correction for light scattering at 650 nm, in a FluoStar Omega plate reader (BMG LabTech, Aylesbury, UK), in a 96-well plate.

Standards were prepared from a fresh solution of ferrous ammonium sulfate (FAS), made by dissolving 0.392 g of FAS in 10 mL of water to make a 0.1 M solution. Stock

solutions of 10mM, 1 mM and 100 μM were prepared by serial dilution in which 1 mL of each concentration was diluted 10 times by addition of 9 mL water. Standards were prepared as indicated in table 4.1. 100 μL of each standard was used in the to obtain data for a standard curve.

Fe (μM)	0	25	50	100	150	200	250	300
FAS stock	-	100 μM	100 μM	100 μM	1 mM	1 mM	1 mM	1 mM
Vol FAS stock, μL	-	25	50	100	15	20	25	30
Vol H ₂ O, μL	100	75	50	-	85	80	75	70

Table 4.1. Preparation of standard concentrations of ferrous iron for the ferrozine assay.

A standard curve obtained from the ferrozine iron assay is given in figure 4.1 The absorbances obtained from the colorimetric assay can be converted into concentrations using the equation obtained for the standard curve.

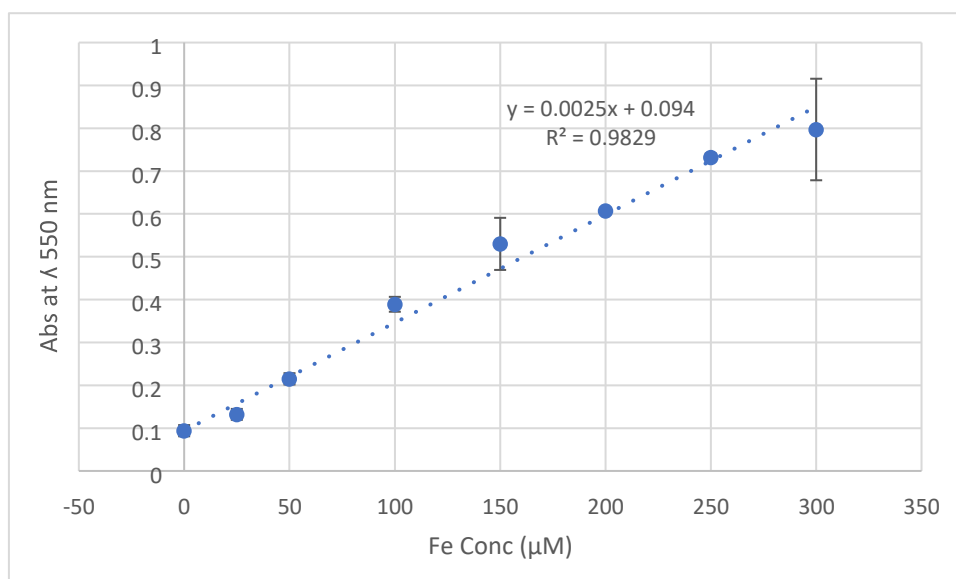


Figure 4.1. Standard curve for the ferrozine assay. The data are means \pm SD of triplicate measurements. R^2 is the square of the correlation coefficient (r) and provides information about how far away the y values are from the predicted line.

A perfect line would have an R^2 value of 1, and most R^2 values for calibration curves are over 0.95. In biomedicine could be excepted below 0.9.

4.2.2.7 Bradford protein assay

This method was used for measuring protein concentration (Cheng *et al.*, 2016), as it is important to know the amount of iron in cells relative to cell number, in this case measured as protein. Coomassie Brilliant Blue G-250 reacts with basic amino acid residues in proteins in the Bradford assay. This method is commonly adopted because of its ease, relative sensitivity, rapidity, and low interference by other materials (Ku *et al.*, 2013).

Bovine serum albumin (BSA) stock solution was made by adding 20 mg to 20mL of 50 mM NaOH, as the cell lysate was in 50mM NaOH as well. A series of standards were made from the stock solution, as shown in the chart below.

Conc BSA $\mu\text{g}/\text{mL}$	Vol of BSA stock solution (μL)	Vol of 50 mM NaOH (μL)
0	0	1000
40	40	960
60	60	940
80	80	920
100	100	900
200	200	800
300	300	720
400	400	600
500	500	500

Table 4.2. Preparation of standard solutions for the Bradford protein assay.

50 μL of each cell lysate and standards were placed in triplicate in a 96 well plate. 50 μL of 50 mM HCl was added to each sample to neutralize the medium. 100 μL

of Bradford reagent was added to the standards and samples. The Bradford reagent was mixed in by shaking the plate for 10 seconds, which was then left it at room temperature for 15 minutes. The absorbance was recorded at 660 nm (Brady and MacNaughtan, 2015).

The standard curve obtained from assay is given below in figure 4.2. This was used for determination of concentration of cells in each treatment.

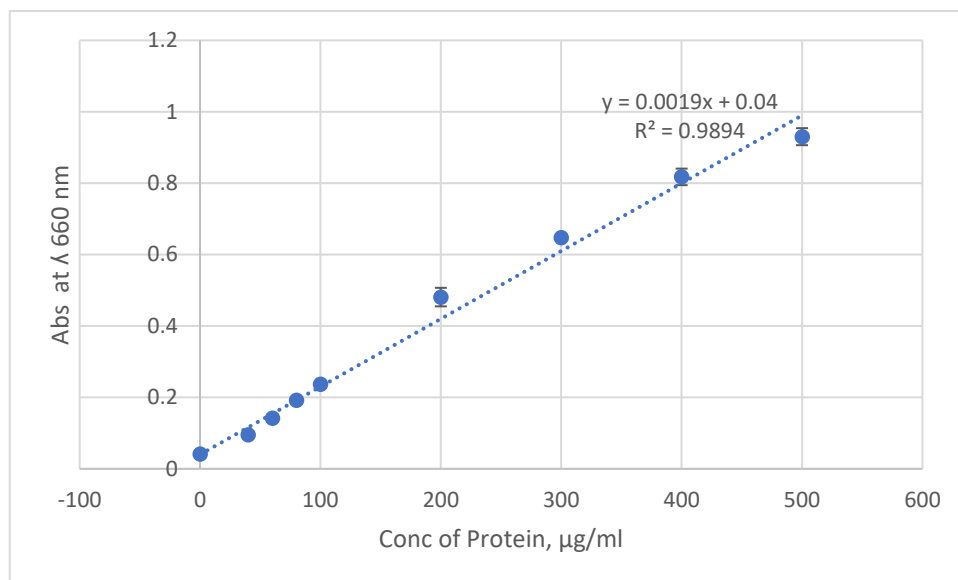


Figure 4.2. Standard curve for determination of concentration of protein in lysed cells. The data are means \pm SD of triplicates. Some of the error bars are hidden due to symbols.

4.3 Results

The experiments were performed to assess the uptake of hemin from dissolved hemin-PVP fibers by cells, to investigate the application of the formulations as a new type of iron supplement to treat anaemia. The hemin uptake is studied in HepG2, THP-1 cells and in Caco-2 cells, respectively.

4.3.1 Uptake of Iron from PVP-Hemin Fibers by HepG2 Cells

Light microscopy was used for initial inspection of the cells' morphology and histological staining, such as Perls' stain for iron uptake (Ahrens *et al.*, 2013; Panier *et al.*, 2013). HepG2 cells for the control and treated plates were directly viewed under the microscope, shown in figure 4.3.

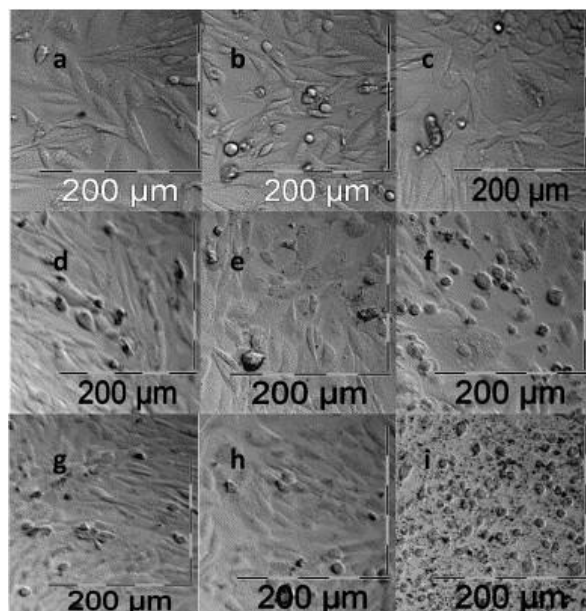


Figure 4.3. Light microscope images of HepG2 cells; (a) control, no treatment, then treatment with (b) 100 μM FAC, (c) PVP-360 only, PVP fibers containing hemin to give (d) 10 μM , (e) 25 μM , (f) 50 μM , (g) 75 μM , (h) 100 μM , and (i) 500 μM concentration of hemin. Cells were treated for 48 hr in serum-free medium and then viewed live. Healthy cells are elongated and flat; stressed cells appear rounded and either bright or granular and dark, which is the predominant appearance in panel (i).

Control, healthy cultures of HepG2 cells are shown in figure 4.3 (a) in which cells had no treatment. When treated with FAC, or with PVP fibers delivering 10, 25, 75 and 100 μM hemin, a small number of rounded stressed cells can be seen (Figure 4.3 b-h). Fibers were generally well tolerated by the cells, but after treatment with PVP fibers containing the highest concentration of hemin there was obvious evidence of cell damage, shown by a large proportion of rounded cells (Figure 4.3i).

To quantify the effect of PVP fiber treatment on cell viability, an MTT assay was carried out after treatments. The MTT assay was selected for this purpose as it is low cost, fast and simple (Pascua-Maestro *et al.*, 2018). The amount of live biomass was measured by formation of formazan through metabolic activity of living cells. Data was measured as the absorbance of formazan at 590 nm, adjusted for light scattering due to debris or insoluble material left after cells are dissolved in DMSO, by the absorbance at 650 nm. To combine data from separate experiments, control values were normalised to 1, and all treatments are expressed as a proportion of control values.

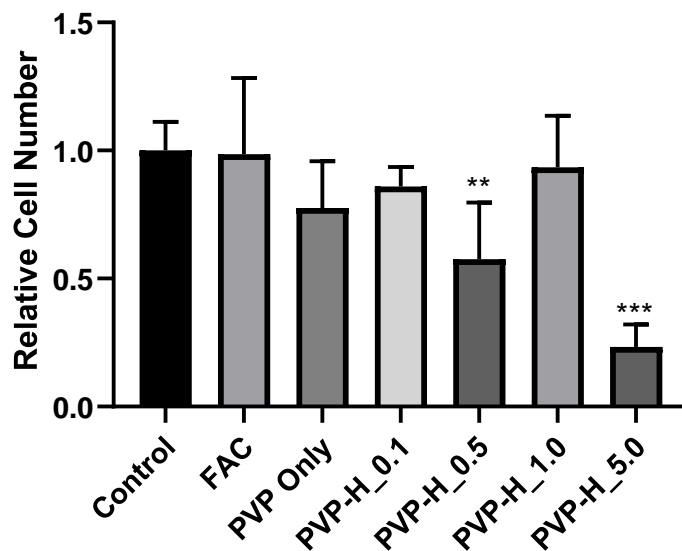


Figure 4.4. Toxicity of PVP-hemin preparations to HepG2 cells. Data are the mean + SD from three sets of data and are normalised to control, untreated cells. Treatments are 100 μ M FAC [FAC], PVP only fibers [PVP Only], PVP-hemin fibers producing: 10 μ M hemin [PVP-H_0.1], 25 μ M hemin [PVP-H_0.25], 50 μ M hemin [PVP-H_0.5], 100 μ M hemin [PVP-H_1.0] and 500 μ M hemin [PVP-H_5.0]. One-way Anova comparison of means indicated a significant difference between the control and cells treated with PVP-H_0.5 [******, $p < 0.01$] and PVP-H_5.0 [******* $p < 0.0001$].

It should be emphasised that in this experiment cells were treated with serum-free preparations, to ensure that the cells would remain locked in the quiescent or G_0 phase of the cell cycle. Under these conditions most treatments did not alter relative cell number significantly (figure 4.4). There is an uneven trend in the relative number of living cells, as the percentage of hemin is increasing. The cell number after treatment with 100 μ M hemin is only 6.6% less than control cells and is higher than after treatments with all other fibers. Treatment with fibers producing 50 μ M hemin produced a significant decrease in cell number of 42.3% and did not follow the trend. This may be due to sampling error or uneven experimental conditions in which cells were not always grown consistently, for example seeded at different densities. Despite the variation the treatment of cells with fibers producing 500 μ M hemin induced a clear, significant ($p < 0.0001$) loss of 76.7% of live cells. This is consistent with the stressed, rounded appearance of HepG2 cells treated with these fibers, shown in figure. 4.3i.

Having established that HepG2 cells remain mostly viable after exposure to PVP fibers including hemin up to 1%, the next step was to assess the ability of the cells to take up the PVP-hemin particles formed after the fibers dissolve in medium. This

is possible by measuring the increase in iron inside the cells that would be expected after uptake of the particles. A simple way of detecting excess iron in cells is by a histological stain called Perls staining, which is still used to detect excess iron loading in liver biopsies and has also been used on HepG2 cells (Cabrita *et al.*, 2004). After treatment of HepG2 cells as described above, cells were fixed and stained. A blue stain is indicative of increased levels of iron in the cells, however none of the treatments gave rise to a visible stain. It is likely that the method is not sensitive enough to detect small changes in iron levels (Sun *et al.*, 2015).

A quantitative and sensitive assay of iron was needed and the chromophore ferrozine was used (Fish, 1988; Im *et al.*, 2013; Jeitner, 2014). The basic principal of this method is that, ferrozine (3-(2-pyridyl)5,6-bis(4-phenylsulfonic acid)-1,2,4-triazine) forms a complex with ferrous iron which absorbs light of wavelength 550 nm with a high extinction coefficient of $27,900 \text{ M}^{-1} \text{ cm}^{-1}$ (Fish, 1988; Jeitner, 2014). Cells are lysed and treated with acidic permanganate to release all the iron bound to heme or protein. Aliquots of cell lysates were assayed both for iron and for protein as a measure of cell biomass.

Standard curves for both assays were used to convert absorbances to concentrations (figures 4.1 and 4.2). The ratio of iron to protein was calculated as a measure of cellular iron content.

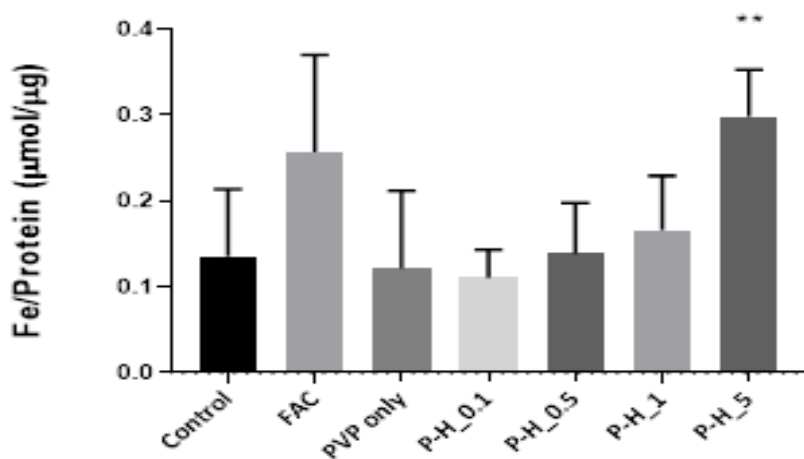


Figure 4.5. Iron uptake by HepG2 cells. Data are the mean + SD from four sets of data. Treatments are 100 µM FAC [FAC], PVP only fibers [PVP Only], PVP-hemin fibers producing: 10 µM hemin [PVP-H_0.1], 50 µM hemin [PVP-H_0.5], 100 µM hemin [PVP-H_1.0] and 500 µM hemin [PVP-H_5.0]. One-way Anova comparison of means indicated a significant difference between the control and cells treated with PVP-H_5.0 [** p < 0.01].

The data (figure 4.5) shown a pattern of modest iron uptake with increasing concentration of hemin in the fibres. Treatments with FAC and PVP-H_1.0 had the same concentration of iron, 100 μ M. Treatment with FAC induced a significant and marked, 89%, increase in cellular iron, but treatment with PVP-hemin fibers induced a more limited increase of 22%. Treatment with fibers containing the highest amount of hemin, 5%, resulted in a significant and marked increase in cellular iron of 119%, as compared to control. However, as demonstrated in figure 4.4i, fibers containing 5% hemin were toxic to cells under these conditions. The 25% of cells that did survive the treatment evidently took up iron well.

Over all the data shows limited uptake of iron from PVP-hemin fibers. As the medium used while treating the HepG2 cell with hemin preparation was serum free, this might be the reason for low uptake of iron. Another reason behind low hemin uptake may be that PVP/hemin nanoparticles did not interact well with HepG2 cells. The PVP/hemin nanoparticles might enter cells by pinocytosis and receptor mediated endocytosis with low efficiency.

4.3.2 Uptake of Iron from PVP-Hemin Fibers by THP-1 cells

This cell line was selected as a second model for hemin uptake studies, as it is a monocyte line that could be used as a model for monocytes circulating in the blood and for macrophage iron recycling and homeostasis. Because THP-1 cells are non-adherent, the experimental set-up is a little different from that used for HepG2 cells. The hemin solutions were made in the same manner as described above, and a set of solutions is shown in figure 4.6.

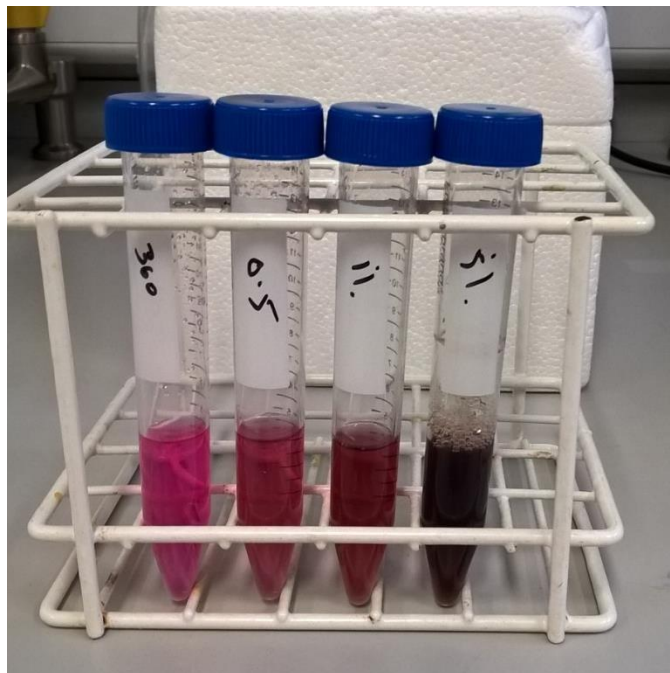


Figure 4.6. Preparations of PVP or PVP-hemin fibers in DMEM. There are four preparations: PVP-360 only, P-H_0.5, P-H_1.0 and P-H_5.0 in DMEM to make 0, 50 μM , 100 μM and 500 μM of hemin solutions with constant concentration of PVP, 0.652% (w/v). As shown in the image, the colour of solution darkened as the percentage of hemin increases.

PVP fibers containing three percentages of hemin (0.5, 1 and 5%) were selected for working on THP-1 cells. For treatments, 1 mL of THP-1 cells (5×10^5 cells) with greater than 95% viability, and in full medium, were mixed with 1mL of hemin preparation in a six-well plate, as shown in figure 4.7. It is important to note that THP-1 cells needed fetal calf serum to survive and so the treatment differs from that of HepG2 cells, which can survive in medium without fetal calf serum for a short period. THP-1 cells were therefore not arrested in the cell cycle and could continue growing in the treatment medium. Four sets of plates were prepared in the same manner. In each well 1 mL of full medium with FCS and 1 mL of preparation were added, and hence the actual concentration of hemin from the fibers was diluted two-fold.

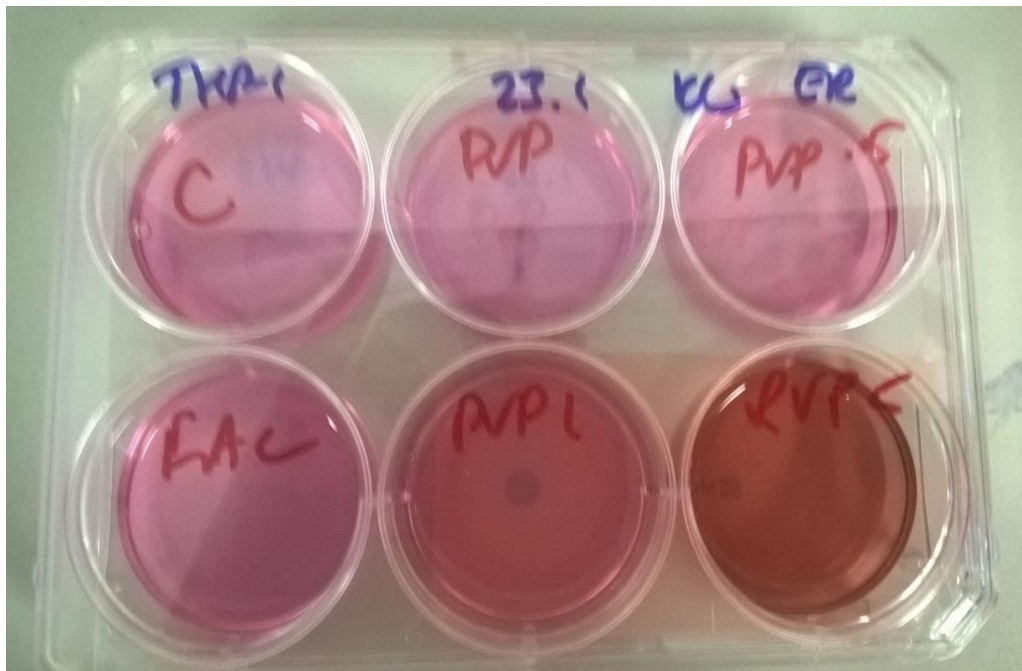


Figure 4.7. Treatment of THP-1 cells with PVP fibers only and PVP fibers containing (0.5, 1.0 and 5.0%) hemin. C is control without any treatment (1 ml of plain DMEM only), FAC contains 100 μ M of ferric ammonium citrate.

After treatments, the wells were visually assessed by microscopy (figures 4.8 and 4.9). The diameters of cells were measured using images from light microscopy analysed using Image J software and a frequency distribution graph obtained (figures 4.8 and 4.9).

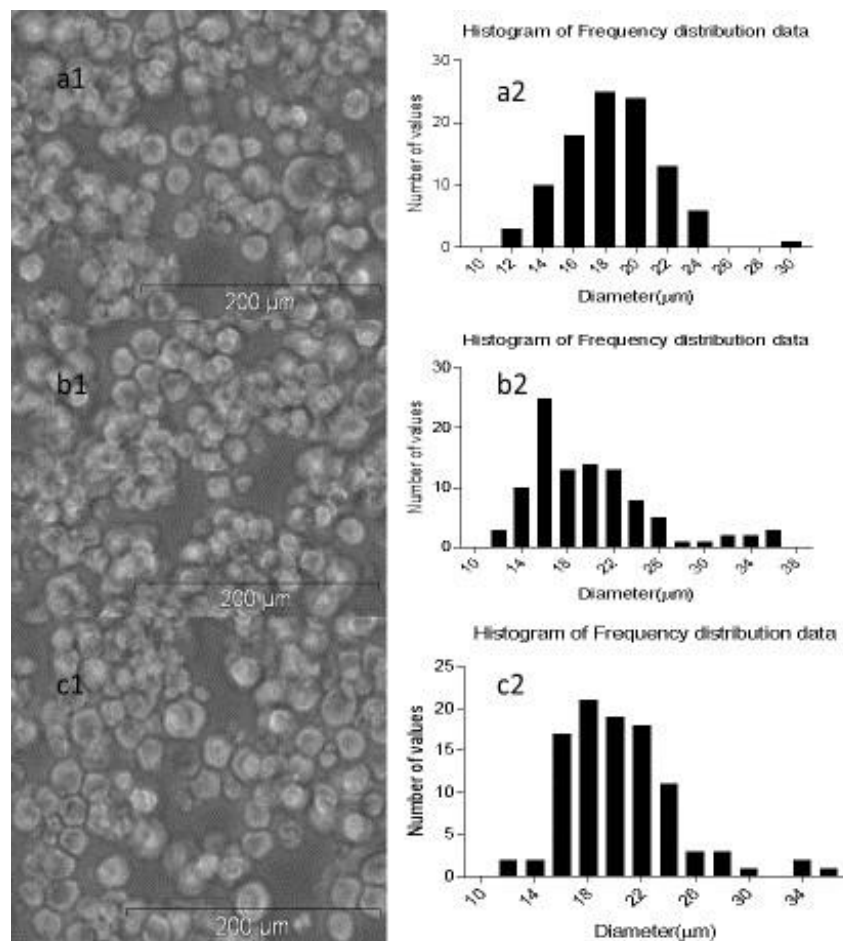


Figure 4.8. Light microscope images of THP-1 cells and frequency distribution graphs of cell diameter. (a1,2) Control cells without any treatment, (b1,2) cells treated with 100 μ M FAC, (c1,2) cells treated with PVP fibers.

Control cells with no treatment, and cells treated with FAC and PVP were found to be healthy, plump, and smooth as shown in figures 4.8 a1, b1 and c1. In contrast, cells treated with PVP-hemin looked stressed shrunken, and there is evidence of dead cells and debris, possibly apoptotic bodies (figure 4.9). Cells treated with 1.0 and 5.0 % hemin containing fibers were especially affected. The diameters of 100 cells were measured manually with the help of Image J, for each image from microscopy, and are plotted as a frequency distribution bar graph using GraphPad Prism software. The mean diameter and standard deviation of cells without treatment, FAC treated and PVP treated are given in table 4.3. The D'Agostino & Pearson, normality test was performed on each data. Control sample passed the normality tests whereas FAC and PVP treated sample failed the normality test. The FAC and PVP treatments seem to induce some cells, which are larger in diameter – this may be due to differentiation.

S.NO	Samples (THP1 cells)	Mean±SD of cell diameter, μm
1	Control	18.5±3.1
2	FAC treated cells	20.0±5.4
3	PVP fibers treated cells	20.2±4.2
4	P-H_0.5 fibers treated cells	16.7±3.4
5	P-H_1.0 fibers treated cells	13.3±2.6
6	P-H_5.0 fibers treated cells	16.2±3.4

Table 4.3. Mean±SD of diameter 100 THP1 cells, measured with image J. Control (cells without treatment), FAC (positive control), PVP-fibers, P-H_0.5, P-H_1.0 and P-H_5.0 treated cells.

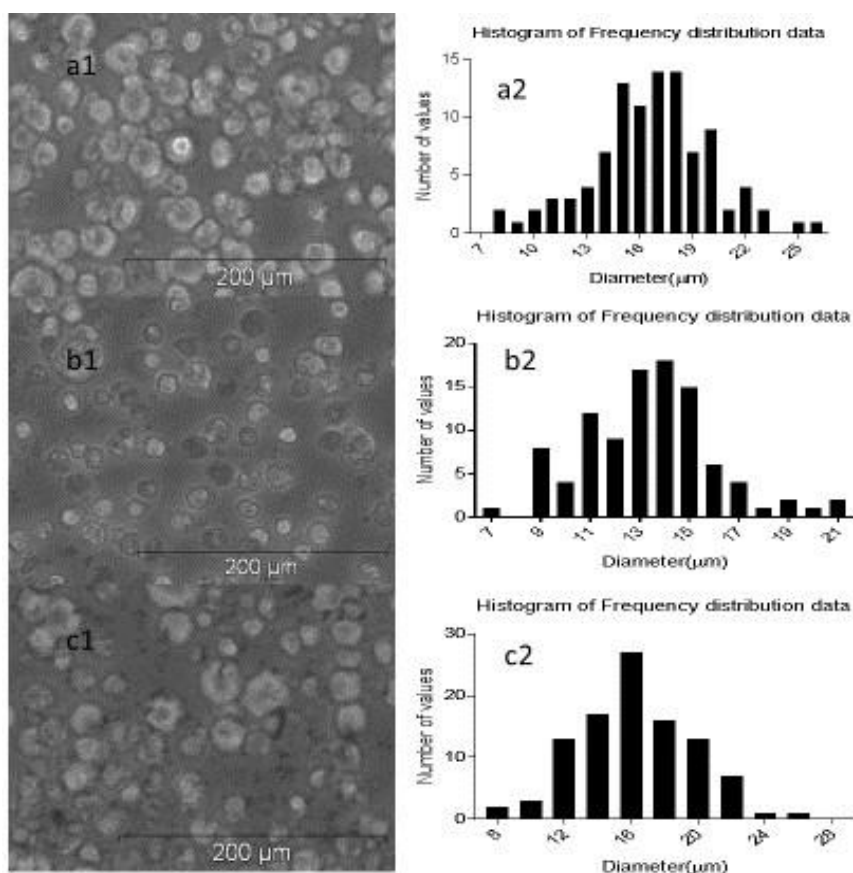


Figure 4.9. Light microscope images of THP-1 cells and frequency distribution graphs of cell diameter. (a1,2) Cells treated with P-H_0.5 fibers, (b1,2) cells treated with P-H_1.0 fibers, (c1,2) cells treated with P-H_5.0 fibers.

The mean diameter and standard deviation of cells treated with hemin containing fibers are mentioned in table 4.3. The mean diameters of untreated control cells (18.5 μm) or cells treated with PVP fibers (20.2 μm) were bigger than diameters of cells treated with hemin containing PVP fibers (13.3 -16.7 μm). The mean diameter of cells treated with 0.5 % hemin containing PVP fibers (16.7 μm) was higher than cells treated with 1% hemin PVP fibers (13.3 μm). Cells treated with 5.0 % hemin PVP fibers, had a mean diameter (16.2 μm) larger than that of the cells treated with 1 % hemin (13.3 μm), but the cells were rough. 0.5, 1.0 and 5% hemin treated samples passed the D'Agostino & Pearson, normality test.

After 48 hr treatment the numbers of live and dead cells were counted by Trypan blue staining using a hemocytometer.

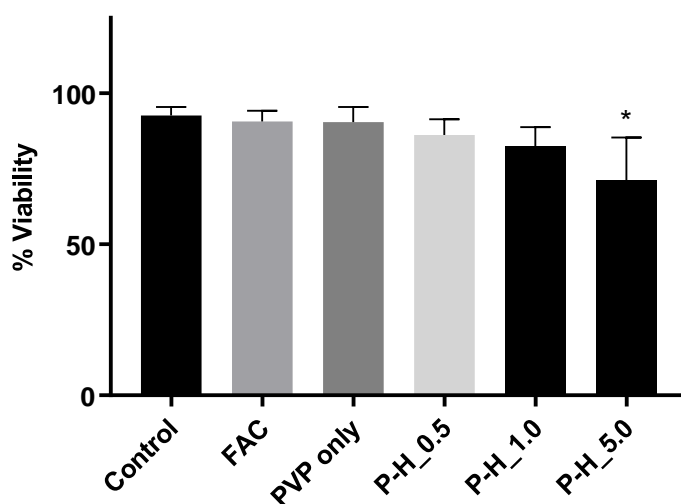


Figure 4.10. Toxicity of hemin preparations to THP-1 cells. Data are mean + SD from four sets of cells. X-axis labels indicate untreated cells (Control), cells treated with 50 μM FAC (FAC) as a positive control, cells treated with dissolved PVP fibers at 0.326% (w/v) (PVP only), cells treated with PVP-hemin fibers to give 25 μM (P-H_0.5), 50 μM (P-H_1.0) and 250 μM (P-H_5.0) hemin. One-way Anova comparison of means indicated a significant difference between the control/ FAC/ PVP only and cells treated with P-H_5.0 [* , $p < 0.01$].

The viability of cells after treatment with FAC or PVP-only fibers is almost the same as control cells without treatment (figure 4.10). Viability of cells treated with PVP-hemin fibers showed a tendency to decrease as the proportion of hemin in the fibers increased, and an average of 70% viability was found in cells treated with PVP fibers containing 5% hemin. There was also a change in appearance of the cells after treatment with PVP-hemin fibers (figure 4.9), with some evidence of cell damage. The viability data showed that the hemin and PVP are not strongly toxic

to the cells, which tolerated the treatments much better than HepG2 cells (figure 4.4).

After treatment with hemin fibers with the higher amounts of hemin, the cells acquired a light brown coloration, indicative of iron uptake. To assess levels of cellular iron the ferrozine assay was used, and the data were normalised to the total cell number, counted using a hemocytometer.

The ratio of total iron taken up by the cells to total number of cells is shown in figure 4.11.

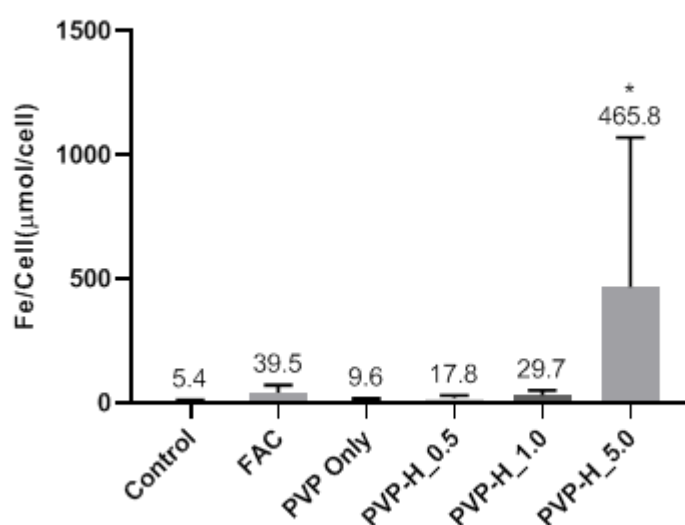


Figure 4.11. Iron uptake by THP-1 cells. Data are mean+SD from five sets of cells. X-axis labels indicate untreated cells (Control), cells treated with 50μM FAC (FAC) as a positive control, cells treated with dissolved PVP fibers at 0.326% (w/v) (PVP only), cells treated with PVP-hemin fibers to give 25 μM (PH_0.5), 50 μM (P-H_1.0) and 250 μM (P-H_5.0) hemin. One-way Anova comparison of means indicated a significant difference between the control/ PVP only and cells treated with P-H_5.0 fibers [**, $p < 0.005$] and there is significant difference between cell treated with P-H_0.5 and P-H_5.0 [* , $p < 0.05$].

As shown in figure 4.11, the highest hemin concentration causes a large uptake of iron but, the cell viability was lower compared to other percentages of PVP-hemin fibers. The iron uptake by FAC is 7 times higher than control. The iron in 0.5, 1% hemin-PVP fibers treated cells were found 17.8 and 29.7 μmol/cell, whereas the iron uptake from 5 % hemin containing fibers by the cells was 100 times higher than control. There is a clear trend in increasing iron uptake with increasing hemin

content in fibers, but due to the big difference in iron uptake from 5% hemin compared with the other preparations the amount of iron uptake from each preparation is indicated for each sample in figure 4.11.

4.3.3 Uptake of Iron from PVP-Hemin Fibers by Caco-2 cells

The Caco-2 cell line was selected as a third model for hemin uptake studies, as it is an intestinal cell line widely used as a model for absorption of dietary components, including different formulations of iron (Tako *et al.*, 2016). Because Caco-2 cells are adherent, the experimental set-up was the same as used for HepG2 cells. The hemin solutions were made in the same manner as described in section 4.2.2.1.

PVP fibers containing three percentages of hemin (1, 2 and 5) were selected for working on Caco-2 cells. For treatments, 0.5 mL of Caco-2 cells (5×10^5 cells) with greater than 95% viability, were grown in full medium, the medium was replaced with 0.5 mL of hemin preparation in a 24-well plate, as shown in figure 4.13. It is important to note that Caco-2 cells needed fetal calf serum to survive and so the treatment differs from that of HepG2 cells, which can survive in medium without fetal calf serum for a short period. Caco-2 cells were therefore not arrested in the cell cycle and continued growing in the treatment medium. Two sets of plates were prepared in the same manner (one for MTT and one for ferrozine test).

Light microscopy was used for initial inspection of the cells' morphology. Caco-2 cells in the control and treated plates were directly viewed under the microscope, shown in figure 4.14.

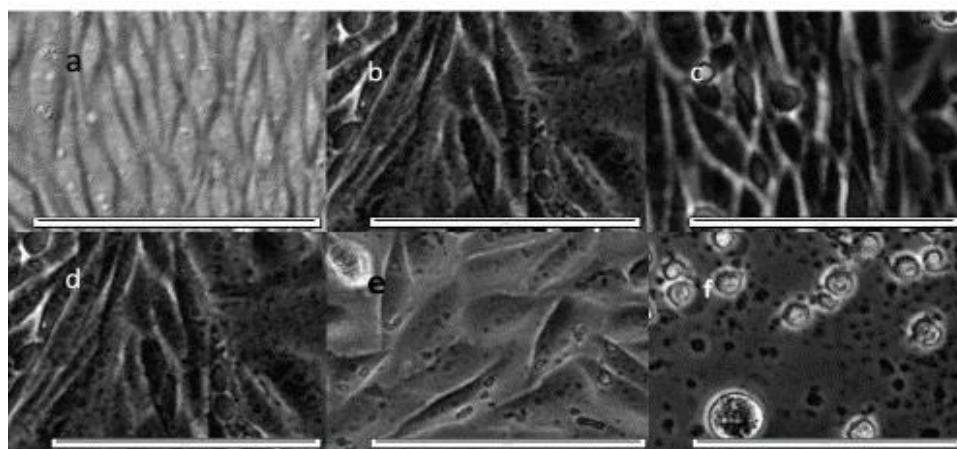


Figure 4.12. Light microscope images of Caco-2 cells; (a) control, no treatment, then treatment with (b) 100 μM FAC, (c) PVP-360 only, PVP fibers containing hemin to

give (d) 100 μM , (e) 200 μM , (f) 500 μM concentration of hemin. The scale bar is 200 μm . Cells were treated for 48 hr in full medium and then viewed live. Healthy cells are elongated and flat; stressed cells appear rounded and either bright or granular and dark, which is the predominant appearance in panel (f).

Control, healthy cultures of Caco-2 cells are shown in figure 4.12 (a) in which cells had no treatment. When treated with FAC, or with PVP fibers delivering 100, and 200 μM hemin, rarely rounded stressed cells can be seen (figure 4.3 b-h). Fibers were generally well tolerated by the cells, but after treatment with PVP fibers containing the highest concentration (500 μM) of hemin there was obvious evidence of cell damage, shown by a large proportion of rounded cells and some round with rough surface (figure 4.12f).

To quantify the effect of PVP fiber treatment on cell viability, an MTT assay was carried out after treatments. The MTT assay was selected for this purpose as it is low cost, fast and simple (PascuaMaestro et al., 2018). The amount of live biomass is measured by formation of formazan through metabolic activity of live cells. Data is measured as the absorbance of formazan at 590 nm, adjusted for light scattering due to debris or insoluble material left after cells are dissolved in DMSO, by the absorbance at 700 nm. To combine data from separate experiments, control values were normalised to 1, and all treatments are expressed as times of control.

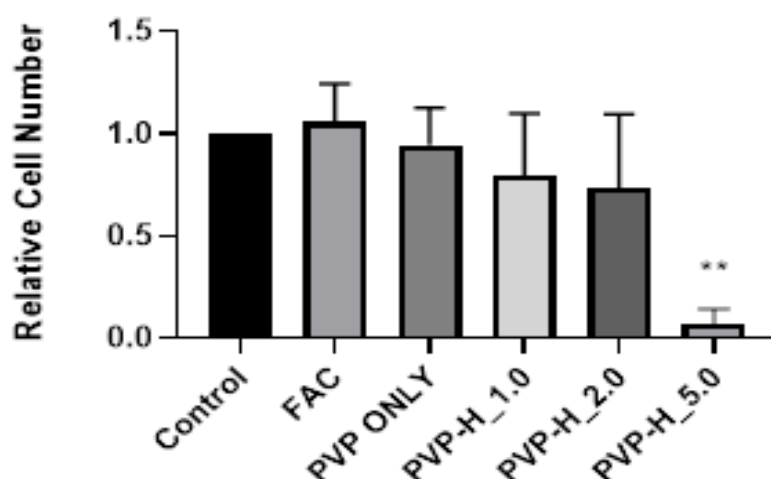


Figure 4.13. Toxicity of PVP-hemin preparations to Caco-2 cells assessed by MTT assay. Data are the mean + SD from three sets of data and are normalised to control, untreated cells. Treatments are 100 μM FAC [FAC], PVP only fibers [PVP Only], PVP-hemin fibers producing: 100 μM hemin [PVP-H_1.0], 200 μM hemin

[PVP-H_2.0] and 500 μ M hemin [PVP-H_5.0]. One-way Anova comparison of means indicated a significant difference between cells treated with PVP-H_5.0 [$** p < 0.05$] and control, FAC, PVP only, PVP-H_1.0 and PVP-H_2.0.

The viability of cells after treatment with FAC or PVP-only fibers is almost the same as control cells without treatment (figure 4.13). Viability of cells treated with PVP-hemin fibers showed a tendency to decrease as the proportion of hemin in the fibers increased, and an average 7.12% viability was found in cells treated with PVP fibers containing 5% hemin. There was also a change in appearance of cells after treatment with PVP-hemin fibers containing 5% hemin (figure 4.12f), with some evidence of cell damage. The viability data showed that a hemin content in PVP fibers up to 2% is not strongly toxic to the cells.

As shown in figure 4.14, the highest hemin concentration causes a large uptake but, the viability was found lower, as compared to other percentages of PVP-hemin fibers. There was no significant increase in iron after treatment of cells with FAC, PVP and PVP-H_1.0 fibers as compared with control cells. Increase in iron content after treatment with 2% hemin-PVP fibers was measured to 42%. The iron uptake from 5% hemin containing fibers increased by 79% compared to control, but most cells were stressed and there were clear signs of toxicity after the treatment (figure 4.15f).

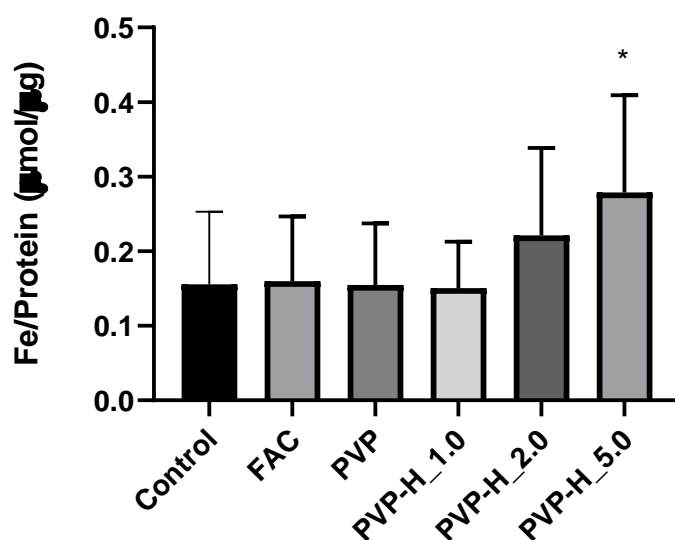


Figure 4.14. Iron uptake by Caco-2 cells. Data are the mean+SD from three sets of data. Treatments are 100 μ M FAC [FAC], PVP only fibers [PVP Only], PVP-hemin fibers producing: 100 μ M hemin [PVPH_1.0], 200 μ M hemin [PVP-H_2.0] and 500 μ M hemin [PVP-H_5.0]. One-way Anova comparison of means indicated a

significant difference between the control and cells treated with PVP-H_5.0 [* p < 0.05].

In cells treated with 5% hemin-PVP fibers Hep-G2 cells had similar iron content 0.29 $\mu\text{mol}/\mu\text{g}$ to Caco-2 cells (0.27 $\mu\text{mol}/\mu\text{g}$). Iron content in Caco2 cells was 0.22 $\mu\text{mol}/\mu\text{g}$ after treatment with 2% hemin PVP fibers. There was no significant increase in quantity of iron with respect to control from 1% hemin-PVP fibers by Caco-2 cells but, in Hep-G2 cells there was some uptake as seen in figure 4.5. There was clear uptake of iron from FAC in Hep-G2 cells compared to Caco-2 cells.

In order to study the effect of microparticulate precipitate on cells, preparations of hemin fibers dissolved in biological medium were spun at 12,000 g for 5 minutes to remove the precipitate. Caco-2 cells were treated with supernatants and MTT and iron assays were carried out (figure 4.15 and 4.16).

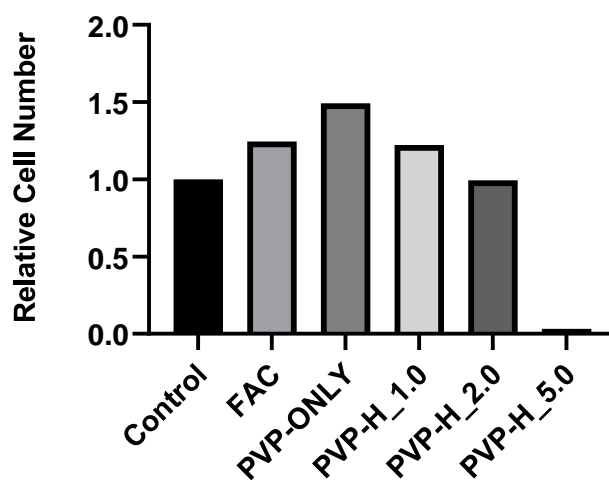


Figure 4.15. Toxicity of centrifuged PVP-hemin preparations to Caco-2 cells assessed by MTT assay. Data are the mean from one set of data and are normalised to control, untreated cells. Treatments are 100 μM FAC [FAC], PVP only fibers [PVP Only], PVP-hemin fibers producing: 100 μM hemin [PVP-H_1.0], 200 μM hemin [PVP-H_2.0] and 500 μM hemin [PVP-H_5.0].

The viability of cells after treatment with FAC, PVP-only fibers and 1% hemin-PVP fibers was higher than the control without treatment (figure 4.15). Viability of cells treated with PVP-hemin fibers showed a tendency to decrease as the proportion of hemin in the fibers increased, and an average 3.20% viability was found in cells treated with PVP fibers containing 5% hemin. The viability data showed that PVP-hemin fibers up to 2% (spun) are not toxic to the cells, but the treatments are

tolerated better by Caco-2 cells than the cells treated with unspun hemin preparations. (figure 4.13).

Iron uptake from spun preparations of PVP-hemin fiber solutions by Caco-2 cells is shown in figure 4.16.

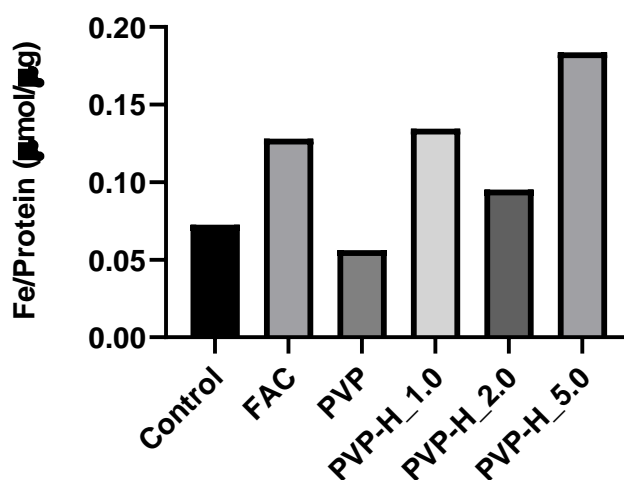


Figure 4.16. Iron uptake by Caco-2 cells treated with centrifuged PVP-hemin fiber solutions. Data are the mean from one set of data. Treatments are 100 μM FAC [FAC], PVP only fibers [PVP Only], PVP-hemin fibers producing: 100 μM hemin [PVPH_1.0], 200 μM hemin [PVP-H_2.0] and 500 μM hemin [PVP-H_5.0].

The data shown in figure 4.16 indicate there is no clear trend in uptake of iron, with uptake less from from 2% hemin-PVP fiber solutions than from 1% hemin-PVP fiber solutions. The uptake of iron from spun preparations of hemin is lower than without spun preparations in Caco-2 cells. In case of 1% hemin-PVP fiber solutions, viability is higher in cells treated with spun preparations than in cells treated with unspun preparations. However, the differences are not large, and experiments need to be repeated to see if they are real or not.

4.4 Discussion

To assess the bioavailability of the iron in the hemin nanoparticles some preliminary studies were carried out *in vitro*, to assess iron uptake from the NPs by three cell culture models. It was also important to assess any potential toxicity of the hemin fibers.

Bioavailability of iron involves the absorption of iron from the intestine into the blood circulation and subsequent utilization of iron in the cells for ordinary metabolic processes. This has five stages: 1. Digestion, release of iron into the lumen of the intestine from the food matrix, 2. Crossing the mucus barrier which coats the intestinal apical cells, 3. The uptake of iron by intestinal enterocytes, 4. The transport of iron through the enterocytes into the blood, 5. The retention, utilization, and storage of iron in the body (Sandberg, 2010). HT 29 cells treated with methotrexate can be used as a model for intestinal mucosa, since these cells are transformed into mucus secreting differentiated cells when treated with methotrexate (Martínez-Maqueda *et al.*, 2015). Caco-2 cells were selected as a combined *in vitro* digestion model which includes stages 1 and 3, and if the cells are cultured on inserts this model also can be used to assess the fourth stage, i.e. the transepithelial transport into the circulation (Sandberg, 2010). HepG2 and THP-1 cells were selected as a model for *in vitro* retention, utilization, and storage of iron, which is stage 5 of iron bioavailability. HepG2 human hepatoma cells were selected as a model for liver cells (hepatocytes). Liver is the major organ of iron storage and helps to maintain the homeostasis of body iron levels (Scott and Guilliams, 2018). The human monocyte cell line THP-1 has been selected as a model for an important cell type that has a major role in systemic iron homeostasis, the monocyte-macrophage system (Andriopoulos and Pantopoulos, 2006; Ludwiczek *et al.*, 2003). Macrophages capture and recycle senescent erythrocytes, extracting the iron from haemoglobin and exporting it for re-use (Silva and Faustino, 2015). This might help in digestion of PVP/hemin nanoparticles which would directly enter in circulation.

Studies on GIT mucosal absorption of particles delivered via the oral route showed that particle size is an important factor in absorption. NPs are able to use three routes for absorption: paracellular transport, transcellular transport and uptake by the M cells of gut (Hosny *et al.*, 2015). A diagram illustrating the different routes for different particle size is shown in figure 4.17.

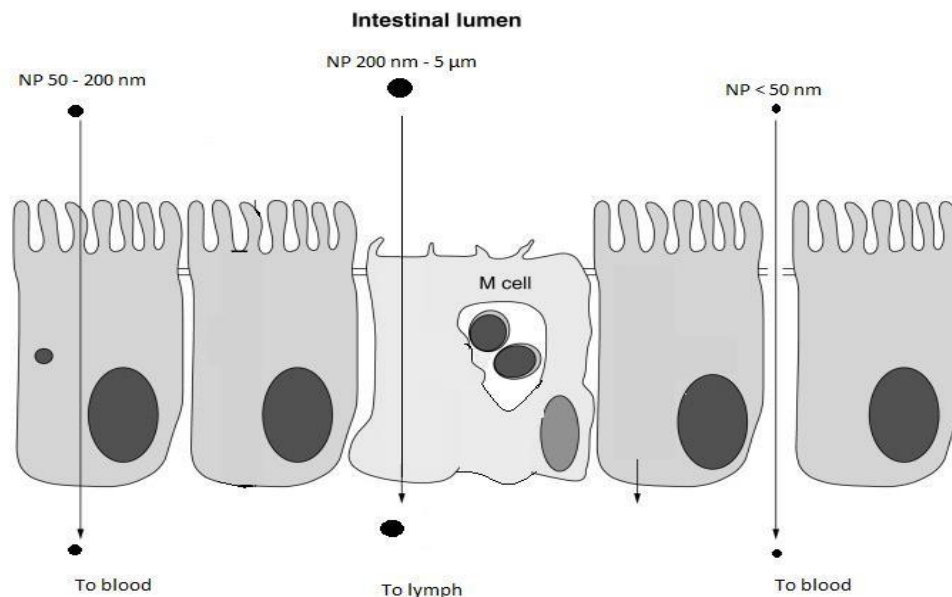


Figure 4.17. Uptake of NPs from the intestinal lumen by paracellular transport (50-200 nm), transcellular transport (< 50 nm) and the M cells (200-5 μm). The uptake by a particular route depends on particle size (Barua and Mitragotri, 2014).

Initially HepG2, the liver cells which help to maintain iron stores were used (Kulaksiz *et al.*, 2004). There is an uneven trend of decreasing cell number in case of HepG2 cells, as the percentage of hemin was increased, but the cell number after treatment with 100 μM hemin is only 6.6% less than control cells and is higher than after treatments with all other fibers. This may be due to sampling error or uneven experimental conditions in which cells were not always grown consistently, for example seeded at different densities or allowed to grow for different periods before treatments. Despite the variation, the treatment of cells with fibers producing 500 μM hemin induced a clear, significant ($p < 0.0001$) loss of 76.7% of live cells. This is consistent with the stressed, rounded appearance of HepG2 cells treated with these fibers, shown in figure. 4.3i. A one-way ANOVA comparison of means in HepG2 cells indicated a significant difference between the control and cells treated with FAC [* , $p < 0.05$] and PVP-H_5.0 [** $p < 0.01$]. Overall, the data show limited uptake of iron from PVP-hemin fibers. This might be due to limited interaction between PVP/hemin NPs and potential endocytic or pinocytotic entry pathways (Lundquist and Artursson, 2016). This can be carried out by improvement or modification in hemin formulation, which is possible by using other polymers or using coaxial electrospinning with a shell polymer with better adhesive properties than PVP, which might improve interaction of formulation with the cells.

The human monocyte cell line THP-1 has been selected as a 2nd model for iron uptake, since it has a major role in systemic iron homeostasis, the monocyte-

macrophage system (Andriopoulos and Pantopoulos, 2006; Ludwiczek, 2003). The viability of THP-1 cells after treatment with FAC or PVP only fibers is almost the same as control cells without treatment (figure 4.10). Viability of cells treated with PVP-hemin fibers showed a tendency to decrease as the proportion of hemin in the fibers increased, and an average 70% viability was found in cells treated with PVP fibers containing 5% hemin. There was also a change in appearance of cells, they were rougher after treatment with 1% and 5% PVP-hemin fibers (figure 4.9), with some evidence of cell damage. The viability data showed that the hemin and PVP is not strongly toxic to the THP1 cells, which tolerated the treatments much better than HepG2 cells (figure 4.4). The highest hemin concentration caused a large uptake (119% increase in iron) and a relatively limited effect on cell viability, reduced to 77%. Compared with HepG2 and Caco-2 cells, which have an epithelial phenotype, THP1 cell tolerated the hemin fibers well and could take up iron. Further work is needed to find optimal conditions for iron loading with hemin fibers and to elucidate the mechanism of uptake. For example, fibers with 3% and 4% (w/w) hemin could be assessed, along with a time-course of uptake. Electron microscopy could be used to visualise uptake to help identify the pathway.

Caco-2 cells, a cell line derived from human colon cancer (Lea, 2015), were selected as a third cell line because they have been widely used as a model for absorption of dietary components, including different formulations of iron (Tako *et al.*, 2016). The viability of cells after treatment with FAC or PVP-only fibers is almost the same as control cells without treatment (figure 4.15). Viability of cells treated with PVP-hemin fibers showed a tendency to decrease as the proportion of hemin in the fibers increased, and an average 7.12% viability was found in cells treated with PVP fibers containing 5% hemin, indicating a marked toxicity of the hemin fibers. There was also a change in appearance of cells after treatment with 5% PVP-hemin fibers (figure 4.14f), with some evidence of cell damage. The highest hemin concentration causes an apparent larger uptake of iron (79%) compared with other treatments, but the toxic effect of this concentration limits the usefulness of the formulation.

Caco-2 cells did not respond to FAC, as compared to Hep-G2 cells. There was little uptake of iron from 1% formulation of hemin in Hep-G2 or Caco-2 cells (figures 4.5 and 4.14). 2% hemin formulation improved the level of iron in Caco-2 cells by about 30 (figure 4.14) and it would be interesting to assess iron uptake from fibers containing hemin at 3% and 4%, to see if it is possible to identify a threshold toxicity.

The possible route for PVP/hemin nanoparticle uptake, being around 50 nm (according to DLS in chapter 3) can be pinocytosis (Schwarz, 2018). However, high molecular weight species, including those larger than 100 nm e.g. carbon nanotubes, face difficulty in such passive translocation. Instead, their transport through the membrane is generally considered to occur by membrane fission and budding, surface aggregation, inclusion in the membrane or lipid membrane permeation (Pogodin *et al.*, 2012). PVP/hemin NPs with diameter more than 100 nm can potentially move into the cell by any of these transport mechanisms. The NPs may also be transported into cells by the folate transporter due to the close structural resemblance between hemin and heme (West and Oates, 2008). The main uptake mechanism for nanoscale material in HepG2 cells was found to be via clathrin-mediated endocytosis and macropinocytosis (Brkić Ahmed *et al.*, 2017). A diagram of the pathway of uptake of NPs from PVP/hemin fibers contained in a gastro-resistant capsule is shown in figure 4.18. Uptake of hemin by the cells is limited, it is a fundamentally important point – how can PVP NPs be efficiently targeted for enhanced bioavailability? To address this problem Jana *et al.* (2002) used Sendai viral envelopes to carry out delivery of hydrogel nanoparticles [cross linked PVP-NP (35-50 nm) containing fluoresceinated dextran (FITC-Dx)] through the process of fusion. Sendai viral envelopes facilitated the fusion of nanoparticles with cell membrane of HepG2 cells.

Mucus immobilizes particles by hydrophobic and electrostatic interactions, which can result in less uptake of NP. To overcome this, it is necessary to develop mucolytic, mucoadhesive or mucus penetrating particles (Barua and Mitragotri, 2014). Mucus penetrating particles (MPP) can rapidly diffuse through the mucus barrier in the intestine. This is made possible by the presence of a dense layer of low molecular PEG-chains on the surface of nanoparticles (Lundquist and Artursson, 2016). Modification of surface characteristics of NPs can offer higher penetration through the mucus membrane. Chitosan NPs with a PEO corona and with a lipid shell of pluronic F127 exhibited comparatively higher efficiency in penetration of the mucus membrane (Barua and Mitragotri, 2014).

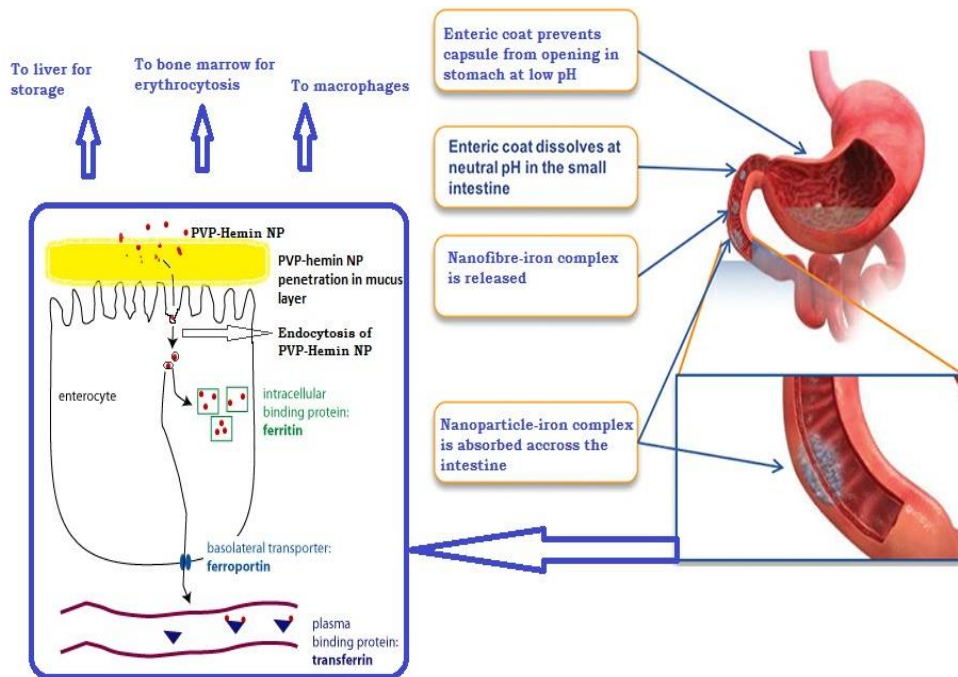


Figure 4.18. Schematic diagram modelling the absorption and uptake of iron from gastro-resistant capsules containing PVP/hemin fibers. Endocytosis is considered as the entrance route of entrance of PVP/hemin NP in intestinal cells, via the heme endocytic pathway. The image of stomach is taken from (“PEPTIDE DELIVERY - The Endometriosis Enigma – Why Can’t There Be a Pill for That?,” 2018)

Chapter 5

Future work

5.1 Potential of nanotechnology in drug delivery for cancer treatment

5.1.1 Burden of cancer

According to recent cancer research, in the UK, 1 in 2 people will be diagnosed with cancer at some stage of their life (Ahmad *et al.*, 2015). This indicates that the burden of cancer disease may be on the rise. According to the Office for National Statistics (2016) 303,135 new cases of cancer were registered in England in 2014. This represents an increase of 3,135 cases from the previous year (excluding nonmelanoma skin cancers).

There are various modalities of cancer treatment, one of which is chemotherapy. Anticancer drugs used in chemotherapy target the cancer cells, however there are potential side effects of these drugs. Some of these issues are linked with drug delivery resulting in poor bioavailability, high dose requirement, low therapeutic indices, and other side effects (Senapati *et al.*, 2018). Hence, efforts are needed to improve cancer treatment options.

5.1.2 5-Fluorouracil: An example of chemotherapeutic drug

5-FU is used to treat solid tumours and is a standard chemotherapeutic agent which has been in use for several decades (Muthu *et al.*, 2013). It is often used in combination for the treatment of colorectal, skin and / or breast cancers (Ito *et al.*, 2008). Colorectal cancer is one of the most common cancers in the UK (national statistics office UK 2016) and 5-FU is used alone as well as in combination with other chemotherapeutics (Wei *et al.*, 2018). The mode of action of 5-FU involves inhibition of the enzyme thymidylate synthase which is involved in DNA replication after it is incorporated in RNA (Kitao *et al.*, 2017).

Here, 5-fluorouracil (5-FU) was selected as the model drug. The structure of 5-FU is shown in figure

5.1.

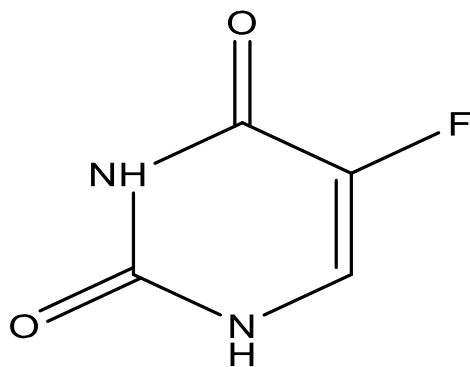


Figure 5.1 Structure of 5-FU

Unfortunately, 5-FU has severe side effects including hand-foot syndrome (Chiara *et al.*, 1997), anorexia, diarrhoea (Boussios *et al.*, 2012), enteritis (Zamani and Helman, 2004), and myelosuppression (Fata *et al.*, 1999). To overcome these side effects, combination therapy and the timing of drug and sequence of drugs in which they are administered is critical (Muthu *et al.*, 2013). Clinical and preclinical studies shown that the toxicity of 5-FU may be reduced, and antitumor activity may be improved by circadian modulation. An increase in 5-FU dose intensity and reduction in 5FU+LV toxicity is possible to obtain by a circadian (nonsinusoidally) modulated infusion. This study showed that toxicity reduction is mainly dependent on the quasi-intermittency (Falcone *et al.*, 1999). 5-FU is absorbed non-uniformly from the intestine, it is also an analogue of pyrimidine uracil as it is metabolised through same metabolic pathway as uracil by uracil reductase or dihydropyrimidine dehydrogenase (Wilson *et al.*, 2012).

An efficient delivery system is required for target delivery of 5-FU, as it is rapidly eliminated. The half-life of parentally administered 5-FU is 8 to 20 minutes. The reason for quick elimination is rapid catabolism in the liver (Diasio and Harris, 1989). Hence an efficient delivery system of 5-FU is required, which should possess characteristics such as small size, physical stability, biodegradability, controllable release, no storage or drug leakage problems and resistant against degradation (Jaferian *et al.*, 2016).

5.1.3 Formulation of 5 FU-PCL Nanoparticles for drug delivery

Several biodegradable polymers have been used for the drug delivery of 5-FU which have increased the stability of the drug and provided controllable release. Alginate is a copolymer and its use has shown an increase in the drug load.

One recent approach involved molecular imprinting of 5-FU nanoparticles (NPs). Acrylamide or N,N'-methylenebis (acrylamide) was used in this study as monomers while AIBN and EDMA were selected as an initiator and crosslinker respectively. The nanoparticles obtained from this work have improved localization of drug with reduced liver side effects (Gardouh *et al.*, 2018). Another appealing approach is to formulate 5-FU loaded nanoparticles by electrospraying.

In the start of this PhD work, attempts were made to produce PCL and 5-FU NPs. Various forms of PCL containing NPs were generated, and they were characterised by using scanning electron microscopy (SEM), infrared spectroscopy (IR), and nuclear magnetic resonance spectroscopy (NMR). The next step involved attempting to form NPs loaded with the model drug and assessing viability of these NPs as potential DDS (drug delivery system) for 5-FU.

Also, attempts to modify the surface characteristics of the NPs as carriers for 5-FU were also undertaken. This involved using co-axial electrospraying (discussed in chapter 1), generating NPs which had PCL in the core and PVP in the shell.

Low molecular weight PVP successfully gave nanoparticles with less than 100 nm but the formulation of PCL (10-14) nanoparticles remained a challenge and there were problems in identifying the presence of PCL in the particles produced. Due to time constraints further work on this aspect of the project was abandoned and as there was no success in getting PCL nanoparticles to incorporate 5-FU.

5.1.4 Potential for a formulation of 5FU-PVP Nanoparticles

Successful formulation of PVP-Hemin could open doors for potential 5FU-PVP formulation. PVP nanoparticles could be used to incorporate 5-FU, which if successful could revolutionise the cancer treatment.

5.2 PVP-Hemin formulation: Improvement in Hemin Formulation

To overcome difficulties of absorption and distribution there is a need to improve the hemin formulation. The PVP fibers could be viewed as a first attempt and subsequent work using electrospinning could include further investigate the use of small PVPs. Use of small molecular weight PVP might increase cellular uptake as discussed by Barua and Mitragotri (2014), according to which smaller polystyrene particles (300nm) showed higher intake in enterocytes and M cells *in vivo* than

larger particles. Using co-axial electrospinning by keeping PVP-hemin in the core and PVP in the shell is another approach to reduce toxicity.

5.2.1 PVP-Hemin Formulation: Scope for further work

Formulation of orally active hemin preparations for the treatment of anaemia may present new opportunities to treat anaemia. The preliminary work described in this thesis has identified a novel way in which hemin can be formulated in a soluble form, but with limited ability to be taken up by epithelial cells and marked toxicity when higher proportions of hemin are present in the formulations. Some suggestions for improvement of the hemin-fiber formulations, or alternatives, are discussed here. As a starting point, other polymers such as CA (cellulose acetate), Eudragit L 100, Eudragit S 100, and Eudragit E 100) could be assessed. These have better mucoadhesive properties than PVP and are resistant to gastric degradation.

The formulations prepared with low molecular weight PVPs can be refined to make better yields, perhaps using coaxial electrospinning of core-shell fibers, with a PVP-hemin core and another, mucoadhesive, polymer in the shell. The shell polymer could enhance mucosal diffusion and uptake. Mucoadhesive polymers such as PLGA, chitosan, PAA and PLGA, poly (sebacic acid) can be used to promote adhesion to the mucus layer to improve absorption of hemin in enterocytes. Removal of the mucus layer with a mucolytic agent can be an alternative method, but there will be chances of bacterial infection (Barua and Mitragotri, 2014). Pulmozyme® [a recombinant human DNase (rhDNase)], Mucinex® (N-acetyl-L-cysteine; NAC) and Nacystelyn are examples of a few mucolytic agents described in the literature (Lai *et al.*, 2009).

The use of SLNs (solid lipid NPs), might be another approach to overcome the bioavailability issue. NPs with improved physicochemical properties, including a positive surface charge, together with high affinity surface ligands [penetratin and Sec peptide] could improve apical endocytosis (Lundquist and Artursson, 2016). SLNs could be a promising carrier for iron with improved bioavailability, (Hosny, 2015).

References

- Abbaspour, N., Hurrell, R., Kelishadi, R., 2014. Review on iron and its importance for human health. *J Res Med Sci* 19, 164–174.
- Abderrahim, B., Abderrahman, E., Mohamed, A., Aicha, A., Reda, B., Abdeslam, A., Isaad, J., Abdesselam, T., 2016. Synthesis and Characterization of Branched Polyester: Thermal and Microbial Degradation Studies. *Journal of Polymer and Biopolymer Physics Chemistry, Journal of Polymer and Biopolymer Physics Chemistry* 4, 16–27. <https://doi.org/10.12691/jpbpc-4-13>
- Abderrahim, B., Abderrahman, E., Mohamed, A., Fatima, T., Abdesselam, T., Krim, O., 2015. Kinetic Thermal Degradation of Cellulose, Polybutylene Succinate and a Green Composite: Comparative Study. *World Journal of Environmental Engineering, World Journal of Environmental Engineering* 3, 95–110. <https://doi.org/10.12691/wjee-3-4-1>
- About the eMC - electronic Medicines Compendium (eMC) [WWW Document], n.d. URL <https://www.medicines.org.uk/emc/about-the-emc> (accessed 5.13.18).
- Ahmad, A.S., Ormiston-Smith, N., Sasieni, P.D., 2015. Trends in the lifetime risk of developing cancer in Great Britain: comparison of risk for those born from 1930 to 1960. *British Journal of Cancer* 112, 943–947. <https://doi.org/10.1038/bjc.2014.606>
- Ahrens, M.B., Orger, M.B., Robson, D.N., Li, J.M., Keller, P.J., 2013. Whole-brain functional imaging at cellular resolution using light-sheet microscopy. *Nat. Methods* 10, 413–420. <https://doi.org/10.1038/nmeth.2434>

- Alfaro De Prá, M.A., Ribeiro-do-Valle, R.M., Maraschin, M., Veleirinho, B., 2017. Effect of collector design on the morphological properties of polycaprolactone electrospun fibers. *Materials Letters* 193, 154–157. <https://doi.org/10.1016/j.matlet.2017.01.102>
- Alyami, H., Dahmash, E., Bowen, J., Mohammed, A.R., 2017. An investigation into the effects of excipient particle size, blending techniques and processing parameters on the homogeneity and content uniformity of a blend containing low-dose model drug. *PLOS ONE* 12, e0178772. <https://doi.org/10.1371/journal.pone.0178772>
- Anaemia - iron deficiency - NICE CKS [WWW Document], n.d. URL <https://cks.nice.org.uk/anaemiairon-deficiency#!backgroundsub> (accessed 4.2.17).
- Anderson, E.R., Shah, Y.M., 2013. Iron Homeostasis in the Liver, in: *Comprehensive Physiology*. American Cancer Society, pp. 315–330. <https://doi.org/10.1002/cphy.c120016>
- Anderson, J.M., Shive, M.S., 1997. Biodegradation and biocompatibility of PLA and PLGA microspheres. *Advanced Drug Delivery Reviews, Biodegradable Microspheres/Therapeutic Peptide Delivery* 28, 5–24. [https://doi.org/10.1016/S0169-409X\(97\)00048-3](https://doi.org/10.1016/S0169-409X(97)00048-3)
- Andriopoulos, B., Pantopoulos, K., 2006. Hepcidin generated by hepatoma cells inhibits iron export from co-cultured THP1 monocytes. *Journal of Hepatology* 44, 1125–1131. <https://doi.org/10.1016/j.jhep.2005.10.025>
- Araya, C.E., Zaritsky, J., 2017. Chapter 88 - Management of Anemia in Children Undergoing Dialysis, in: Nissenson, A.R., Fine, R.N. (Eds.), *Handbook of Dialysis Therapy (Fifth Edition)*. Elsevier, pp. 1023-1033.e3. <https://doi.org/10.1016/B978-0-323-39154-2.00088-6>

- Aria, M.M., Irajizad, A., Astaraei, F.R., Shariatpanahi, S.P., Sarvari, R., 2016. Ethanol sensing properties of PVP electrospun membranes studied by quartz crystal microbalance. *Measurement* 78, 283–288. <https://doi.org/10.1016/j.measurement.2015.10.018>
- Balci, M., 2005. *Basic 1H- and 13C-NMR Spectroscopy*. Elsevier.
- Bancroft, John, 1982. *Theory and practice of histological techniques*. p. 366.
- Banerjee, A., Pathak, S., Subramaniam, V.D., G., D., Murugesan, R., Verma, R.S., 2017. Strategies for targeted drug delivery in treatment of colon cancer: current trends and future perspectives. *Drug Discovery Today* 22, 1224–1232. <https://doi.org/10.1016/j.drudis.2017.05.006>
- Barrero, A., López-Herrera, J.M., Boucard, A., Loscertales, I.G., Márquez, M., 2004. Steady cone-jet electrosprays in liquid insulator baths. *Journal of Colloid and Interface Science* 272, 104–108. <https://doi.org/10.1016/j.jcis.2003.10.035>
- Barth, A., 2007. Infrared spectroscopy of proteins. *Biochimica et Biophysica Acta (BBA) - Bioenergetics* 1767, 1073–1101. <https://doi.org/10.1016/j.bbabi.2007.06.004>
- Barua, S., Mitragotri, S., 2014. Challenges associated with penetration of nanoparticles across cell and tissue barriers: A review of current status and future prospects. *Nano Today* 9, 223–243. <https://doi.org/10.1016/j.nantod.2014.04.008>
- Baskakova, A., Awwad, S., Jiménez, J., 2016. Electrospun formulations of acyclovir, ciprofloxacin and 2 cyanocobalamin for ocular drug delivery.
- Berg, J.M., Tymoczko, J.L., Stryer, L., Berg, J.M., Tymoczko, J.L., Stryer, L., 2002. *Biochemistry*, 5th ed. W H Freeman.

- Bergamaschi, G., Sabatino, A.D., Pasini, A., Ubezio, C., Costanzo, F., Grataroli, D., Masotti, M., Alvisi, C., Corazza, G.R., 2017. Intestinal expression of genes implicated in iron absorption and their regulation by hepcidin. *Clinical Nutrition* 36, 1427–1433. <https://doi.org/10.1016/j.clnu.2016.09.021>
- Bertini, I., Borghi, E., Canti, G., Luchinat, C., 1979. Investigation of the system cobalt(ii) bovine carbonic anhydrase b-trichloroacetaldehyde. *J. Inorg. Biochem.* 11, 49–56.
- Bhardwaj, N., Kundu, S.C., 2010. Electrospinning: A fascinating fiber fabrication technique. *Biotechnology Advances* 28, 325–347. <https://doi.org/10.1016/j.biotechadv.2010.01.004>
- Bilensoy, E., Sarisozen, C., Esendağlı, G., Doğan, A.L., Aktaş, Y., Sen, M., Mungan, N.A., 2009. Intravesical cationic nanoparticles of chitosan and polycaprolactone for the delivery of Mitomycin C to bladder tumors. *Int J Pharm* 371, 170–176. <https://doi.org/10.1016/j.ijpharm.2008.12.015>
- Bock, N., Dargaville, T.R., Woodruff, M.A., 2012. Electro spraying of polymers with therapeutic molecules: State of the art. *Progress in Polymer Science* 37, 1510–1551. <https://doi.org/10.1016/j.progpolymsci.2012.03.002>
- Bose, S., Vu, A.A., Emshadi, K., Bandyopadhyay, A., 2018. Effects of polycaprolactone on alendronate drug release from Mg-doped hydroxyapatite coating on titanium. *Materials Science and Engineering: C* 88, 166–171. <https://doi.org/10.1016/j.msec.2018.02.019>
- Boussios, S., Pentheroudakis, G., Katsanos, K., Pavlidis, N., 2012. Systemic treatment-induced gastrointestinal toxicity: incidence, clinical presentation and management. *Ann Gastroenterol* 25, 106–118.

Brady, P.N., Macnaughtan, M.A., 2015. Evaluation of colorimetric assays for analyzing reductively methylated proteins: Biases and mechanistic insights. *Analytical Biochemistry* 491, 43–51.
<https://doi.org/10.1016/j.ab.2015.08.027>

British National Formulary (BNF) 70, n.d. 1397.

Brkić Ahmed, L., Milić, M., Pongrac, I.M., Marjanović, A.M., Mlinarić, H., Pavičić, I., Gajović, S., Vinković Vrček, I., 2017a. Impact of surface functionalization on the uptake mechanism and toxicity effects of silver nanoparticles in HepG2 cells. *Food and Chemical Toxicology* 107, 349–361.
<https://doi.org/10.1016/j.fct.2017.07.016>

Brkić Ahmed, L., Milić, M., Pongrac, I.M., Marjanović, A.M., Mlinarić, H., Pavičić, I., Gajović, S., Vinković Vrček, I., 2017b. Impact of surface functionalization on the uptake mechanism and toxicity effects of silver nanoparticles in HepG2 cells. *Food and Chemical Toxicology* 107, 349–361.
<https://doi.org/10.1016/j.fct.2017.07.016>

Brown, S.B., Lantzke, I.R., 1969. Solution structures of ferrihaem in some dipolar aprotic solvents and their binary aqueous mixtures. *Biochem. J.* 115, 279–285.

Cabrita, M., Pereira, C.F., Rodrigues, P., Cardoso, E.M., Arosa, F.A., 2004. Altered expression of CD1d molecules and lipid accumulation in the human hepatoma cell line HepG2 after iron loading: CD1d upregulation in iron-loaded HepG2 cells. *FEBS Journal* 272, 152–165.
<https://doi.org/10.1111/j.1432-1033.2004.04387.x>

Cadafalch Gazquez, G., Smulders, V., Veldhuis, S.A., Wieringa, P., Moroni, L., Boukamp, B.A., Ten Elshof, J.E., 2017. Influence of Solution Properties and Process Parameters on the Formation and Morphology of YSZ and NiO Ceramic Nanofibers by Electrospinning. *Nanomaterials* 7, 16.

<https://doi.org/10.3390/nano7010016>

Cancer registration statistics, England - Office for National Statistics [WWW Document], n.d. URL <https://www.ons.gov.uk/peoplepopulationandcommunity/healthandsocialcare/conditionsanddiseases/bulletins/cancerregistrationstatisticsengland/final2016> (accessed 8.27.18).

Carrier, J., Aghdassi, E., Cullen, J., Allard, J.P., 2002. Iron supplementation increases disease activity and vitamin E ameliorates the effect in rats with dextran sulfate sodium-induced colitis. *J. Nutr.* 132, 3146–3150. <https://doi.org/10.1093/jn/131.10.3146>

Cavalli, R., Bisazza, A., Bussano, R., Trotta, M., Civra, A., Lembo, D., Ranucci, E., Ferruti, P., 2011. Poly(amidoamine)-Cholesterol Conjugate Nanoparticles Obtained by Electrospraying as Novel Tamoxifen Delivery System [WWW Document]. *Journal of Drug Delivery*. <https://doi.org/10.1155/2011/587604>

Cetin, M., Atila, A., Kadioglu, Y., 2010. Formulation and In vitro Characterization of Eudragit® L100 and Eudragit® L100-PLGA Nanoparticles Containing Diclofenac Sodium. *AAPS PharmSciTech* 11, 1250–1256. <https://doi.org/10.1208/s12249-010-9489-6>

Ceylan, M., Jiang, J., Asmatulu, R., Yang, S.-Y., 2013. Gene Delivery with PCL Nanofiber in Vitro 9, 2.

Chakraborty, S., Liao, I.-C., Adler, A., Leong, K.W., 2009. Electrohydrodynamics: A facile technique to fabricate drug delivery systems. *Advanced Drug Delivery Reviews, Nanofibers in Regenerative Medicine and Drug Delivery* 61, 1043–1054. <https://doi.org/10.1016/j.addr.2009.07.013>

- Chauhan, R., Reddy, A., Abraham, J., 2015. Biosynthesis of silver and zinc oxide nanoparticles using *Pichia fermentans* JA2 and their antimicrobial property. *Appl Nanosci* 5, 63–71. <https://doi.org/10.1007/s13204-014-0292-7>
- Cheng, Y., Wei, H., Sun, R., Tian, Z., Zheng, X., 2016. Rapid method for protein quantitation by Bradford assay after elimination of the interference of polysorbate 80. *Analytical Biochemistry* 494, 37–39. <https://doi.org/10.1016/j.ab.2015.10.013>
- Chew, S.Y., Hufnagel, T.C., Lim, C.T., Leong, K.W., 2006. Mechanical properties of single electrospun drug-encapsulated nanofibres. *Nanotechnology* 17, 3880–3891. <https://doi.org/10.1088/0957-4484/17/15/045>
- Chiara, S., Nobile, M.T., Barzacchi, C., Sanguineti, O., Vincenti, M., Somma, C.D., Meszaros, P., Rosso, R., 1997. Hand-foot syndrome induced by high-dose, short-term, continuous 5-fluorouracil infusion. *European Journal of Cancer* 33, 967–969. [https://doi.org/10.1016/S09598049\(96\)00497-2](https://doi.org/10.1016/S09598049(96)00497-2)
- Cho, E.J., Holback, H., Liu, K.C., Abouelmagd, S.A., Park, J., Yeo, Y., 2013. Nanoparticle characterization: State of the art, challenges, and emerging technologies. *Mol Pharm* 10, 2093–2110. <https://doi.org/10.1021/mp300697h>
- Coad, J., Pedley, K., 2014. Iron deficiency and iron deficiency anemia in women. *Scandinavian Journal of Clinical and Laboratory Investigation* 74, 82–89. <https://doi.org/10.3109/00365513.2014.936694>
- Conrad, M.E., Umbreit, J.N., 2002. Pathways of Iron Absorption. *Blood Cells, Molecules, and Diseases* 29, 336–355. <https://doi.org/10.1006/bcmd.2002.0564>

Controlled drug delivery vehicles for cancer treatment and their performance | Signal Transduction and Targeted Therapy [WWW Document], n.d. URL <https://www.nature.com/articles/s41392-017-0004-3> (accessed 8.27.18).

Danafar, H., 2016. MPEG–PCL copolymeric nanoparticles in drug delivery systems. *Cogent Medicine* 3, 1142411. <https://doi.org/10.1080/2331205X.2016.1142411>

De Jong, W.H., Borm, P.J., 2008. Drug delivery and nanoparticles: Applications and hazards. *Int J Nanomedicine* 3, 133–149.

Diasio, R.B., Harris, B.E., 1989. Clinical Pharmacology of 5-Fluorouracil. *Clin-Pharmacokinet* 16, 215– 237. <https://doi.org/10.2165/00003088-198916040-00002>

Ding, Q., Alborzi, S., Bastarrachea, L.J., Tikekar, R.V., 2018. Novel sanitization approach based on synergistic action of UV-A light and benzoic acid: Inactivation mechanism and a potential application in washing fresh produce. *Food Microbiology* 72, 39–54. <https://doi.org/10.1016/j.fm.2017.11.004>

Distribution of Body Iron – All About Blood [WWW Document], n.d. URL <https://allaboutblood.com/2014/01/16/distribution-of-body-iron/> (accessed 5.13.20).

Doppalapudi, S., Jain, A., Khan, W., 2014. Biodegradable polymers—an overview - Doppalapudi - 2014 - Polymers for Advanced Technologies - Wiley Online Library [WWW Document]. URL <https://onlinelibrary.wiley.com/doi/pdf/10.1002/pat.3305> (accessed 12.31.18).

Egan, T.J., Hempelmann, E., Mavuso, W.W., 1999a. Characterisation of synthetic beta-haematin and effects of the antimalarial drugs quinidine, halofantrine, desbutylhalofantrine and mefloquine on its formation. *J.*

Inorg. Biochem. 73, 101–107.
[https://doi.org/10.1016/S01620134\(98\)10095-8](https://doi.org/10.1016/S01620134(98)10095-8)

Egan, T.J., Hempelmann, E., Mavuso, W.W., 1999b. Characterisation of synthetic beta-haematin and effects of the antimalarial drugs quinidine, halofantrine, desbutylhalofantrine and mefloquine on its formation. *J. Inorg. Biochem.* 73, 101–107.
[https://doi.org/10.1016/S01620134\(98\)10095-8](https://doi.org/10.1016/S01620134(98)10095-8)

Enayati, M., Ahmad, Z., Stride, E., Edirisinghe, M., 2010. Size mapping of electric field-assisted production of polycaprolactone particles. *Journal of The Royal Society Interface* 7, S393–S402.
<https://doi.org/10.1098/rsif.2010.0099.focus>

Ezzati, M., Lopez, A.D., Rodgers, A., Vander Hoorn, S., Murray, C.J.L., Comparative Risk Assessment Collaborating Group, 2002. Selected major risk factors and global and regional burden of disease. *Lancet* 360, 1347–1360.
[https://doi.org/10.1016/S0140-6736\(02\)11403-6](https://doi.org/10.1016/S0140-6736(02)11403-6)

Falcone, A., Allegrini, G., Antonuzzo, A., Brunetti, I., Pfanner, E., Lencioni, M., Masi, G., Danesi, R., Del Tacca, M., Conte, P., 1999. Infusions of fluorouracil and leucovorin: effects of the timing and semi-intermittency of drug delivery. *Oncology* 57, 195–201. <https://doi.org/10.1159/000012031>

Fie, C., 2015. Iron Deficiency Anemia: A Guide to Oral Iron Supplements – Clinical Correlations. URL <https://www.clinicalcorrelations.org/2015/03/26/iron-deficiency-anemia-a-guide-to-oraliron-supplements/> (accessed 11.17.18).

Finch, C.A., 1984. Water-soluble synthetic polymers: Properties and behaviour. Edited by P. Molyneux, CRC Press, Florida, 1983. Volume I, Pp xi + 225, Price \$75 (USA); \$87 (overseas). ISBN 0849361354. Volume 11, Pp xii + 266, Price \$83 (USA); \$95 (overseas). ISBN 0849361362.

British Polymer Journal 16, 157–158.

<https://doi.org/10.1002/pi.4980160315>

- Finkel (PharmD.), R., Clark, M.A., Cubeddu, L.X., 2009. Pharmacology. Lippincott Williams & Wilkins.
- Fish, W.W., 1988. [27] Rapid colorimetric micromethod for the quantitation of complexed iron in biological samples, in: *Methods in Enzymology, Metallobiochemistry Part A*. Academic Press, pp. 357–364. [https://doi.org/10.1016/0076-6879\(88\)58067-9](https://doi.org/10.1016/0076-6879(88)58067-9)
- Fuqua, B.K., Vulpe, C.D., Anderson, G.J., 2012. Intestinal iron absorption. *Journal of Trace Elements in Medicine and Biology, IX ISTERH Conference. Trace elements in health and disease: Essentiality, toxicity* 26, 115–119. <https://doi.org/10.1016/j.jtemb.2012.03.015>
- Gaitán, D., Olivares, M., Lönnerdal, B., Brito, A., Pizarro, F., 2012. Non-heme Iron as Ferrous Sulfate Does Not Interact with Heme Iron Absorption in Humans. *Biological Trace Element Research* 150, 68–73. <https://doi.org/10.1007/s12011-012-9496-4>
- Ganipineni, L.P., Ucakar, B., Joudiou, N., Bianco, J., Danhier, P., Zhao, M., Bastiancich, C., Gallez, B., Danhier, F., Prétat, V., 2018. Magnetic targeting of paclitaxel-loaded poly(lactic-co-glycolic acid)-based nanoparticles for the treatment of glioblastoma. *Int J Nanomedicine* 13, 4509– 4521. <https://doi.org/10.2147/IJN.S165184>
- Gardouh, A.R., Barakat, B.M., Qushawy, M.K.E., El-kazzaz, A.Y., Sami, M.M., Zaitone, S.A., 2018. Antitumor activity of a molecularly imprinted nanopreparation of 5-fluorouracil against Ehrlich's carcinoma solid tumors grown in mice: Comparison to free 5-fluorouracil. *ChemicoBiological Interactions*. <https://doi.org/10.1016/j.cbi.2018.04.019>

- Garmarudi, A.B., Khanmohammadi, M., Khoddami, N., Shabani, K., 2010. Feasibility Investigation of Near Infrared Spectrometry for Particle Size Estimation of Nano Structures 4, 3.
- Gazulla, M.F., Rodrigo, M., Blasco, E., Orduña, M., 2013. Nitrogen determination by SEM-EDS and elemental analysis: Nitrogen determination by SEM-EDS and elemental analysis. *X-Ray Spectrometry* 42, 394–401. <https://doi.org/10.1002/xrs.2490>
- Golnak, R., Xiao, J., Atak, K., Khan, M., Suljoti, E., Aziz, E.F., 2015. Local energy gap opening induced by hemin dimerization in aqueous solution. *J Phys Chem B* 119, 3058–3062. <https://doi.org/10.1021/jp509966q>
- Gomez Perez, M., Fourcade, L., Mateescu, M.A., Paquin, J., 2017. Neutral Red versus MTT assay of cell viability in the presence of copper compounds. *Analytical Biochemistry* 535, 43–46. <https://doi.org/10.1016/j.ab.2017.07.027>
- Gómez-Mascaraque, L.G., Sanchez, G., López-Rubio, A., 2016. Impact of molecular weight on the formation of electrosprayed chitosan microcapsules as delivery vehicles for bioactive compounds. *Carbohydrate Polymers* 150, 121–130. <https://doi.org/10.1016/j.carbpol.2016.05.012>
- Gutul, T., Rusu, E., Condur, N., Ursaki, V., Goncarencu, E., Vlazan, P., 2014. Preparation of poly(*N* vinylpyrrolidone)-stabilized ZnO colloid nanoparticles. *Beilstein Journal of Nanotechnology* 5, 402–406. <https://doi.org/10.3762/bjnano.5.47>
- Han, J., Zhou, Z., Bu, X., Zhu, S., Zhang, H., Sun, H., Yang, B., 2013. Employing aqueous CdTe quantum dots with diversified surface functionalities to discriminate between heme (Fe(II)) and hemin (Fe(III)). *Analyst* 138, 3402–3408. <https://doi.org/10.1039/c3an00310h>

- Hanudel, M.R., Rappaport, M., Chua, K., Gabayan, V., Qiao, B., Jung, G., Salusky, I.B., Ganz, T., Nemeth, E., 2018. Levels of the erythropoietin-responsive hormone erythroferrone in mice and humans with chronic kidney disease. *Haematologica* 103, e141–e142.
<https://doi.org/10.3324/haematol.2017.181743>
- Himmelfarb, J., 2007. Iron Regulation. *Journal of the American Society of Nephrology* 18, 379–381.
<https://doi.org/10.1681/ASN.2006101097>
- Hirayama, T., Nagasawa, H., 2017. Chemical tools for detecting Fe ions. *J Clin Biochem Nutr* 60, 39–48.
<https://doi.org/10.3164/jcbrn.16-70>
- Hosny, K.M., Banjar, Z.M., Hariri, A.H., Hassan, A.H., 2015. Solid lipid nanoparticles loaded with iron to overcome barriers for treatment of iron deficiency anemia. *Drug Des Devel Ther* 9, 313–320.
<https://doi.org/10.2147/DDDT.S77702>
- Hotaling, N.A., Bharti, K., Kriel, H., Simon, C.G., 2015. DiameterJ: A Validated Open Source Nanofiber Diameter Measurement Tool. *Biomaterials* 61, 327–338.
<https://doi.org/10.1016/j.biomaterials.2015.05.015>
- İçoğlu, H.İ., Oğulata, R.T., 2017. Effect of ambient parameters on morphology of electrospun poly (trimethylene terephthalate) (ptt) fibers. *Tekstil ve Konfeksiyon* 27, 215–223.
- Illangakoon, U.E., Gill, H., Shearman, G.C., Parhizkar, M., Mahalingam, S., Chatterton, N.P., Williams, G.R., 2014a. Fast dissolving paracetamol/caffeine nanofibers prepared by electrospinning. *International Journal of Pharmaceutics* 477, 369–379.
<https://doi.org/10.1016/j.ijpharm.2014.10.036>

- Illangakoon, U.E., Nazir, T., Williams, G.R., Chatterton, N.P., 2014b. Mebeverine-Loaded Electrospun Nanofibers: Physicochemical Characterization and Dissolution Studies. *Journal of Pharmaceutical Sciences* 103, 283–292. <https://doi.org/10.1002/jps.23759>
- Im, J., Lee, J., Löffler, F.E., 2013. Interference of ferric ions with ferrous iron quantification using the ferrozine assay. *Journal of Microbiological Methods* 95, 366–367. <https://doi.org/10.1016/j.mimet.2013.10.005>
- Imaging fibers with a SEM: how to obtain a flawless quality analysis [WWW Document], n.d. URL <http://blog.phenom-world.com/imaging-fibers-sem-quality-analysis> (accessed 8.14.18).
- Inamura, I., Isshiki, M., Araki, T., 1989. Solubilization of hemin in neutral and acidic aqueous solutions by forming complexes with water-soluble macromolecules [WWW Document]. ResearchGate. URL https://www.researchgate.net/publication/239265815_Solubilization_of_hemin_in_neutral_and_acidic_aqueous_solutions_by_forming_complexes_with_watersoluble_macromolecules (accessed 8.21.18).
- Intravenous iron and serious hypersensitivity reactions: strengthened recommendations [WWW Document], n.d. GOV.UK. URL <https://www.gov.uk/drug-safety-update/intravenous-ironand-serious-hypersensitivity-reactions-strengthened-recommendations> (accessed 5.13.18).
- Iron Deficiency Anemia: A Guide to Oral Iron Supplements | Clinical Correlations, n.d. URL <https://www.clinicalcorrelations.org/?p=8405> (accessed 5.13.18).
- Iron Deficiency Anemia [WWW Document], 2017. URL </Patients/Anemia/Iron-Deficiency.aspx> (accessed 5.13.18).

- Ito, T., Tanabe, K., Yamada, H., Hatta, H., Nishimoto, S., 2008. Radiation- and Photo-induced Activation of 5-Fluorouracil Prodrugs as a Strategy for the Selective Treatment of Solid Tumors. *Molecules* 13, 2370–2384. <https://doi.org/10.3390/molecules13102370>
- Jaberolansar, E., Kameli, P., Ahmadvand, H., Salamati, H., 2016. Synthesis and characterization of PVPcoated $\text{Co}_0.3\text{Zn}_0.7\text{Fe}_2\text{O}_4$ ferrite nanoparticles. *Journal of Magnetism and Magnetic Materials* 404, 21–28. <https://doi.org/10.1016/j.jmmm.2015.12.012>
- Jabur, A.R., Al-Hassani, E.S., Al-Shammari, A.M., Najim, M.A., Hassan, A.A., Ahmed, A.A., 2017. Evaluation of Stem Cells' Growth on Electrospun Polycaprolactone (PCL) Scaffolds Used for Soft Tissue Applications. *Energy Procedia* 119, 61–71. <https://doi.org/10.1016/j.egypro.2017.07.048>
- Jabur, A.R., Najim, M.A., Al- Rahman, S.A.A., 2018. Study the effect of flow rate on some physical properties of different polymeric solutions. *Journal of Physics: Conference Series* 1003, 012069. <https://doi.org/10.1088/1742-6596/1003/1/012069>
- Jaferian, S., Negahdari, B., Eatemadi, A., 2016. Colon cancer targeting using conjugates biomaterial 5flurouracil. *Biomedicine & Pharmacotherapy* 84, 780–788. <https://doi.org/10.1016/j.biopha.2016.10.004>
- Jagtap, Y.M., Bhujbal, R.K., Ranade, A.N., Ranpise, N.S., 2012. Effect of Various Polymers Concentrations on Physicochemical Properties of Floating Microspheres. *Indian J Pharm Sci* 74, 512–520. <https://doi.org/10.4103/0250-474X.110578>
- Jana, S.S., Bharali, D.J., Mani, P., Maitra, A., Gupta, C.M., Sarkar, D.P., 2002a. Targeted cytosolic delivery of hydrogel nanoparticles into HepG2 cells

through engineered Sendai viral envelopes. *FEBS Letters* 515, 184–188.
[https://doi.org/10.1016/S0014-5793\(02\)02467-5](https://doi.org/10.1016/S0014-5793(02)02467-5)

Jana, S.S., Bharali, D.J., Mani, P., Maitra, A., Gupta, C.M., Sarkar, D.P., 2002b. Targeted cytosolic delivery of hydrogel nanoparticles into HepG2 cells through engineered Sendai viral envelopes. *FEBS Letters* 515, 184–188.
[https://doi.org/10.1016/S0014-5793\(02\)02467-5](https://doi.org/10.1016/S0014-5793(02)02467-5)

Jeitner, T.M., 2014. Optimized ferrozine-based assay for dissolved iron. *Analytical Biochemistry* 454, 36–37. <https://doi.org/10.1016/j.ab.2014.02.026>

Johnson, C.D.L., D'Amato, A.R., Gilbert, R.J., 2016. Electrospun fibers for drug delivery after spinal cord injury and the effects of drug incorporation on fiber properties. *Cells Tissues Organs* 202, 116–135.
<https://doi.org/10.1159/000446621>

Johnson-Wimbley, T.D., Graham, D.Y., 2011. Diagnosis and management of iron deficiency anemia in the 21st century. *Therap Adv Gastroenterol* 4, 177–184. <https://doi.org/10.1177/1756283X11398736>

Kew, M.C., 2014. Hepatic iron overload and hepatocellular carcinoma. *Liver Cancer* 3, 31–40.
<https://doi.org/10.1159/000343856>

Kadajji, V.G., Betageri, G.V., 2011. Water Soluble Polymers for Pharmaceutical Applications. *Polymers* 3, 1972–2009.
<https://doi.org/10.3390/polym3041972>

Kitao, H., Iimori, M., Kataoka, Y., Wakasa, T., Tokunaga, E., Saeki, H., Oki, E., Maehara, Y., 2017. DNA replication stress and cancer chemotherapy. *Cancer Science* 109, 264–271. <https://doi.org/10.1111/cas.13455>

Kiyak, Y.E., Cakmak, E., 2014. Nanofiber Production Methods. *Electronic Journal of Vehicle Technologies* 8, 49–60.

Knutson, M.D., 2017. Iron transport proteins: Gateways of cellular and systemic iron homeostasis. *Journal of Biological Chemistry* 292, 12735–12743. <https://doi.org/10.1074/jbc.R117.786632>

Kortman, G.A.M., Boleij, A., Swinkels, D.W., Tjalsma, H., 2012. Iron Availability Increases the Pathogenic Potential of Salmonella Typhimurium and Other Enteric Pathogens at the Intestinal Epithelial Interface. *PLOS ONE* 7, e29968. <https://doi.org/10.1371/journal.pone.0029968>

Košťáková, E., Zemanová, E., Mikeš, P., Soukupová, J., Matheisová, H., Klouda, K., 2012. Electrospinning and electrospraying of polymer solutions with spherical fullerenes 5.

Kotula, A.P., Snyder, C.R., Migler, K.B., 2017. Determining conformational order and crystallinity in polycaprolactone via Raman spectroscopy. *Polymer* 117, 1–10. <https://doi.org/10.1016/j.polymer.2017.04.006>

Kraszewski, S., Bianco, A., Tarek, M., Ramseyer, C., 2012. Insertion of Short Amino-Functionalized Single-Walled Carbon Nanotubes into Phospholipid Bilayer Occurs by Passive Diffusion. *PLOS ONE* 7, e40703. <https://doi.org/10.1371/journal.pone.0040703>

Kremer, M.L., 1989. The reaction of hemin with H₂O₂. *European Journal of Biochemistry* 185, 651–658. <https://doi.org/10.1111/j.1432-1033.1989.tb15162.x>

- Ku, H.-K., Lim, H.-M., Oh, K.-H., Yang, H.-J., Jeong, J.-S., Kim, S.-K., 2013. Interpretation of protein quantitation using the Bradford assay: Comparison with two calculation models. *Analytical Biochemistry* 434, 178–180. <https://doi.org/10.1016/j.ab.2012.10.045>
- Kulaksiz, H., Gehrke, S.G., Janetzko, A., Rost, D., Bruckner, T., Kallinowski, B., Stremmel, W., 2004. Prohepcidin: expression and cell specific localisation in the liver and its regulation in hereditary haemochromatosis, chronic renal insufficiency, and renal anaemia. *Gut* 53, 735–743. <https://doi.org/10.1136/gut.2003.022863>
- Lai, S.K., Wang, Y.-Y., Hanes, J., 2009. Mucus-penetrating nanoparticles for drug and gene delivery to mucosal tissues. *Adv Drug Deliv Rev* 61, 158–171. <https://doi.org/10.1016/j.addr.2008.11.002>
- Latunde-Dada, G.O., Pereira, D.I., Tempest, B., Ilyas, H., Flynn, A.C., Aslam, M.F., Simpson, R.J., Powell, J.J., 2014. A Nanoparticulate Ferritin-Core Mimetic Is Well Taken Up by HuTu 80 Duodenal Cells and Its Absorption in Mice Is Regulated by Body Iron¹². *J Nutr* 144, 1896–1902. <https://doi.org/10.3945/jn.114.201715>
- Le Blanc, S., Garrick, M.D., Arredondo, M., 2012. Heme carrier protein 1 transports heme and is involved in heme-Fe metabolism. *American Journal of Physiology-Cell Physiology* 302, C1780–C1785. <https://doi.org/10.1152/ajpcell.00080.2012>
- Lea, T., 2015a. Caco-2 Cell Line, in: *The Impact of Food Bioactives on Health*. Springer, Cham, pp. 103–111. https://doi.org/10.1007/978-3-319-16104-4_10
- Lea, T., 2015b. Caco-2 Cell Line, in: Verhoeckx, K., Cotter, P., López-Expósito, I., Kleiveland, C., Lea, T., Mackie, A., Requena, T., Swiatecka, D., Wichers, H. (Eds.), *The Impact of Food Bioactives on Health: In Vitro and Ex Vivo Models*. Springer, Cham (CH).

- Lee, Y.Y., Erdogan, A., Rao, S.S.C., 2014. How to Assess Regional and Whole Gut Transit Time With Wireless Motility Capsule. *J Neurogastroenterol Motil* 20, 265–270. <https://doi.org/10.5056/jnm.2014.20.2.265>
- Lepoittevin, B., Devalckenaere, M., Pantoustier, N., Alexandre, M., Kubies, D., Calberg, C., Jérôme, R., Dubois, P., 2002. Poly(ϵ -caprolactone)/clay nanocomposites prepared by melt intercalation: mechanical, thermal and rheological properties 43, 9.
- Li, L., Jiang, Z., Xu, J., Fang, T., 2013. Predicting poly(vinyl pyrrolidone)'s solubility parameter and systematic investigation of the parameters of electrospinning with response surface methodology. *Journal of Applied Polymer Science* 131. <https://doi.org/10.1002/app.40304>
- Litton, E., Xiao, J., Ho, K.M., 2013. Safety and efficacy of intravenous iron therapy in reducing requirement for allogeneic blood transfusion: systematic review and meta-analysis of randomised clinical trials. *BMJ* 347, f4822.
- Li, Z., Wang, C., 2013. Effects of Working Parameters on Electrospinning, in: Li, Z., Wang, C. (Eds.), *OneDimensional Nanostructures: Electrospinning Technique and Unique Nanofibers*, SpringerBriefs in Materials. Springer, Berlin, Heidelberg, pp. 15–28. https://doi.org/10.1007/978-3-642-36427-3_2
- Loon, J.C.V., Barefoot, R.R., 2013. *Analytical Methods For Geochemical Exploration*. Elsevier.
- Lopez, F.L., Shearman, G.C., Gaisford, S., Williams, G.R., 2014. Amorphous Formulations of Indomethacin and Griseofulvin Prepared by Electrospinning. *Mol. Pharmaceutics* 11, 4327–4338. <https://doi.org/10.1021/mp500391y>

- Lozoya-Agullo, I., Araújo, F., González-Álvarez, I., Merino-Sanjuán, M., González-Álvarez, M., Bermejo, M., Sarmiento, B., 2018. PLGA nanoparticles are effective to control the colonic release and absorption on ibuprofen. *European Journal of Pharmaceutical Sciences* 115, 119–125.
<https://doi.org/10.1016/j.ejps.2017.12.009>
- Ludwiczek, S., 2003. Cytokine-mediated regulation of iron transport in human monocytic cells. *Blood* 101, 4148–4154. <https://doi.org/10.1182/blood-2002-08-2459>
- Lundquist, P., Artursson, P., 2016. Oral absorption of peptides and nanoparticles across the human intestine: Opportunities, limitations and studies in human tissues. *Advanced Drug Delivery Reviews*, Oral delivery of peptides 106, 256–276.
<https://doi.org/10.1016/j.addr.2016.07.007>
- Luo, C., Okubo, T., Nangrejo, M., Edirisinghe, M., 2015. Preparation of polymeric nanoparticles by novel electrospray nanoprecipitation: Novel electrospray nanoprecipitation. *Polymer International* 64, 183–187.
<https://doi.org/10.1002/pi.4822>
- Lynch, S.R., Cook, J.D., 1980. Interaction of vitamin C and iron. *Ann. N. Y. Acad. Sci.* 355, 32–44.
<https://doi.org/10.1111/j.1749-6632.1980.tb21325.x>
- Macchi, E., Zema, L., Maroni, A., Gazzaniga, A., Felton, L.A., 2015. Enteric-coating of pulsatile-release HPC capsules prepared by injection molding. *European Journal of Pharmaceutical Sciences* 70, 1–11.
<https://doi.org/10.1016/j.ejps.2014.12.020>
- Mahl, D., Diendorf, J., Meyer-Zaika, W., Eppe, M., 2011. Possibilities and limitations of different analytical methods for the size determination of a bimodal dispersion of metallic nanoparticles. *Colloids and Surfaces A:*

Physicochemical and Engineering Aspects 1–3, 386– 392.

<https://doi.org/10.1016/j.colsurfa.2011.01.031>

Martínez-Maqueda, D., Miralles, B., Recio, I., 2015. HT29 Cell Line, in: Verhoeckx, K., Cotter, P., LópezExpósito, I., Kleiveland, C., Lea, T., Mackie, A., Requena, T., Swiatecka, D., Wichers, H. (Eds.), *The Impact of Food Bioactives on Health: In Vitro and Ex Vivo Models*. Springer, Cham (CH).

Matak, P., Chaston, T.B., Chung, B., Srail, S.K., McKie, A.T., Sharp, P.A., 2009. Activated macrophages induce hepcidin expression in HuH7 hepatoma cells. *Haematologica* 94, 773–780.

<https://doi.org/10.3324/haematol.2008.003400>

McDowell, L., 2017. *Mineral Nutrition History: The Early Years*. First Edition Design Pub.

Melent'eva, T.A., Barybin, A.S., Didenko, I.V., Pekel', N.D., 1980. Preparation of adducts of metallic complexes of octadehydrocorrins with polyvinylpyrrolidone and their biological activity. *Pharm Chem J* 14, 781–783. <https://doi.org/10.1007/BF00765622>

Mignani, S., El Kazzouli, S., Bousmina, M., Majoral, J.-P., 2013. Expand classical drug administration ways by emerging routes using dendrimer drug delivery systems: A concise overview. *Advanced Drug Delivery Reviews*, EDITOR'S COLLECTION 2013 65, 1316–1330. <https://doi.org/10.1016/j.addr.2013.01.001>

Missel, P.J., Mazer, N.A., Benedek, G.B., Young, C.Y., Carey, M.C., 1980. Thermodynamic analysis of the growth of sodium dodecyl sulfate micelles. *The Journal of Physical Chemistry* 84, 1044– 1057. <https://doi.org/10.1021/j100446a021>

- Modi, M.P., Mathew, S.T., Abraham, A., 2012. Formulation and evaluation of enteric coated time r elease press coated tablets of theophylline for chronopharmacotherapy [WWW Document]. URL <https://www.semanticscholar.org/paper/Formulation-and-evaluation-of-entericcoated-time-r-Modi-Mathew/2c453a52ca1f2a3df1ed88a51a15465183c031c7> (accessed 4.29.20).
- Molinari, B.L., Tasat, D.R., Palmieri, M.A., Cabrini, R.L., 2005. Kinetics of MTT-formazan exocytosis in phagocytic and non-phagocytic cells. *Micron* 36, 177–183. <https://doi.org/10.1016/j.micron.2004.08.002>
- Mosmann, T., 1983. Rapid colorimetric assay for cellular growth and survival: application to proliferation and cytotoxicity assays. *J. Immunol. Methods* 65, 55–63.
- Muthu, R., Thangavel, P., Selvaraj, N., Ramalingam, R., Vaiyapuri, M., 2013. Synergistic and individual effects of umbelliferone with 5-fluorouracil on the status of lipid peroxidation and antioxidant defense against 1, 2-dimethylhydrazine induced rat colon carcinogenesis. *Biomedicine & Preventive Nutrition* 3, 74–82. <https://doi.org/10.1016/j.bionut.2012.10.011>
- Nagaraju, S.P., Cohn, A., Akbari, A., Davis, J.L., Zimmerman, D.L., 2013. Heme iron polypeptide for the treatment of iron deficiency anemia in non-dialysis chronic kidney disease patients: a randomized controlled trial. *BMC Nephrol* 14, 64. <https://doi.org/10.1186/1471-2369-14-64>
- Nanoparticle-Induced Permeability of Lipid Membranes [WWW Document], n.d. URL <https://pubs.acs.org/doi/pdf/10.1021/nn3028858> (accessed 10.8.18).
- Ndegwa, S., Banks, R., n.d. Heme Iron Polypeptide (Proferrin®) versus Oral and Injectable Iron Products for the Treatment of Anemia.

Ngadiman, N.H.A., Noordin, M.Y., Idris, A., Shakir, A.S.A., Kurniawan, D., 2015. Influence of Polyvinyl

Alcohol Molecular Weight on the Electrospun Nanofiber Mechanical Properties. *Procedia Manufacturing* 2, 568–572.
<https://doi.org/10.1016/j.promfg.2015.07.098>

Office of Dietary Supplements - Iron [WWW Document], n.d. URL <https://ods.od.nih.gov/factsheets/Iron-HealthProfessional/> (accessed 8.29.18).

Okutan, N., Terzi, P., Altay, F., 2014. Affecting parameters on electrospinning process and characterization of electrospun gelatin nanofibers. *Food Hydrocolloids* 39, 19–26.

<https://doi.org/10.1016/j.foodhyd.2013.12.022>

Oliveira, C.P., Ribeiro, M.E.N.P., Ricardo, N.M.P.S., Souza, T.V. de P., Moura, C.L., Chaibundit, C., Yeates, S.G., Nixon, K., Attwood, D., 2011. The effect of water-soluble polymers, PEG and PVP, on the solubilisation of griseofulvin in aqueous micellar solutions of Pluronic F127.

International Journal of Pharmaceutics 421, 252–257.

<https://doi.org/10.1016/j.ijpharm.2011.10.010>

Oréface, R.L., Hench, L.L., Brennan, A.B., 2001. Effect of particle morphology on the mechanical and thermo-mechanical behavior of polymer composites. *Journal of the Brazilian Society of Mechanical Sciences* 23, 1–8.

<https://doi.org/10.1590/S0100-73862001000100001>

Owais, M., Varshney, G.C., Choudhury, A., Chandra, S., Gupta, C.M., 1995. Chloroquine encapsulated in malaria-infected erythrocyte-specific antibody-bearing liposomes effectively controls chloroquine-resistant *Plasmodium berghei* infections in mice. *Antimicrob. Agents Chemother.* 39, 180–184.

- Panier, T., Romano, S.A., Olive, R., Pietri, T., Sumbre, G., Candelier, R., Debrégeas, G., 2013. Fast functional imaging of multiple brain regions in intact zebrafish larvae using selective plane illumination microscopy. *Front Neural Circuits* 7, 65. <https://doi.org/10.3389/fncir.2013.00065>
- Panyam, J., Labhasetwar, V., 2004. Sustained cytoplasmic delivery of drugs with intracellular receptors using biodegradable nanoparticles. *Mol. Pharm.* 1, 77–84.
- Park, J., Fong, P.M., Lu, J., Russell, K.S., Booth, C.J., Saltzman, W.M., Fahmy, T.M., 2009. PEGylated PLGA nanoparticles for the improved delivery of doxorubicin. *Nanomedicine* 5, 410–418. <https://doi.org/10.1016/j.nano.2009.02.002>
- Pascua-Maestro, R., Corraliza-Gomez, M., Diez-Hermano, S., Perez-Segurado, C., Ganfornina, M.D., Sanchez, D., 2018. The MTT-formazan assay: Complementary technical approaches and in vivo validation in *Drosophila* larvae. *Acta Histochemica* 120, 179–186. <https://doi.org/10.1016/j.acthis.2018.01.006>
- Patil, M., Mehta, D.S., Guvva, S., 2008. Future impact of nanotechnology on medicine and dentistry. *Journal of Indian Society of Periodontology* 12, 34. <https://doi.org/10.4103/0972-124X.44088>
- PEPTIDE DELIVERY - The Endometriosis Enigma – Why Can't There Be a Pill for That?, 2018. . *Drug Development and Delivery*. URL <https://drug-dev.com/peptide-delivery-the-endometriosisenigma-why-cant-there-be-a-pill-for-that/> (accessed 12.26.18).
- Pereira, D.I.A., Bruggraber, S.F.A., Faria, N., Poots, L.K., Tagmount, M.A., Aslam, M.F., Frazer, D.M., Vulpe, C.D., Anderson, G.J., Powell, J.J., 2014.

Nanoparticulate iron(III) oxo-hydroxide delivers safe iron that is well absorbed and utilised in humans. *Nanomedicine* 10, 1877–1886.
<https://doi.org/10.1016/j.nano.2014.06.012>

Pillay, V., Dott, C., Choonara, Y.E., Tyagi, C., Tomar, L., Kumar, P., du Toit, L.C., Ndesendo, V.M.K., 2013. A Review of the Effect of Processing Variables on the Fabrication of Electrospun Nanofibers for Drug Delivery Applications. *Journal of Nanomaterials* 2013, 1–22.
<https://doi.org/10.1155/2013/789289>

Pinto Reis, C., Neufeld, R.J., Ribeiro, A.J., Veiga, F., 2006. Nanoencapsulation II. Biomedical applications and current status of peptide and protein nanoparticulate delivery systems. *Nanomedicine: Nanotechnology, Biology and Medicine* 2, 53–65.
<https://doi.org/10.1016/j.nano.2006.04.009>

Pogodin, S., Baulin, V.A., 2010. Can a carbon nanotube pierce through a phospholipid bilayer? *ACS Nano* 4, 5293–5300.
<https://doi.org/10.1021/nn1016549>

Pogodin, S., Slater, N.K.H., Baulin, V.A., 2011. Surface Patterning of Carbon Nanotubes Can Enhance Their Penetration through a Phospholipid Bilayer. *ACS Nano* 5, 1141–1146.
<https://doi.org/10.1021/nn102763b>

Pogodin, S., Werner, M., Sommer, J., 2012a. Nanoparticle-Induced Permeability of Lipid Membranes
[WWW Document]. URL <https://pubs.acs.org/doi/pdf/10.1021/nn3028858>
(accessed 12.19.18).

Powell, J.J., Bruggaber, S.F.A., Faria, N., Poots, L.K., Hondow, N., Pennycook, T.J., Latunde-Dada, G.O., Simpson, R.J., Brown, A.P., Pereira, D.I.A., 2014. A

nano-disperse ferritin-core mimetic that efficiently corrects anemia without luminal iron redox activity. *Nanomedicine* 10, 1529–1538.
<https://doi.org/10.1016/j.nano.2013.12.011>

Prasad, M., Palepu, R., Moulik, S.P., 2006. Interaction between sodium dodecyl sulfate (SDS) and polyvinylpyrrolidone (PVP) investigated with forward and reverse component addition protocols employing tensiometric, conductometric, microcalorimetric, electrokinetic, and DLS techniques. *Colloid and Polymer Science* 284, 871–878.
<https://doi.org/10.1007/s00396-0051453-8>

Ramakrishna, S., 2005. *An Introduction to Electrospinning and Nanofibers*. World Scientific.

Rasekh, M., Karavasili, C., Soong, Y.L., Bouropoulos, N., Morris, M., Armitage, D., Li, X., Fatouros, D.G., Ahmad, Z., 2014. Electrospun PVP–indomethacin constituents for transdermal dressings and drug delivery devices. *International Journal of Pharmaceutics* 473, 95–104.
<https://doi.org/10.1016/j.ijpharm.2014.06.059>

Regazzoni, S., Pesce, G., Marini, G., Cavalli, F., Goldhirsch, A., 1996. Low-dose continuous intravenous infusion of 5-fluorouracil for metastatic breast cancer. *Annals of Oncology* 7, 807–813.
<https://doi.org/10.1093/oxfordjournals.annonc.a010759>

Reinholz, J., Landfester, K., Mailänder, V., 2018. The challenges of oral drug delivery via nanocarriers. *Drug Delivery* 25, 1694–1705. <https://doi.org/10.1080/10717544.2018.1501119>

Riemer, J., Hoepken, H.H., Czerwinska, H., Robinson, S.R., Dringen, R., 2004. Colorimetric ferrozinebased assay for the quantitation of iron in cultured cells. *Analytical Biochemistry* 331, 370–375.
<https://doi.org/10.1016/j.ab.2004.03.049>

Robb, B., Lennox, B., 2011. 3 - The electrospinning process, conditions and control, in: Bosworth, L.A., Downes, S. (Eds.), *Electrospinning for Tissue Regeneration*, Woodhead Publishing Series in Biomaterials. Woodhead Publishing, pp. 51–66.
<https://doi.org/10.1533/9780857092915.1.51>

Rodríguez-Tobías, H., Morales, G., Ledezma, A., Romero, J., Saldívar, R., Langlois, V., Renard, E., Grande, D., 2016. Electrospinning and electrospraying techniques for designing novel antibacterial poly(3-hydroxybutyrate)/zinc oxide nanofibrous composites. *J Mater Sci* 51, 8593–8609.
<https://doi.org/10.1007/s10853-016-0119-x>

Roughead, Z.K. (Fariba), Zito, C.A., Hunt, J.R., 2002. Initial uptake and absorption of nonheme iron and absorption of heme iron in humans are unaffected by the addition of calcium as cheese to a meal with high iron bioavailability. *The American Journal of Clinical Nutrition* 76, 419–425.
<https://doi.org/10.1093/ajcn/76.2.419>

Sadeghian, I., Khalvati, B., Ghasemi, Y., Hemmati, S., 2018. TAT-mediated intracellular delivery of carboxypeptidase G2 protects against methotrexate-induced cell death in HepG2 cells. *Toxicology and Applied Pharmacology* 346, 9–18.
<https://doi.org/10.1016/j.taap.2018.03.023>

Sandberg, A.-S., 2010. The Use of Caco-2 Cells to Estimate Fe Absorption in Humans - a Critical Appraisal. *International Journal for Vitamin and Nutrition Research* 80, 307–313.
<https://doi.org/10.1024/0300-9831/a000038>

Santiago, P., 2012. Ferrous versus Ferric Oral Iron Formulations for the Treatment of Iron Deficiency:
A Clinical Overview. *The Scientific World Journal* 2012, 1–5. <https://doi.org/10.1100/2012/846824>

- Sawawi, M., Wang, T.Y., Nisbet, D.R., Simon, G.P., 2013. Scission of electrospun polymer fibres by ultrasonication. *Polymer* 54, 4237–4252. <https://doi.org/10.1016/j.polymer.2013.05.060>
- Sazawal, S., Black, R.E., Ramsan, M., Chwaya, H.M., Stoltzfus, R.J., Dutta, A., Dhingra, U., Kabole, I., Deb, S., Othman, M.K., Kabole, F.M., 2006. Effects of routine prophylactic supplementation with iron and folic acid on admission to hospital and mortality in preschool children in a high malaria transmission setting: community-based, randomised, placebo-controlled trial. *Lancet* 367, 133–143. [https://doi.org/10.1016/S0140-6736\(06\)67962-2](https://doi.org/10.1016/S0140-6736(06)67962-2)
- Schiller, G.J., Goldstein, L., Finn, R., Busuttil, R., 2004. Intravenous Hemin as Prophylaxis of Allograft Function Following Second Liver Transplant for Erythropoietic Protoporphyrria. *Blood* 104, 3677–3677. <https://doi.org/10.1182/blood.V104.11.3677.3677>
- Schwarz, W., 2018. Pvp: A Critical Review of the Kinetics and Toxicology of Polyvinylpyrrolidone (Povidone). Routledge.
- Scott, C.L., Guilliams, M., 2018. The role of Kupffer cells in hepatic iron and lipid metabolism. *Journal of Hepatology* 69, 1197–1199. <https://doi.org/10.1016/j.jhep.2018.02.013>
- Senapati, S., Mahanta, A.K., Kumar, S., Maiti, P., 2018. Controlled drug delivery vehicles for cancer treatment and their performance. *Signal Transduction and Targeted Therapy* 3, 7. <https://doi.org/10.1038/s41392-017-0004-3>
- Seo, K., Sinha, K., Novitskaya, E., Graeve, O.A., 2018. Polyvinylpyrrolidone (PVP) effects on iron oxide nanoparticle formation. *Materials Letters* 215, 203–206. <https://doi.org/10.1016/j.matlet.2017.12.107>

Seril, D.N., Liao, J., Ho, K.-L.K., Warsi, A., Yang, C.S., Yang, G.-Y., 2002. Dietary iron supplementation enhances DSS-induced colitis and associated colorectal carcinoma development in mice. *Dig. Dis. Sci.* 47, 1266–1278.

Shafie, n.d. The effects of nanoparticles containing iron on blood and inflammatory markers in comparison to ferrous sulfate in anemic rats [WWW Document]. URL <http://www.ijpvmjournal.net/article.asp?issn=2008-7802;year=2016;volume=7;issue=1;spage=117;epage=117;aulast=Shafie> (accessed 5.16.18).

Shang, L., Nienhaus, K., Nienhaus, G.U., 2014. Engineered nanoparticles interacting with cells: size matters. *Journal of Nanobiotechnology* 12, 5. <https://doi.org/10.1186/1477-3155-12-5>

Shi, J., Votruba, A.R., Farokhzad, O.C., Langer, R., 2010. Nanotechnology in Drug Delivery and Tissue Engineering: From Discovery to Applications. *Nano Lett* 10, 3223–3230. <https://doi.org/10.1021/nl102184c>

Silva, B., Faustino, P., 2015. An overview of molecular basis of iron metabolism regulation and the associated pathologies. *Biochimica et Biophysica Acta (BBA) - Molecular Basis of Disease* 1852, 1347–1359. <https://doi.org/10.1016/j.bbadis.2015.03.011>

Silverstein, S.B., Rodgers, G.M., 2004. Parenteral iron therapy options. *Am. J. Hematol.* 76, 74–78. <https://doi.org/10.1002/ajh.20056>

Smeets, A., Clasen, C., Van den Mooter, G., 2017. Electrospraying of polymer solutions: Study of formulation and process parameters. *European Journal of Pharmaceutics and Biopharmaceutics* 119, 114–124. <https://doi.org/10.1016/j.ejpb.2017.06.010>

- Span, K., Verhoef, J.J.F., Hunt, H., van Nostrum, C.F., Brinks, V., Schellekens, H., Hennink, W.E., 2016a. A novel oral iron-complex formulation: Encapsulation of hemin in polymeric micelles and its in vitro absorption. *European Journal of Pharmaceutics and Biopharmaceutics* 108, 226–234. <https://doi.org/10.1016/j.ejpb.2016.09.002>
- Span, K., Verhoef, J.J.F., Hunt, H., van Nostrum, C.F., Brinks, V., Schellekens, H., Hennink, W.E., 2016b. A novel oral iron-complex formulation: Encapsulation of hemin in polymeric micelles and its in vitro absorption. *Eur J Pharm Biopharm* 108, 226–234. <https://doi.org/10.1016/j.ejpb.2016.09.002>
- Stuart, B.H., 2004. *Infrared Spectroscopy: Fundamentals and Applications: Stuart/Infrared Spectroscopy: Fundamentals and Applications, Analytical Techniques in the Sciences.* John Wiley & Sons, Ltd, Chichester, UK. <https://doi.org/10.1002/0470011149>
- Sun, H., Walsh, A.J., Lebel, R.M., Blevins, G., Catz, I., Lu, J.-Q., Johnson, E.S., Emery, D.J., Warren, K.G., Wilman, A.H., 2015. Validation of quantitative susceptibility mapping with Perls' iron staining for subcortical gray matter. *NeuroImage* 105, 486–492. <https://doi.org/10.1016/j.neuroimage.2014.11.010>
- Sun, T., King, H.E., 1996. Aggregation Behavior in the Semidilute Poly(N-vinyl-2-pyrrolidone)/Water System. *Macromolecules* 29, 3175–3181. <https://doi.org/10.1021/ma951734c>
- Tako, E., Bar, H., Glahn, R.P., 2016. The Combined Application of the Caco-2 Cell Bioassay Coupled with In Vivo (*Gallus gallus*) Feeding Trial Represents an Effective Approach to Predicting Fe Bioavailability in Humans. *Nutrients* 8. <https://doi.org/10.3390/nu8110732>

Teodorescu, M., Bercea, M., 2015. Poly(vinylpyrrolidone) – A Versatile Polymer for Biomedical and Beyond Medical Applications. *Polymer-Plastics Technology and Engineering* 54, 923–943.

<https://doi.org/10.1080/03602559.2014.979506>

Thakur, V.K., Thakur, M.K., Kessler, M.R., 2017. *Handbook of Composites from Renewable Materials, Nanocomposites: Advanced Applications*. John Wiley & Sons.

The Combined Application of the Caco-2 Cell Bioassay Coupled with In Vivo (*Gallus gallus*) Feeding Trial Represents an Effective Approach to Predicting Fe Bioavailability in Humans [WWW

Document], n.d. URL

<https://www.ncbi.nlm.nih.gov/pmc/articles/PMC5133116/> (accessed 5.5.18).

Tsiftoglou, A.S., Tsamadou, A.I., Papadopoulou, L.C., 2006. Heme as key regulator of major mammalian cellular functions: Molecular, cellular, and pharmacological aspects.

Pharmacology & Therapeutics 111, 327–345.

<https://doi.org/10.1016/j.pharmthera.2005.10.017>

Ulubayram, K., Calamak, S., Shahbazi, R., Eroglu, I., 2015. Nanofibers Based Antibacterial Drug Design,

Delivery and Applications. *Current pharmaceutical design* 21.

<https://doi.org/10.2174/1381612821666150302151804>

Vroman, I., Tighzert, L., 2009. Biodegradable Polymers. *Materials* 2, 307–344.

<https://doi.org/10.3390/ma2020307>

- Waldvogel-Abramowski, S., Waeber, G., Gassner, C., Buser, A., Frey, B.M., Favrat, B., Tissot, J-D., 2014. Physiology of Iron Metabolism. *TMH* 41, 213–221. <https://doi.org/10.1159/000362888>
- Wei, Y., Yang, P., Cao, S., Zhao, L., 2018. The combination of curcumin and 5-fluorouracil in cancer therapy. *Arch. Pharm. Res.* 41, 1–13. <https://doi.org/10.1007/s12272-017-0979-x>
- West, A.R., Oates, P.S., 2008. Mechanisms of heme iron absorption: Current questions and controversies. *World J Gastroenterol* 14, 4101–4110. <https://doi.org/10.3748/wjg.14.4101>
- Whatmore, R.W., 2006. Nanotechnology—what is it? Should we be worried? *Occupational Medicine* 56, 295–299. <https://doi.org/10.1093/occmed/kql050>
- WHO | Anaemia [WWW Document], n.d. WHO. URL <http://www.who.int/topics/anaemia/en/> (accessed 4.2.17).
- Wilczewska, A.Z., Niemirowicz, K., Markiewicz, K.H., Car, H., 2012a. Nanoparticles as drug delivery systems. *Pharmacological Reports* 64, 1020–1037. [https://doi.org/10.1016/S17341140\(12\)70901-5](https://doi.org/10.1016/S17341140(12)70901-5)
- Wilczewska, A.Z., Niemirowicz, K., Markiewicz, K.H., Car, H., 2012b. Nanoparticles as drug delivery systems. *Pharmacol Rep* 64, 1020–1037.
- Wilson, B., Ambika, T.V., Dharmesh Kumar Patel, R., Jenita, J.L., Priyadarshini, S.R.B., 2012. Nanoparticles based on albumin: Preparation, characterization and the use for 5-fluorouracil delivery. *International Journal of Biological Macromolecules* 51, 874–878. <https://doi.org/10.1016/j.ijbiomac.2012.07.014>

- Xi, J., Qin, J., Fan, L., 2012. Chondroitin sulfate functionalized mesostructured silica nanoparticles as biocompatible carriers for drug delivery. *Int J Nanomedicine* 7, 5235–5247.
<https://doi.org/10.2147/IJN.S34128>
- Xu, Y., Li, J.-J., Yu, D.-G., Williams, G.R., Yang, J.-H., Wang, X., 2017. Influence of the drug distribution in electrospun gliadin fibers on drug-release behavior. *European Journal of Pharmaceutical Sciences* 106, 422–430.
<https://doi.org/10.1016/j.ejps.2017.06.017>
- Yadav, S.K., 2009. *Nanoscale Materials in Targeted Drug Delivery, Theragnosis and Tissue Regeneration*. Springer.
- Yamamoto, M., Nishida, A., Otsuka, K., Komai, T., Fukushima, M., 2010. Evaluation of the binding of iron(II) to humic substances derived from a compost sample by a colorimetric method using ferrozine. *Bioresource Technology* 101, 4456–4460. <https://doi.org/10.1016/j.biortech.2010.01.050>
- Yang, L., Zhang, Y., Wang, J., Huang, Z., Gou, L., Wang, Z., Ren, T., Piao, J., Yang, X., 2016. Non-Heme Iron Absorption and Utilization from Typical Whole Chinese Diets in Young Chinese Urban Men Measured by a Double-Labeled Stable Isotope Technique. *PLOS ONE* 11, e0153885.
<https://doi.org/10.1371/journal.pone.0153885>
- Yang, N.J., Hinner, M.J., 2015. Getting Across the Cell Membrane: An Overview for Small Molecules, Peptides, and Proteins. *Methods Mol Biol* 1266, 29–53.
https://doi.org/10.1007/978-1-49392272-7_3
- Yilmaz, E., Soylak, M., 2018. A novel and simple deep eutectic solvent based liquid phase microextraction method for rhodamine B in cosmetic products and water samples prior to its spectrophotometric determination. *Spectrochimica Acta Part A: Molecular and Biomolecular Spectroscopy* 202, 81–86. <https://doi.org/10.1016/j.saa.2018.04.073>

- Yu, D.-G., Xu, Y., Li, Z., Du, L.-P., Zhao, B.-G., Wang, X., 2014. Coaxial Electrospinning with Mixed Solvents: From Flat to Round Eudragit L100 Nanofibers for Better Colon-Targeted Sustained Drug Release Profiles. *Journal of Nanomaterials* 2014, 1–8. <https://doi.org/10.1155/2014/967295>
- Zema, L., Loreti, G., Melocchi, A., Maroni, A., Palugan, L., Gazzaniga, A., 2013. Gastroresistant capsular device prepared by injection molding. *International Journal of Pharmaceutics* 440, 264–272. <https://doi.org/10.1016/j.ijpharm.2012.05.071>
- Zhang, L., Huang, J., Si, T., Xu, R.X., 2012. Coaxial electrospray of microparticles and nanoparticles for biomedical applications. *Expert Rev Med Devices* 9, 595–612. <https://doi.org/10.1586/erd.12.58>
- Zhang, S., Kawakami, K., 2010. One-step preparation of chitosan solid nanoparticles by electrospray deposition. *International Journal of Pharmaceutics* 397, 211–217. <https://doi.org/10.1016/j.ijpharm.2010.07.007>
- Zheng, G., Xue, W., Chen, H., Sun, L., Jiang, J., Wang, X., Guo, S., Li, W., 2019. Measurement and Time Response of Electrohydrodynamic Direct-Writing Current. *Micromachines* 10, 90. <https://doi.org/10.3390/mi10020090>
- Zhou, F.-L., Hubbard Cristinacce, P.L., Eichhorn, S.J., Parker, G.J.M., 2016. Preparation and characterization of polycaprolactone microspheres by electrospraying. *Aerosol Science and Technology* 50, 1201–1215. <https://doi.org/10.1080/02786826.2016.1234707>
- Zhu, G., Zhao, L.Y., Zhu, L.T., Deng, X.Y., Chen, W.L., 2017. Effect of Experimental Parameters on Nanofiber Diameter from Electrospinning with Wire Electrodes. *IOP Conf. Ser.: Mater. Sci. Eng.* 230, 012043. <https://doi.org/10.1088/1757-899X/230/1/012043>

Zimmermann, M.B., Chassard, C., Rohner, F., N’Goran, E.K., Nindjin, C., Dostal, A., Utzinger, J., Ghattas, H., Lacroix, C., Hurrell, R.F., 2010. The effects of iron fortification on the gut microbiota in African children: a randomized controlled trial in Côte d’Ivoire. *Am J Clin Nutr* 92, 1406–1415.

<https://doi.org/10.3945/ajcn.110.004564>

Zong, H., Xia, X., Liang, Y., Dai, S., Alsaedi, A., Hayat, T., Kong, F., Pan, J.H., 2018. Designing functionoriented artificial nanomaterials and membranes via electrospinning and electrospraying techniques. *Materials Science and Engineering: C* 92, 1075–1091.

<https://doi.org/10.1016/j.msec.2017.11.007>

Appendices

Appendix A

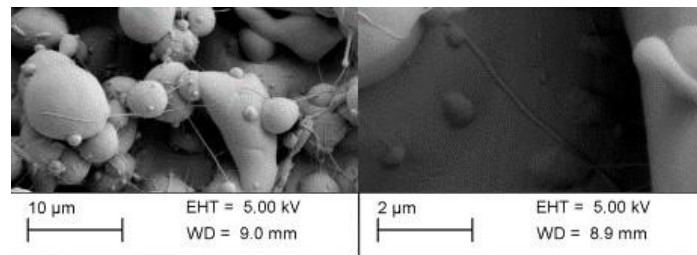


Figure A1. SEM of particles obtained from 5% (w/v) sample SP_{CH} (with a 1ml/hr flow rate, 15 kV voltage 15 cm distance from tip to collector).

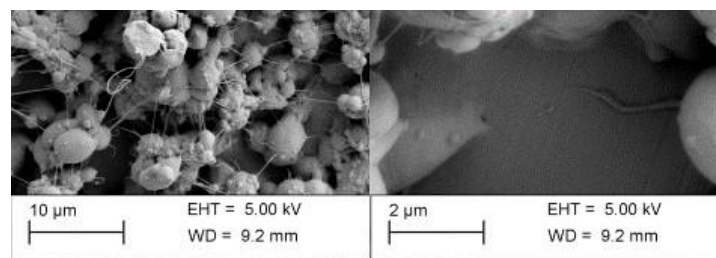


Figure A2. SEM of particles obtained from 2% (w/v) sample SP_{CH} (with a 0.5ml/hr flow rate, 15.01 kV voltage 18.7 cm distance from tip to collector).

Appendix B

Sample code	Voltage/ kV	Tip to collector distance/ cm	Flow rate/ mL/hr	Observation
SP _{CH} 1	15.00	18.00	1.00	Electrospraying
SP _{CH} 2	15.00	20.00	1.00	Electrospraying
SP _{CH} 3	15.00	16.00	1.00	Electrospraying
SP _{CH} 4	15.00	16.00	1.50	Electrospraying
SP _{CH} 5	15.00	18.00	1.50	Electrospraying
SP _{CH} 6	17.63	18.00	1.00	Electrospraying
SP _{CH} 7	14.00	20.00	1.00	Spitting + spraying
SP _{CH} 8	14.00	16.00	1.50	Spitting + spraying
SP _{CH} 9	14.00	18.00	1.50	Dripping
SP _{CH} 10	13.00	16.00	1.50	Spitting + spraying
SP _{CH} 11	13.00	18.00	1.50	Dripping
SP _{CH} 12	15.00	20.00	1.50	Electrospraying
SP _{CH} 13	12.00	16.00	1.00	Spitting + electrospaying

Table B1. Processing parameters used for SP_{CH} of 0.5 % (w/v) solution in 1,2-dichloroethane.

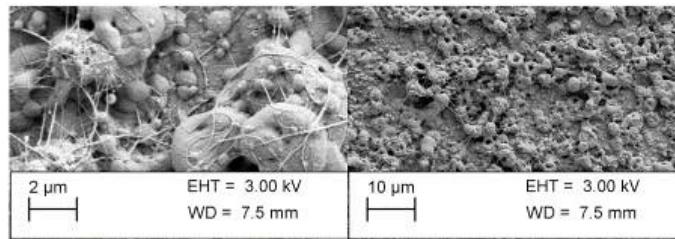


Figure B1. SEM micrograph of sample SP_{CH} 4 from table B1.

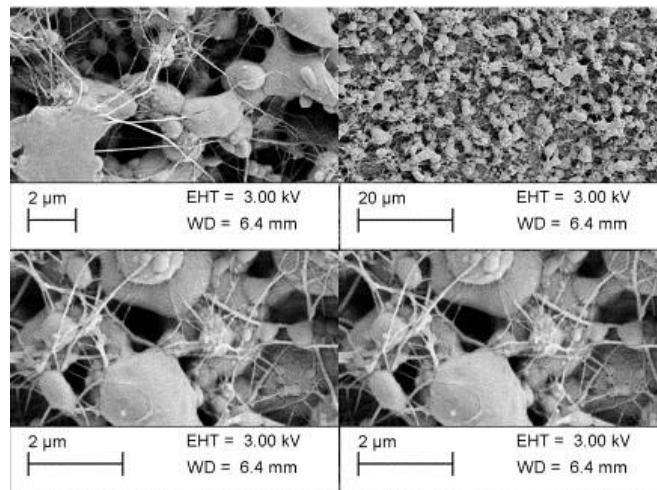


Figure B2. SEM micrograph of sample SP_{CH} 1 from table B1.

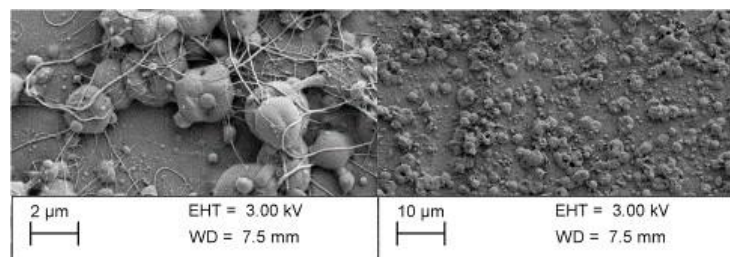


Figure B3. SEM micrograph obtained for sample SP_{CH} 5 from table B1.

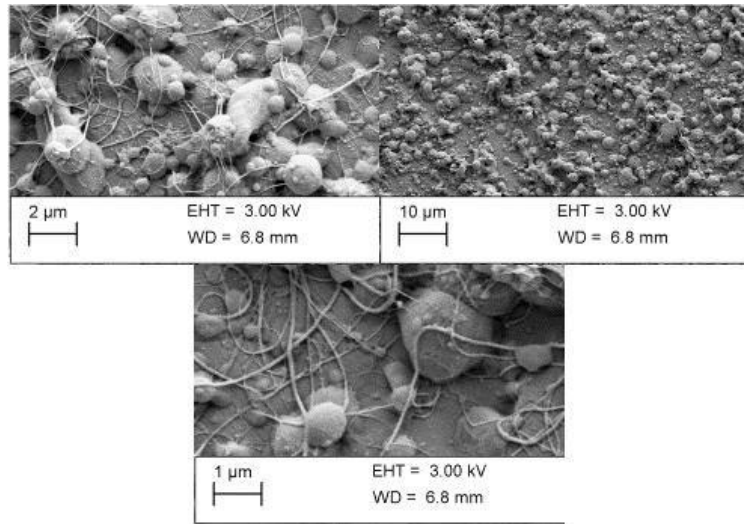


Figure B4. SEM micrograph obtained for sample SP_{CH} 2 from table B1.

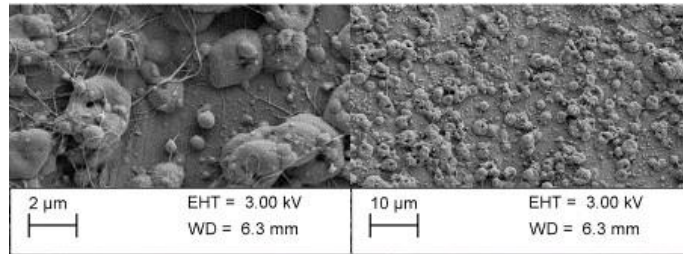


Figure B5. SEM micrograph obtained for sample SP_{CH} 12 from table B1.

Appendix C

Sample code	PCL flow rate (mLhr ⁻¹)	PVP flow rate(mLhr ⁻¹)	Distance(cm)	Voltage(kV)	Observation
CP _{VCH} 1	0.5	1.5	10	15	Electrospraying
CP _{VCH} 2	0.25	1.5	10	15	Solution dripping/no electrospraying
CP _{VCH} 3	0.25	1.5	15	15	Electrospraying
CP _{VCH} 4	0.5	1.5	10	20	Electrospraying
CP _{VCH} 5	0.5	1.5	15	20	Electrospraying
CP _{VCH} 6	0.5	1.5	20	20	Electrospraying
CP _{VCH} 7	0.25	1.5	10	20	Electrospraying
CP _{VCH} 8	0.25	1.5	15	20	Solution dripping/no electrospraying
CP _{VCH} 9	0.25	1.5	20	20	Solution dripping/no electrospraying

Table C1. Processing parameters used for CP_{VCH}. 4% solution of PCL in 1,2-dichloroethane and 5% PVP in water was used.

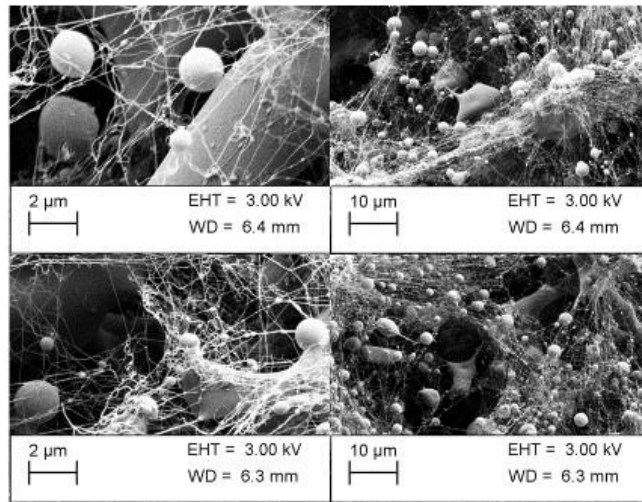


Figure C1. SEM micrograph of sample CP_{VCH} 5 from table C1.

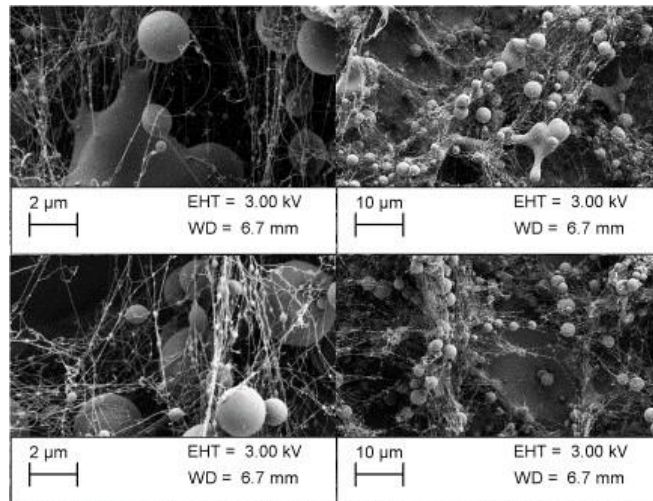


Figure C2. SEM micrograph of sample CP_{VCH} 6 from table C1.

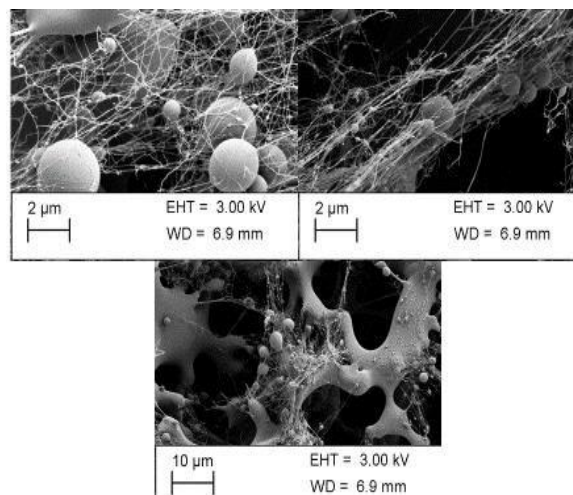


Figure C3. SEM micrograph of sample CP_{VCH} 4 from table C1.

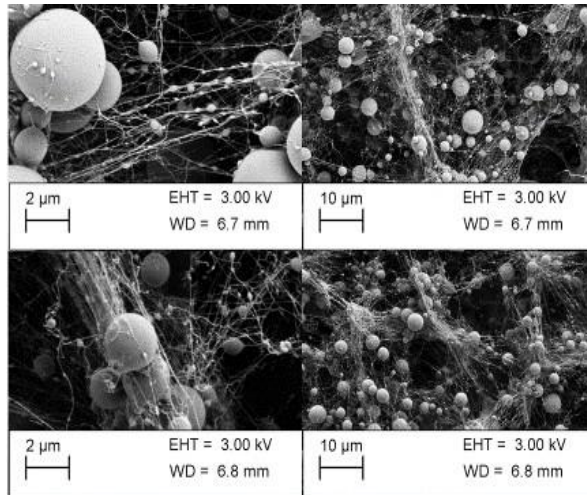


Figure C4. Figure C3. SEM micrograph of sample CP_{VCH} 3 from table C1.

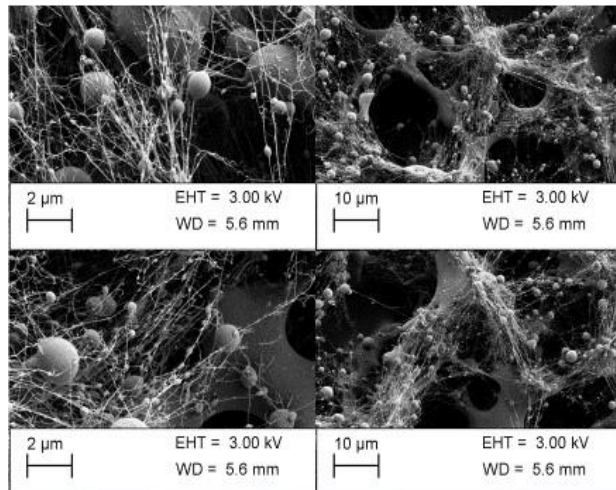


Figure C5. Figure C3. SEM micrograph of sample CP_{VCH} 7 from table C1.

Appendix D

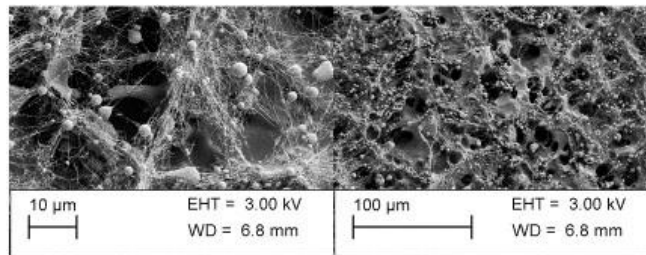


Figure D1. SEM micrograph image of CP_{V2H} 5% (w/v) PVP outside (1.5ml/hr) and 10% (w/v) PVP inside (0.5ml/hr) at 15 kV and 10cm tip to collector distance.

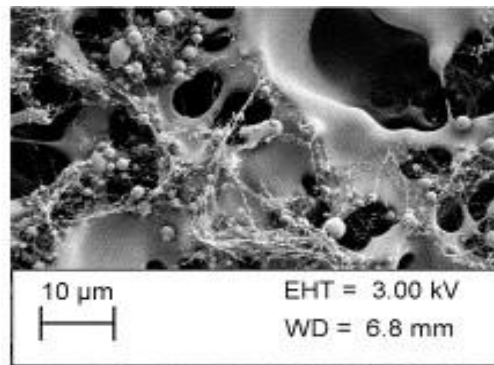


Figure D2. SEM micrograph image of CP_{V2H} 5% (w/v) PVP outside (1.5ml/hr) and 5% (w/v) PVP inside (0.25 ml/hr) at 15 kV and 10 cm tip to collector distance (outer ring).

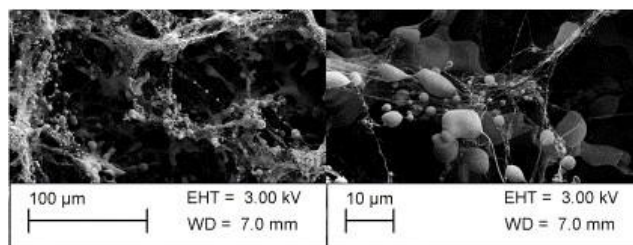


Figure D3. SEM micrograph of CP_{V2H} 5% (w/v) PVP outside (1.5ml/hr) and 4% (w/v) PVP inside (0.25 ml/hr) at 15 kV and 10 cm tip to collector distance

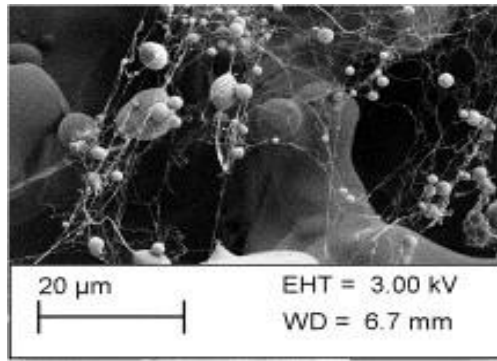


Figure D4. SEM micrograph of CP_{V2H} 5% (w/v) PVP outside (1.5ml/hr) and 2% (w/v) PVP inside (0.25 ml/hr) at 20 kV and 10 cm tip to collector distance (outer ring).

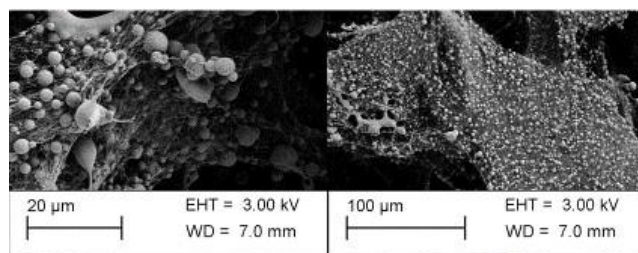


Figure D5. SEM micrograph of CP_{V2H} 5% (w/v) PVP outside (1.5ml/hr) and 1% (w/v) PVP inside (0.25ml/hr) at 15 kV and 10 cm tip to collector distance.

Appendix E

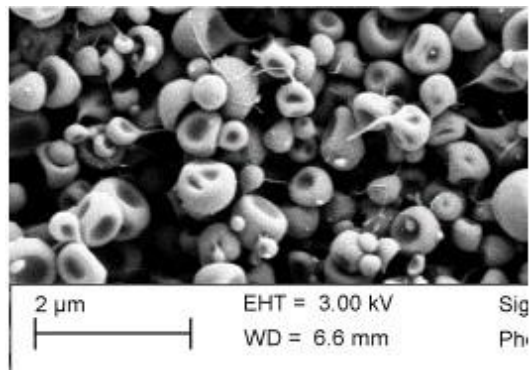


Figure E1. SEM of sample CP_{V2M} 21 from table 2.1.

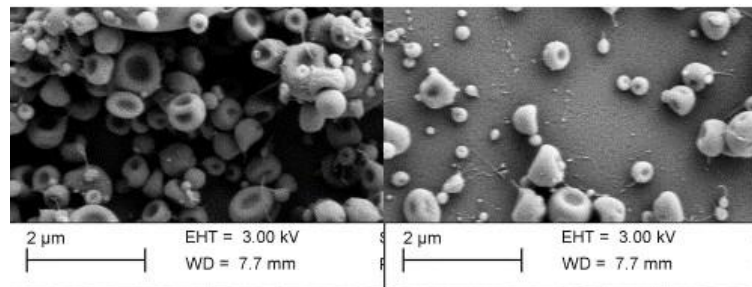


Figure E2. SEM of sample CP_{V2M} 23 from table 2.1.

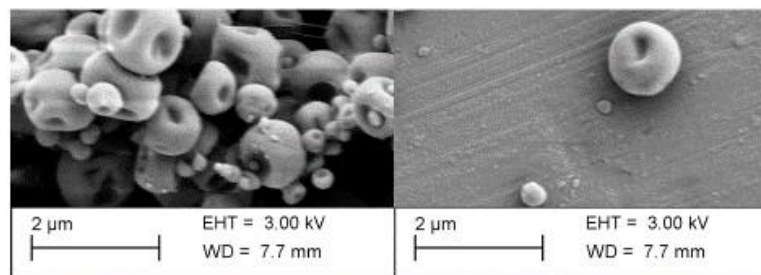


Figure E3. SEM of sample CP_{V2M} 22 from table 2.1.

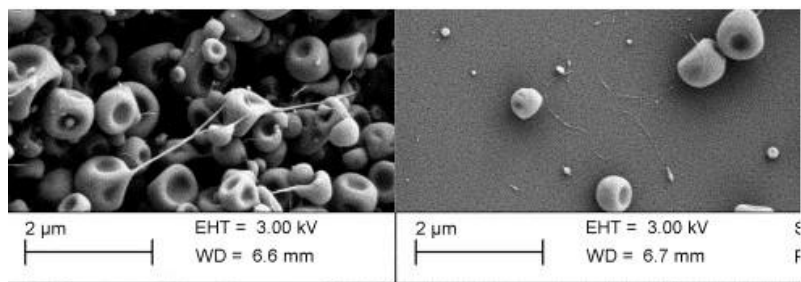


Figure E4. SEM of sample CP_{V2M} 12 from table 2.1.

Appendix F

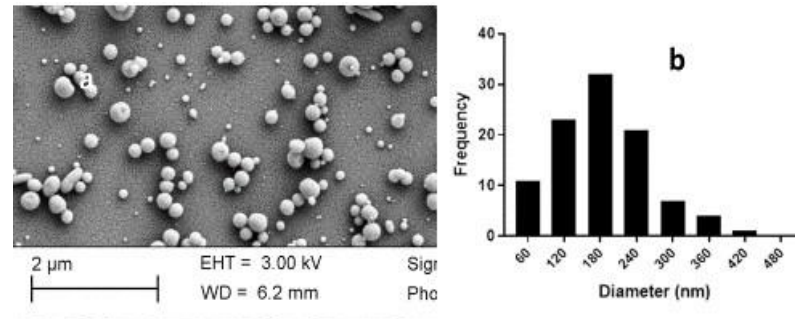


Figure F1. (a) SEM of particles (b) frequency distribution graph particles obtained for sample CP_{v2L} 12 from table 2.2

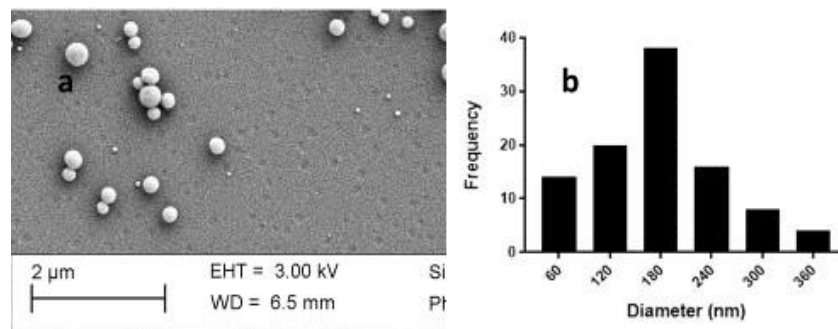


Figure F2. (a) SEM of particles (b) frequency distribution graph particles obtained for sample CP_{v2L} 23 from table 2.3.

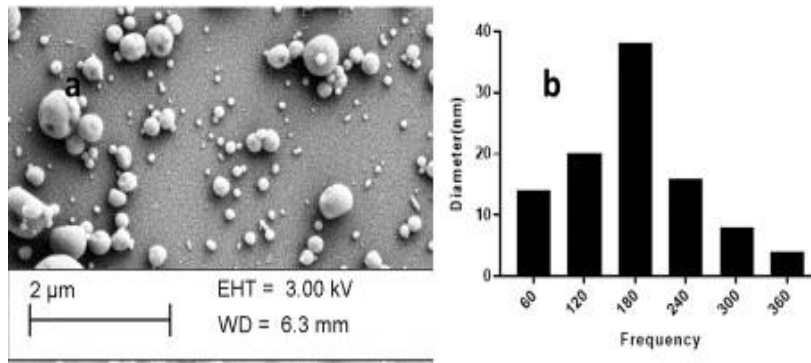


Figure F3. (a) SEM of particles (b) frequency distribution graph particles obtained for sample CP_{v2L} 23 from table 2.4.

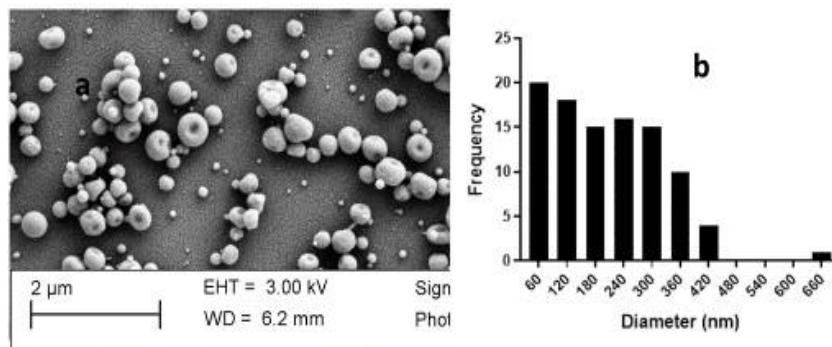


Figure F4. (a) SEM of particles (b) frequency distribution graph particles obtained for sample CP_{v2L} 8 from table 2.4.

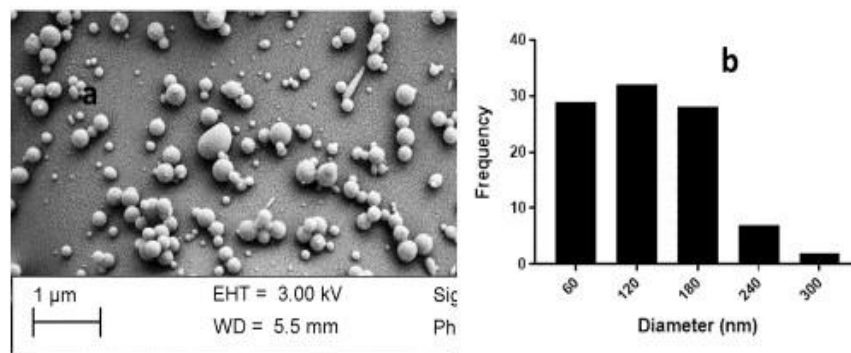


Figure F5. (a) SEM of particles (b) frequency distribution graph particles obtained for sample CP_{v2L} 3 from table 2.2.

Appendix G

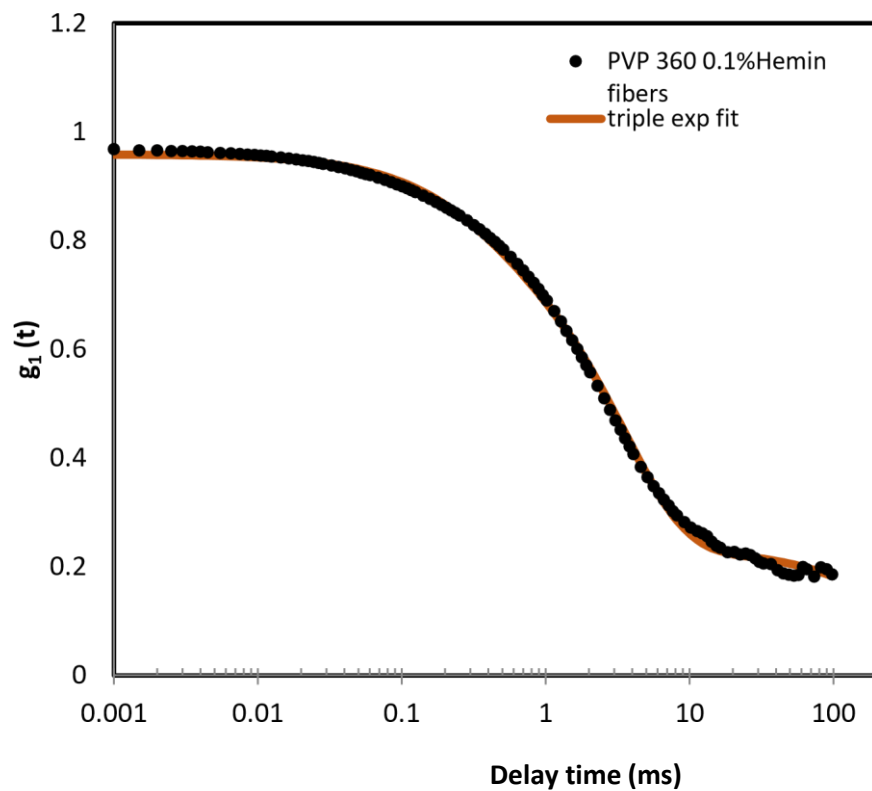


Figure G1. Triple exponential fit for PVP 360 containing 0.1% hemin fibers in water at 25 °C (SSR= **0.007**)

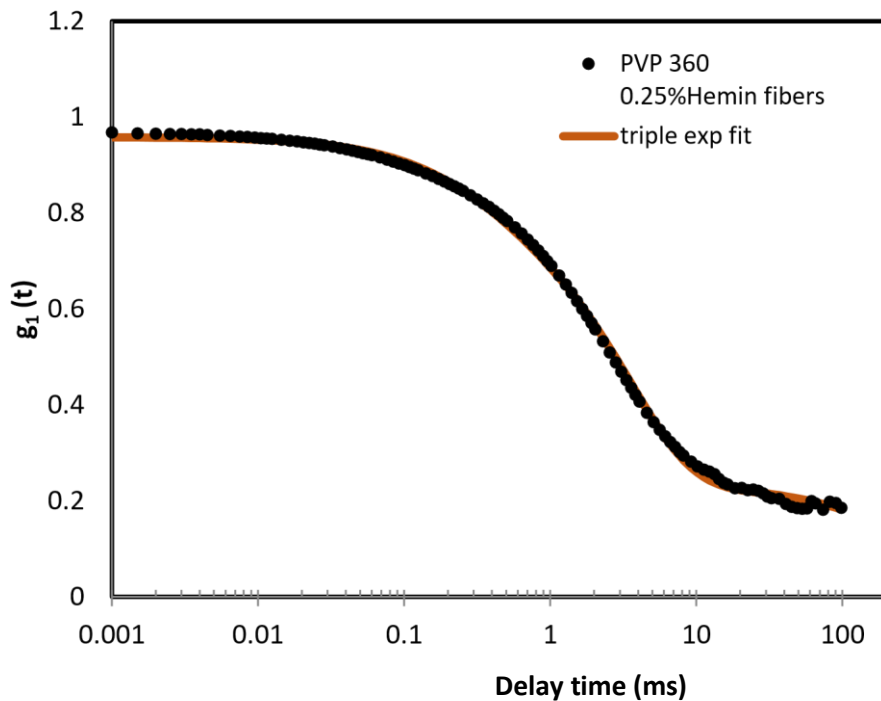


Figure G2. Triple exponential fit for PVP 360 containing 0.25% hemin fibers in water at 25 °C (SSR= 0.002)

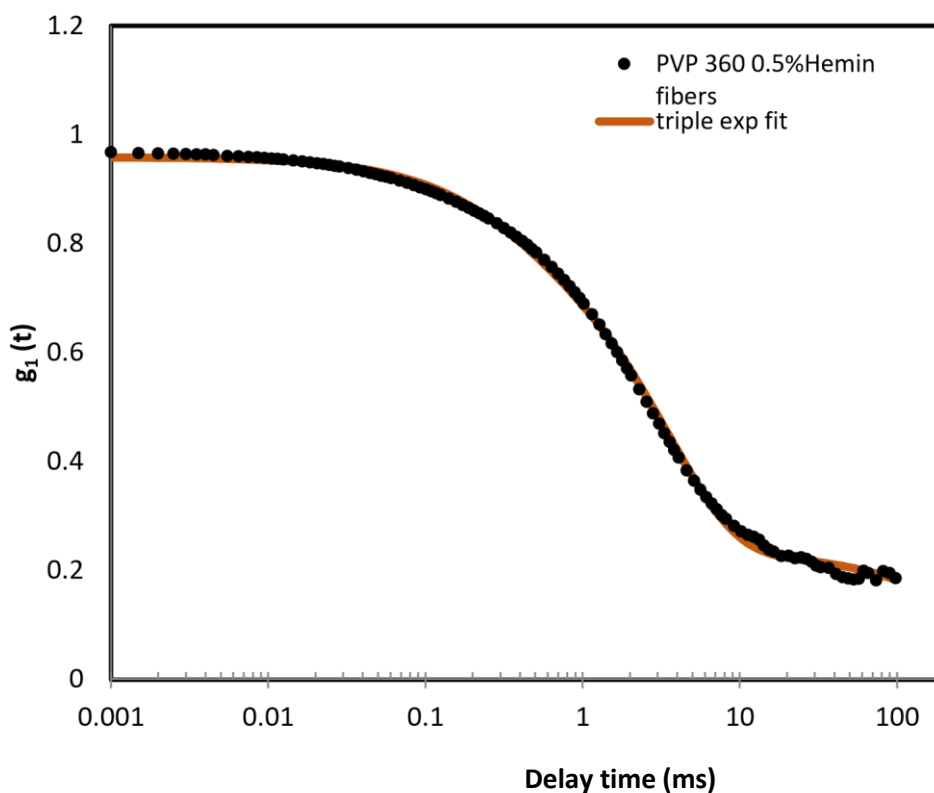


Figure G3. Triple exponential fit for PVP 360 containing 0.5% hemin fibers in water at 25 °C (SSR= **0.007**)

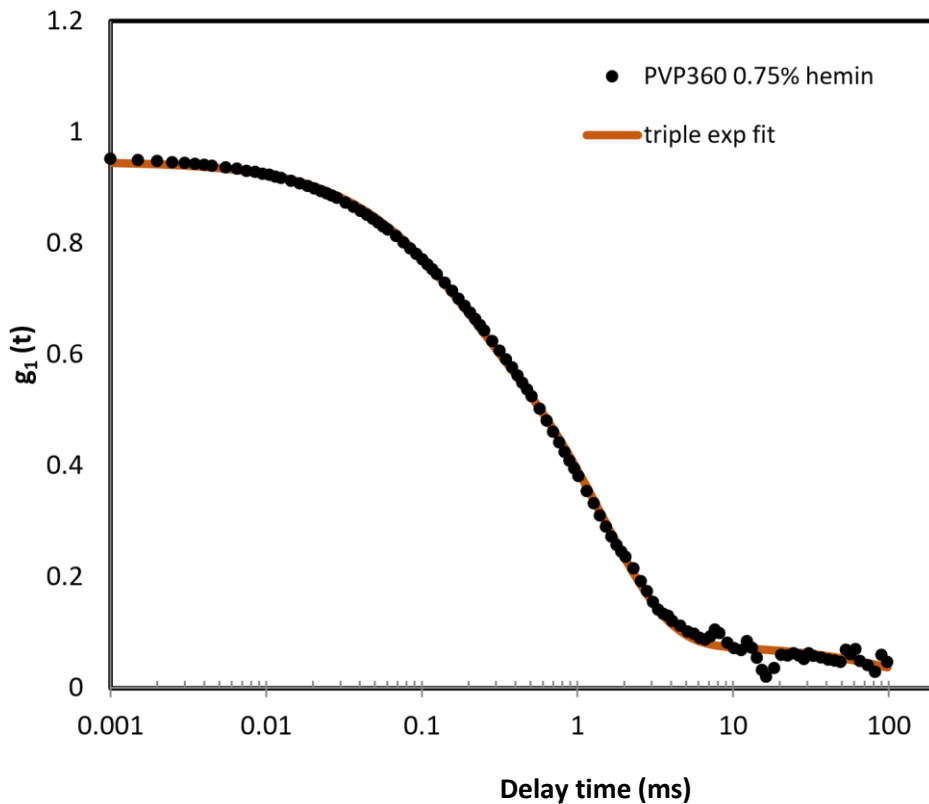


Figure G4. Triple exponential fit for PVP 360 containing 0.75% hemin fibers in water at 25 °C (SSR= **0.004**)

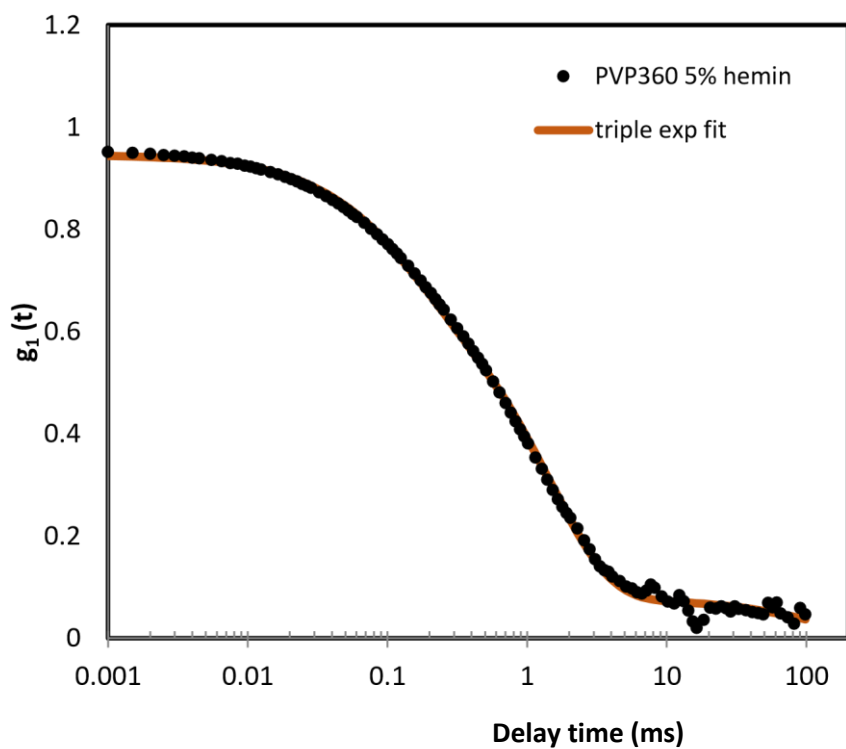


Figure G5. Triple exponential fit for PVP 360 containing 5% hemin fibers in water at 25 °C (SSR= **0.003**)

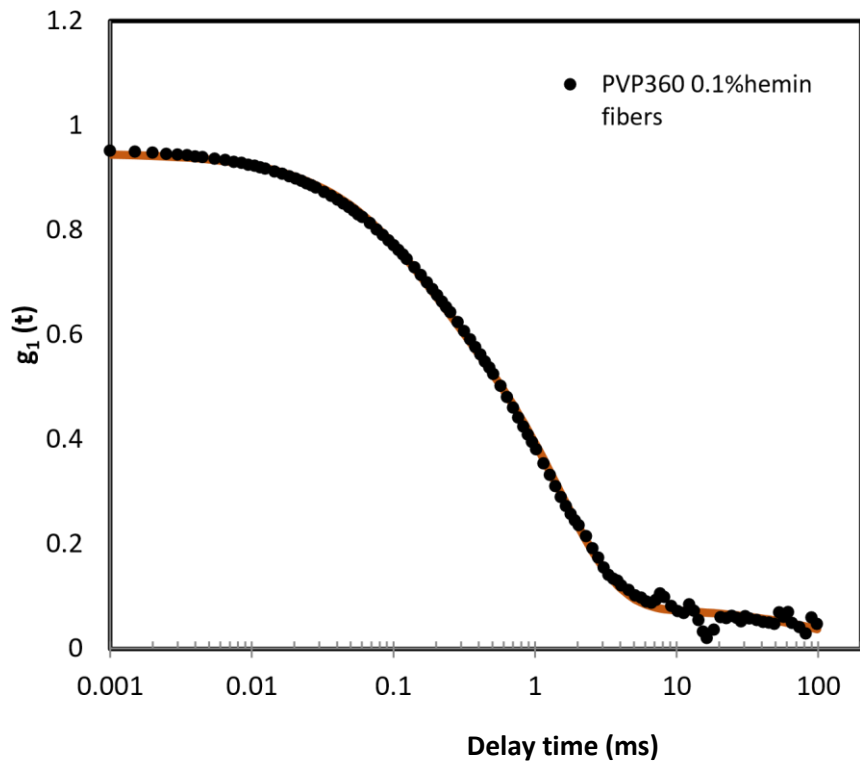


Figure G6. Triple exponential fit for PVP 360 containing 0.1% hemin fibers in PBS at 25 °C (SSR= **0.003**)

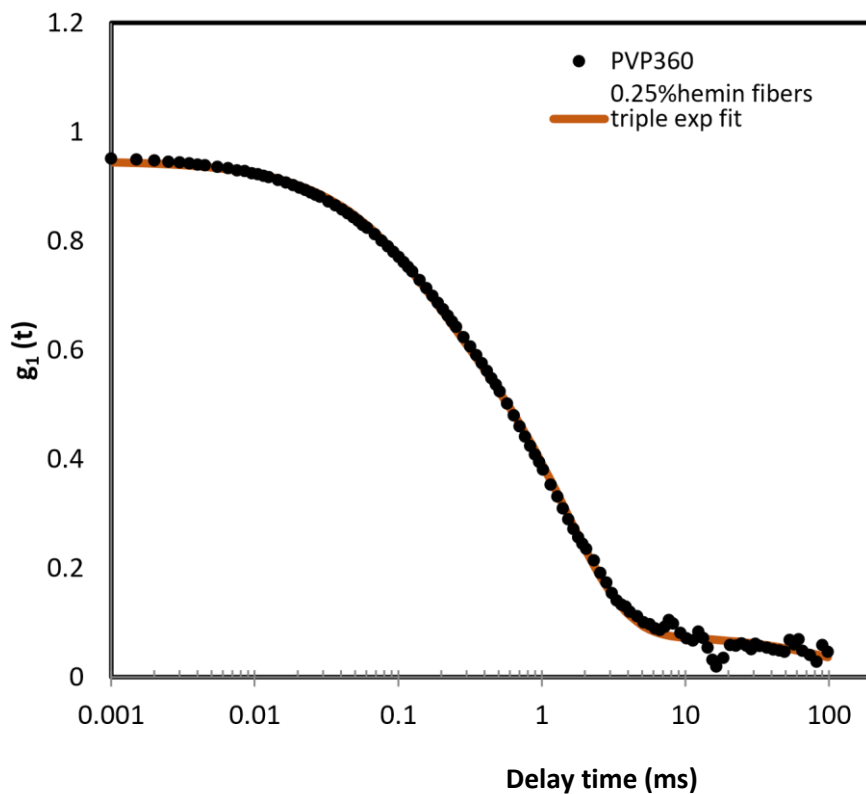


Figure G7. Triple exponential fit for PVP 360 containing 0.25% hemin fibers in PBS at 25 °C (SSR= **0.005**)

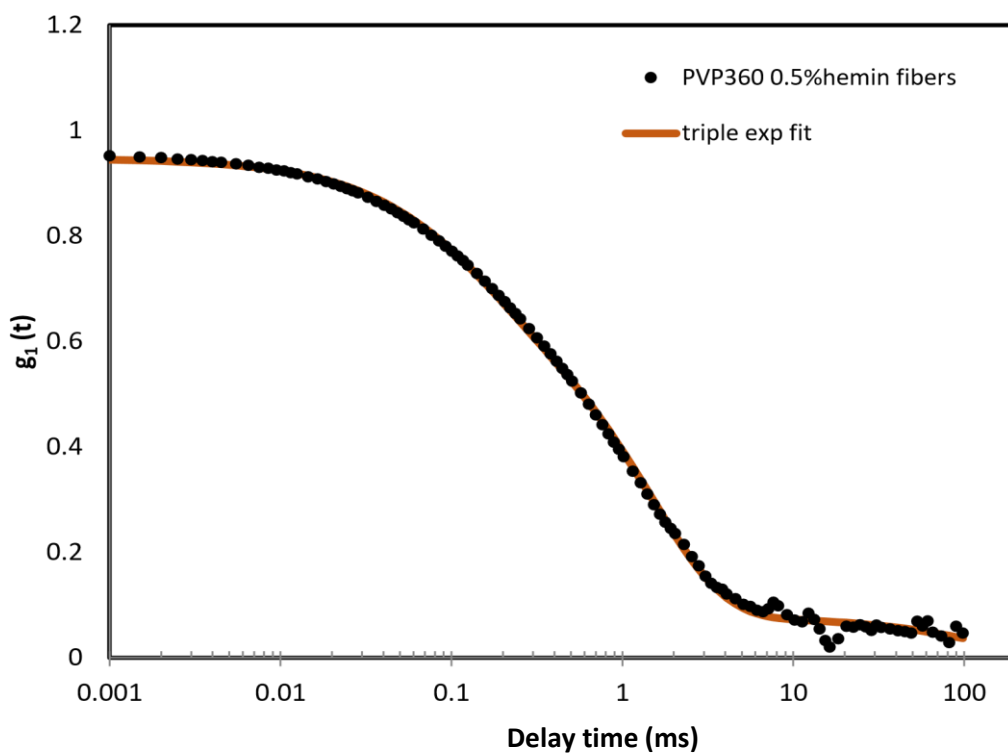


Figure G8. Triple exponential fit for PVP 360 containing 0.5% hemin fibers in PBS at 25 °C (SSR= **0.012**)

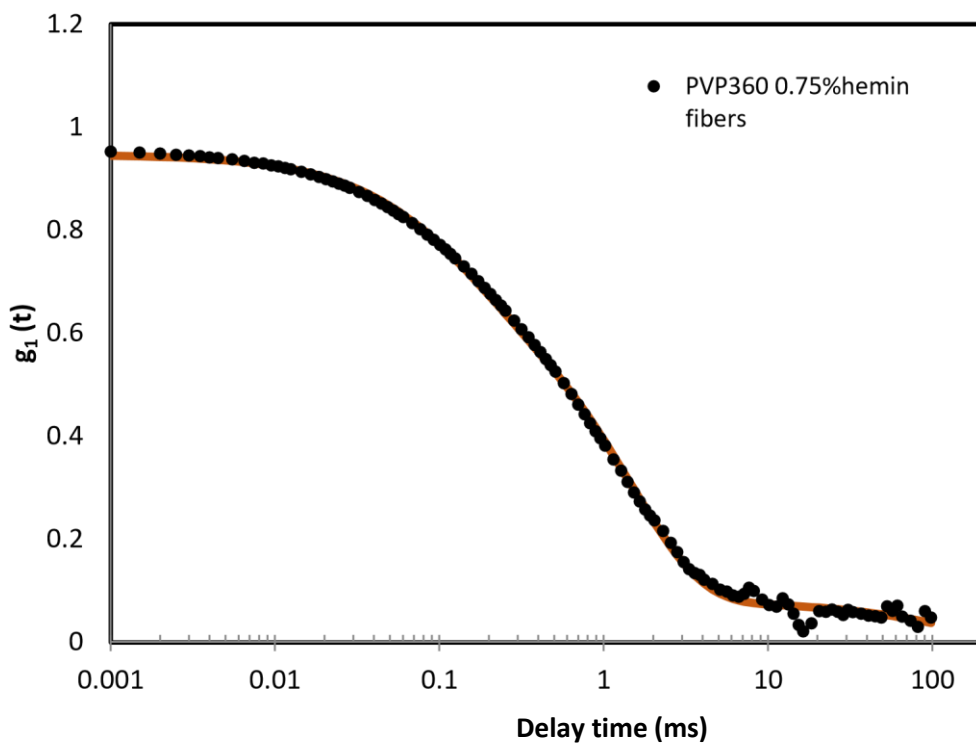


Figure G9. Triple exponential fit for PVP 360 containing 0.75% hemin fibers in PBS at 25 °C (SSR= **0.006**)